Charles University

Faculty of Science

Study programme: Geology

Branch of study: Geology

Mgr. Nikol Novotná

Deformation, metamorphism and metasomatism in the Gemer-Vepor Contact Zone in the Western Carpathians and the possible links to the Greywacke Zone in the Eastern Alps

Deformace, metamorfóza a metasomatóza v gemersko-veporské kontaktní zóně v Západních Karpatech a možné vazby na Greywacke Zone ve Východních Alpách

Doctoral thesis

Supervisor: RNDr. Petr Jeřábek, PhD.

Prague, 2019

Acknowledgements
It would not have been possible to compile this thesis without the patience of my supervisor Petr Jeřábek, who has always tried to "extract" the best from me and was always there to discuss any issues I had. Therefore, my biggest support-related thanks go to him. In second place, I would like to thank Pavel Pitra not just for the superb co-supervision of a major part of my thesis, but for providing helpful hints on how to continue the work when I felt desperate and lost somewhere between the Milky Way, the Western Carpathians and other galaxies! I also wish to thank Martin Racek, Ondro Lexa and other colleagues and classmates from the Institute of Petrology and Structural Geology. This work is the result of continuous contributions from many colleagues and friends. Thanks also go to Jitka Míková, Vojtěch Janoušek, František Veselovský, Ralf Schuster and Zita Bukovská, who was the best "field-buddy" I could ever have hoped to find. I thank my family for their moral support. This work was supported by research funding from the Charles University in Prague (GAUK 5545/2012) and was compiled under the so-called "co-tutelle" supervision system supported by a scholarship provided by the French Government.

I declare that this thesis is a result of my own work and that I have cited all the resources and literature. Neither this thesis nor its substantial part has been submitted to fulfill requirements for any other academic degree. The results of the thesis are my own work or the product of collaboration with other members of the research team.

In Prague, 7/18/2019 .....

Abstract

The studied area extends from the Ochtiná Unit in Western Carpathians to the Veitsch Nappe Eastern Alps. The thesis represents a complex multidisciplinary work that combines the structural analysis, petrology and geochronology. The three main objectives of this thesis: reevaluation of the structure, deformation and metamorphic records, and original position of the Ochtiná Unit, understanding the distinct metasomatic processes recorded along the contact of two major units of the Central Western Carpathians – in the Gemer-Vepor Contact Zone – and their relation to distinct tectono-metamorphic events, testing the possible links between the Ochtiná Unit in the Gemer-Vepor Contact Zone of the Western Carpathians and the Veitsch Nappe in the Greywacke Zone of the Easten Alps, both well known for the Lower Carboniferous shale/schist sequence accompanied by the abundant presence of magnesite ore bodies.

Keywords: Central Western Carpathians, Greywacke Zone, Ochtiná Unit, Veitsch Nappe, U-Pb zircon dating, Phase equilibrium modelling

Abstrakt

Studovaná oblast se rozkládá z Ochtinské jednotky v Západních Karpatech po Veitschský příkrov ve Východních Alpách. Řešení výzkumných otázek je postaveno na komplexním multidisciplinárním přístupu, který kombinuje metody strukturní analýzy, petrologie a geochronologie. Tato práce shrnuje odpovědi na následující výzkumné otázky: reevaluace strukturního, deformačního a metamorfního záznamu Ochtinské jednotky, porozumění jednotlivým metasomatickým procesům zaznamenaným v Gemesko-Veporské styčné zóně a jejich vztah k odlišným tektono-metamorfním událostem, ověření možných propojení mezi Ochtinskou jednotkou v Gemersko-Veporské styčné zóně v Západních Karpatech a Veitschským příkrovem ve Východních Alpách, přičemž obě tyto jednotky jsou tvořeny Spodně-Karbonskými sedimentárními sekvencemi s výskyty magnezotivých ložisek.

Klíčová slova: Centrální Západní Karpaty, Greywacke Zone, Ochtinská jednotka, Veitschský příkrov, U-Pb datování zirkonů, modelování fázových rovnováh

Table of contents

INTRODUCTION

The studied area is located in the Central Western Carpathians and its continuation towards the Eastern Alps. Although the Western Carpathians are intensively studied over decades, details on its evolution remain unsolved. The Ochtiná Unit – described in this work, with magnesite ore deposits provides a link towards the Eastern Alps and its so-called Veitsch Nappe. We have brought some new data from this area and have also looked more in detail on the Central Western Carpathians Alpine evolution.

This work combines field work, metamorphic petrology, structural geology and geochemistry to clarify some of the unknown processes within this region.

1 GEOLOGICAL SETTING

The Alps and Western Carpathians constitute that part of the Alpine-Mediterranean orogenic belt which advances furthest to the north into Central Europe. They were formed by a series of Jurassic to Tertiary subduction and collision events affecting several Mesozoic ocean basins, continental margins, and continental fragments. The Western Alps form a pronounced, westward-convex arc around which the strike of the tectonic units changes by almost 180°. The Western Carpathians are a northward-convex arc of similar size but minor curvature. The two arcs are connected by an almost straight, WSW–ENE striking portion including the Eastern Alps (Froitzheim et al., 2008, Fig. 1).

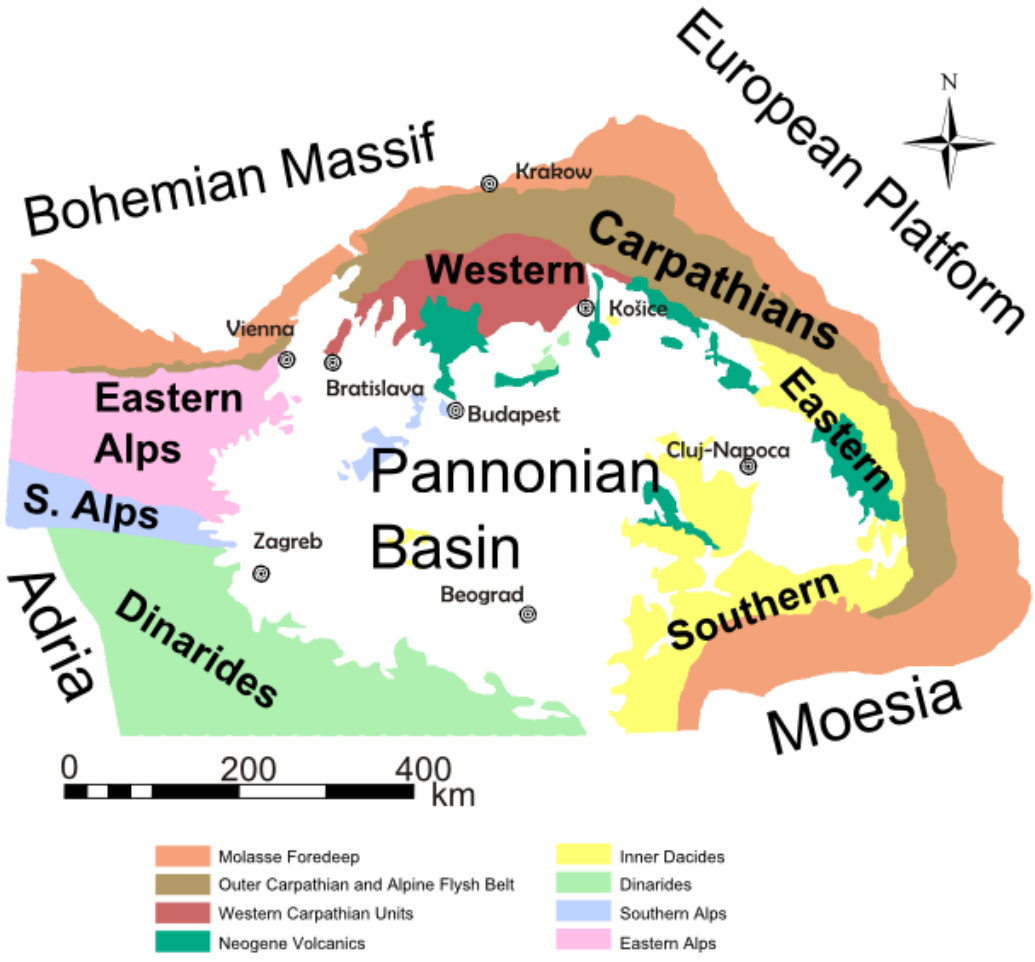

Fig. 1: *Schematic tectonic map of the Eastern Alpine—Western Carpathian—Pannonian basin region (modified after Froitzheim et al. 2008; Lillie et al. 1994).*

1.1 WESTERN CARPATHIANS

The Western Carpathians represent the northernmost segment of the European Alpine belt that connects the Eastern Alps to the west and the Eastern Carpathians to the east. The Central Western Carpathians comprise three major crystalline basement units, from the north to the south, the Tatra, Vepor and Gemer Units (e.g. Matějka and Andrusov, 1931). These units represent segments of the Variscan crust overlain by Late Palaeozoic–Mesozoic cover, which were amalgamated and tectonically overlain by allochthonous Mesozoic nappes during the Cretaceous Eo-Alpine convergence (Plašienka et al., 1997).

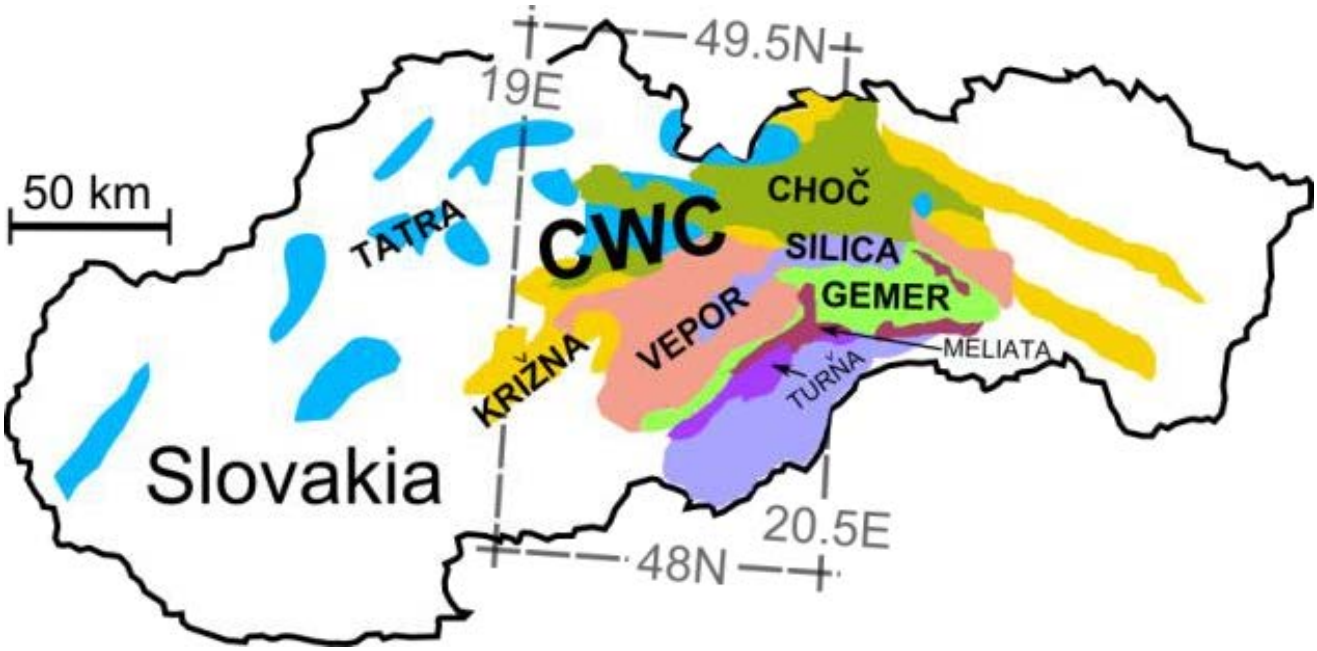

Fig. 2: *Simplified geological map of Slovakia with the major units and nappe. Map based on the geological map of the Slovak Republic, 1:50 000 http://mapserver.geology.sk.*

1.1.1 CENTRAL WESTERN CARPATHIANS

In the Western Carpathians, the Tatra Unit comprises variscan high-grade crystalline basement with its Late Paleozoic to Mesozoic sedimentary cover. It is overlain by a superficial nappe system represented by the structurally lower Krížna (Fig. 2) nappe and structurally upper Choč nappe (Fig. 2), which also overlays the northern part of the Vepor Unit. The Krížna and Choč nappes are composed of Mesozoic sedimentary sequences dominated by Triassic carbonate platform sediments (e. g. Michalík et al., 2007). It is generally accepted that the Krížna nappe represents a sedimentary infill of the Zliechov basin originally located between the present day Tatra and Vepor units (Prokešová et al., 2012 and references therein). On the other hand, the location of the basin associated with the Choč nappe has not been resolved (e.g. Plašienka, 2003; Tomek, 1993).

1.1.2 GEMER-VEPOR CONTACT ZONE

The studied region straddles the Gemer – Vepor Contact Zone and comprises three Alpine units/nappes. The structurally lower Vepor Unit consists of Variscan basement rocks dominated by micaschists (Hladomorná Dolina Complex, Klinec, 1966), intruded by Carboniferous granitoids (Bibikova et al., 1988; Michalko et al., 1998). In the southern and central part of the Vepor Unit, the basement rocks are overlain by the para-autochthonous Permian–Triassic cover comprising meta-arkose, meta-conglomerate and quartzite (Foederata unit, Rozlozsnik, 1935), as well as minor kyanite-chloritoid-bearing schists (Lupták et al., 2003; Vrána, 1964). The structurally intermediate Ochtiná Unit (also called the Ochtiná "nappe", Kozur and Mock, 1997) represents a few kilometres wide ENE-WSW trending belt located at the border between the Gemer and Vepor Units. The Ochtiná Unit shows a complex lithological assemblage dominated by dark flysch-like phyllites and meta-sandstones, which enclose metric to hectometric lenses of amphibolite, serpentinite, chloritoid schists, magnesite and Visean to Serpukhovian limestone (Abonyi, 1971; Kozur et al., 1976; Němejc, 1946). The carbonates are usually interpreted as part of the Ochtiná sedimentary sequence while the other rocks are commonly seen as exotic (e.g. Vozárová, 1990). Although this complex was earlier interpreted as the Lower Carboniferous cover of the Gemer Unit (Němejc, 1946; Planderová and Vozárová, 1978), more recently a separate evolution of the Ochtiná Unit was proposed based on the study

of fluid inclusions and possible correlation of lithostragraphic horizons (Kozur and Mock, 1997; Németh et al., 2006). Further to the east, the Gemer-Vepor Contact Zone is marked by a similar lithological complex – the Črmel nappe (e.g. Grecula et al., 2009; Vozárová, 1996). The structurally upper Gemer Unit is dominated by a basement comprising three groups with distinct lithology and metamorphic grade (Faryad, 1991a; Grecula, 1982). The structurally uppermost Gelnica group in the south comprises volcano-sedimentary rocks intruded by Permian granitoids (Grecula, 1982; Poller et al., 2002), the structurally lower Rakovec group is dominated by metavolcanites (Hovorka and Ivan, 1985), and the lowermost Klátov group in the north consists of paragneiss and amphibolite (Faryad, 1990; Hovorka et al., 1997). The Gelnica and Rakovec groups are uncomfortably overlain by Upper Carboniferous shales and Permian meta-conglomerates (Šucha and Eberl, 1992). The Gemer Unit is tectonically overlain by the Meliata subduction-accretionary complex of Jurassic age (Faryad and Henjes-Kunst, 1997; Mock et al., 1998) and by the uppermost Triassic Turňa and Silica nappe systems (Fig. 3).

The Variscan metamorphic fabrics of greenschist- to amphibolite-facies grade are dominant in the Gemer Unit (e.g. Faryad, 1995). Maximum P–T conditions are documented in the Klátov complex (550-700 °C at 7-10 kbar, Faryad, 1995), intermediate P–T in the Rakovec complex (440-480 °C at 7-10 kbar, Faryad, 1999) and low P–T in the Gelnica complex (up to 350-450 °C at 3-5 kbar, (Faryad, 1994). The Variscan metamorphism in the southern Vepor basement reached 570-670 °C at 6-8.5 kbar (Jeřábek et al., 2008).

The Cretaceous tectono-metamorphic overprint was higher grade and more intense in the Vepor Unit than in the Gemer Unit. In the Gemer Unit, the Alpine metamorphic overprint reached generally lower greenschist-facies conditions (330-350 °C at 4.5-6 kbar in the Permian granitoids, Faryad and Dianiška, 1999) and 200-250 °C in the cover (Šucha and Eberl, 1992). In the Vepor basement, the Alpine metamorphic conditions range in a variety of P–T conditions depending on the structural position of the studied samples (430-620 °C at 5-11 kbar; Janák et al., 2001; Jeřábek et al., 2012, 2008; Plašienka et al., 1999). In the Gemer-Vepor Contact Zone (Fig. 3), the Alpine metamorphism reached 520-550 °C at 8-9 kbar in the basement schists (Jeřábek et al., 2008). The P–T conditions in the Foederata cover overlying the central portion of the Vepor basement are 350-400 °C at 4-4.5 kbar (Lupták et al., 2003), whereas in the Gemer-Vepor Contact Zone the Permian cover recorded 530-560 °C at 4.5-8 kbar (Lupták et al., 2000), similar to the underlying Vepor basement schists.

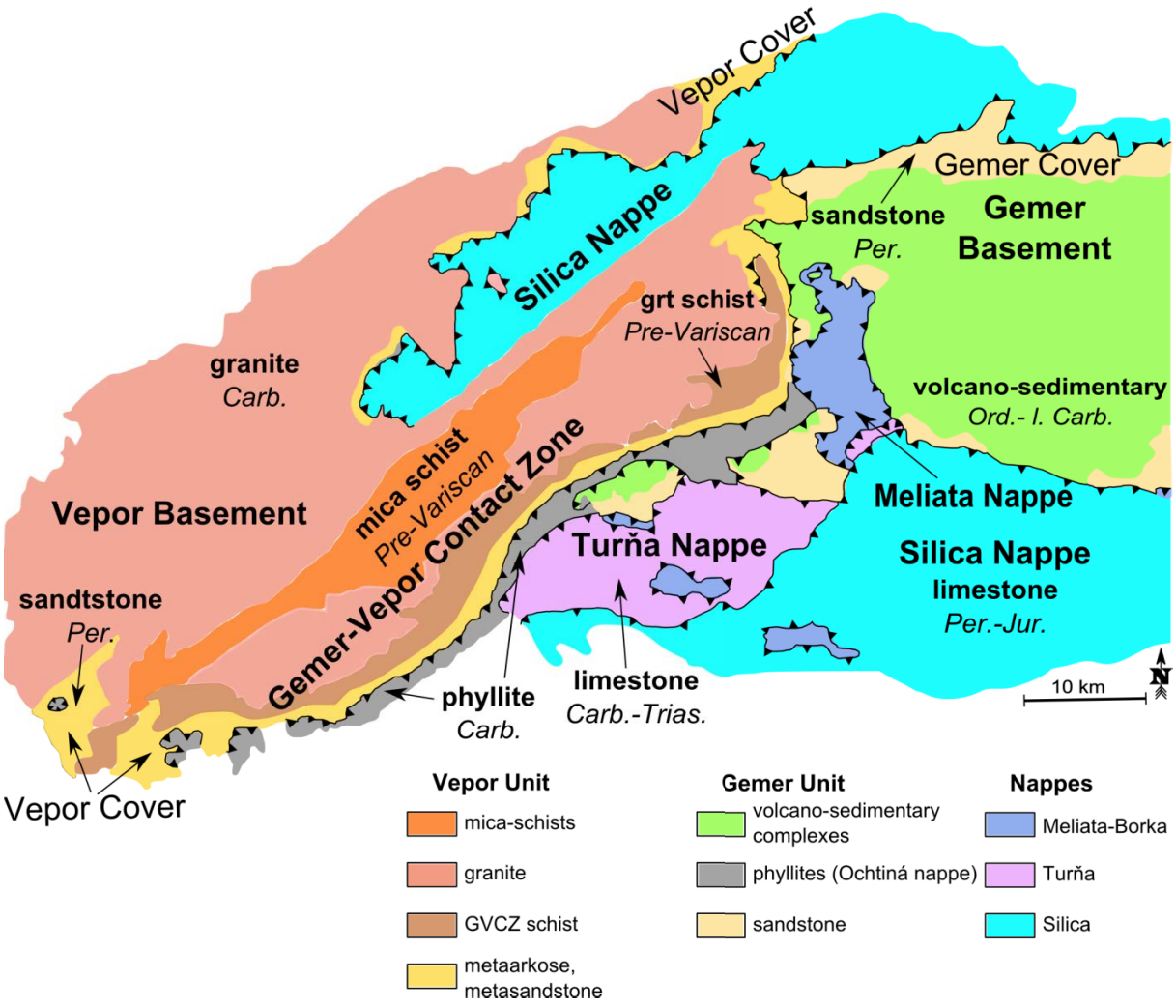

Fig. 3: *Lithotectonic map of the Gemer–Vepor Contact Zone and surrounding units. Map based on the geological map of the Slovak Republic, 1:50 000 http://mapserver.geology.sk.*

1.1.3 ORE DEPOSITS IN GEMER-VEPOR CONTACT ZONE

Numerous magnesite and talc ore deposits are documented along the ENE-WSW striking Gemer-Vepor Contact Zone (Tab. 1, Fig. 4). The Gemer-Vepor Contact Zone is characterized by an alternation of lithological complexes. The ore deposits are located on both sides of this contact zone. They form large (up to 100 m) blocks of lenticular shape. In the southern of Vepor zone the ore deposits are located in the so-called "Sinec zone" and to the south from Gemer-Vepor Contact Zone they are located within the Ochtiná Unit. However, although the southern part of Vepor Unit is dominated by Carboniferous granitoids, the magnesite and talc ore deposits are hosted in Lower Paleozoic chlorite-sericite schists, biotite- and garnet micaschists intercalated with black shales and carbonates, serpentinite bodies, amphibolites and talc schists (e.g. Hurai et al., 2008a and reference therein). In Ochtiná Unit, the magnesite ore deposits occur within the Upper Turnaisian-Viséan (Bajaník and Planderová, 1985; Planderová and Vozárová, 1982) Hrádok Formation and Upper Viséan-Serpukhovian (Kozur et al., 1976) Lubeník Formation, the deposits of Ochtiná Unit are hosted in sericite-graphite schist, sericite-chlorite schist and black shales (see table 1 for details). The second productive horizon is documented in the Lower Paleozoic rocks of the Gelnica Group of Gemeric Unit (Košice, Gemerská Poloma). The Mg-carbonates occur in volacano-sedimentary complexes composed of black shales, chlorite sericite schists, metarhyolites, basic pyroclastics and porphyroids of the Bystrý Potok and Vlachovo Formations (Grecula et al., 1995; Tréger et al., 2004). Moreover, the replacement-type siderite-Fe-dolomite-ankerite deposits occur in Silurian limestones along with the magrnesite deposits hosted predominantly by Carboniferous marine carbonates along the Gemer-Vepor Contact Zone (Bernard, 1961; Grecula et al., 1995, Nižná Slaná,). In spite of the extensive mining the origin of the metasomatic deposits remains controversial.

Locality	Map Ref.	Unit	Structure	Lithology	Reference
Gemerská Poloma	1	Gemer	W-E trending magnesite-talc lense, length: 1000 m, width up to 300 m	Lower Paleozoic carbonate- and lydite-bearing sequence of Gelnica Group, Hanging wall: laminated phyllites, footwall: Permian granite	Kilík, 1997
Košice	X	Gemer	Two irregular lenses, oriented NW-SE, dip 40°-70° SW, directional length 1600-1800m, max. thickness 280 m	Early Carboniferous graphite-sericite schist with interlaces of dark dolostone	Grecula et al., 1995
Ochtiná	2	Ochtiná	Several subhorizontal NW-SE oriented lenses, max. thickness 55-230 m, length 1000 m, width 400 m	Early Carboniferous sericite-graphite schist	Grecula et al., 1995; Mihalík and Tréger, 1995
Jelšava	4	Gemer	Several E-W oriented lenses, dip 45°-85° SE, directional length 4500 m, max. thickness 600-1000 m. Magnesite rich parts are 5-80 m thick and up to 1500 m long	Early Carboniferous black shale with gabbro-amphibolites in footwall, interlaces of diabase tuff and tuffite with chlorite-, sericite-chlorite and black schist in hanging wall	Grecula et al., 1995; Mihalík and Tréger, 1995
Lubeník	3	Ochtiná	Lense-shaped, direction NE-SW, dip 55°-60° SE, cropping out in directional length 300 m, total directional length 880 m, max. thickness 200m	Early Carboniferous black schist	Gánovský, 1995
Ploské	5	Ochtiná	One major and 4 small lenses oriented NE-SW, dip 60° SE, directional length 180 m, max. thickness 18-25 m	Footwall: Early Carboniferous graphitic schist, slaty dolomite and metabasalt. Hanging wall: metapsamite, sericite-graphite schist	Grecula et al., 1995; Varga 1992
Burda	6	Ochtiná	One lense oriented NE-SW, dip 25°-55° SE, directional length 1500 m, thickness 200 m	Footwall: Early Carboniferous chlorite-sericite schist. Hanging wall: black shale, quartz phyllite with slaty crystalline limestone	
Mútnik	8	Vepor	Several irregular lenses 20-100 m thick, dip 45° S, W-E oriented	Footwall: sericite-chlorite schist, talc schist, garnet-mica schist and amphibolite. Hanging wall: sericite and chlorite schist	Varga, 1992; Lisý, 1971
Kokava	7	Vepor	Several mylonitized lenses oriented NE-SW, dip 55° SE	Chlorite-sericite schist	Lisý, 1971

Tab. 1: *The main magnesite and talc ore deposits in Central Western Carpatnians (after Radvanec et al., 2010).*

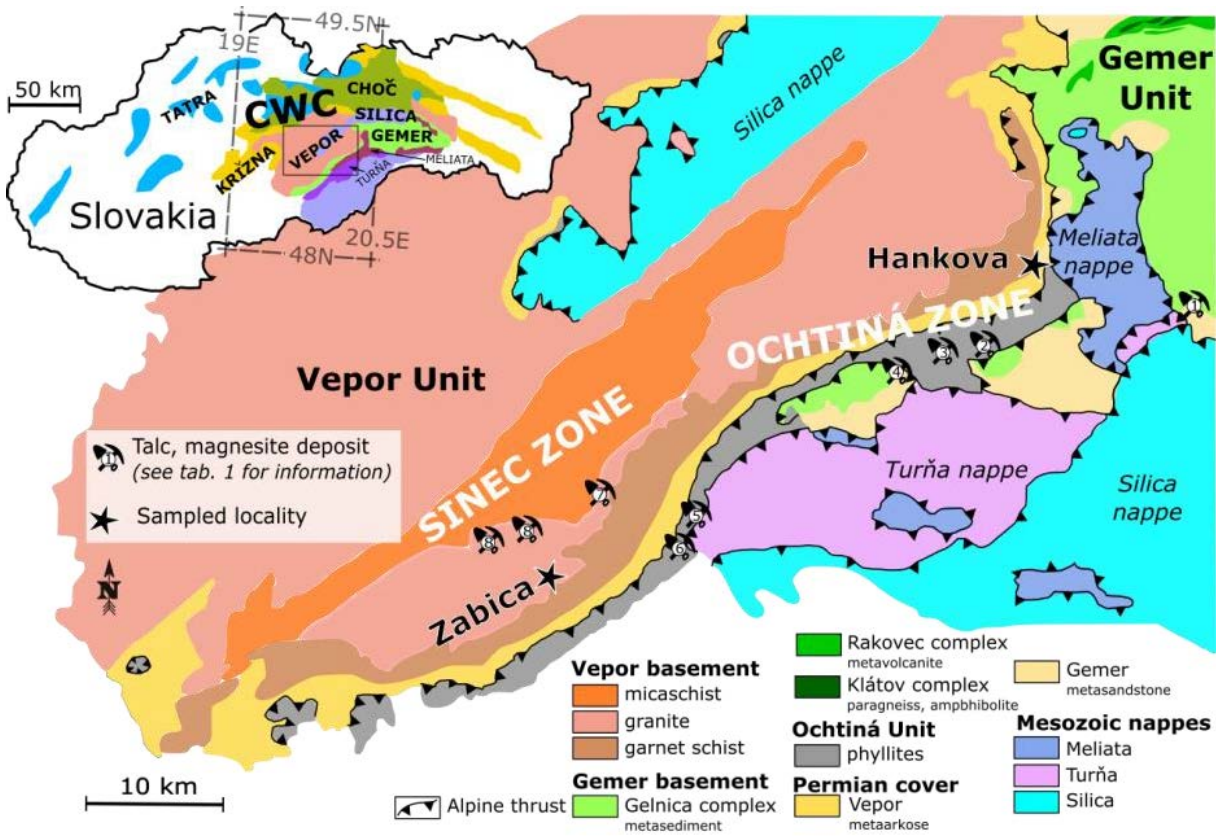

Fig. 4: *Lithotectonic map of the Gemer-Vepor Contact Zone and surrounding units with location of the studied localities (black star) and the main magnesite and talc bodies (see tab. 1 for reference). The position of the Sinec and Ochtiná Zone are also marked. Map based on the geological map of the Slovak Republic, 1:50 000* http://mapserver.geology.sk

The ore deposits in Sinec zone are surrounded by the rocks reaching up to amphibolites facies condition. The origin of these strongly mylonitized talc and magnesite ore deposists remains unsolved. Some authors interpreted the magnesite ore deposits to be derived from Vepor basement (Molák at al., 1995). Another group of authors has proposed the model of calcite in Carboniferous limestone being replaced by talc and dolomite during the Permo-Triassic rifting stage, the temperatures of magnesite formation are 280-400 °C (Neméth et al., 2004 and references therein). The temperatures ~370-420 °C were determined for the megnesite in Ochtiná Unit (Koděra and Radvanec, 2002; Radvanec and Prochaska, 2001). Furthermore, some of the more recent publications propose an Alpine metasomamic event responsible for the talc evolution (Hurai et al., 2011).

This situation in Central Western Carpathians resembles to the Eastern Alps Greywacke Zone, where the replacement-type siderite deposits occur in Devonian limestone, and Carboniferous marine carbonates are replaced by metasomatic sparry magnesite. The

siderite veins of the Eastern Alps penetrate Carboniferous and Permian strata, similar to those in the Gemer-Vepor Contact Zone (Grecula et al., 1995; Hurai et al., 2008b; Prochaska, 1999,). The magnesite and talc ore deposits are located in so-called Veitsch Nappe, which is regarded to be the counterpart of Ochtiná Unit in the Eastern Alps (Neubauer and Vozárová, 1990).

1.2 EASTERN ALPS

The Eastern Alps consists of poly-phase deformed and partly metamorphosed sedimentary and crystalline rocks of the Austroalpine Units. The Austroalpine nappes are subdivided into Lower and Upper Austroalpine, and the Upper Austroalpine nappes themselves are grouped in several nappe systems (Schmid et al., 2004). The nappe systems are stacked on top of each other and separated by either flat-lying shear zones or by major steep strike-slip faults from each other. From North to South and from top to bottom the Upper Austroalpine Unit is furthermore subdivided Northern Calcareous Alps, Greywacke Zone and the Crystalline basement units (Froitzheim et al. 2008, Fig. 5 and 6).

The Northern Calcareous Alps are an elongated thrust belt of more than 500 km length from the Rhein valley in the west to Vienna in the east. They are located north of the Greywacke Zone and south of the Penninic flysch zone. The Northern Calcareous Alps consist of Permo-Mesozoic sediments affected by several tectonic and metamorphic events, which led to a complex internal structure. In the studied area, the following tectonic units can be distinguished according to Frisch and Gawlick 2003: The Upper Bavaric Unit, the Tirolic Unit with the Hallstatt Mélange, the Ultra Tirolic Unit and an imbricated belt (Fig. 6).

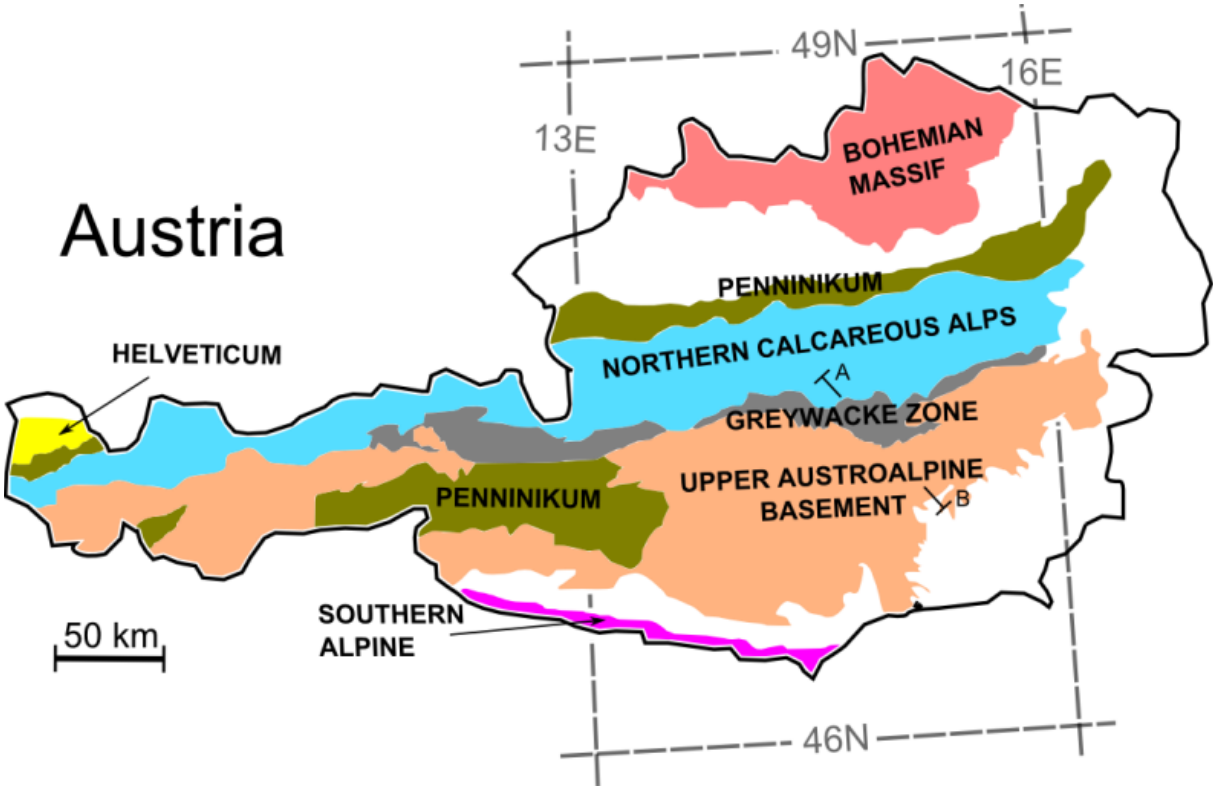

Fig. 5: *Simplified geological map of Austria with the major units and nappes (after Egger et al. 1999)*

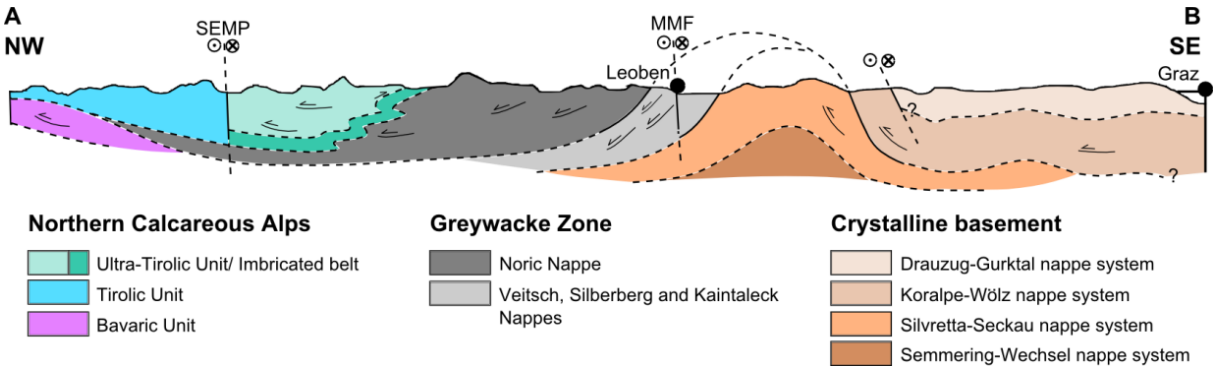

Fig. 6: *Simplified geological profile through the Eastern Alps. Abbreviations: SEMP = Salzach-Ennstal fault system, MMF = Mur-Mürz fault system. Profile trace is indicated on Fig. 5 (After Gasser et al., 2009).*

The continuation of the Central Western Carpathians (CWC) in the Eastern Alps is regarded to be the nappe system of the Greywacke Zone (Fig. 5 and 6). This Zone underlies the Tirolic Nappe System and includes from bottom to the top the Veitsch, Silbersberg, Vöstenhof-Kaintaleck and Noric nappes (Neubauer et al. 1994, Fig. 6). The lowermost Veitsch Nappe mainly comprises Carboniferous clastic and carbonaceous metasediments (Froitzheim et al., 2008), the overlying Silbersberg Nappe consists of phyllites with intercalations of chlorite schists and the Gloggnitz riebeckite gneiss, the Vöstenhof-Kaintaleck Nappe is formed by a basement of paragneisses, mica schists and amphibolites with overlying post-Mid-Devonian clastic metasediments. The crystalline rocks of this nappe show a Variscan amphibolite-facies imprint (Froitzheim et al., 2008 and references therein). The largest and uppermost Noric Nappe comprises a Lower Palaeozoic to Upper Carboniferous sedimentary successions. This is transgressively overlain by the Permian-age strata of the Tirolic Nappe System (Fig. 6). Within the nappe pile of the Greywacke Zone the Eo-Alpine metamorphic grade increases downward to upper greenschist facies in parts of the lowermost nappe. Only the uppermost Noric Nappe is in stratigraphic contact with the Tirolic Nappe System of the Northern Calcareous Alps; the other nappes are not (Froitzheim et al., 2008 and references therein).

The Crystalline basement units to the south underlie the Greywacke Zone can be separated again into several nappe systems. They are from bottom to top the Semmering-Wechsel, Silvretta-Seckau, Koralpe-Wölz, ÖtztalBundschuh and Drauzug-Gurktal nappe systems (after Schmid & al. 2004 and Froitzheim et al. 2008, Fig. 6). These units consist of series of low- to high-grade Paleozoic and Mesozoic metamorphic rocks with complex poly-phase tectonic and metamorphic histories.

1.3 OBJECTIVES

During the progress of the thesis, we defined three main objectives for the presented work:

1. Reevaluation of the structure, deformation and metamorphic records, and original position of the "Ochtiná Unit" in the Gemer-Vepor Contact Zone, which was traditionally recognized as the part of the Gemer Unit cover sequence.

2. Understanding the distinct metasomatic processes recorded along the contact of two major units of the Central Western Carpathians – in the Gemer-Vepor Contact Zone – and their relation to distinct tectono-metamorphic events and to formation of talc and magnesite ore deposits abundant in this region.

3. Testing the possible links between the Ochtiná Unit in the Gemer-Vepor Contact Zone of the Western Carpathians and the Veitsch Nappe in the Greywacke Zone of the Easten Alps, both well known for the Lower Carboniferous shale/schist sequence accompanied by the abundant presence of magnesite ore bodies.

2 METHODOLOGY

In order to better understand the poly-phase evolution of the studied area the subsequent methodology of study was chosen. This work comprises of large amount of field structural measurements, as well as the detailed study of over 300 thin sections and over 1000 structural measurements in the field. After the field work selected samples were analyzed more in detail.

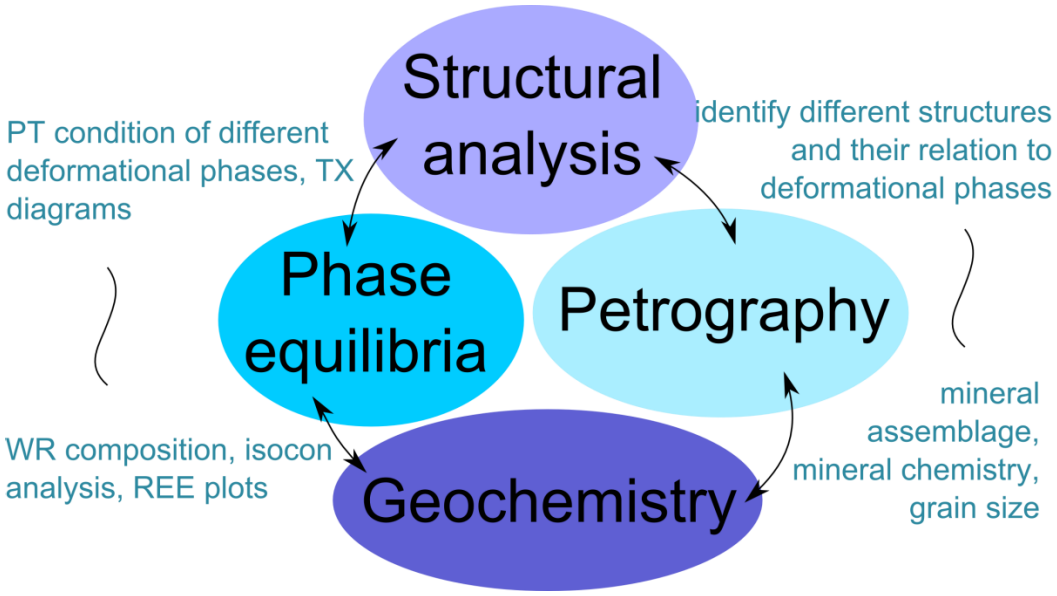

2.1 WHOLE ROCK CHEMICAL COMPOSITIONS

Whole rock chemical compositions were obtained from the ACME Labs, Vancouver, Canada. Samples were finely ground in an agate tray and the whole rock major and minor elements compositions were obtained by ICP-ES following a lithium borate fusion and dilute acid digestion of a 0.2 g pulp. Trace element contents were obtained by ICP-MS. Detection limits for major elements are 0.01 %, for the trace elements the detection limit varies from 0.01 ppm (Hg) to 1 ppm (Ba, Be, Sn).

2.2 MINERAL COMPOSITIONS

Mineral compositions were determined using the electron microprobe Cameca SX100 in wavelength-dispersive mode at the Joint Laboratory of Electron Microscopy and Microanalysis, of the Masaryk University, Brno, and the Czech Geological survey and scanning electron microscope TESCAN Vega with energy-dispersive spectrometer X-MAX 50 (silicon drift detector, SDD) from Oxford Instruments controlled by the INCA software at the Institute of Petrology and Structural Geology, Charles University in Prague. On both instruments, the analyses were obtained with an accelerating potential of 15 kV and a beam current of 1 nA for the TESCAN Vega and a beam current of 20 nA for the Cameca SX100. The precision control was held by repeated measurements of known phases, mainly standards.

2.3 P-T ESTIMATES

To obtain P-T estimates from the samples, P–T pseudosections and compositional isopleths were calculated using the thermodynamic modelling software Perple_X version 6.6.8 (Connolly, 2005) and THERMOCALC version 3.33 (Powell and Holland, 1988).

2.4 DETRITAL ZIRCON U-PB DATING

About 5 kg of fresh rock of each of 8 selected samples were collected in the Ochtiná Zone and in the Veitsch Nappe. The samples were crushed and zircon grains were separated using conventional methods such as magnetic and heavy liquid separations at the Czech Geological Survey in Prague.

The zircon concentrates were after that handpicked under a binocular microscope for morphological types and selected grains were mounted in epoxy discs, grounded and finally polished (see fig. 7). The internal zircon structure and zoning patterns in individual grains were checked by cathodoluminescence (CL) imaging using CAMECA SX-100 electron microprobe equipped with a MonoCL3 CL spectrometer at the Institute of Petrology and Structural Geology, Charles University in Prague.

***Fig.** 7: The final mounts of 8 selected samples before coating.*

The U-Pb dating of zircons from four samples (NN142, R40, GG89, GG141) was performed using an ArF excimer 193 nm laser ablation system (Resolution M-50) coupled with a Nu Plasma HR MC-ICP-MS at the Department of Earth Sciences of the University of Hong Kong, following the analytical procedure described by Xia et al. (2011). Most analyses were performed with a beam diameter of 40 μm, 5 Hz repetition rate and energy of ~ 5 J/cm^2 per pulse. Zircon standard 91500 was used for calibration. The mass fractionation correction and isotopic results were calculated by ICPMSDataCal (version 7.0, Liu Y et al. 2008). The age calculations and concordia plots were done using Isoplot (Ludwig 2008) and IsoplotR (Vermeesch, 2018). Individual analyses are presented with 1σ error in the data table and in concordia diagrams, and uncertainties in mean age calculations are quoted at the 95% level (2σ).

Two samples (TU5, GG69) were analyzed performed by using an AnalyteExcite 193 nmexcimer laser-ablation system(LA; ProtonMachines), equipped with a two-volume HelEx ablation cell, in tandem with an Agilent 7900x ICPMS (Agilent Technologies Inc., Santa Clara,

USA) at the Czech Geological Survey in Prague. Samples were ablated in He atmosphere (0.8 l min−1) at a pulse repetition rate of 5 Hz using a spot size of 25 μm and laser fluence of 7.59 J/cm^2. Each measurement consisted of 20 s of blank acquisition followed by ablation of the sample for further 40 s of signal collection at masses ^{202}Hg, ^{204}Pb, ^{206}Pb, ^{207}Pb, ^{208}Pb, ^{232}Th and ^{238}U using the SEM detector, with one point per mass peak and the respective dwell times of 10, 10, 15, 30, 20, 10 and 15 ms per mass (total sweep time of 0.134 s). Instrumental drift was monitored by repeat measurements of 91500 reference zircon (Wiedenbeck et al., 1995) after every 20 unknowns. Data reduction using Iolite software followed the method described by Paton et al. (2010), including an 'on peak' gas blank subtraction followed by correction for laser-induced elemental fractionation (LIEF) by comparison with the behaviour of the 91500 reference zircon (Wiedenbeck et al., 1995). The concordia age for reference materials has been calculated by Isoplot (Ludwig, 2008). For primary reference material 91500, a zircon age of 1063 ±2Ma for the TU5 sample was obtained and 1062,9 ±2.1 Ma for the GG69. No common Pb correction was applied as useful data could not be obtained for 204Pb due to the high level of isobaric Hg interferences derived from the carrier gases. In addition zircon reference samples GJ-1 (~609 Ma, Jackson et al., 2004) and Plešovice (~337Ma, Sláma et al., 2008) were analyzed periodically during this study and yielded concordia ages of 607.6 ± 1.3 Ma (TU5 and 337.15 ±0.89 for GG69) and 337.4 ± 0.93 Ma (2σ), respectively (TU5 and 606.4 ±2.2 for GG69).

3. THE GEMER-VEPOR CONTACT ZONE (GVCZ) – REPEATED SLIP ALONG A MAJOR DECOUPLING HORIZON BETWEEN CRUSTAL-SCALE NAPPES

A mélange is defined as a rock body containing exotic blocks without internal strata continuity. Mélanges can form in different geological environments. Recently, six main categories of mélanges were distinguished, based on the process and geodynamic context of their formation (Festa et al., 2010 and references therein) and classified into those related to extensional tectonics, passive margin evolution, strike-slip tectonics, subduction zones, collisional tectonics, and intracontinental deformation.

The Ochtiná Unit is located along the boundary between the Gemer and Vepor Units (Central Western Carpathians, Slovakia), in the ENE-WSW-trending so-called Gemer-Vepor Contact Zone. It comprises Carboniferous syn- to late-orogenic sediments, which deposited in a narrow orogenic foredeep basin described as the Nötsch-Veitsch-Szabadbattyán-Ochtiná Zone (Neubauer and Vozárová, 1990). The Ochtiná Unit has its counterpart in the Eastern Alps represented by the so-called Veitsch nappe (Neubauer and Vozárová, 1990). The Ochtiná Unit consists of a complex lithological assemblage with large amount of meter- to hectometer-sized blocks embedded in a dark flysch-like phyllite matrix. Blocks consist of amphibolite, serpentinite, magnesite and Visean to Serpukhovian limestone (Kozur et al., 1976), as well as chloritoid schists and the actinolite-chlorite schists. This complex block-in-matrix assemblage, characterized by the mixing of polymictic blocks of exotic nature with respect to the matrix, closely resemble a tectonic mélange formed at deep structural levels (Festa et al., 2010 and references therein), associated with the Gemer and Vepor nappes stacking. The goal of this study is to test this hypothesis.

In this chapter we focus on the characterization of a complex lithological assemblage present in the Ochtiná Unit see fig. 8 for sample location. We provide geochemical data to characterize the sedimentary origin of the dominant phyllites in this complex. Furthermore, detailed petrological analysis of amphibolites and chloritoid schists from lenticular blocks enclosed in phyllite points out contrasting pressure–temperature (P–T) evolution possibly related to tectonic mixing of mutually incompatible rocks from different tectonic units. The structural record in the Ochtiná Unit identifies this zone as one of the major Eo-Alpine thrust and detachment zones in the Western Carpathians.

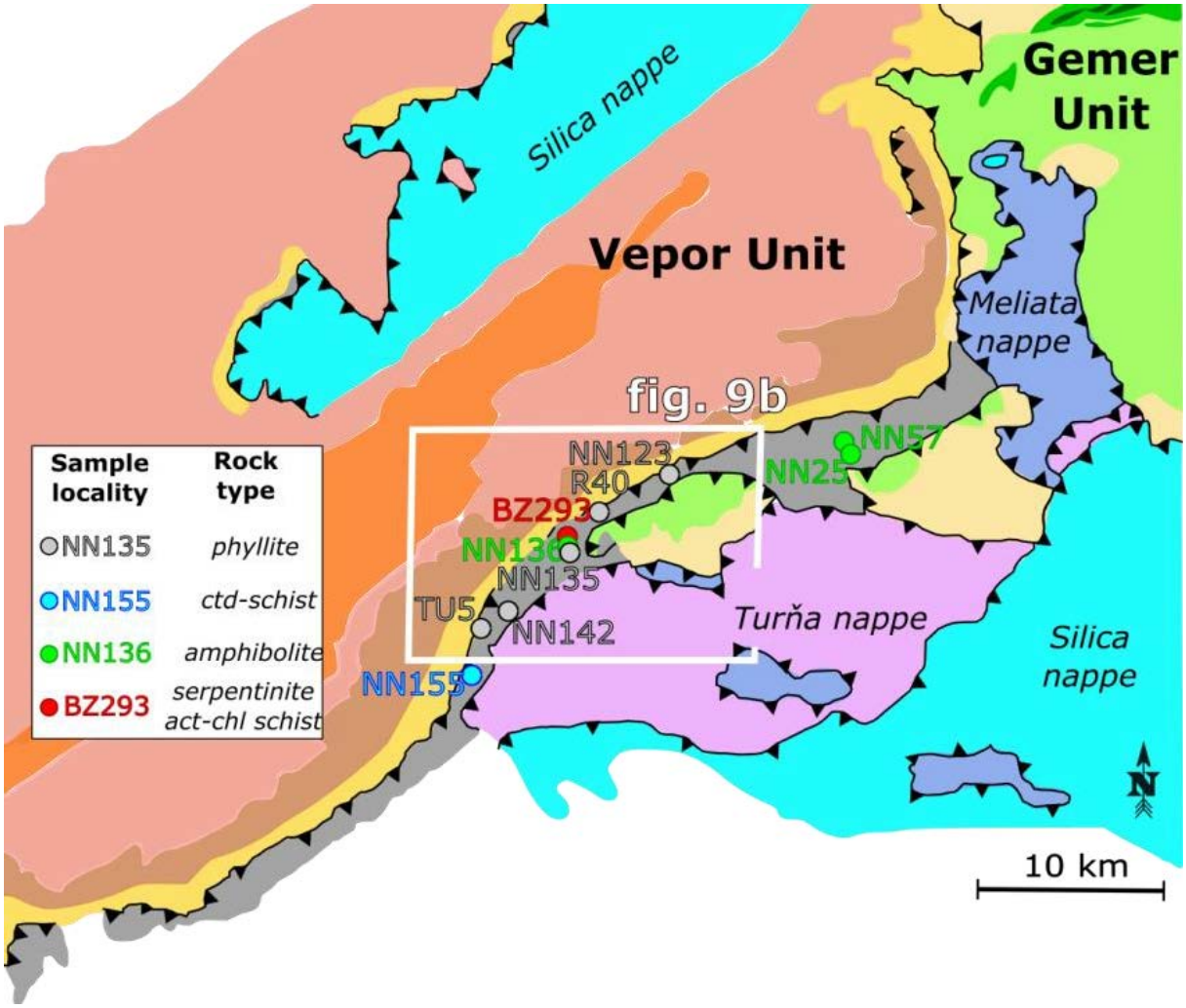

Fig. 8: *Lithotectonic map of the Gemer–Vepor Contact Zone and surrounding units with location of studied samples. Inset corresponds to Fig.9b. Map based on the geological map of the Slovak Republic, 1:50 000* http://mapserver.geology.sk.

3.1 STRUCTURAL RECORD IN THE GEMER-VEPOR CONTACT ZONE

Four major deformation fabrics were distinguished in the Gemer-Vepor Contact Zone: (i) heterogeneously preserved Variscan metamorphic fabric S_V, (ii) main Alpine deformational fabric S_{A1}, and (iii) and (iv) heterogeneously developed Alpine fabrics S_{A2} and S_{A3} (Fig.9). The three Alpine fabrics document the polyphase Cretaceous evolution of the studied area. In the studied area, the Gemer-Vepor Contact Zone is marked by nearly 45° change in trend of the dominant lithological belts (Fig. 9b), from ENE-WSW in the NE to NNE-SSW in the SW. For this reason, individual deformation structures in figure 9a are shown separately for the domains marked by ENE-WSW trend (solid symbols), and NNE-SSW trend (open symbols), respectively.

In the Vepor basement schists, the Variscan metamorphic foliation S_V comprises garnet-biotite-plagioclase-muscovite-quartz (Fig. 11a) and it is mainly preserved in the north, close to the contact with the leucogranite (Fig. 9, 10), which intrudes the schists and forms numerous dykes crosscutting the S_V fabric. The S_V fabric in this region is generally SE-dipping at various angles due to the subsequent Alpine deformation overprint (Fig. 9a, 10). Both the schists and the leucogranite are overprinted by the first Alpine metamorphic fabric S_{A1} comprising grossular-rich garnet, biotite, albite, epidote, white mica and quartz (Fig. 11a).

The heterogeneous development of the S_{A1} fabric in the leucogranite and the neighbouring schists contrasts with its pervasive development and the associated complete obliteration of the Variscan foliation S_V by the S_{A1} cleavage towards the SE (Fig. 10). Further to the SE, in the vicinity of the Permian Vepor cover, the S_{A1} fabric is isoclinally folded and overprinted by a lower grade muscovite- and chlorite-bearing second Alpine cleavage S_{A2} (Fig. 10 and 11b). Here the S_{A1} and S_{A2} cleavages are subparallel and generally SE-dipping (Fig. 9a, 10). Both fabrics bear a mineral and stretching lineation defined by the shape of mica and quartz aggregates.

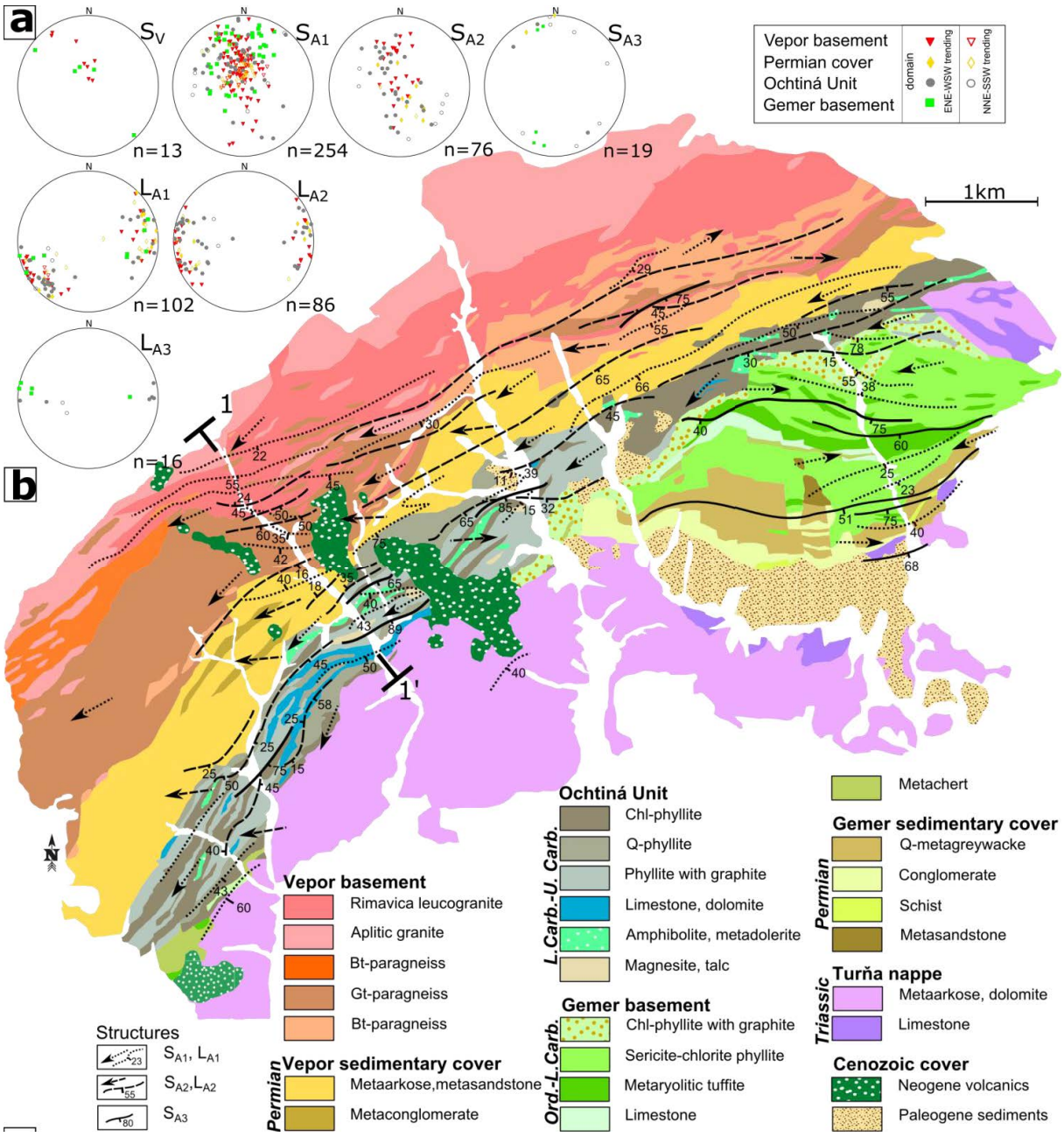

Fig. 9: *(**a**) Pole figures (lower hemisphere, equal-area Schmidt projection) of documented deformation structures. For the structural measurements, solid symbols correspond to the ENE–WSW-trending part of the belt and open symbols to the NNE–SSW-trending part. (**b**) Detailed lithological and structural map of the selected area in the Gemer–Vepor Contact Zone (see Fig. 8 for location). Map based on the geological map of the Slovak Republic, 1:50 000 http://mapserver.geology.sk.*

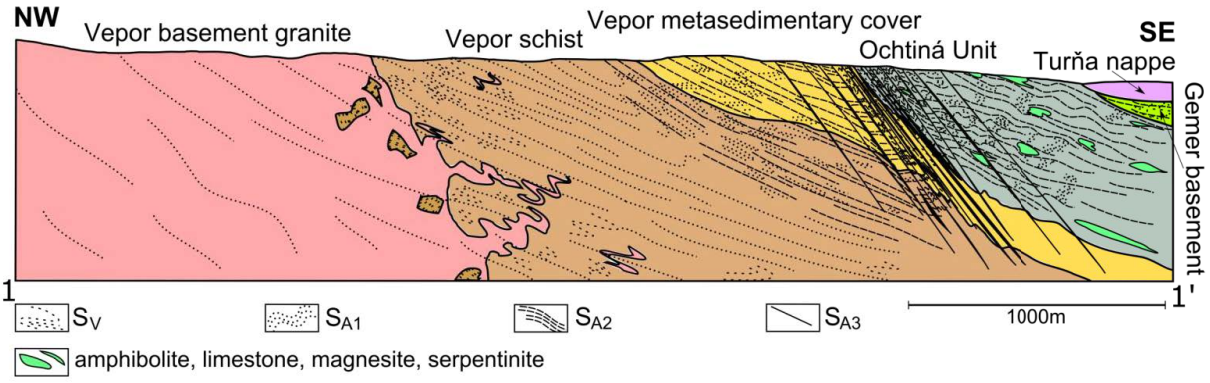

Fig. 10: *Detailed NW–SE trending geological–structural cross section across the Gemer–Vepor Contact Zone. Profile trace is indicated on Fig. 9b.*

The Veporic Permian cover shows two deformation fabrics S_{A1} and S_{A2} associated with distinct metamorphic grade marked by higher grade chloritoid-kyanite and lower grade chlorite-muscovite assemblages in the schist as well as distinct quartz deformation microstructures in the meta-arkose (Bukovská et al., 2013). The superposition of the two fabrics leads to the common development of S-C-type geometries (Fig. 11c). Towards the southern contact with the hanging wall Ochtiná Unit, the S_{A1} and S_{A2} cleavages become locally overprinted by kink bands and open folds F3 with generally ENE-WSW trending axial planes S_{A3} (Fig. 9a).

The phyllites of the Ochtiná Unit show a complex polyphase deformation with relics of the higher-grade fabric S_{A1} being mostly obliterated by the lower-grade muscovite-chlorite bearing S_{A2} cleavage (Figs. 10, 11d, 12a), and subsequent F3 folding associated with local development of very low-grade cleavage S_{A3} (Fig. 12b). F3 folds have subhorizontal axes and their axial planes, parallel to the S_{A3} cleavage, are steep and generally ENE-WSW trending (Fig. 9b, 10 and 12b).

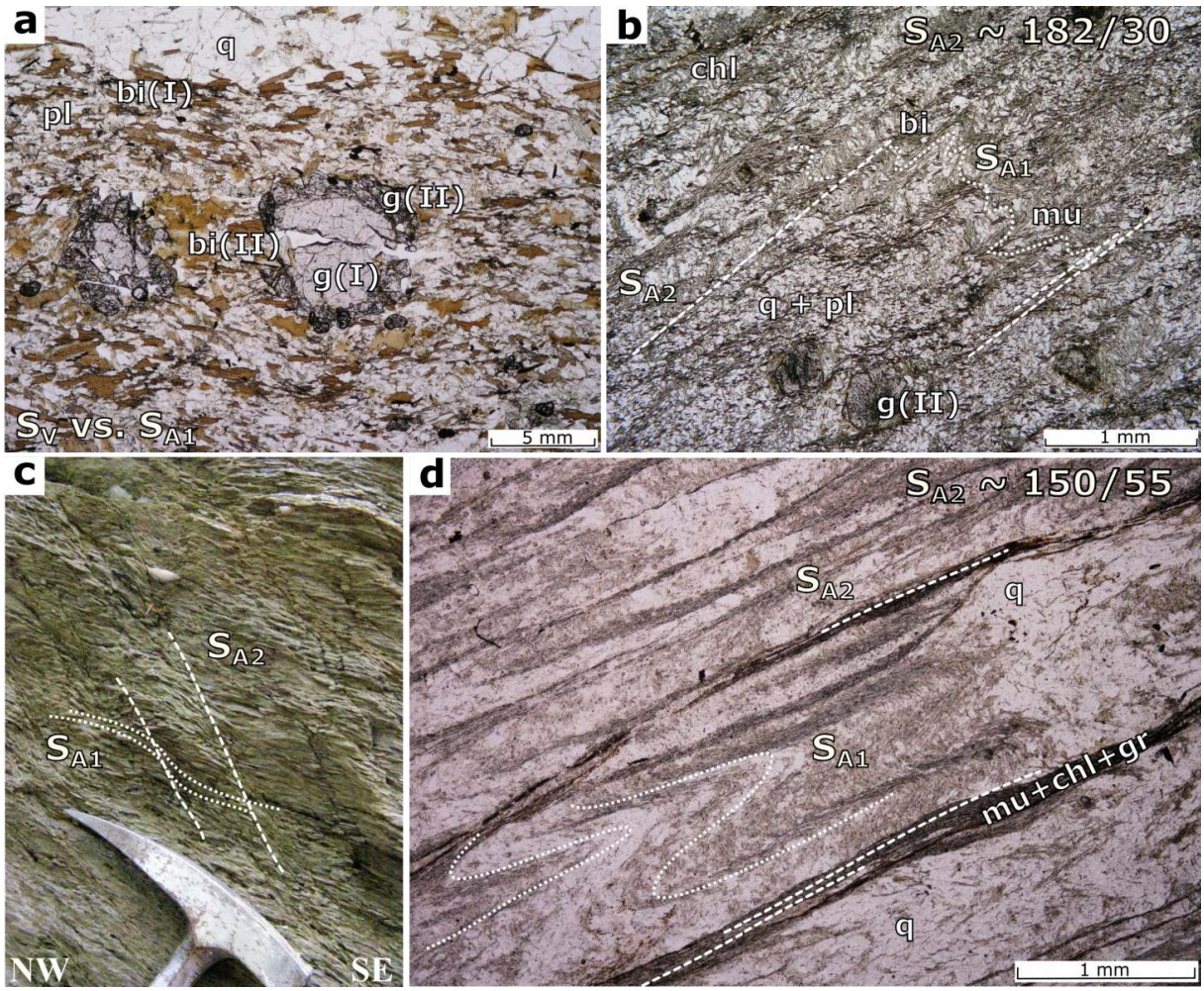

Fig. 11: *(**a**) Micrograph of the Vepor basement schist showing the relationship between the S_V assemblage represented by relic cores of garnets, biotite porphyroblasts and plagioclase being overprinted by S_{A1} fabric represented by garnet rims, biotite(II), albite, epidote and white mica (locality: Blh-Krokávka). (**b**) Micrograph of the Vepor basement schist with the relationship between S_{A1} and S_{A2} fabrics. S_{A1} is associated with newly formed garnet(II). Muscovite- and chlorite-bearing cleavage S_{A2} subsequently folds and overprints S_{A1} (locality: Krokávka, S_{A2} ~182/30). (**c**) Field photograph from the Vepor metasedimentary cover with the higher grade fabric S_{A1} being overprinted by the lower grade cleavage S_{A2} (locality: Hanková–Klihov). (**d**) Micrograph of the Ochtiná Unit phyllite showing overprint of the S_{A1} fabric-represented mainly by the distinct quartz microstructure by the lower grade cleavage S_{A2} represented by muscovite, chlorite and graphite (locality: Nižná Burda, S_{A2} ~150/55). Mineral abbreviations are after Holland and Powell (1998).*

In all the above-described lithologies, the S_{A1} and S_{A2} fabrics are subparallel and their poles are distributed along broad girdles related to the development of the F3 folds (Fig. 9a). In places where the main lithological belts are WSW-ENE-trending (Figs. 8 and 9b), the girdles are oriented NNW-SSE, whereas where the belts are NNE-SSW-trending, the girdles are oriented WNW-ESE (cf. solid and open symbols in Fig. 9a). Accordingly such change in orientation also applies to the intersections of S_{A1} and S_{A2} showing parallel orientation to the trend of the belts. In contrast, lineations L_{A1} and L_{A2} do not change their orientation with changing trend of the foliations. L_{A1} is oriented WSW-ENE to SW-NE whereas L_{A2} is roughly E-W trending (Fig. 9a). This suggests that the changes in trends of the lithological belts and S_{A1} and S_{A2} fabrics do not result from subsequent folding but more likely reflect the shape of the underlying Vepor basement.

The Gemer basement in the studied area shows relics of Variscan metamorphic fabric S_V (Fig. 9a), which are nearly completely obliterated by the lower grade muscovite- and chlorite-bearing cleavage S_{A1}. This S_{A1} cleavage generally dips to the south at variable angles ranging from steep to shallow. S_{A1} cleavage in the Permian conglomerates of the Gemer cover is steep and E-W trending, and overprints subhorizontal bedding. In contrast to the Vepor Unit, S_{A2} cleavage was not identified in the studied portion of the Gemer Unit. Orientations of both S_V and S_{A1} fabrics in the Gemer Unit were subsequently modified by larger scale folds F3 with steep, generally E-W trending axial planes and subhorizontal axes (Fig. 9a). Also, several localized transpressional zones associated with left-lateral movements develop within the Vepor and Gemer basements.

The blocks of heteregeneous lithologies found in the Ochtiná Unit have in general elongated, lenticular shape with long axes parallel to main foliations S_{A1} and S_{A2} as well as to locally developed S_{A3}. Although the size of these blocks varies, both the small meter-sized blocks as well as large (up to several hundred meters) blocks are wrapped by the phyllite matrix. Due to the limited number of outcrops, the extent of the larger blocks is only documented by geological mapping. Because it is not clear from the field observations which of the fabrics is responsible for incorporation of the blocks into phyllite matrix a detailed petrographic-petrological study had been carried out.

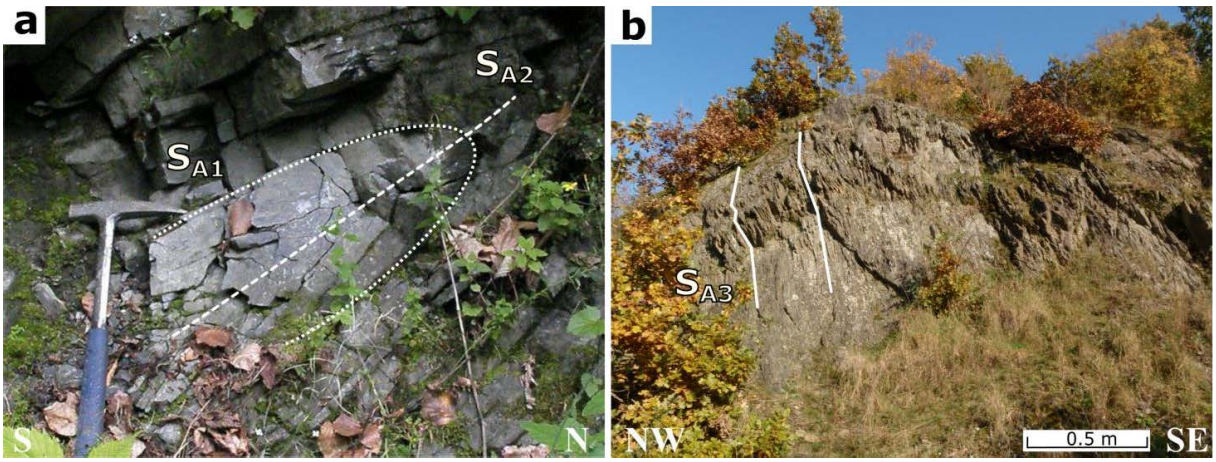

Fig. 12: *(**a**) Field photograph from the Ochtiná Unit with S_{A1} fabric being folded in association with the S_{A2} cleavage development (locality: Ploské–Ratková). (**b**) Steep S_{A3} cleavage developed due to the Trans-Gemer Shear Zone formation in the Ochtiná Unit (locality: Hrančiarská ves).*

3.2 LITHOLOGICAL CHARACTERIZATION OF THE OCHTINÁ UNIT

In order to understand the tectonic evolution of the Ochtiná Unit, the petrologically most informative lithologies were sampled and analysed to check the supposed mélange character of the unit. These include the dominant phyllites, as well as chloritoid schists, amphibolites, serpentinites and actinolite schists sampled from the lenticular blocks (Fig. 8). Because very little is known about the primary depositional environment of the phyllites of the Ochtiná Unit, five samples were collected for geochemical characterization of these rocks (Fig. 8, Tab. 2).

Sample	NN 123	NN 135	NN 142	R 40	TU 5	NN 155	UCC	Sample	NN 123	NN 135	NN 142	R 40	TU 5	NN 155	UCC
SiO_2	51.16	69.83	65.19	71.30	58.58	66.95	66.60	Y	23.8	13.5	27.4	27.9	32.7	40	21
Al_2O_3	14.24	13.54	22.20	13.62	21.35	16.95	15.40	La	26.1	17.1	31.9	38.5	40.5		31
Fe_2O_3	7.98	5.10	2.27	2.21	6.52	8.27	5.40	Ce	55.6	33.2	79.7	78.8	78.8		63
MgO	5.06	2.21	0.35	0.68	1.49	1.34	2.48	Pr	6.47	3.59	8.44	8.78	10.92		7.1
CaO	7.10	0.17	0.07	2.07	0.19	0.04	3.59	Nd	23.9	12.2	27.9	31	40.5		27
Na_2O	2.61	2.44	2.06	2.04	0.91	0.62	3.27	Sm	4.95	2.31	5.48	5.75	8.03		4.7

Sample	NN 123	NN 135	NN 142	R 40	TU 5	NN 155	UCC	Sample	NN 123	NN 135	NN 142	R 40	TU 5	NN 155	UCC
K_2O	1.24	2.28	3.34	4.23	4.10	1.50	2.80	Eu	1.30	0.55	1.20	1.03	1.74		1
TiO_2	1.42	0.63	0.73	0.26	0.97	0.90	0.64	Gd	4.80	2.24	5.13	5.28	7.31		4
P_2O_5	0.29	0.12	0.02	0.06	0.07	0.06	0.15	Tb	0.76	0.38	0.80	0.83	1.08		0.7
MnO	0.14	0.04	0.03	0.05	0.04	0.06	0.10	Dy	4.20	2.51	4.83	4.80	6.06		3.9
Cr_2O_3	0.04	0.01	0.02	0.01	0.02	0.02		Ho	0.85	0.51	1.04	1.02	1.21		0.83
								Er	2.59	1.68	2.86	2.99	3.74		2.3
Ni	120	<20	32	22	41	63	47	Tm	0.37	0.22	0.46	0.42	0.52		0.3
Sc	20	10	15	7	21	17	14	Yb	2.20	1.48	3.17	2.82	3.65		2
Ba	349	619	810	519	720	439	628	Lu	0.34	0.26	0.50	0.44	0.52		0.31
Be	3	3	6	6	12			Cr							92
Co	29.4	6.1	9.1	4.8	10.2			Mo	0.5	0.3	0.2	0.2	0.4		
Cs	1.1	2.3	6.5	3	5.7		4.9	Cu	50.3	22.1	11.4	4.1	32.9		28
Ga	16	14.5	23.6	14.8	23		17.5	Pb	3.4	2.4	3.6	2.2	3.2		17
Hf	4.4	5.6	5.4	2.9	5.6		5.3	Zn	61	50	19	4	70		67
Nb	21.2	9.7	14.7	9.5	13.8	11	12	Ni	103.8	19.7	12.7	7.1	39.5		
Rb	31.8	67.7	143.4	120.8	162.1		82	As	15.8	43.6	14.3	2.8	29.8		
Sn	2	2	4	2	3			Cd	0.1	<0.1	<0.1	<0.1	<0.1		
Sr	223.9	39.4	260.8	25.3	114.3	68	320	Sb	0.2	0.4	<0.1	0.3	0.4		
Ta	1.3	0.7	1.2	0.9	1.1		0.9	Bi	<0.1	<0.1	0.5	<0.1	0.6		
Th	5.9	9.3	14.8	14.8	15		10.5	Ag	<0.1	<0.1	<0.1	<0.1	<0.1		
U	1.8	2	2.9	2.6	5.8		2.7	Au	3.2	<0.5	35.6	<0.5	3.6		
V	174	80	64	31	126		97	Hg	<0.01	0.01	<0.01	0.01	0.02		
W	0.7	0.9	1.9	2.2	2.3			Tl	<0.1	<0.1	<0.1	<0.1	0.1		
Zr	170.1	223	188.9	116.1	220.9	325	193	Se	<0.5	<0.5	<0.5	<0.5	<0.5		

Tab. 2: *Whole rock analyses of phyllite, chloritoid schist and amphibolite from the Ochtiná Nappe. Values are of oxides are given in wt. %, of elements in ppm.*

3.2.1 PHYLLITES

The phyllites are the dominant lithology of the Ochtiná Unit. They have a well developed slaty cleavage S_{A1} with local overprint by cleavage S_{A2} (Fig. 11d). The slaty cleavage S_{A1} is marked by the preferred orientation of fine-grained white mica and chlorite and locally graphite. The foliation is anastomosing around stronger domains of quartz or larger crystals of mica. Calcite, tourmaline, plagioclase, hematite, ilmenite, rutile, zircon and monazite are locally present. The size of the crystals ranges from 0.1 mm to 0.5 mm.

Based on the whole rock analyses, the studied phyllites show a relatively wide compositional range (Tab. 2). The SiO_2/Al_2O_3 index, used to characterize the sedimentary maturation, ranges from 2.7 to 5.2 – close to values characteristic for igneous source rocks (Roser et al., 1996). On the other hand, the rather diverse character of the studied phyllites may indicate both basic (SiO_2/Al_2O_3 = 2.7-3.6, samples NN123, NN142 and TU5) and acidic source rocks (SiO_2/Al_2O_3 ~ 5.2, samples NN135 and R40), and/or sedimentary maturation in the latter case.

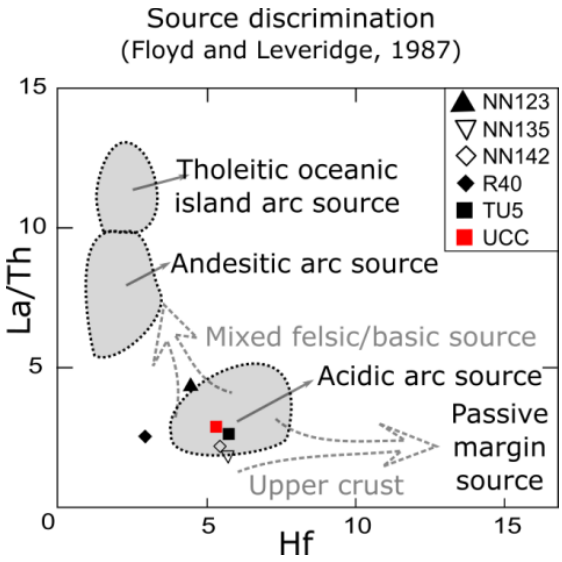

Fig. 13: *Source rock and tectonic setting discrimination diagrams for the phyllites from Ochtiná Nappe, the UCC (Upper Continental Crust after Rudnick and Gao, 2003) standard is plotted for comparism: La/Th vs. Hf diagram (after Floyd and Leveridge, 1987), indicating mixing of felsic and intermediate sources with minor influence of an old sediment component.*

Compared to the Upper Continental Crust standard (UCC after Rudnick and Gao, 2003, Tab. 2), the phyllites are depleted in Na_2O and CaO – except for sample NN123 (Tab. 2) characterized by high calcite and apatite contents. The transition elements, large ion litophile (LIL), high field strength (HFS) and rare earth elements (REE) show values comparable to the UCC. To discuss the tectonic setting and the source rocks for the sedimentary protolith of the phyllites, the discrimination diagrams of Floyd and Leveridge (1987) and Bhatia and Crook (1986) were used. In the diagram La/Th vs. Hf , the analyzed samples show proximity to the acidic arc source field (Fig. 13).

In the Ti/Zr vs. La/Sc and La-Th-Sc-Zr/10 diagrams (Fig. 14), most phyllite samples exhibit an affinity to continental arc source. An exception is sample NN123, which differs significantly from the rest of studied samples (see Table 2) and indicates an island arc affinity (Fig. 14).

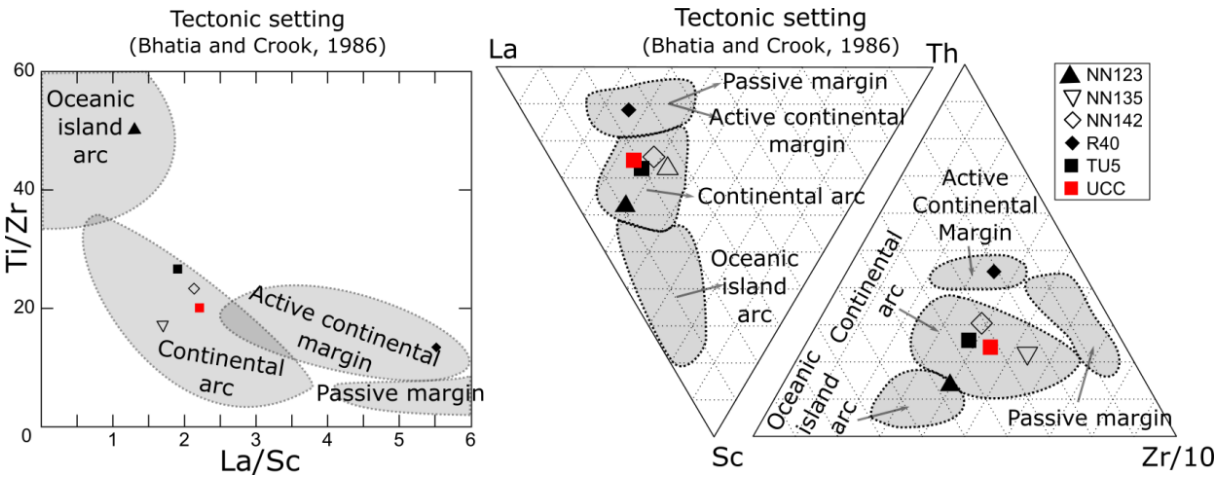

Fig. 14: *Source rock and tectonic setting discrimination diagrams for the phyllites from Ochtiná Nappe, the UCC (Upper Continental Crust after Rudnick and Gao, 2003) standard is plotted for comparism. Left: Ti/Zr vs La/Sc diagram (after Bhatia and Crook, 1986), right: triangular trace element tectonic discrimination diagram (Bhatia and Crook, 1986).*

3.2.2 CHLORITOID SCHISTS

Chloritoid schists are fine-grained quartz- and white mica-dominated rocks (Fig. 15, 16, 17). They display a compositional layering with layers rich in chloritoid and white mica and layers rich in chlorite and quartz. Layering is parallel to a foliation defined by the preferred orientation of muscovite (Si = 3.04-3.07 a.p.f.u, X_{Na}= $Na_2O/(Na_2O+K_2O)$ = 0.13-0.15, Fig. 15). Deformed porphyroclasts of muscovite (up to 0.5 mm) wrapped by the foliation are locally present. Paragonite (X_{Na} = 0.74-0.85, X_{Ca} = 0-0.2) occurs locally in close association with chloritoid and it commonly intergrows with muscovite (Fig. 17).

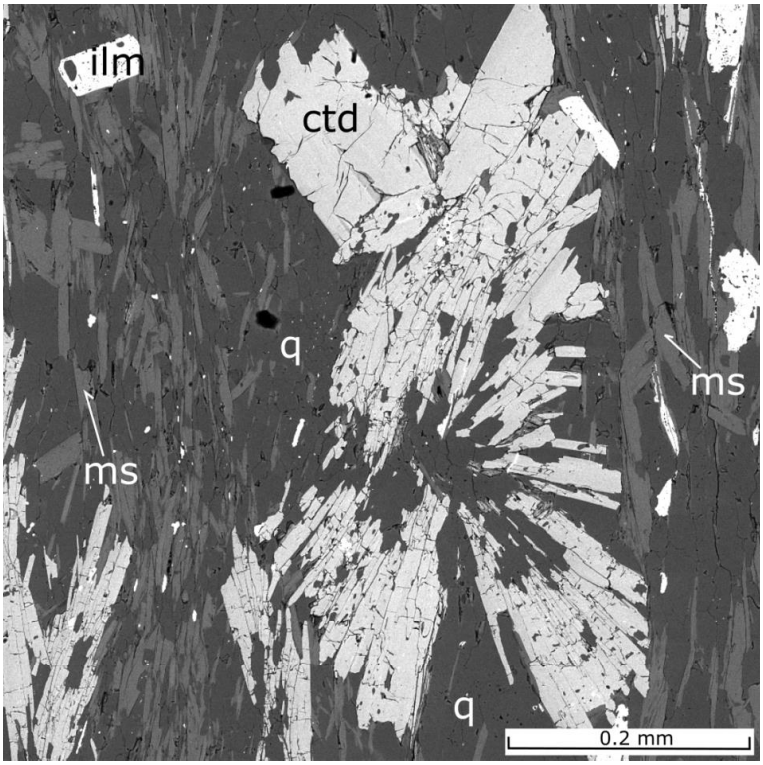

Fig. 15: *Back Scattered Electron (BSE) image from chloritoid schist sample NN155 - radial chloritoid spherulites. Mineral abbreviations are after Holland and Powell (1998).*

Recrystallized quartz aggregates (up to 1 mm) stretched parallel to and wrapped by the foliation are common. Chloritoid (X_{Mg} = $Mg/(Fe^{2+}+Mg)$ = 0.14-0.15) forms euhedral prismatic unzoned porphyroblasts (up to 0.3 mm, Fig. 15 and 17), commonly associated into radial aggregates up to 1 mm in size (Fig. 15). Aggregates and individual crystals are typically wrapped by the foliation, but crystals parallel to the foliation are also common. Ilmenite, rutile and quartz form inclusions in chloritoid (Fig. 17).

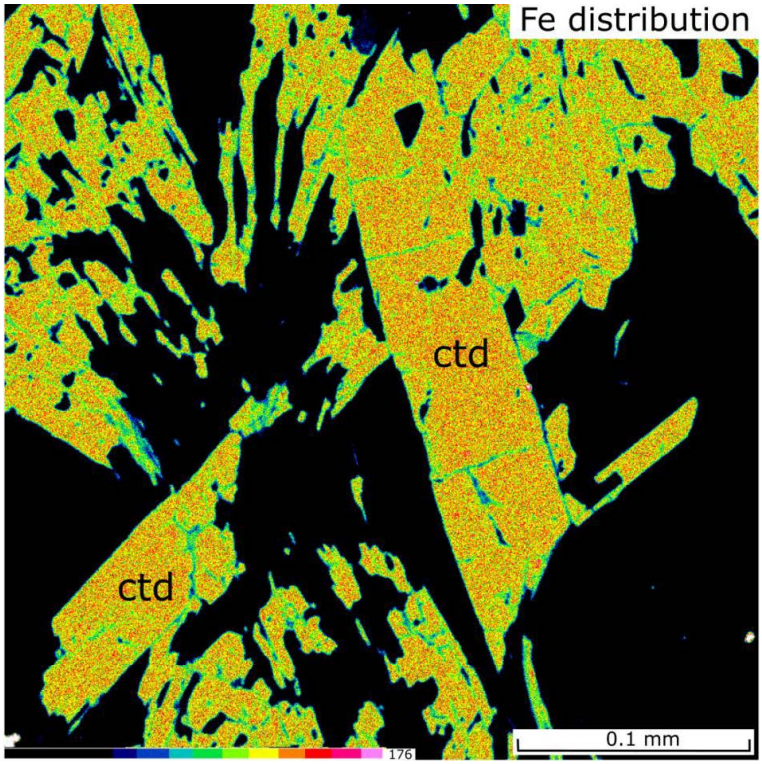

Fig. 16: *BSE image from chloritoid shist sample NN155 - element distribution map of iron demonstrating lack of chemical zoning in chloritoid. Mineral abbreviations are after Holland and Powell (1998).*

Chlorite (X_{Mg} = 0.36-0.40) forms flakes (≈0.5 mm) parallel to the foliation. Chlorite is very rare in the chloritoid-rich layers and vice versa. However, around the interface of both types of layers, chloritoid and chlorite coexist in an apparent textural equilibrium. Additionally, the foliation contains subhedral prisms of tourmaline, ilmenite, rutile and locally hematite. Based on the microstructural relations the inferred synfolial equilibrium assemblage comprises chloritoid, chlorite, muscovite, paragonite, rutile, ilmenite, hematite and quartz (for representative mineral analyses see Table 3).

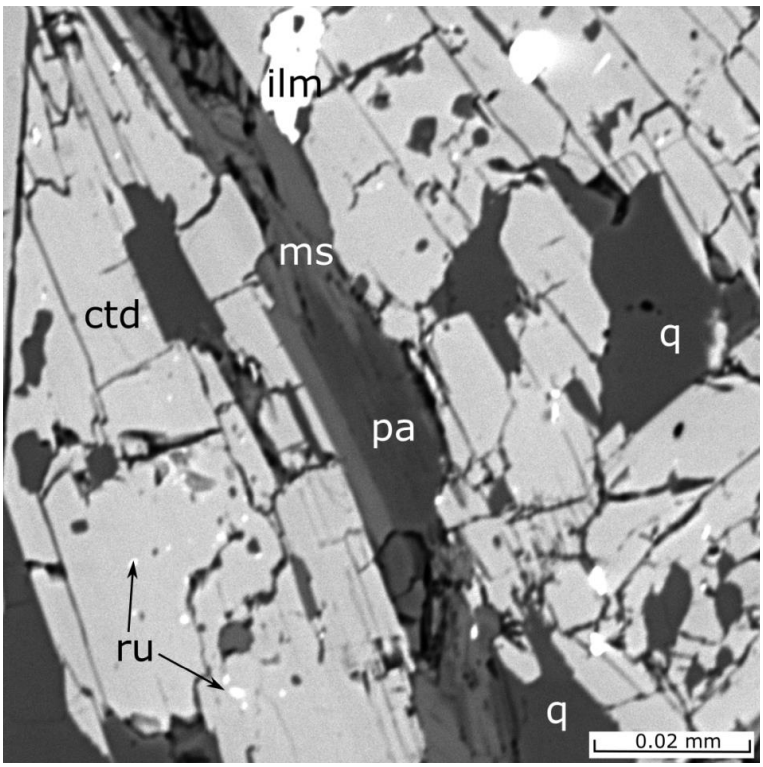

Fig. 17: *BSE image of the sample NN 155 showing the relationship of muscovite and paragonite. Mineral abbreviations are after Holland and Powell (1998).*

3.2.3 AMPHIBOLITES

Amphibolites are homogeneous fine-grained rocks generally lacking preferred orientation and only locally displaying a faint cleavage parallel to discrete micro shear zones (Fig. 18, 19 and 20). They contain porphyroblasts of calcic clinoamphibole (up to 1 mm) and titanite (up to 0.5 mm) in a fine grained matrix, which is composed of epidote, plagioclase, titanite and small amounts of chlorite, clinoamphibole and quartz (Fig. 18, 19 and 20, Tab. 3).

Amphibole porphyroblasts (Fig. 20) contain inclusions of titanite and locally also epidote and have a core of actinolite (Si = 7.5-7.8 p.f.u., $X_{Na} = Na_{M4}/(Na_{M4}+Ca) = 0.002\text{-}0.022$, $X_{Mg} = 0.61\text{-}0.67$, recalculated $Fe^{3+} = 0.02\text{-}0.08$, $XAl_{M2} = (Si+Al-8)/2 = 0.08\text{-}0.14$), rimmed by hornblende s.l. (Si = 6.3-6.9 p.f.u., $X_{Na} = 0.005\text{-}0.027$, $X_{Mg} = 0.45\text{-}0.53$, $XAl_{M2} = 0.37\text{-}0.51$, Fig. 21). However, in some places actinolite and hornblende are intergrown, without clear core-rim relation (Fig. 18).

Titanite porphyroblasts are locally partly recrystallized to smaller titanite crystals. Epidote forms randomly oriented subhedral prims (0.05-0.5 mm) in the matrix (Figs. 18 and 20) and commonly displays oscillatory zoning ($X_{Fe3+} = Fe^{3+}/(Fe^{3+}+Al–2)$ = 0.50-0.70). Matrix plagioclase is albite (up to 5 % anorthite) with locally preserved relict cores of oligoclase (10-15 % of anorthite, Fig. 19). Chlorite (X_{Mg} = 0.50-0.55) is relatively rare in the matrix, but oriented crystals are commonly present in the micro shear zones cross-cutting the sample (Fig. 18).

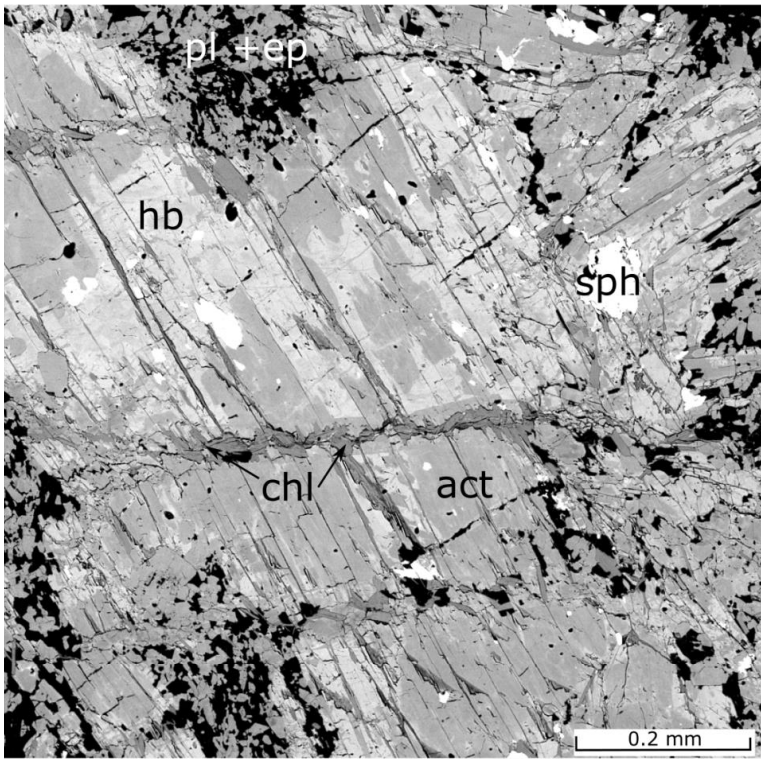

Fig. 18: *BSE image from amphibolite sample NN25- zoned calcic clinoamphiboles, the epidote and plagioclase matrix and the chlorite present in micro shear zones cross-cutting the amphibole porphyroblast. Mineral abbreviations are after Holland and Powell (1998).*

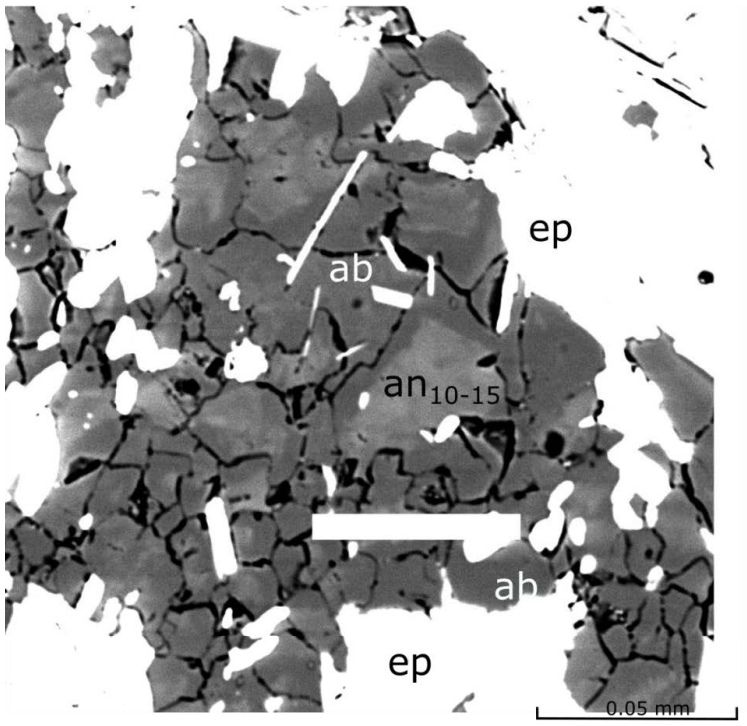

Fig. 19: *BSE image from amphibolite sample NN25- relic oligoclase overgrown by albite. Mineral abbreviations are after Holland and Powell (1998).*

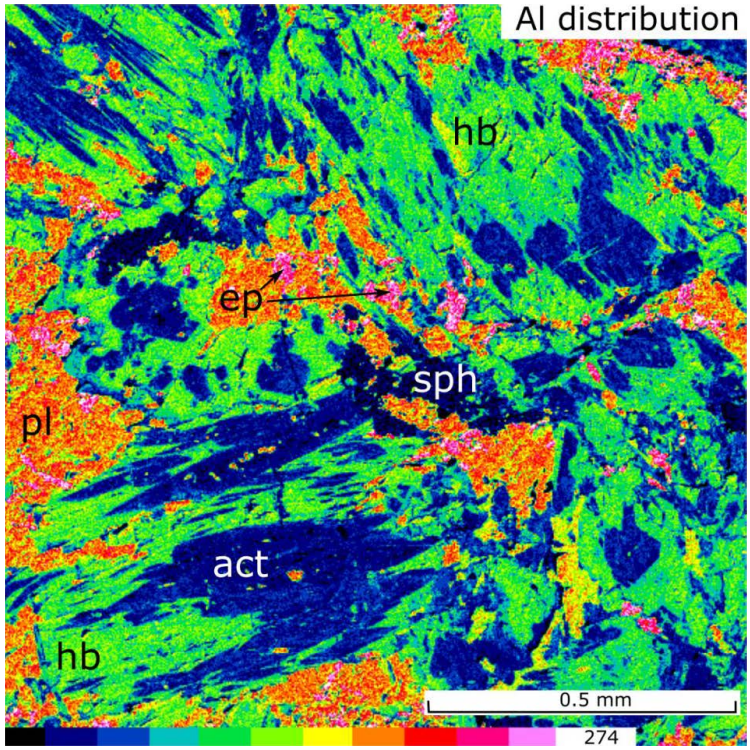

Fig. 20: *BSE image from amphibolite sample NN25- element distribution map of Al showing the amphibole zonation and the cores of actinolite composition rimmed by hornblende. Mineral abbreviations are after Holland and Powell (1998).*

Based on the microstructural relations, we infer that the matrix assemblage albite-epidote±actinolite±chlorite overprints an earlier assemblage that comprised oligoclase, hornblende, titanite ± epidote, ± quartz. It is not clear whether actinolite cores of large porhyroblasts were part of this early equilibrium assemblage. While the intergrowths of actinolite with hornblende are in favour of this interpretation, actinolite cores surrounded by hornblende may point to actinolite being the precursor of hornblende along a prograde P–T evolution. The growth of chlorite in the shear zones is interpreted as a late local feature, possibly related to fluid circulation and could be in association with the matrix assemblage.

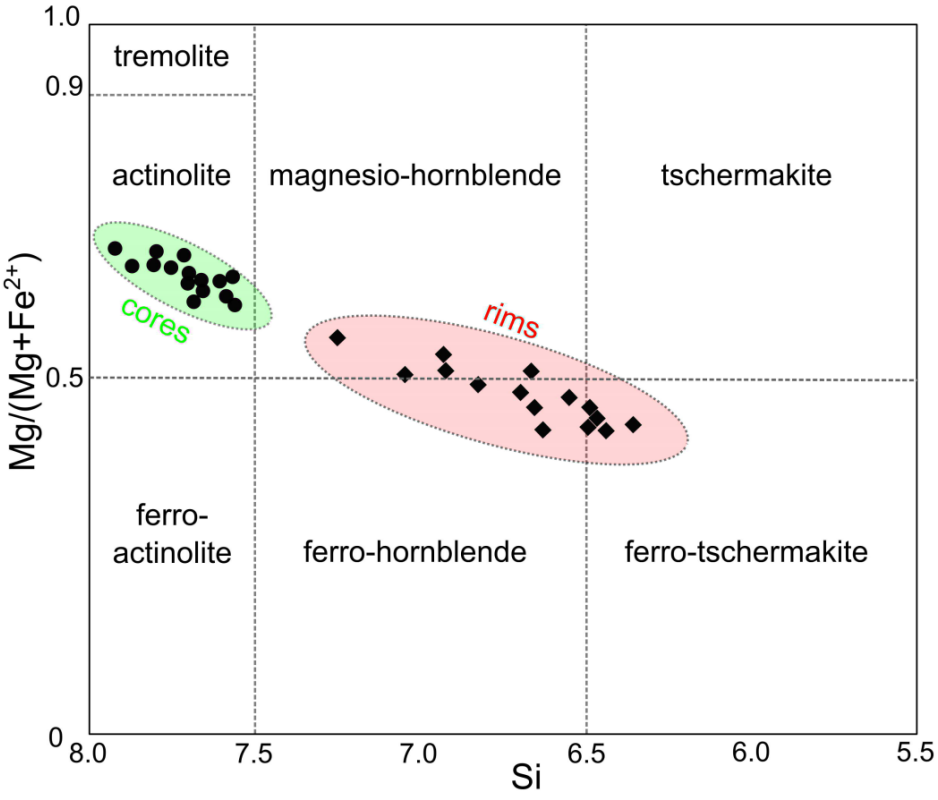

Fig. 21: *Classification diagram for the calcic clinoamphiboles after IMA (International Mineralogical Association, Leake et al., 1997) from the Ochtiná amphibolites samples NN25, NN57 and NN136. For representative analyses of amphibole see Table 3.*

From the whole rock chemical data, the studied amphibolites enclosed within phyllites of the Ochtiná Unit show a restricted compositional range (Table 2). Based on the immobile trace elements, the amphibolites correspond to subalkaline basaltic rocks in the Zr-Ti vs. SiO_2

discrimination diagram (Fig. 22, after Winchester and Floyd, 1977) and indicates transition from N-MORB (mid-ocean ridge basalt) to E-MORB (enriched mid-ocean ridge basalt) in the Th-Hf/3-Ta discrimination diagram (Fig. 23a, after Wood, 1980).

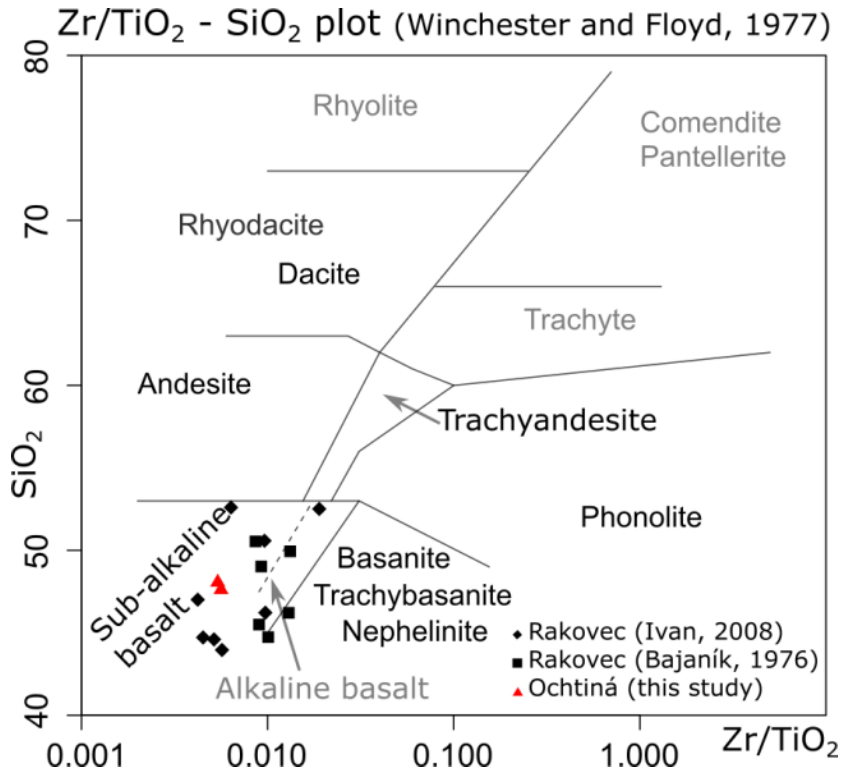

Fig. 22: *Zr-Ti vs. SiO_2 discrimination diagram (after Winchester and Floyd, 1977). The previously published data from amphibolites of the Gemer basement (Bajaník, 1976; Ivan, 2008) are shown for comparison in. The Geochemical Data Toolkit (GCDkit, Janoušek et al., 2006) was used to create these diagrams.*

In the Zr/Y vs. Zr diagram for basic rocks (Fig. 23b, after Pearce and Norry, 1979), the studied samples also correspond to mid-ocean ridge basalts. In all the diagrams in figure 22, 23a, 23b, the Ochtiná amphibolite is compared with the previously published geochemical data from amphibolites of the Gemer basement (Bajaník, 1976; Ivan, 2008), which show similar affinity to the mid-ocean ridge basalts field and indicate a possible correlation between these amphibolites.

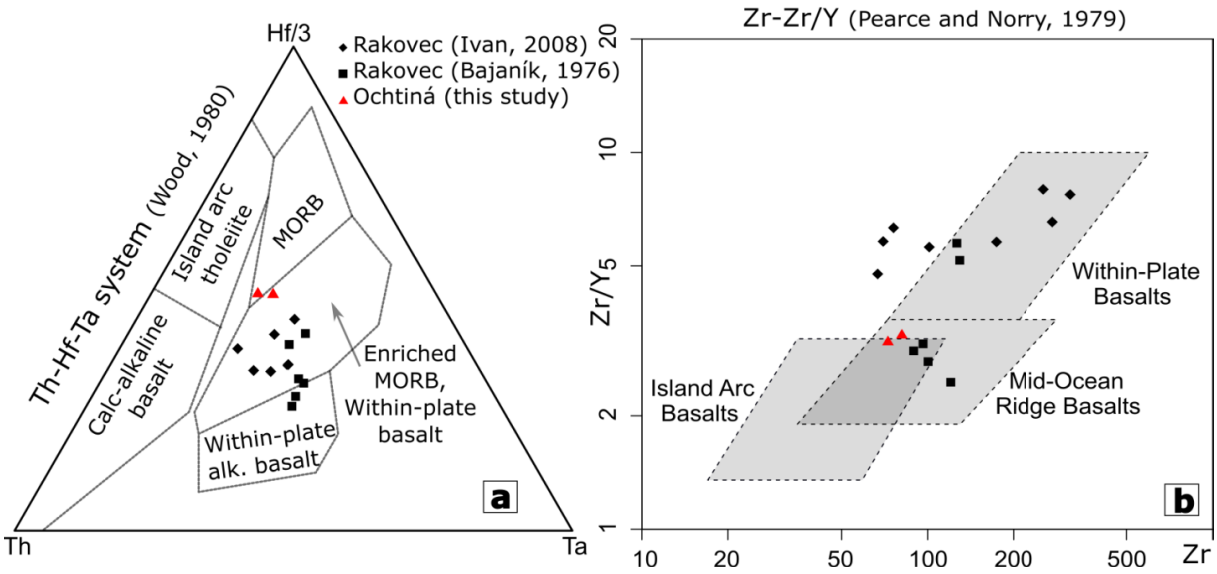

Fig. 23: *(**a**) Classification provided by the Th-Hf/3-Ta discrimination diagram (Wood, 1980). (**b**) Zr/Y vs. Zr diagram for basic rocks (after Pearce and Norry, 1979). The previously published data from amphibolites of the Gemer basement (Bajaník, 1976; Ivan, 2008) are shown for comparison. The Geochemical Data Toolkit (GCDkit, Janoušek et al., 2006) was used to create these diagrams. Abbreviations: MORB= middle ocean ridge basalt.*

3.2.4 SERPENTINITES AND ACTINOLITE-CHLORITE SCHISTS

The serpentinites are dominated by fine grained serpentine and magnetite. Serpentine flakes (<0.1 mm) are randomly oriented and neither the core-and-rim mesh microstructures, nor bastites are observed. Very fine-grained magnetite is concentrated in thin layers that form an anastomosing network and separate lenses (in general 0.2-0.5 mm long) of nearly pure serpentine. Talc and coarser-grained magnetite (up to 0.5 mm) together with subordinate chlorite fill fractures that crosscut the rock (Fig. 24). The serpentine lenses probably represent pseudomorphed crystals of olivine. These rocks are interpreted as former peridotites, although no relics of the original minerals or microstructures were found.

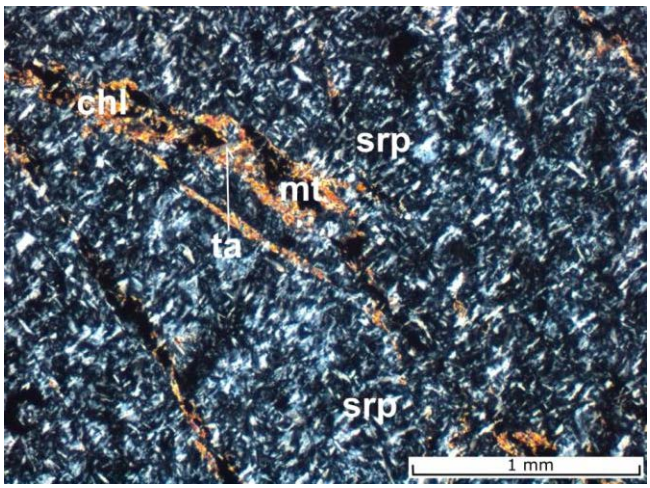

Fig. 24: *Micrograph of the serpentinite, showing the randomly oriented serpentine and the talc, magnetite and chlorite filling the fractures.*

An actinolite-chlorite schist crops out in the vicinity of one of the serpentinite bodies. The schist contains 2-10 mm large domains of recrystallised polycrystalline quartz (0.1-0.3 mm) and domains of oriented, Mg-rich chlorite with numerous tiny grains of titanite, commonly aligned in thin bands. These domains are surrounded by a quartz-chlorite matrix that shows a well developed foliation. The matrix contains thin prismatic crystals of actinolite (up to 1.5 mm long) (Fig. 25), which are in some cases oriented parallel to the foliation, although, in other occurrences they are wrapped by the foliation and show variable orientations. This peculiar schist may be interpreted as a volcano-sedimentary rock containing quartz pebbles in a matrix of rather mafic composition.

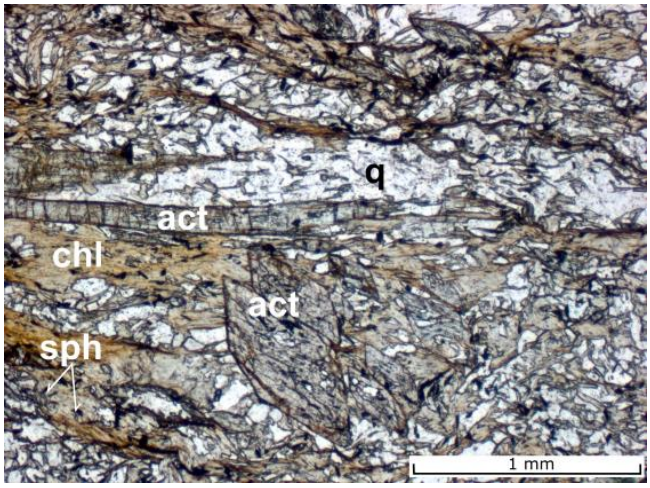

Fig. 25: *Micrograph of the actinolite schist. Prismatic crystals of actinolite which are in some cases parallel to the foliation and in some they show variable orientation.*

	Apmhibolites					Ctd schists			
Analysis	Hb2	Act2	Ab5	Ep5	Chl6	Ctd13	Chl2	Mu11	Mu8
Mineral	**hb**	**act**	**pl**	**ep**	**chl**	**ctd**	**chl**	**mu**	**pa**
wt . %									
SiO_2	42.71	52.56	65.86	37.79	23.81	23.48	23.77	46.48	45.34
TiO_2	0.36	0.06	0.00	0.13	0.00	0.00	0.00	0.17	0.00
Al_2O_3	14.34	3.83	21.44	26.74	40.47	40.44	21.96	36.35	40.00
Cr_2O_3	0.01	0.02	0.00	0.00	0.00	0.00	0.00	0.00	0.00
Fe_2O_3	0.52	0.15	0.00	6.80	1.10	1.92	0.08	0.00	0.00
FeO	16.56	13.98	0.00	1.37	24.16	23.74	30.82	1.44	0.56
MnO	0.24	0.27	0.00	0.13	0.27	0.26	0.27	0.00	0.00
MgO	7.89	13.99	0.00	0.21	2.27	2.28	10.82	0.69	0.00
CaO	11.79	12.82	2.38	23.45	0.00	0.00	0.00	0.00	0.29
Na_2O	1.55	0.46	10.16	0.03	0.00	0.00	0.00	1.31	6.83
K_2O	0.41	0.12	0.10	0.00	0.00	0.00	0.00	8.98	1.20
Totals	**96.38**	**98.26**	**99.95**	**96.64**	**87.18**	**92.07**	**87.72**	**95.42**	**94.21**
Oxygen equivalents	**23**	**23**	**8**	**12.5**	**14**	**6**	**14**	**11**	**11**
Si	6.46	7.59	2.89	3.00	2.68	0.99	2.59	3.07	2.94
Ti	0.04	0.01	0.00	0.01	0.00	0.00	0.00	0.01	0.00
Al	2.56	0.65	1.11	2.50	2.63	1.99	2.82	2,83	3,06
Cr	0.00	0.00	0.00	0.00	0.00	0.00	0.00	0.00	0.00
Fe^{3+}	0.06	0.02	0.00	0.41	0.01	0.03	0.01	0.00	0.00
Fe^{2+}	2.09	1.69	0.00	0.09	2.18	0.84	2.81	0.08	0.03
Mn	0.03	0.03	0.00	0.01	0.03	0.01	0.03	0.00	0.00
Mg	1.78	3.01	0.00	0.03	2.45	0.14	1.76	0.07	0.00
Ca	1.91	1.99	0.11	1.99	0.01	0.00	0.00	0.00	0.02
Na	0.45	0.13	0.87	0.01	0.00	0.00	0.00	0.17	0.86
K	0.08	0.02	0.01	0.00	0.00	0.00	0.00	0.76	0.10
Sum	**15.48**	**15.15**	**4.99**	**8.04**	**9.99**	**4.00**	**10.00**	**6.97**	**7.01**
X_{Mg}	0.46	0.64			0.53	0.14	0.38		
XAl_{M2}	0.51	0.12							
XNa_{A}	0.40	0.12							
XNa_{M4}	0.05	0.01							
X_{Ca}			0.11						
X_{Fe3+}				0.14					
X_{Na}								0.13	0.85

***Tab. 3**: Representative chemical analyses of selected minerals.*

3.3 P-T ESTIMATES

One sample of a chloritoid schist (NN155) and one of an amphibolite (NN25) from two lenses in the Ochtiná Unit were selected for a petrological study based on their suitable mineral assemblage. The use of THERMOCALC (Powell and Holland, 1988) was preferred because it is more reliable in handling the most up-to-date complex solid solutions, like those for amphiboles. However, it appeared impossible to complete the P–T pseudosection for the chloritoid schist with THERMOCALC because of software problems during calculation of equilibria involving muscovite-paragonite and ilmenite-hematite solvi. Thus Perple_X (v. 6.6.8, Connolly, 2005) was used instead for this rock. Nevertheless, the results of the two techniques can be compared, since it has been demonstrated that Perple_X and THERMOCALC yielded identical results when the same thermodynamic dataset was used (Hoschek, 2013, 2004).

3.3.1 CHLORITOID SCHIST

The P-T pseudosection for chloritoid schist sample NN155 was constructed by using Perple_X (Connolly, 2005) v. 6.6.8 and the internally consistent thermodynamic dataset hp04 (Holland and Powell, 1998) in the model system MnO-Na_2O-K_2O-FeO-MgO-Al_2O_3-SiO_2-H_2O-TiO_2-Fe_2O_3 (MnNKFMASHTO). The whole rock composition used to calculate the P-T section is presented in figure 26 and table 2. All CaO (0.04 wt.%) is combined with P_2O_5 to form apatite and therefore CaO component was excluded from the calculation. The amount of O_2 was recalculated from the whole rock composition with respect to the estimated ratio of Fe^{3+}/Fe^{total} 0.05. The mixing models for chloritoid (Holland and Powell, 1998), chlorite (Holland and Powell, 1998), biotite (White et al., 2007), white mica (Auzanneau et al., 2010; Coggon et al., 2002), garnet (White et al., 2000), ilmenite (White et al., 2000) and staurolite (Holland and Powell, 1998) were used. In the resulting P-T pseudosection (Fig. 26), the observed equilibrium assemblage chloritoid, chlorite, muscovite, paragonite, ilmenite, rutile, hematite and quartz corresponds to a narrow stability field ranging between 480-520 °C and 7.5-12 kbar. This stability field is limited by the disappearance of rutile towards higher temperatures and by the disappearance of paragonite towards lower pressures and higher temperatures. The modelled compositional isopleths for chloritoid and muscovite were used to

further constrain the equilibration P–T conditions (Fig. 26). X_{Mg} in the analysed chloritoid grains ranges 0.14–0.15 yielding a temperature interval of 500-520 °C. The Si content in the analysed muscovite ranges 3.04–3.07 a.p.f.u. which corresponds to 9-11 kbar in the calculated P–T pseudosection (Fig. 26).

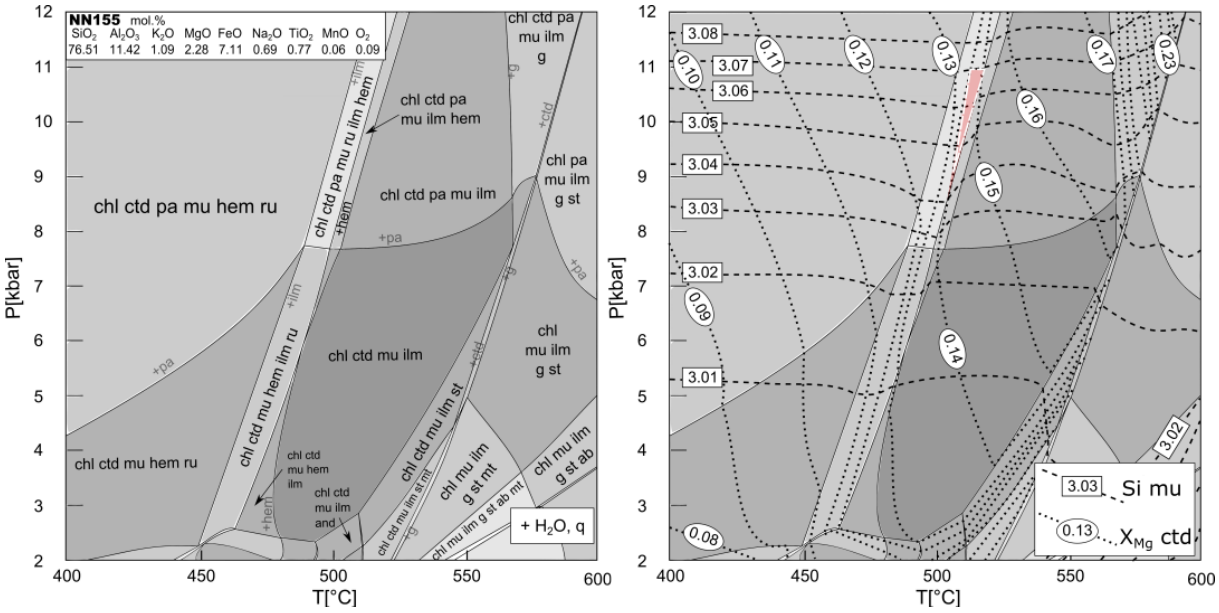

Fig. 26: *P-T section for chloritoid schist sample NN155 with compositional isopleths of X_{Mg} in chloritoid and X_{Si} in muscovite. Resulting P-T conditions are highlighted by pinkish polygon. The section was calculated in the MnNKFMASHTO system using the Perple_X v. 6.6.8 with quartz and water in excess. The bulk rock composition in molar proportion is indicated above the section.*

3.3.2 AMPHIBOLITES

The P–T pseudosection for amphibolite sample NN25 was calculated using THERMOCALC 3.33 (Powell and Holland, 1988) and the internally-consistent thermodynamic dataset 5.5 (Holland and Powell, 2003 upgrade, 1998) in the model system Na_2O-CaO-FeO-MgO-Al_2O_3-SiO_2-H_2O-TiO_2- Fe_2O_3 (NCFMASHTO) for the analysed whole-rock composition (Fig. 27, Table 2). The amount of Fe_2O_3 was analysed by wet chemical titration. Because activity-composition relations for Mn-bearing solid solutions, in particular amphiboles, are poorly constrained and the studied sample has a low MnO content (0.22 wt. %), MnO was not included in the chemical model system. The whole rock composition used to calculate the P-T section is presented in figure 27 and Table 2. K_2O was excluded from the

calculation because (i) potassium-bearing micas and K-feldspar are absent in the studied sample, (ii) the existing mixing model for amphibole does not incorporate K_2O and (iii) the amount of K_2O in the studied sample is low (0.1 wt.%; Tab. 3). The mixing models of clinoamphibole (Diener and Powell, 2012), clinopyroxene (Diener and Powell, 2012), chlorite (Holland and Powell, 1998), garnet (White et al., 2007), epidote (Holland and Powell, 1998), plagioclase (Holland and Powell, 2003), ilmenite and hematite (White et al., 2000) were used in the calculation.

In the resulting pseudosection (Fig. 27), the early equilibrium assemblage of hornblende, plagioclase, titanite, ± epidote and quartz corresponds to the stability field spanning between 500-600 °C and 4-7 kbar. For a more precise determination of the peak P-T conditions, the compositional isopleths of X_{Ca} (= Ca/(Ca+Na)) in plagioclase and the proportion of octahedral Al in hornblende (XAl_{M2}) were calculated. In the resulting pseudosection (Fig. 27), the early equilibrium assemblage of hornblende, plagioclase, titanite, ± epidote and quartz corresponds to the stability field spanning between 500-600 °C and 4-7 kbar. For a more precise determination of the peak P-T conditions, the compositional isopleths of X_{Ca} (= Ca/(Ca+Na)) in plagioclase and the proportion of octahedral Al in hornblende (XAl_{M2}) were calculated.

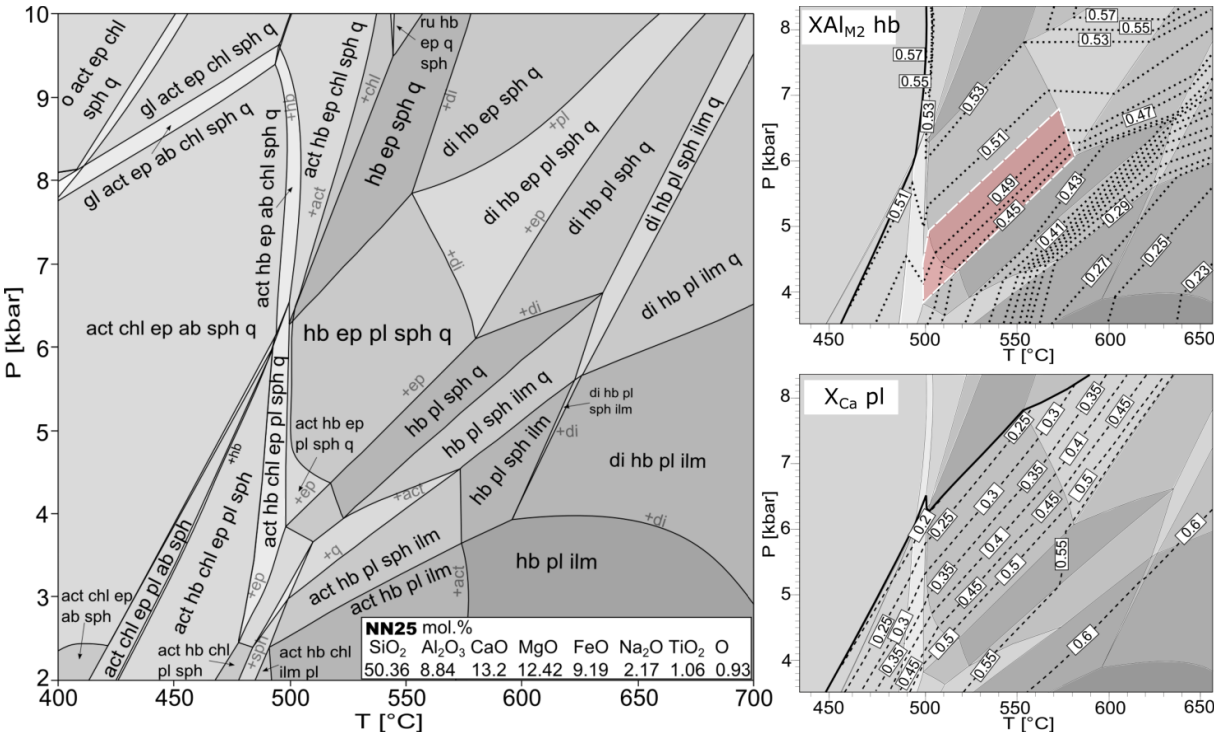

Fig. 27: *P-T section for amphibolite sample NN25 with compositional isopleths of XAl_{M2} in hornblende and X_{Ca} in plagioclase. Resulting P-T conditions are highlighted by pinkish polygon. The section was calculated in the NCFMASHTO system using the THERMOCALC v. 3.33. The bulk rock composition in molar proportion is indicated above the section.*

The analysed plagioclase, inferred to be in equilibrium with hornblende, contains up to 15 % of anorthite component. However, the minimum modelled X_{Ca} value in plagioclase is of ca. 0.20 (Fig. 27) and the analysed values are not modelled in the pseudosection. This could be related to uncertainties on the actual Fe_2O_3/FeO ratio, which is easily affected by late alteration and has influence on the position of the compositional isopleths (e.g. López-Carmona et al., 2013). A P-X_{Fe2O3} pseudosection has been constructed in order to check this influence (Fig. 28). However, even at very low values of Fe_2O_3 the proportion of anorthite in plagioclase does not reach values significantly lower than 0.2. Consequently, we infer that the plagioclase composition must reflect later local partial reequilibration (cf. below). Based on the pseudosection, the peak P-T conditions of the studied amphibolite sample correspond to 500-600 °C at 4-6.5 kbar. The later matrix mineral assemblage of actinolite, epidote, albite and chlorite re-equilibrated in the broad field spanning from the beginning of the section at 400-470 °C and 3-8 kbar (Fig. 27).

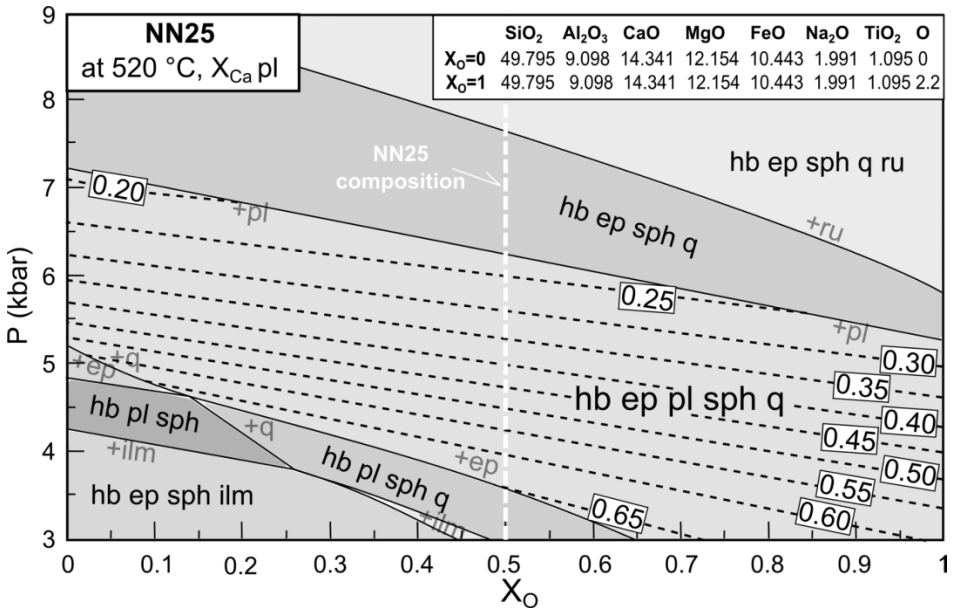

Fig. 28: *The P-X section calculated at 520° C for NN25. The modeled values in P-T section for X_{Ca} in plagioclase start at the value of ca. 0.20 (Fig. 27), this does not correspond to the analysed values. The P-X section was constructed to check, whether this may be influenced by the actual Fe_2O_3/FeO ratio. Even at very low values of Fe_2O_3 the proportion of anorthite in plagioclase does not reach values lower than 0.2. The 2 compositions in molar proportion are indicated above the section.*

3.4 DISCUSSION

The Ochtiná Unit marks the tectonic contact between the Gemer and Vepor Units in the Central Western Carpathians. It comprises flysch-like phyllites and meta-sandstones that contain diverse exotic lenticular blocks up to hundreds of meters in size. In earlier concepts, these rocks were considered part of the upper plate Gemer Unit and their sedimentary cover relationship to the Gemer basement has been favoured. The lenticular blocks of amphibolite and serpentinite were associated with imbrications of the Gemer basement (Vozárová, 1990). However, the studied blocks revealed a different metamorphic history and correspond to contrasting transient geothermal gradients (Fig. 29). The equilibration conditions of the amphibolite lens are of 4-6.5 kbar at 500-600 °C, later re-equilibrated at 3-8 kbar and 400-470 °C, whereas the chloritoid schist equilibrated at 9-11 kbar and ~500 °C. Consequently, our results show that the occurrence of exotic strong blocks enclosed within the weak phyllite matrix of the Ochtiná Unit can be regarded as a mappable block-in-matrix rock unit (i.e., mélange sensu Silver and Beutner, 1980; Raymond, 1984; Festa et al., 2012).

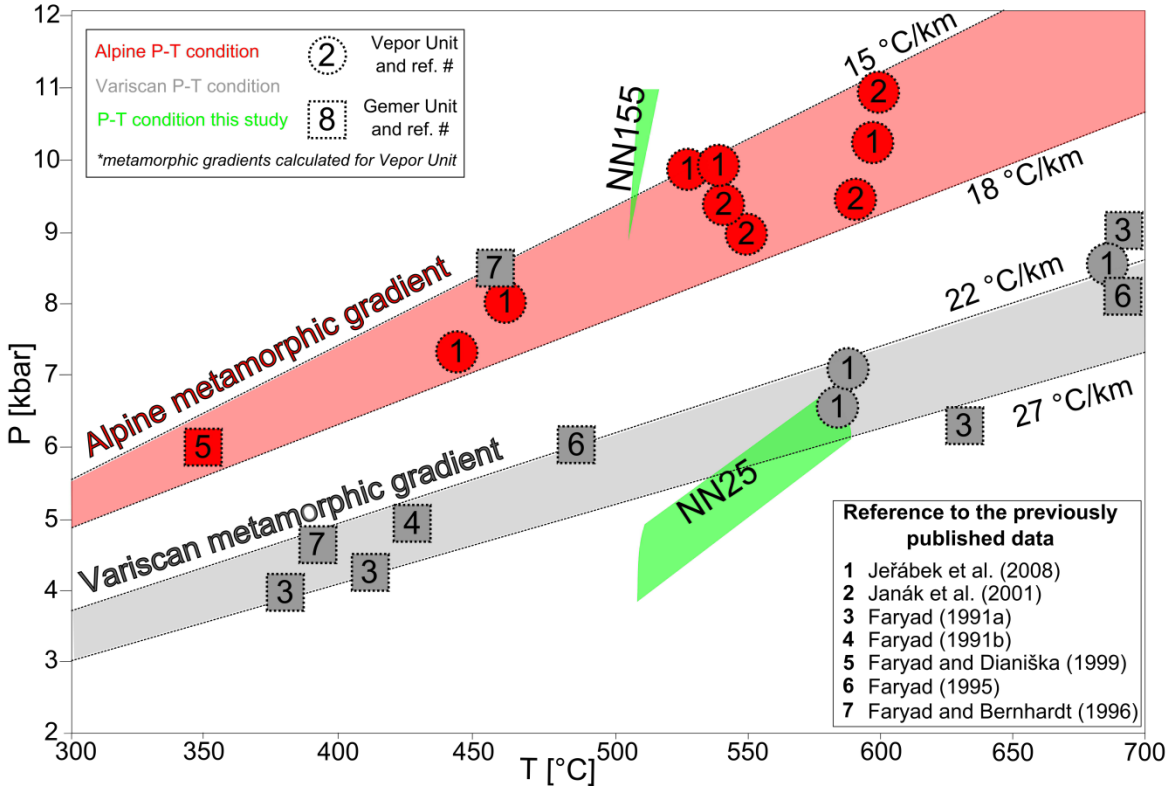

Fig. 29: *Summary P-T diagram showing P-T estimates for chloritoid schist sample NN155 (Fig. 26) and amphibolite sample NN25 (Fig. 27) as well as selected published P-T data from Gemer and Vepor units. The data for the Ochtiná Nappe samples reveal two contrasting metamoprhic field gradients for Variscan and Alpine metamorphism. The metamorphic field gradients are after Jeřábek et al., 2008.*

3.4.1 THE TECTONIC SIGNIFICANCE OF THE OCHTINÁ UNIT

The Ochtiná Unit and the similar lithological complex of the Črmel nappe further east delineate a major boundary between the crustal scale Vepor and Gemer units. Since Andrusov (1936) this boundary has been recognized as a major thrust of the Gemer Unit over the Vepor Unit. In the studied area, this event is associated with the development of S_{A1} deformation fabrics, which are relatively steep and E-W trending in the Gemer Unit and subhorizontal with an E-W stretching component in the Vepor Unit (Fig. 30a). This process is associated with prograde metamorphism during crustal thickening and burial of the Vepor Unit (Jeřábek et al., 2008; Jeřábek et al., 2012). The development of the S_{A2} fabric is mainly documented in the vicinity of the contact between the Gemer and Vepor units, but did not affect the hanging wall Gemer Unit. It is interpreted that the Ochtiná Unit localized the detachment responsible for the unroofing of the Vepor basement (Fig. 30b; Plašienka et al., 1999; Janák et al., 2001; Bukovská et al., 2013). Finally, the F3 folding and the heterogeneous development of the S_{A3} fabric can be associated with the localization in the southern part of the Ochtiná Unit of sinistral transpressive movements along the Trans Gemer Shear Zone (Fig. 30c; Lexa et al., 2003).

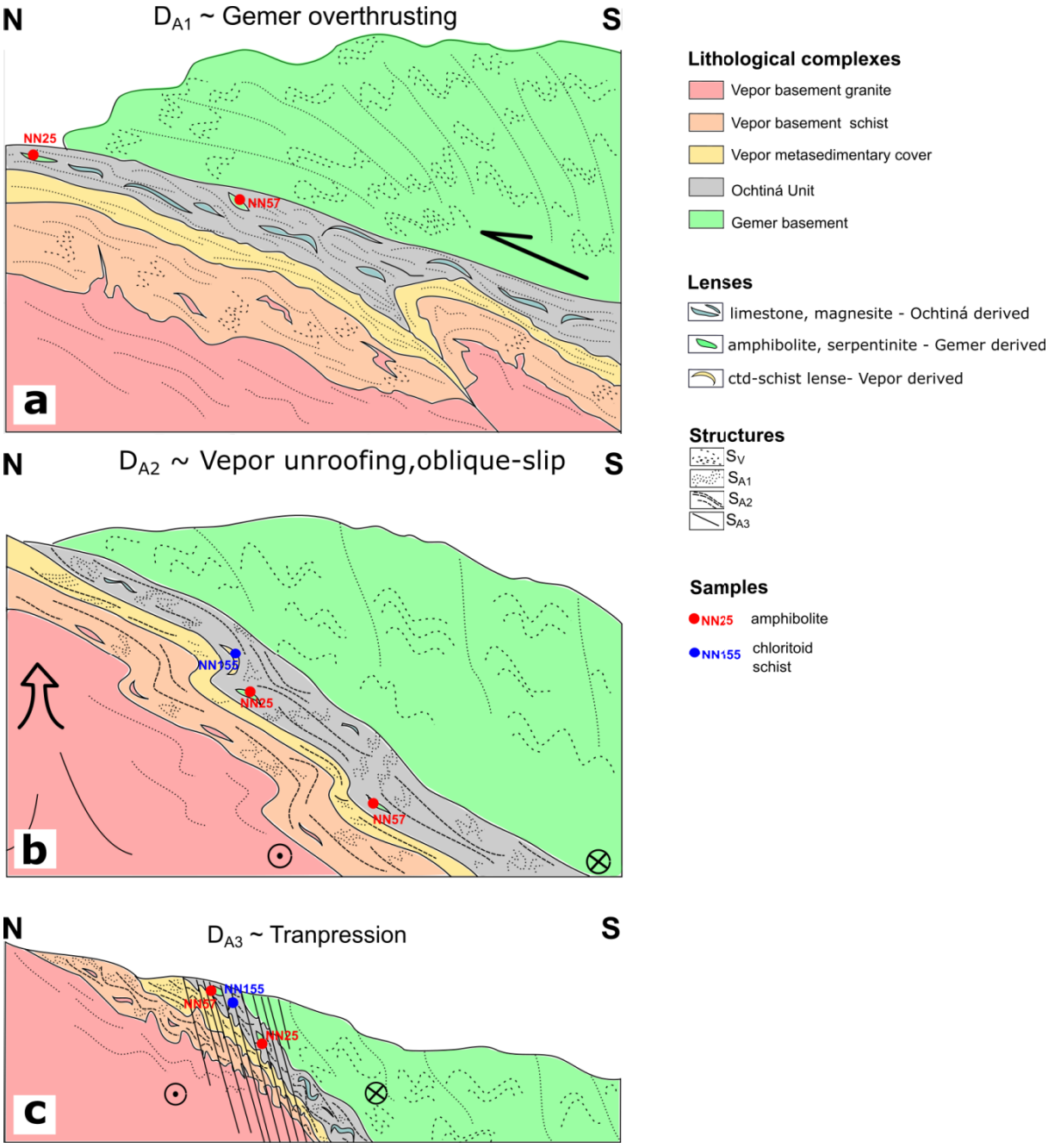

Fig. 30: *Proposed model of Ochtiná mélange evolution during the D_{A1}, D_{A2} and D_{A3} deformational phases (see text). The amphibolite samples are in red (NN25 and NN57), the chloritoid schist (NN155) is in blue. (a) D_{A1} phase, the Gemer Unit is thrusting over the Vepor Unit, which leads to its burial. (b) D_{A2} phase, subsequent exhumation and unroofing of Vepor Unit, (c) D_{A3} phase Trans-Gemer Shear Zone (TGSZ) formation due to the transpressional lateral escape of Gemer Unit.*

3.4.2 ORIGIN OF THE LITHOLOGICAL ASSEMBLAGE IN THE OCHTINÁ UNIT MÉLANGE

Based on the geological, metamorphic and geochemical evidence, the complex lithological assemblage of the blocks in the phyllite matrix of the Ochtiná Unit is associated with three different source regions. 1) The limestone, dolomite and magnesite blocks are interpreted to represent a dismembered carbonate horizon of Lower Carboniferous age within the Ochtiná sedimentary sequence (Abonyi and Abonyiová, 1981). In contrast, 2) the amphibolite and serpentinite blocks show affinity to the Gemer basement while 3) the chloritoid schists are most likely derived from the Vepor cover.

1) Supportive evidence for this interpretation comes from an identical lithological assemblage of flysch sediments and carbonates reported from the Carboniferous Veitsch nappe (Ratschbacher, 1986), which is considered as a counterpart of the Ochtiná Unit in the Graywacke zone of the Eastern Alps (e.g. Neubauer and Vozárová, 1990) and which lacks the complex lithological assemblage recorded in the Ochtiná Unit. The limestones in both nappes locally experienced metasomatic replacement of calcite by dolomite and magnesite that has been associated with Permian rifting (Prochaska, 2000) or Cretaceous collision (Hurai et al., 2011).

2) Amphibolites are frequent in the Gemer basement mainly in the Rakovec and Klátov complexes and occur in a close proximity to the Gemer-Vepor contact zone (Fig. 4). Serpentinised peridotites also occur in the Gemer basement (Hovorka and Zlocha, 1974) although little is known about their origin. Estimates of the peak PT conditions of the studied amphibolite in the Ochtiná Unit range between 500-600 °C and 4-6.5 kbar and show very good correlation with the previously published PT data from the Gemer amphibolites (Fig. 29, Faryad, 1995, 1991a). The formation of the Gemer amphibolites is associated with the Variscan tectono-metamorphic event (Faryad, 1990), thus the age of the peak metamorphism in the Ochtiná amphibolite is most likely also Variscan as previously proposed by Vozárová (1990). The correlation of the Ochtiná and Gemer amphibolites is further supported by comparing the geochemical data from the Ochtiná amphibolite (Table 2, Fig. 22 and 23) with the previously published data from the Rakovec complex (Bajaník, 1976; Ivan, 2008). Both data sets show relatively good match indicating a mid-ocean ridge to within plate basalts affinity of the analysed amphibolites (Fig. 22 and 23). The Ochtiná amphibolite and serpentinite are thus interpreted to represent parts of the upper plate Gemer basement that were incorporated into the

Ochtiná phyllites during the Early Cretaceous thrusting of the Gemer Unit over the Vepor Unit (see discussion below).

3) Southern portions of the Vepor Foederata cover, located in direct structural footwall of the overlying Ochtiná Unit, contain chloritoid-kyanite schists (Lupták et al., 2000; Vrána, 1964). These schists probably represent an aluminium-rich sedimentary horizon in the Permian sequence that was subjected to Cretaceous metamorphism. The metamorphic conditions of these schists range 530-560 °C and 4.5-8 kbar (Lupták et al., 2000) and their Cretaceous (~97 Ma) metamorphic age has been recently constrained by U-Pb dating of monazite (Bukovská et al., 2013). Chloritoid-schists enclosed within the Ochtiná phyllite typically occur close to the boundary with the Vepor Unit (Fig. 4, 8). These rocks show identical microstructural relationships as those described in chloritoid schists of the Vepor cover (Bukovská et al., 2013; Lupták et al., 2000) and are characterized by similar PT conditions of ~ 500 °C and 9-11 kbar (Fig. 29). Based on these similarities, the chloritoid schists of the Ochtiná Unit are interpreted as parts of the Vepor cover that were incorporated into the Ochtiná phyllites during the unroofing of the Vepor Unit (see discussion below).

3.4.3 THE MECHANISM OF INCORPORATION OF EXOTIC BLOCKS INTO THE OCHTINÁ UNIT MÉLANGE

Mélanges related to collisional tectonic settings are capable of incorporating material from both upper and lower plates during a single kinematic event (Chang et al., 2001; Festa et al., 2010; Huang et al., 2008). Careful characterization of the tectono-metamorphic record of the Ochtiná mélange, however, does not allow for a simple kinematic model. Instead, the incorporation of the Gemer and Vepor derived rocks is explained by repeated reactivation along the rheologically weak sediments of the Ochtiná sequence transformed into a major décollement horizon between the two crustal-scale units. Because field observations don't allow to establish a clear structural relationship between the blocks and the surrounding phyllites, this interpretation is based purely on comparison of metamorphic record in the matrix phyllites and incorporated blocks.

The metamorphic overprint associated with the Cretaceous nappe stacking and northward overthrusting of the Gemer Unit over the Vepor Unit and the development of S_{A1} is of relatively low grade in the Gemer basement (350 °C, 5-6 kbar; Fig. 29; Faryad and Dianiška, 1999) and the underlying Ochtiná Unit. S_{A1}-related micro shear zones in the Gemer-derived blocks of Variscan amphibolites yield 3-8 kbar and 400-470 °C. It is thus likely that it is during the northward overthrusting of the Gemer Unit when the amphibolite blocks have been sheared off from the bottom Gemer basement and incorporated into the Ochtiná phyllites (Fig. 30a).

On the other hand, the PT conditions related to the S_{A1} fabric in the direct footwall of the Ochtiná Unit in the studied area reached up to 9 kbar at 550 °C for the southern Veporic cover and the underlying basement schists (Jeřábek et al., 2008; Lupták et al., 2000). These PT conditions document a metamorphic gap across the boundary between the lower grade Ochtiná Unit in the hanging wall and the higher grade Vepor metasediments in the footwall. Such a metamorphic gap is consistent with the existence of a décollement shear zone associated with the exhumation and unroofing of the Vepor Unit. In the studied area, this décollement is associated with the development of lower grade subhorizontal cleavage S_{A2}, which mainly affected the Vepor cover and Ochtiná phyllite but has not been identified in the hanging wall Gemer Unit (Fig. 30b). Moreover, the blocks of chloritoid schists within the Ochtiná phyllite occur exclusively in the vicinity of the contact with the Vepor Unit and record similar PT conditions as the nearby Vepor cover metasediments. It is thus likely that the top parts of the

Vepor Unit have been sheared off and incorporated into the hanging wall Ochtiná phyllites during exhumation of the Vepor Unit (Fig. 30b).

The last Upper Cretaceous deformation phase documented in the studied area corresponds to the left-lateral transpressional movements between the Gemer and Vepor Units, which are recorded by the development of steep cleavages and shear zones S_{A3} mainly in the Ochtiná phyllites (Lexa et al., 2003). These horizontal movements are again accommodated by the Ochtiná Unit along the southern edge of the Vepor Unit (Fig. 30c). The strike slip derived tectonic mélange (Dela Pierre et al., 2007; Festa et al., 2010) represents an alternative scenario for incorporation of both Gemer and Vepor rocks into the Ochtiná Unit. However, no significant transpressional movements were documented in the Črmel nappe (Lexa et al., 2003) that contains a similar block-in-matrix lithological assemblage and delineates the contact between the Gemer and Vepor units further to the east (Vozárová, 1996).

3.4.4 THE EFFECT OF WEAK DÉCOLLEMENT HORIZON ON THE STYLE OF COLLISION BETWEEN MAJOR CRUSTAL NAPPES

The rheological characteristics of the sediments of the Ochtiná Unit dominated by phyllites represent an ideal décollement horizon to promote major relative movements between the neighbouring Gemer and Vepor Units. The repeated reactivation of this horizon may explain the mechanically uncoupled behaviour during deformation documented by the contrasting structural record in the Gemer suprastructure and the Vepor infrastructure (Jeřábek et al., 2012; Lexa et al., 2003). 1) The overthrusting is associated with steep E-W trending cleavages in the Gemer suprastructure and subhorizontal fabrics with characteristic E-W orogen-parallel stretching in the Vepor infrastructure. 2) The unroofing of the Vepor Unit is associated with the development of detachment fabric in the Vepor infrastructure but the suprastructure has not been affected by this deformation. 3) Several localized transpressional zones associated with left-lateral movements develop within the Vepor and Gemer basements suggesting coupled behaviour of the two units and no major role of the Ochtiná nappe in this late Cretaceous process.

It is concluded that the Ochtiná décollement zone served repeatedly as a high-strain shear zone promoting decoupled behaviour between the orogenic suprastructure and infrastructure in the Eo-Alpine Western Carpathians orogenic wedge. The development of such suprastructure-infrastructure transition zones is commonly associated with thermo-mechanical relaxation of a thickened crust resulting in upward propagating mechanical weakening. Therefore the position of suprastructure-infrastructure transition zone commonly changes through time (Beaumont et al., 2006; Culshaw et al., 2006). In contrast, the Ochtiná Unit represents an unusual example of a suprastructure-infrastructure transition zone with its position being predefined and fixed by the mechanical weakness of this sedimentary horizon.

3.4.5 IMPLICATIONS FOR THE PRE-CONVERGENT SETTING OF THE OCHTINÁ SEDIMENTS

If the Ochtiná Unit represents a tectonic mélange, which formed at the base of the overriding Gemer Unit, it appears rather suspicious that it does not contain rocks of the Gemer cover nor of the overlying subduction-accretionary complex of the Meliata ocean (Faryad and Henjes-Kunst, 1997). A possible explanation of this phenomenon involves the post-Lower Carboniferous evolution of the Ochtiná basin as well as the initial stages of Cretaceous collision.

The previously assumed cover relationship of the Ochtiná metasediments to the Gemer basement is contradicted by the fact that the rocks of the Ochtiná Unit never occur upon the Gemer basement, which in turn is discordantly overlain by the Upper Carboniferous succession of the Dobšiná group and Permian conglomerates (Kozur et al., 1976; Rakusz, 1932). For this reason some authors proposed the existence of a basin separating the Vepor and Gemer during Late Paleozoic–Mesozoic (e.g., Abonyi, 1971; Kozur and Mock, 1997) and others associate the sediments of the Ochtiná Unit with the Vepor Unit (Németh et al., 2006). Indeed, the geochemical data from phyllites and meta-sandstones presented in this work point to acidic continental arc protolith source, which may be sought in the Vepor basement dominated by Carboniferous granitoids. Furthermore, a recent study of detritic zircons in one meta-sandstone sample from the Ochtiná Unit shows a dominance of Upper Devonian-Carboniferous zircons (Vozárová et al., 2013), which are frequent in the Vepor basement but nearly absent in Gemer (cf. Michalko et al., 1998; Vozárová et al., 2010). Although very little is known about the basin separating the Gemer and Vepor units, it is sometimes considered as a root zone for a thick Mesozoic carbonate sequence preserved in the rootless Choč nappe overriding the Krížna nappe in the northern Vepor and Tatra Units. There is a remarkable stratigraphic coincidence between the Lower Carboniferous metasediments of the Ochtiná Unit and the basal part of the Choč nappe formed by Upper Carboniferous shales and conglomerates. The origin of the Choč nappe in the Ochtiná basin may actually explain the lack of upper crustal rocks in the Ochtiná mélange. As the Cretaceous convergence in the Western Carpathians started in the south with the closure of the Ochtiná basin between the Gemer and Vepor blocks, it appears likely that the rheologically weak horizon of the Ochtiná sediments acted as a décollement zone already for the overlying strong carbonate platform of the Upper Carboniferous-Cretaceous deposits of the future Choč sequence. The Choč nappe was thus pushed northwards from its root zone by the

thickening Gemer Unit, however at the same time it served as a lid preventing the Gemer derived debris from getting into the basal thrust zone. This scenario is further supported by the overlap of the recently published ages related to thickening of the Gemer Unit starting at ca. 137 Ma (Hurai et al., 2008a; Vozárová et al., 2014) with the youngest Valagian sediments in the the Choč nappe (Jablonský et al., 2001). These sediments comprise chromium-spinel bearing turbidites, which may be associated with denudation of the Meliata accretionary complex overlying the thickening Gemer Unit. This scenario may also explain the lack of the Gemer and Meliata derived debris in the Ochtiná basal thrust zone.

3.5 PARTIAL CONCLUSIONS

1. The Ochtiná Unit is characterized by a complex lithological assemblage of exotic hard blocks, lenticular in shape enclosed in a weak phyllite matrix. Petrological analysis by means of phase equilibrium modelling revealed that the lenses are characterised by contrasting metamorphic histories with peak PT conditions of 500-600 °C and 4-6.5 kbar for amphibolite, and 500-520 °C and 9-11 kbar for chloritoid schist. These PT estimates document two distinct metamorphic field gradients presumably related to Variscan and Alpine metamorphic events, respectively. The heterogeneous lithological and metamorphic record is consistent with a block-in-matrix type of rock assemblage and consequently the Ochtiná Unit is interpreted as deep seated tectonic mélange.

2. The mélange formed during the Cretaceous Eo-Alpine collision at the boundary between two major crustal nappes of the Western Carpathians – the Gemer and Vepor Units. The mélange evolved via repeated slip along the rheologically weak sediments of the Ochtiná Unit during the building and collapse of the Central Western Carpathians orogenic wedge. Deformation record indicates that the mélange separates two distinct structural domains marked by a decoupled behaviour, i.e. the orogenic suprastructure represented by the Gemer Unit and infrastructure represented by the Vepor Unit. With this respect, the Ochtiná Unit represents an unusual example of a suprastructure-infrastructure transition zone with its position being controlled by the mechanical weakness of this sedimentary horizon and not by the usual thermal maturation.

3. The lack of the upper crustal rocks derived from the Gemer Unit within the Ochtiná Unit mélange may be explained by the presence of the Mesozoic carbonates of the Choč nappe in the Ochtiná basin prior to the Cretaceous collision.

4. METASOMATISM WITHIN THE ZONE OF ACTIVE DEFORMATION IN THE GVCZ

Mg-rich schistose rocks are relatively common in alpine orogenic belts, such as the Alps and the Carpathians, or the Pyrenees. They are usually associated with shear zones and ore deposits of magnesian rocks (such as talc and magnesite; Goncalves et al., 2012, Marquer, 1987 etc.). They are commonly enriched in Mg. Originally their genesis was ascribed to isochemical metamorphism of a sedimentary protolith (Chopin, 1981, Schertl et al., 1991). Due to their leucocratic character, they are referred to as leucophyllites or whiteschists. Nowadays they are in general interpreted as metasomatic rocks generated by fluid-assisted exchange of elements (Demény et al., 1997) or by relative enrichment of MgO due to fluid-assisted removal of other components (Prochaska 1985, 1991).

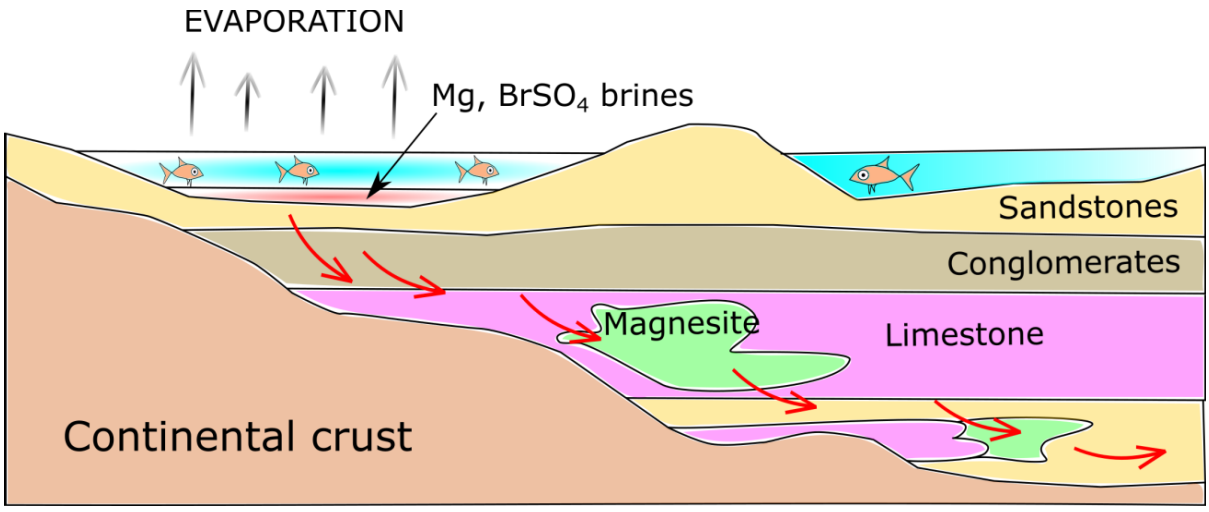

Fig. 31: *Genetic model for magnesite formation by the circulation of evaporitic residual brines rich in Mg during Permotriassic rifting stage (after Prochaska, 2000).*

The metasomatising fluids may have different sources. A first type of models suggests the involvment of late-magmatic hydrothermal systems (Pawling and Baumgartner, 2001). A second group of models involves the formation of fluids due to seawater evaporation,

circulation of enriched evaporitic brines through carbonates and the formation of ore deposits (Fig. 31). This model is traditionally used to explain the magnesite formation in the Eastern Alps (Prochaska, 2000, Fig. 31). A third group of models involves the interaction of fluids with mantle rocks in various tectonic settings. In a first case, seawater interacts with mantle rocks during rift-related ocean continent transition stage and the enriched fluids are channelized along large-scale detachments (Ferrando et al., 2012; Manatschal et al., 2000 and reference therein, Fig. 32a). A second type of tectonic setting is a continental subduction, where parts of the fluids are released during (ultra)high-pressure (HP/UHP) dehydration of slices of oceanic serpentinites and are channelized along main convergent structures (Agard et al., 2009; Ferrando et al., 2012, Fig. 32b). In a third case, metasomatic fluids are generated during continental collision by local dehydration of serpentinites and are channelized along major extensional shear zones (Agard et al., 2009; Ferrando et al., 2012 and reference therein, Fig. 32c).

The talc and magnesite ore deposits in the Central Western Carpathians occur along a large-scale tectonic contact (Fig. 4). In order to understand the distinct metasomatic processes within the Western Carpathians, and their position in the structural and tectonic framework of the orogenic evolution, local shear zones with different alteration trends and a well-constrained structural framework were sampled (Fig. 4).

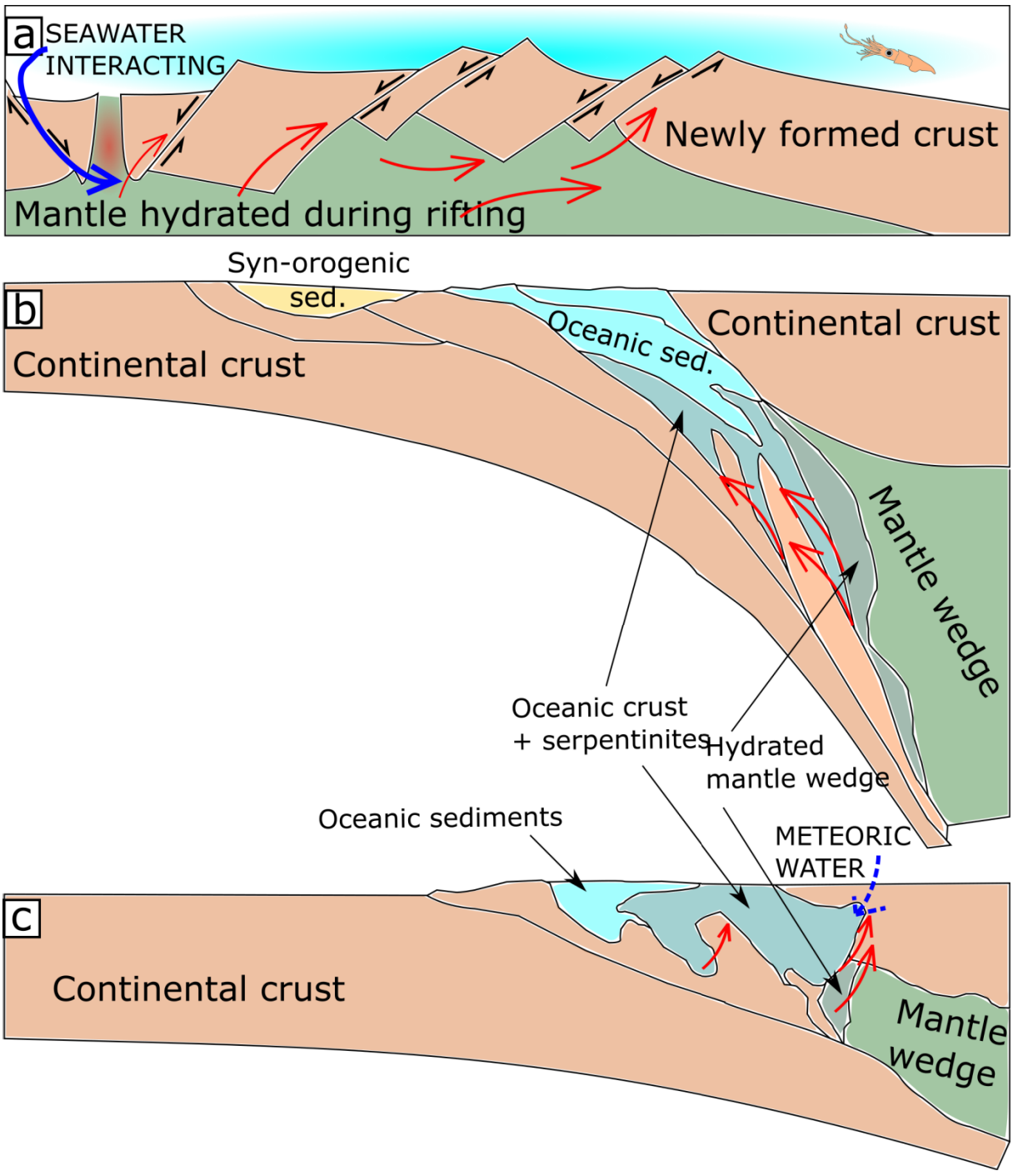

Fig. 32: ***(a)*** *A seawater interacts with mantle rocks during rift-related ocean continent transition stage and the enriched fluids are channelized along large-scale detachments.* ***(b)*** *Continental subduction, where parts of the fluids are released during (ultra)high-pressure (HP/UHP) dehydration of slices of oceanic serpentinites and are channelized along main convergent structures.* ***(c)*** *Metasomatic fluids are generated during continental collision by local dehydration of serpentinites and are channelized along major extensional shear zones (figure after Ferrando et al., 2012 and reference therein).*

4.1 DEFORMATION HISTORY

As indicated in chapter 3, the Gemer-Vepor Contact Zone is characterized by the presence of narrow SW-NE trending lithological complexes. From the bottom to the top these are (1) Vepor basement granite, (2) Vepor basement schists, (3) Vepor basement Cover, (4) Ochtiná Unit and (5) Gemer basement (Fig. 10). The 4 major deformation fabrics (S_V, S_{A1}, S_{A2} and S_{A3}) are observed in the Gemer-Vepor Contact Zone (Fig. 9, 10), but they are preserved heterogeneously in each lithological complex. The S_{A1} deformational is the main deformation fabric developed through the region (Fig. 33a).

Lithological complex	**Observed structures**
Vepor basement granite	S_{A1}
Vepor schist	$S_V \rightarrow S_{A1} \rightarrow S_{A2}$
Vepor metasedimentary cover	$S_{A1} \rightarrow S_{A2}$
Ochtiná Unit	$S_{A1} \rightarrow S_{A2} \rightarrow S_{A3}$
Gemer basement	S_0 & $S_V \rightarrow S_{A1} \rightarrow S_{A3}$

Tab. 4*: Observed structural fabrics within different lithological complexes in the studied area.*

The Vepor basement schists were affected by Variscan and Alpine regional metamorphism of medium grade (Jeřábek et al., 2008). The Alpine deformation-metamorphic overprint is indicative of low strains in the vicinity of leucogranite while towards the south the Variscan schistosity S_V is obliterated by the Alpine S_{A1} cleavage. The degree of metamorphism in the schists generally decreases towards SE where, however, the higher grade garnet bearing first Alpine fabric is overprinted by a lower grade muscovite-chlorite bearing second Alpine S_{A2} cleavage (Fig. 33b). The Vepor cover is characterized by the presence of two Alpine deformation fabrics of different metamorphic grade that is mainly manifested by distinct quartz deformation microstructures (Jeřábek et al., 2007 and Jeřábek et al., 2008). The presumably Carboniferous phyllites of the Ochtiná Unit show polydeformation record characterized by

relics of higher grade fabric being S_{A1} nearly obliterated by the low grade muscovite-chlorite bearing S_{A2} cleavage. The above-described first and second Alpine cleavages are subparallel dipping to the S or SE at moderate angles (Fig. 33d). In Gemer basement rocks in the studied area, the relics of SV S-SE oriented fabric are locally preserved. However, they are obliterated by the S_{A1} fabric represented by a cleavage of lower grade oblieterating the older fabrics, dipping steeply to S-SE The two main metamorphic fabrics in the rocks of Ochtiná Unit and Gemer basement and are subsequently folded by the F3 open folds with a subhorizontal, SW-NE trending axes, locally developing a steep discrete cleavage S_{A3} (Fig. 33c, 33d).

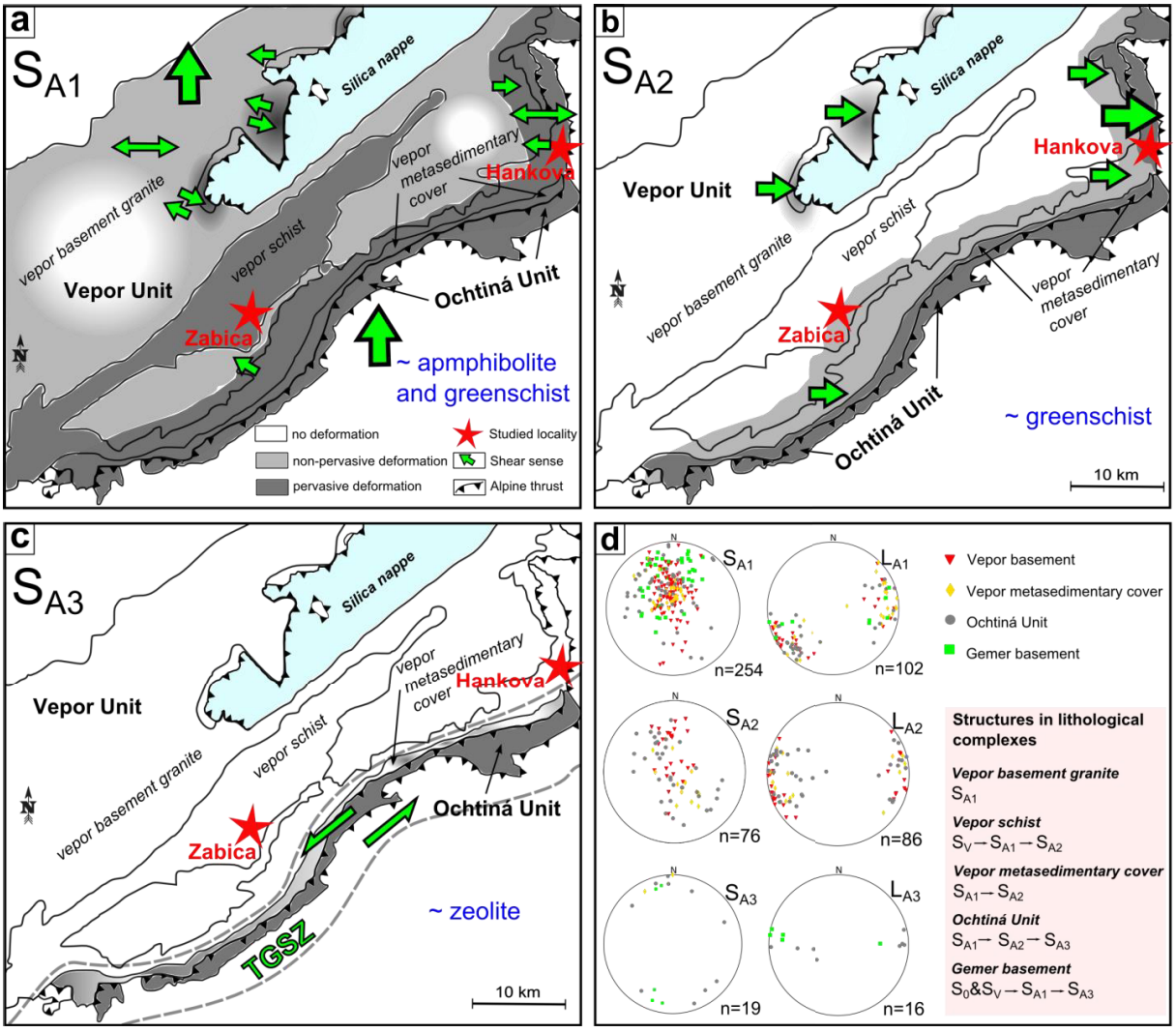

Fig. 33: (a), (b), (c) *Structural maps of individual Alpine fabrics showing trajectories and dips of metamorphic foliations and cleavages and associated lineation or fold axes. The background gray-scale manifests spatial extent and intensity of individual deformation events. Major thrusts and detachments together with shear sense for individual fabrics are also indicated (after Jeřábek et al., 2012). The studied localities in different lithological complexes are marked (red star).* ***(d)*** *Pole figures (lower hemisphere, equal-area Schmidt projection) of documented structures and documented structures within different lithological complexes (inset table, see also fig. 9 for details).*

In order to understand the distinct metasomatic events in the region during the Cretaceous polyphase deformation we have decided to sample two smaller local shear zones with its different manifestations of deformational fabrics.

4.1.1 ŽABICA LOCALITY

In the Žabica locality, the Carboniferous Vepor basement granite complex (Fig. 4, 33) is cut across by a 10m long, 2 m wide and gently dipping westward shear zone. Several other gently to moderately southward dipping shear zones develop in neighbouring outcrops. In this shear zone, the metagranite is progressively transformed into a quartz-white mica±chlorite bearing whiteschist. This zone was affected by the S_{A1}, and S_{A2} metamorphic fabrics (Fig. 33a), the older metamorphic fabric S_{A1} is represented by the kyanite, muscovite and chlorite. This metamorphic fabric was subsequently overprinted by lower grade second Alpine S_{A2} muscovite-chlorite bearing cleavage. Therefore, the development of the shear zone is ascribed to a second Alpine metamorphic fabric S_{A2}. Late kinking is responsible for local variations of the fabric orientation and in particular the westward dip direction of the studied shear zone.

4.1.2 HANKOVÁ LOCALITY

The Hanková locality is a local shear zone situated in the Vepor metasedimenatry cover complex (Fig. 4). The shear zone crops out in 8 m wide section, gently dips towards the East, and bears a SW-NE trending stretching lineation. It is marked by muscovite-chlorite-quartz bearing whiteschists, developed at the expense of chloritoid-kyanite-bearing schist. The rocks show two deformation fabrics S_{A1} and S_{A2} associated with distinct metamorphic grade (Fig. 33a, 33b) marked by higher grade chloritoid-kyanite (S_{A1}) subsequently overprinted by lower grade chlorite-muscovite assemblages (S_{A2}) in the schist as well as distinct quartz deformation microstructures in the meta-arkose (Bukovská et al., 2013). The superposition of the two fabrics leads to the common development of S-C-type geometries.

4.2 PETROGRAPHY AND MINERAL CHEMISTRY

Smaller local shear zones develop in the Carboniferous granitoid of Vepor Unit (Žabica) and in the Vepor metasedimentary cover (Hanková, Fig. 4).

4.2.1 ŽABICA LOCALITY

In the Žabica locality (Fig. 4, 33), proceeding from metagranite (stage I) through transition rocks (stage II) to white schists (stage III, Fig. 34), with increasing strain the grain size is reduced and the amount of phyllosilicates increases. The metagranite (BZ299A, Fig. 34a) is characterized by an igneous porphyritic texture, with phenocrysts of former K-feldspars (up to 0.5 cm). In the metagranite of Žabica the older metamorphic fabric is preserved (Fig. 34a). This fabric is mainly represented by replacement of the magmatic biotite phenocrysts by chlorite(I) and muscovite (I, Fig. 34 and 35), rich in rutile inclusions and the growth of newly formed subhedral kyanite (Fig. 35a) which forms randomly oriented porphyroblasts (up to 4 mm large, Fig. 35a). The older muscovite is characterized by low X_{Fe} ($X_{Fe}=Fe^{2+}/(Fe^{2+}+Mg+Mn)$=0.2-0.50, X_{Na}= Na/(Na+K) ~ 0-0.15, Si ~ 3.10-3.20 a.p.f.u., Fig. 36a, tab. 5. The Mg content in muscovite is increasing with increasing strain rate (up to X_{Mg}= 0.75-79). In the so-called whiteschists, the originally magmatic K-feldspars are completely replaced by fine grained white mica aggregates (size of grains ~ 0.1 mm, Fig. 34, 35, 36e), Si ~ 3.02- 3.11 a.p.f.u., with higher X_{Na} (0.15-0.30) in comparison to older muscovite(I), Fig. 36a, tab. 5. Quartz is found in all studied samples, however the amount varies with the deformation stage in rocks and with the increased strain the phyllosilicates continuously dominate the rocks and in general, grain size is towards the shear zone reduced (e.g. Fig. 35). With increasing strain intensity, the metagranite progressively evolves into a fine grained mylonite – white schist, rich in Mg-chlorite(II), Fig. 34. With increasing strain the X_{Fe} in newly formed Mg-chlorite(II), Fig. 36b is decreasing from ~ 0.22 (stage I) to 0.18 (stage III, Fig. 36b, tab. 5)., only few relics of magmatic chlorite (X_{Fe}= 0.39-0.42, Al= 0.58-0.61) were found in the sample of BZ299A. Tourmaline, rutile and apatite are present as accessories. In most deformed samples – magnesite aggregates (up to 0.2 mm in diameter) could be locally found in veins (Fig. 32d). For representative mineral analyses see tab. 5.

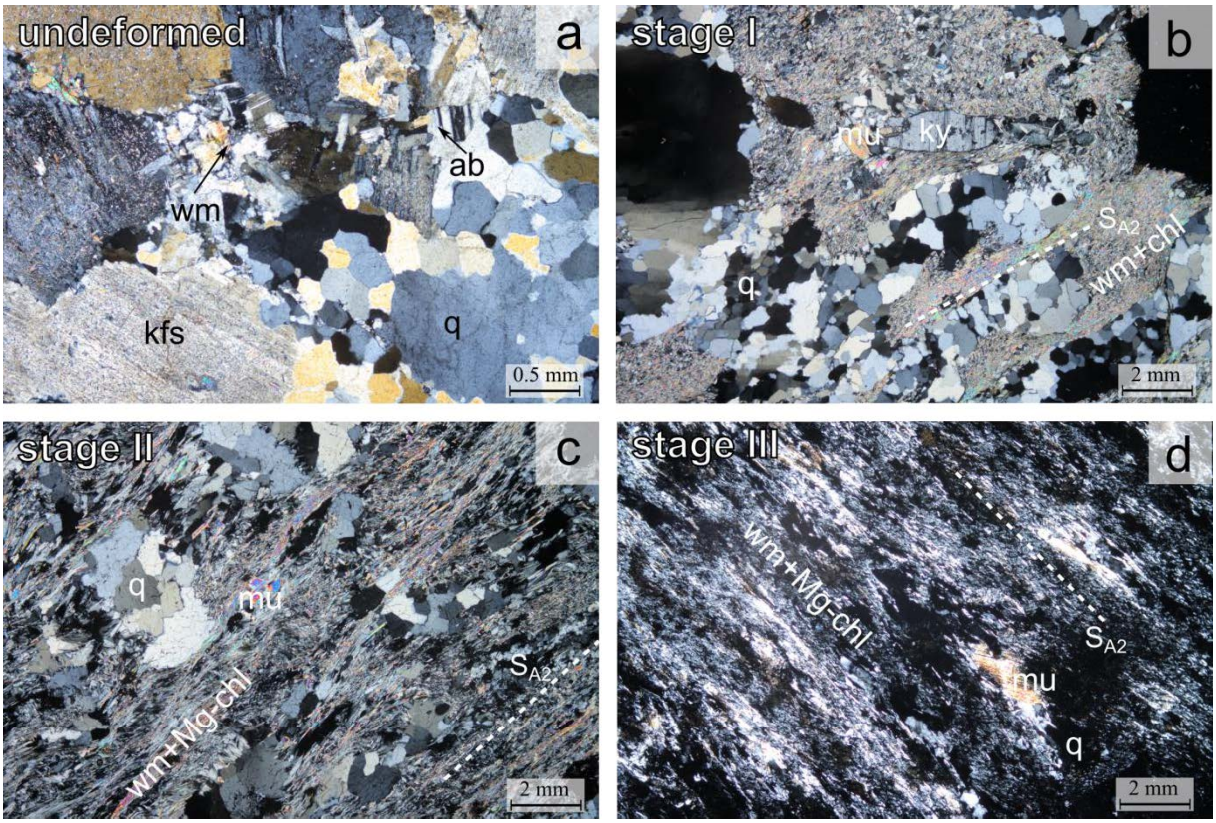

Fig. 34*: Micrographs of deformed metagranite from Žabica locality – crossed polars.* ***(a)*** *Detail on the least deformed domain with relic feldspars in the sample BZ299A.* ***(b)*** *The SA1 metamorphic fabric with kyanite porhyroblasts in BZ299A, stage I of deformation.* ***(c)*** *Stage II of deformation in the sample NK2C, no kyanite is observed, grain size is reduced.* ***(d)*** *Stage III of deformation in Žabica metagranite – "white schist" with dominant Mg-chlorite in the sample NK2A.*

Fig. 35: *Back scattered electron (BSE) images from metagranite samples.* ***(a)*** *Kyanite cross-cutting the foliation defined by white mica and chlorite (BZ299A).* ***(b)*** *Altered muscovite(I) and Mg-chlorite(II) progressively growing in the foliation (NK2C).* ***(c)*** *Element distribution map of magnesium demonstrating the Mg-enrichment in muscovite along fractures (NK2C).* ***(d)*** *Mg-carbonates are locally found in veins, during the deformation all fabrics are with increasing strain obliterated by Mg-chlorite (NK2A).* ***(e)*** *Mg-chlorite and white mica in the matrix and large porphyroblast of rutile (NK2A).* ***(f)*** *Element distribution map of magnesium demonstrating the Mg-enrichment in newly formed chlorite(II) and lack of chemical zoning.*

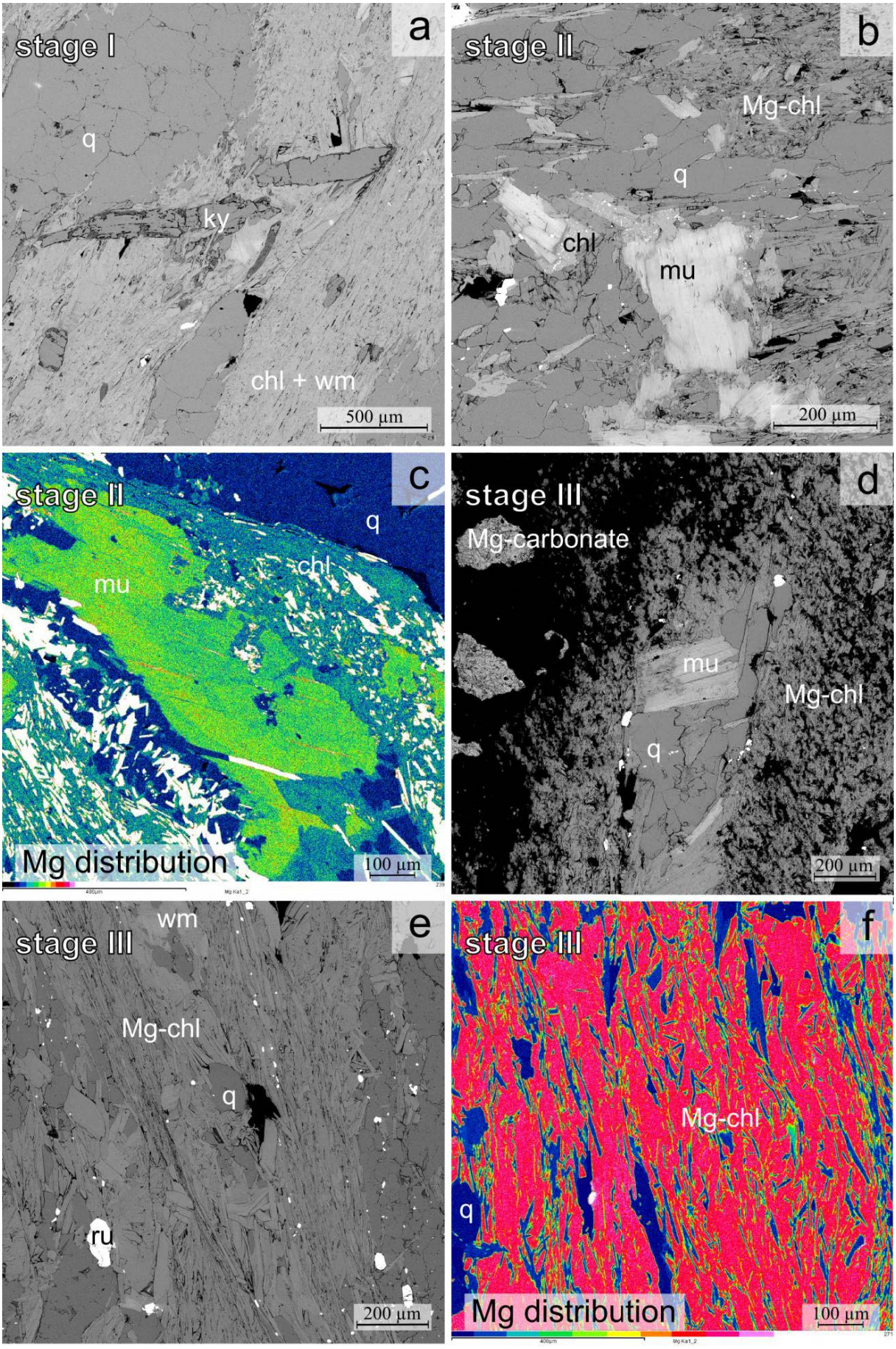
a
stage I
q
ky
chl + wm
500 µm
b
stage II
Mg-chl
q
chl
mu
200 µm
c
stage II
q
chl
mu
Mg distribution
100 µm
d
stage III
Mg-carbonate
mu
Mg-chl
q
200 µm
e
wm
stage III
Mg-chl
q
ru
200 µm
f
stage III
Mg-chl
q
Mg distribution
100 µm

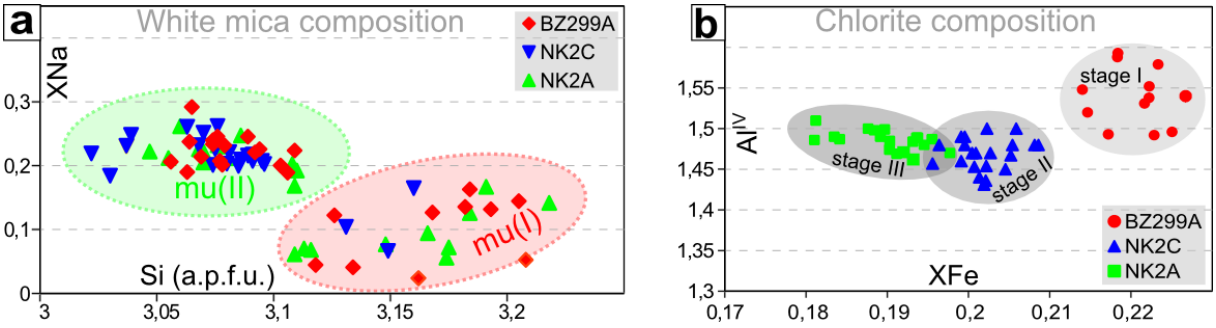

Fig. 36: (a) *Chemical composition of white micas in Žabica locality.* ***(b)*** *Chemical composition of chlorite in Žabica locality.*

4.2.2 HANKOVÁ LOCALITY

In Hanková locality (Fig. 4, 33), the chloritoid-schists with a well developed fabric S_{A1} (stage I), Fig. 37a, b, proceed to fine-grained quartz- and white mica-dominated domains (grain size ~ 0.1 mm phyllonites) with relic chloritoid porphyroblasts completely obliterated by the S_{A2} foliation (stage III, Fig. 37d).

In the least deformed samples (stage I), the well preserved S_{A1} fabric is represented by chloritoid, muscovite(I), phengite, kyanite and rutile. The S_{A2} fabric is represented by muscovite(II), paragonite, chlorite and ilmenite in deformed domains. Chloritoid (X_{Fe}= 0.60-0.72), tab. 5, forms euhedral prismatic zoned porphyroblasts (up to 2 mm, Fig. 37a, b, c and Fig. 38, 39), the X_{Fe} is decreasing towards the rim. Chloritoid is commonly associated into radial aggregates (up to 5 mm), wrapped by the S_{A2} foliation. However with increasing strain, chloritoid prisms rotate to be parallel with the S_{A2} foliation (Fig. 38b) and in most deformed samples chloritoid (X_{Mg} 0.23-0.26 in NK1F) is often replaced by chlorite (pseudomorphs are observed in NK1F sample, Fig. 38c, d). Muscovite(I), Si= 3.01-3.05 a.p.f.u., X_{Na}= 0.17-0.36, tab. 5, is preserved in porphyroclasts (up to 0.3 mm, Fig. 38a), as relic cores of larger white mica porphyroblasts and/or in close spatial association with chloritoid (Fig.38, 40a). Locally, white mica of phengite composition (Si= 3.18-3.20 a.p.f.u., X_{Na} ~ 0.18) was found adjacent to muscovite(I), Fig. 40a. Muscovite(I) porphyroclasts are wraped by the foliation mainly composed of muscovite(II) and chlorite. In the foliation, the fine grained (up to 0.5 mm) muscovite(II), Si= 3.05-3.14 a.p.f.u., X_{Na}= 0.15-0.20, Fig. 10a, tab. 5, together with chlorite

(X_{Fe}= 0.33-36, with increasing deformation the X_{Fe} is increasing up to ~ 0.39, Fig. 40b), are anastomosing around the chloritoid porphyroblasts. With increasing strain the muscovite(II), paragonite (Si= 2.9-3.0 a.p.f.u., X_{Na}= 0.75-0.85, Fig. 40a) and chlorite dominate the rock and form flakes parallel to the S_{A2} foliation (Fig. 38b,c). Kyanite is presented as randomly oriented aggregates (Fig. 38a) and could be found only in least deformed samples and/or domains (eg. NK1I and NK1F – relics of kyanite are preserved in less deformed domains). Recrystallized quartz aggregates (up to 5 mm) stretched parallel to and wrapped by the foliation are common in all studied samples. Ilmenite, rutile and quartz form inclusions in chloritoid. Additionally, the studied samples contain ilmenite, rutile, monazite and zircon.

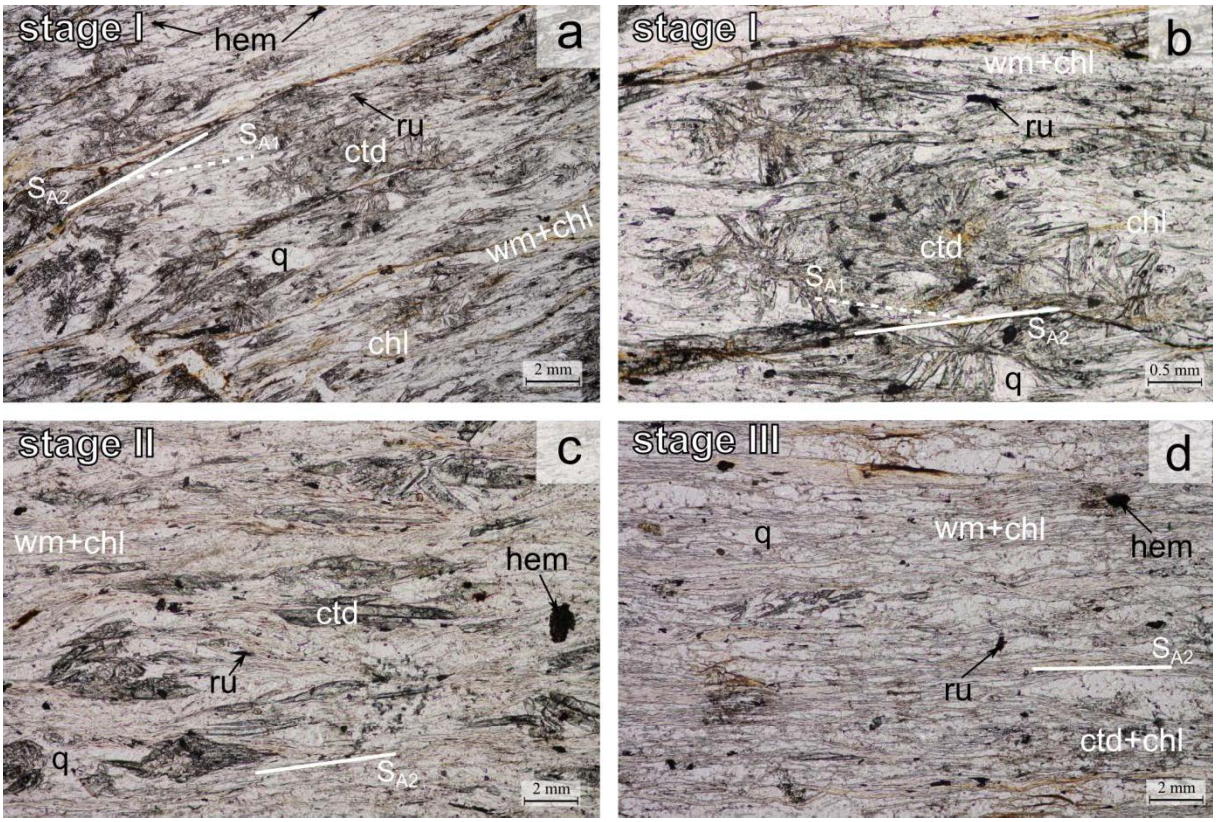

***Fig. 37**: Micrographs of deformed schists from Hanková locality. **(a)** The S_{A1} and S_{A2} metamorphic fabrics in ctd-ky schist, stage I of deformation (NK1I). **(b)** Detail on the deformed chloritoid and the S_{A2} deformation fabric defined by white mica and chlorite, stage I of deformation (NK1I). **(c)** Stage II of deformation in the sample NK1E, no kyanite is observed, chloritoid porphyroblasts are rotated to S_{A2} fabric. **(d)** Stage III of deformation in Hanková locality, chlorite pseudomorphs after chloritoid, white micas and chlorite are dominant (NK1F).*

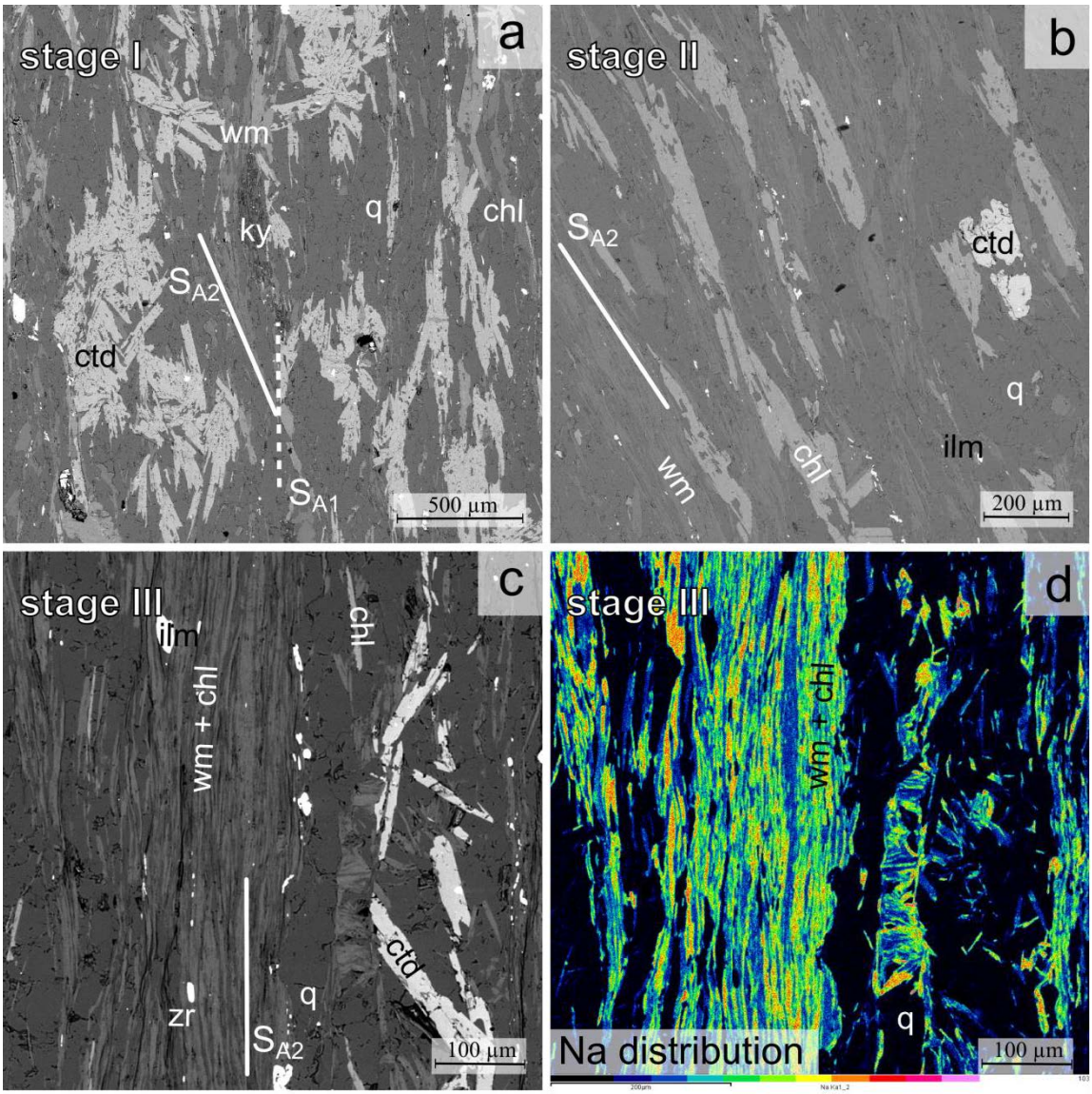

Fig. 38: *Back scattered electron (BSE) images from ctd-ky schist samples.* ***(a)*** *Radial aggregates of chloritoid prisms and kyanite aggregates (NK1I).* ***(b)*** *Chloritoid prisms are parallel to the S_{A2} foliation and partly replaced by chlorite (NK1E).* ***(c)*** *In most cases, chloritoid is replaced by chlorite, the phyllosilicates are dominant in the shear bands – the deformed domains (NK1F)* ***(d)*** *Element distribution map of sodium demonstrating the Na-enrichment in newly formed paragonite.*

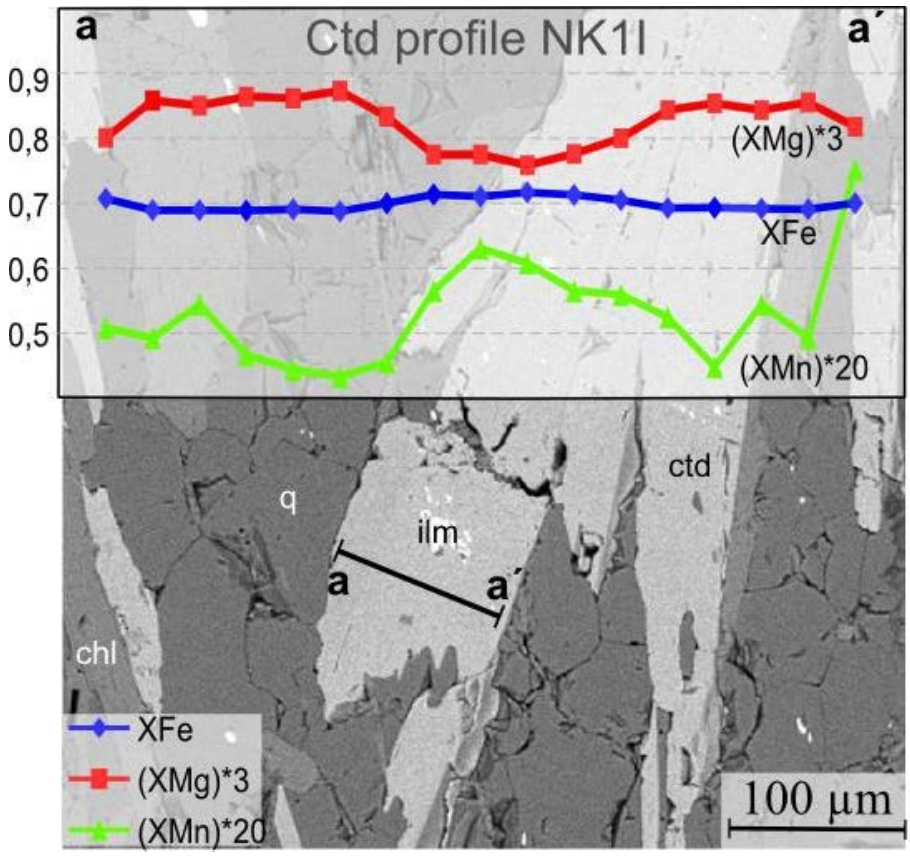

Fig. 39: *Composition profile of chloritoid in the sample NK1I with distribution of X_{Fe}, X_{Mg} (3x exaggerated) and X_{Mn} (20x exaggerated).*

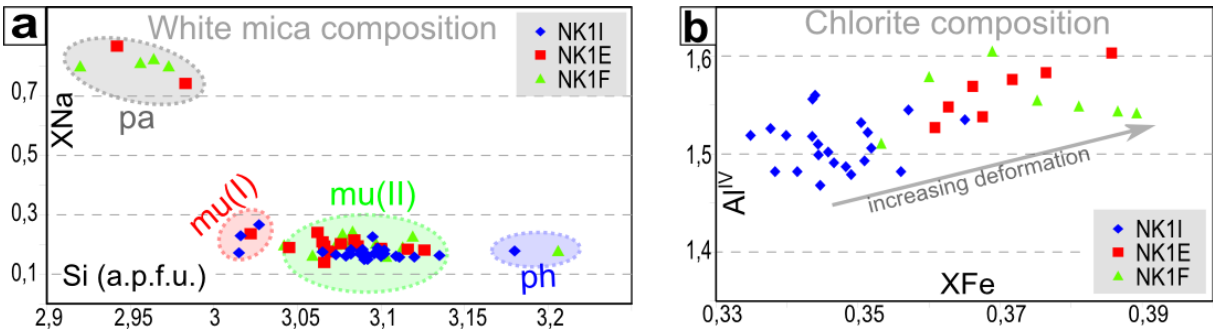

Fig. 40: ***(a)*** *Chemical composition of white micas in Hanková locality.* ***(b)*** *Chemical composition of chlorite in Hanková locality.*

	Metagranite BZ299A			Transition rock NK2C			White schist NK2A		
Analysis	17	15	10	15	28	11	78	76	77
Mineral	**chl**	**mu(I)**	**mu(II)**	**chl**	**mu(I)**	**mu(II)**	**chl**	**mu(I)**	**mu(II)**
wt . %									
SiO_2	26.34	46.89	46.76	27.34	46.76	48.38	27.67	47.36	46.76
TiO_2	0.00	0.00	0.21	0.00	0.86	0.19	0.00	0.65	0.32
Al_2O_3	23.67	33.53	36.83	23.62	32.91	38.13	24.70	33.04	37.68
MgO	22.67	1.17	0.38	23.95	1.46	0.49	24.87	1.71	0.47
FeO	11.51	1.26	0.61	10.84	1.23	0.44	9.81	1.27	0.31
MnO	0.00	0.00	0.00	0.00	0.00	0.00	0.00	0.00	0.00
CaO	0.00	0.00	0.00	0.00	0.00	0.00	0.00	0.00	0.00
Na_2O	0.00	0.91	1.80	0.00	0.49	2.10	0.00	0.67	1.65
K_2O	0.00	9.52	8.66	0.00	10.47	8.62	0.00	9.69	8.80
H_2O	11.51	4.43	4.56	10.84	4.45	4.71	12.35	4.48	4.60
Totals	**96.00**	**97.71**	**99.81**	**97.84**	**98.63**	**102.97**	**99.40**	**98.87**	**100.59**
Si	2.67	3.17	3.07	2.71	3.15	3.08	2.69	3.17	3.05
Ti	0.00	0.00	0.01	0.00	0.04	0.01	0.00	0.03	0.02
Al	2.83	2.67	2.85	2.76	2.61	2.86	2.83	2.60	2.89
Mg	3.43	0.12	0.04	3.54	0.15	0.05	3.60	0.17	0.05
Fe^{2+}	0.98	0.07	0.03	0.90	0.07	0.02	0.80	0.07	0.02
Mn	0.00	0.00	0.00	0.00	0.00	0.00	0.00	0.00	0.00
Ca	0.00	0.00	0.00	0.00	0.00	0.00	0.00	0.00	0.00
Na	0.00	0.12	0.23	0.00	0.06	0.25	0.00	0.09	0.21
K	0.00	0.82	0.73	0.00	0.90	0.70	0.00	0.83	0.73
OH	8.00	2.00	2.00	8.00	2.00	2.00	8.00	2.00	2.00
Sum	**17.91**	**8.97**	**8.97**	**17.91**	**8.98**	**8.96**	**17.90**	**8.96**	**8.96**
X_{Fe}	0.22			0.20			0.18		
X_{Na}		0.13	0.24		0.07	0.26		0.09	0.22

	Ctd-ky schist NK1I				Transition rock NK1E				
Analysis	27	49	12	19	11	32	31	26	5
Mineral	**mu(I)**	**mu(II)**	**chl**	**ctd**	**mu(I)**	**mu(II)**	**chl**	**ctd**	**pa**
wt . %									
SiO_2	44.96	46.55	25.54	24.26	45.90	47.07	25.43	24.49	44.97
TiO_2	0.24	0.20	0.00	0.00	0.15	0.00	0.00	0.00	0.00
Al_2O_3	35.77	35.69	23.10	41.54	38.18	36.48	23.89	40.91	39.91
MgO	0.62	0.68	18.51	4.31	0.36	0.56	17.29	4.40	0.00
FeO	3.28	0.39	17.04	20.40	0.27	0.43	18.40	20.68	0.14
MnO	0.00	0.00	0.12	0.79	0.00	0.00	0.27	0.77	0.00
CaO	0.00	0.00	0.00	0.00	0.19	0.00	0.00	0.00	0.59
Na_2O	1.21	1.25	0.00	0.00	2.63	1.39	0.00	0.00	6.19
K_2O	8.91	9.40	0.00	0.00	6.59	9.18	0.07	0.00	1.43
H_2O	4.47	4.49	11.46	7.30	4.55	4.55	11.51	7.28	4.58
Totals	**99.46**	**98.65**	**95.78**	**98.59**	**98.83**	**99.66**	**96.86**	**98.53**	**97.80**
Si	3.02	3.10	2.67	1.00	3.02	3.10	2.65	1.01	2.94
Ti	0.01	0.01	0.00	0.00	0.01	0.00	0.00	0.00	0.00
Al	2.83	2.80	2.85	2.01	2.96	2.83	2.93	1.98	3.08
Mg	0.06	0.07	2.89	0.26	0.04	0.06	2.68	0.27	0.00
Fe^{2+}	0.18	0.02	1.49	0.70	0.02	0.02	1.60	0.71	0.01
Mn	0.00	0.00	0.01	0.03	0.00	0.00	0.02	0.03	0.00
Ca	0.00	0.00	0.00	0.00	0.01	0.00	0.00	0.00	0.04
Na	0.16	0.16	0.00	0.00	0.34	0.18	0.00	0.00	0.79
K	0.76	0.80	0.00	0.00	0.55	0.77	0.01	0.00	0.12
OH	2.00	2.00	8.00	2.00	2.00	2.00	8.00	2.00	2.00
Sum	**9.02**	**8.97**	**17.91**	**6.00**	**8.94**	**8.96**	**17.89**	**6.00**	**8.97**
X_{Na}	0.17	0.17			0.37	0.19			0.83
X_{Fe}			0.34	0.73			0.37	0.73	
X^{Mg}			0.66	0.27			0.63	0.27	

	Phyllonite NK1F				
Analysis	70	75	76	1	103
Mineral	**mu(II)**	**chl**	**ctd**	**pa**	**ph**
wt . %					
SiO_2	46.87	25.30	24.97	45.82	49.35
TiO_2	0.17	0.00	0.00	0.00	0.18
Al_2O_3	36.00	22.89	40.04	40.15	34.57
MgO	0.63	16.73	3.50	0.06	1.19
FeO	0.58	19.80	19.62	0.23	0.57
MnO	0.00	0.12	0.70	0.00	0.00
CaO	0.00	0.00	0.00	0.47	0.09
Na_2O	1.18	0.00	0.00	5.69	1.28
K_2O	9.35	0.00	0.35	1.81	8.88
H_2O	4.53	11.30	7.15	4.63	4.61
Totals	**99.31**	**95.42**	**96.33**	**98.86**	**100.72**
Si	3.10	2.68	1.05	2.96	3.21
Ti	0.01	0.00	0.00	0.00	0.01
Al	2.81	2.86	1.98	3.06	2.65
Mg	0.06	2.64	0.22	0.01	0.12
Fe^{2+}	0.03	1.69	0.69	0.01	0.03
Mn	0.00	0.01	0.03	0.00	0.00
Ca	0.00	0.00	0.00	0.03	0.01
Na	0.15	0.00	0.00	0.71	0.16
K	0.79	0.00	0.02	0.15	0.74
OH	2.00	8.00	2.00	2.00	2.00
Sum	**8.96**	**17.89**	**5.97**	**8.94**	**8.91**
X_{Na}	0.16			0.80	0.18
X_{Fe}		0.39	0.76		
X^{Mg}		0.61	0.24		

Tab. 5: *Representative chemical analyses of selected minerals from the Žabica (BZ299A, NK2C and NK2A) and Hanková(NK1EI, NK1E and NK1F) localities. Chloritoid analyses were normalized to 12 oxygens, chlorite was normalized to 14 oxygens and white mica analyses were normalized to 11 oxygens. Values are given in wt. %. Mineral abbreviations are after Holland and Powell (1998).*

4.3 WHOLE ROCK CHEMISTRY

4.3.1 ŽABICA LOCALITY

The metagranite of the Žabica locality has the composition of a peraluminous granite (A/CNK = 4.99), tab. 6. As it approaches the centre of the shear zone, the hosting metagranite appears progressively enriched in micas and in Mg-rich minerals (Fig. 35f). Our samples allow to define three metasomatic stages, representative for a progressive increase in metasomatism and deformation, starting from the least deformed sample of metagranite (BZ299A) – stage(I), to the deformed mylonitic white schist sample (NK2A) – stage(III). With respect to the average continental crust, the samples show selective enrichments in Th, U, La, Ce, Pr, Nd, Zr and Sm (this trend is decreasing with increasing deformation from stage(I) to stage(III)) and strong depletions in Cs, Ba, Pb, Sr, and P, moderate depletions in Eu, Ti, Y, Yb and Lu. With increasing deformation, the rocks are depleted in Rb (Fig.41, tab. 6). Comparison of the two rocks in an isocon diagram (Fig. 41) is allowed by the field observation from which we infer that the whiteschist (NK2A) was derived from the metagranite (BZ299A) through fluid-rock interaction. This genetic relation is a posteriori confirmed by the good correlation defined by the elements that are classically considered immobile during fluid-rock interaction at mid-crustal conditions (Al, Ti, P, Th, Nb, Ta, Zr, Hf, Y- the immobility of these elements was confirmed through the wedge plots construction, after Ague, 1994, not shown here). These elements define a line, which corresponds to an isocon (Grant 1986). The slope of the isocon allows for the calculation of the mass variation during alteration. The slope value (y = 1.47) points to about 32% loss of mass, which corresponds to a major decrease in volume during alteration, provided that the rock densities were not significantly affected by metasomatism. Elements that plot below the isocon were lost during alteration. From Fig. 41, we infer that leaching of SiO_2 and K_2O account for most of the mass lost. An interesting feature is the increased amount of MgO, FeO, NiO and MnO. The enrichment of MgO was described in other shear zones well known in the Alps (Ferrando, 2012 and references therein), however not in the association of the FeO, NiO and MnO enrichment.

Sample	BZ299A	NK2A	NK1I	NK1F		BZ299A	NK2A	NK1I	NK1F
SiO_2	70.07	32.09	65.43	74.59	La	29	12.5	27.2	26.2
Al_2O_3	15.14	25.32	19.71	16.47	Ce	61.3	23.3	57	52.8
Fe_2O_3	2.86	9.42	5.77	0.87	Pr	7.16	2.72	6.47	5.66
MgO	4.94	21.03	1.52	0.48	Nd	27.8	9.1	25.3	20.2
CaO	0.05	0.02	0.24	0.22	Sm	6.5	2.05	5.13	3.87
Na_2O	0.44	0.27	0.38	1.37	Eu	0.55	0.14	0.93	0.89
K_2O	2.05	1.2	2.57	2.39	Gd	4.8	1.33	4.89	4.14
TiO_2	0.27	0.37	0.93	0.71	Tb	0.64	0.16	0.82	0.69
P_2O_5	0.06	0.02	0.2	0.1	Dy	2.72	0.76	4.9	4.11
MnO	0.01	0.03	0.06	0.02	Ho	0.48	0.1	0.97	0.91
Cr_2O_3	<0.002	<0.002	0.011	0.008	Er	1.02	0.27	2.8	2.81
Sc	4	8	17	9	Tm	0.15	0.07	0.42	0.45
Ba	136	67	413	221	Yb	1.12	0.68	2.84	3.09
Be	2	<1	2	1	Lu	0.13	0.1	0.39	0.4
Co	1.8	8.4	7.7	6.8	Mo	<0.1	<0.1	<0.1	<0.1
Cs	0.4	0.2	9.2	10	Cu	0.7	0.6	18.5	38.9
Ga	16.2	28.5	23.7	18.4	Pb	0.7	0.6	1.6	1.4
Hf	4.4	5.6	5.5	6.6	Zn	4	10	6	2
Nb	6.4	8.3	18.7	14.4	Ag	<0.1	<0.1	<0.1	<0.1
Rb	72.7	37.8	104.4	88.5	Ni	1.8	8.5	20.2	6.4
Sn	<1	4	4	3	As	<0.5	<0.5	1.9	33.1
Sr	25.8	15.5	124.5	223.5	Au	<0.5	<0.5	<0.5	1
Ta	0.4	0.8	1.5	1.1	Cd	<0.1	<0.1	<0.1	<0.1
Th	14.5	21.3	13.4	11.4	Sb	<0.1	<0.1	0.2	0.1
U	3.7	2.7	2.4	2.8	Bi	<0.1	<0.1	<0.1	0.1
V	19	42	115	95	Hg	<0.01	<0.01	0.01	0.02
W	<0.5	<0.5	3.6	2.8	Tl	<0.1	<0.1	<0.1	<0.1
Zr	139.3	195.6	198.1	224.7	Se	<0.5	<0.5	<0.5	<0.5
Y	13	3.7	26.8	24.8					

***Tab. 6**: Whole rock analyses of selected samples. Values are given in wt.%.*

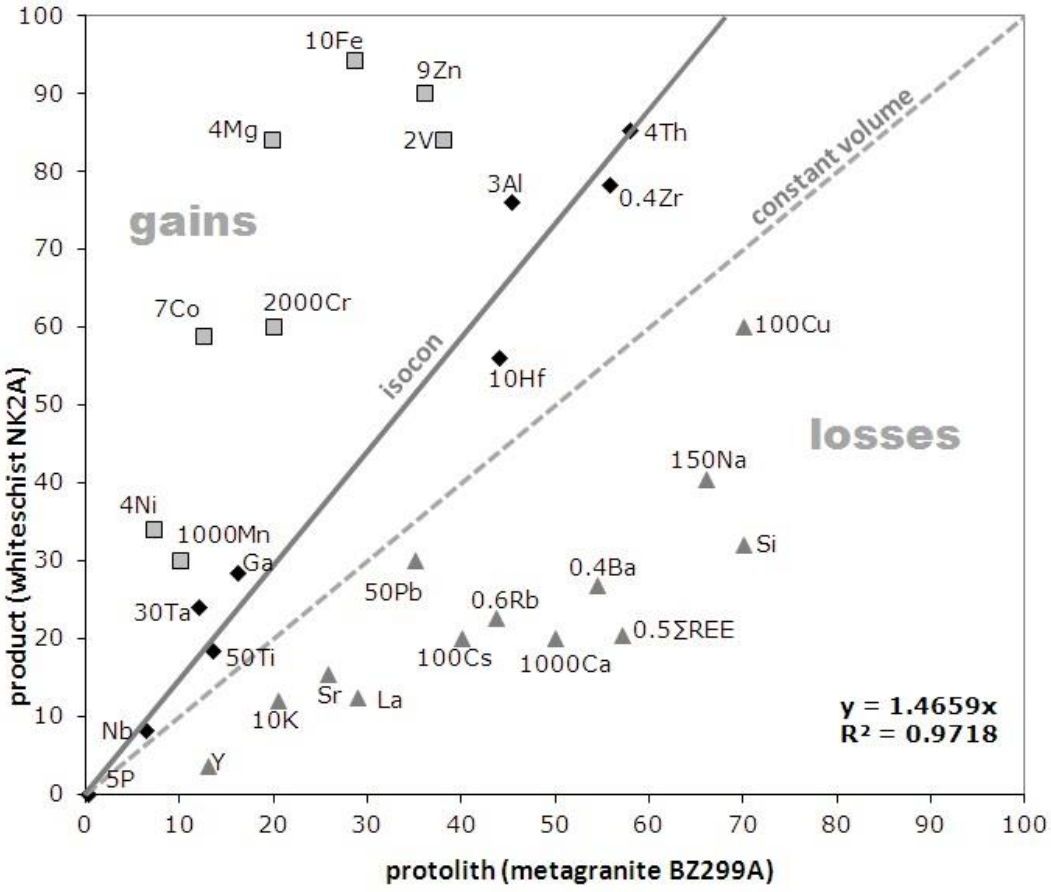

Fig. 41: *Isocon diagram (Grant 1986) showing variations in element concentration between the metagranite (protolith) and the whiteschist (product). Major elements are plotted as wt% oxide and trace elements as ppm (Table 6). Scaling factors are indicated. Straight line is the isocon fit to immobile elements (black diamonds). Slope and correlation coefficient (R2) the lower right corner of the diagram. Squares and triangles indicate elements that increased and decreased in amount, respectively, during metasomatism.*

4.3.2 HANKOVÁ LOCALITY

Contrary to the Mg, Fe-enrichment in Žabica locality, in Hanková we have observed different alteration trend in the chloritoid-kyanite schists. The studied samples allow three metasomatic stages to be defined. Stage(I) is represented by the least deformed sample of ctd-ky schist (NK1I) with well developed S_{A1} metamorphic fabric. Stage(I) proceeds through stage(II) to stage(III) which is represented by fine grained phyllonite (domains in NK1F), completely obliterated by the S_{A2} metamorphic fabric. However, due to the "domain" structural character of the NK1F sample, the whole rock composition resembles to the composition of transition phase from stage(I) to stage(III). The majority of elements show variation across the

shear zone. Comparison of the two extreme rocks (stage(I) vs. stage(III)), Fig.42 is supported by the field observation from which we infer that the phyllonite domain (NK1F) was derived from the ctd-ky schist (NK1I) through fluid-rock interaction. Based on the isocon analysis the ctd-ky schists compared the fine grained phyllonites are enriched in Na_2O, SiO_2, K_2O, Sr, Zr and depleted in MgO, FeO, NiO. Based on the wedge plots (Ague, 1994), the P, Cr, Nb, V, Y, La, Ta, Ti, Th, Al, Pb, Co and Ga were considered as immobile during the metasomatic process. The slope value (y = 0.82) points to about 22% gain of mass, which corresponds to an increase in volume during alteration. This observed trend of the alteration seems to be opposite to the trend observed in Žabica locality.

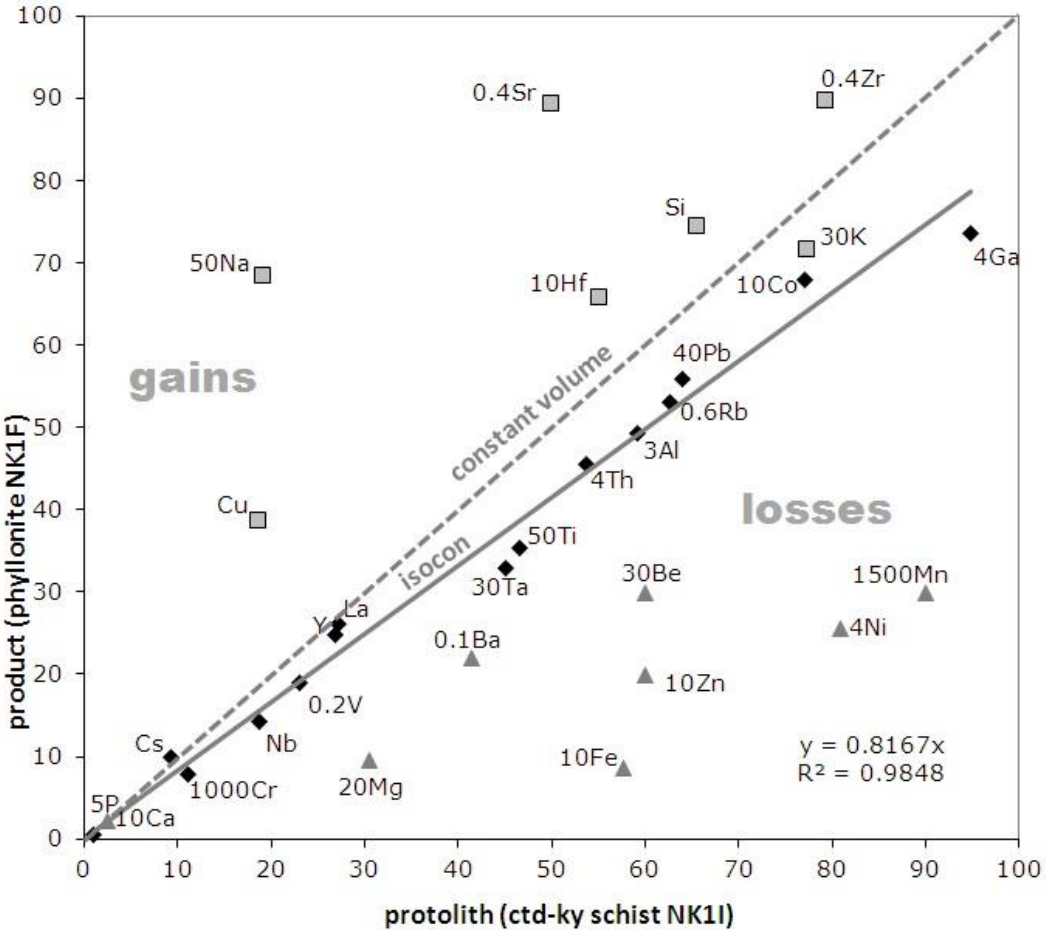

Fig. 42: *Isocon diagram (Grant 1986) showing variations in element concentration between the ctd-ky schist (protolith) and the phyllonite (product). Major elements are plotted as wt% oxide and trace elements as ppm (Table 6). Scaling factors are indicated. Straight line is the isocon fit to immobile elements (black diamonds). Slope and correlation coefficient (R2) the lower right corner of the diagram. Squares and triangles indicate elements that increased and decreased in amount, respectively, during metasomatism.*

4.4 P-T ESTIMATES

A petrological study of the samples from two different shear zones was performed. The majority of elements show continuous changes in relation to their deformational stage. The least and the most deformed samples were selected to obtain P-T estimates. P-T pseudosections and compositional isopleths were calculated using the thermodynamic modelling software Perple_X version 6.6.8 (Connoly, 2005) and the internally consistent thermodynamic dataset hp04 (Holland and Powell, 1998).

4.4.1 ŽABICA LOCALITY

To model the P-T pseudosection for metagranitic sample (BZ299A) and the whiteschist sample (NK2A) the system MnO-Na_2O-K_2O-FeO-MgO-Al_2O_3-SiO_2-H_2O-TiO_2 (MnNKFMASHT). The whole rock composition used to calculate the P-T section is presented in Fig. 43 and tab. 6. All CaO (0.05 wt.%) is combined with P_2O_5 to form apatite and therefore CaO component was excluded from the calculation. The mixing models for white mica (Auzanneau et al., 2010; Coggon et al., 2002), chlorite (Holland and Powell, 1998), chloritoid (Holland and Powell, 1998), garnet (White et al., 2000), ilmenite (White et al., 2000) and staurolite (Holland and Powell, 1998) were used. In the resulting P-T pseudosection for the sample BZ299A (Fig. 43), the equilibrium assemblage chlorite, muscovite, kyanite, rutile and quartz corresponds to a large stability field (450-700 °C, 4-12 kbar). The stability filed is limited by disappearance of kyanite towards higher temperatures and appearance of chloritoid towards the lower temperatures. The modelled compositional isoplethes for chlorite X_{Fe} in the analysed chlorite grains is ~ 0.22 which was used to further constrain the equilibration P-T conditions. This corresponds well to the equilibrium assemblage values (not shown in pseudosection, see Fig. 44). For the NK2A sample in the resulting P-T pseudosection, the equilibrium assemblage chlorite, muscovite, rutile and quartz corresponds to a narrow stability field yielding a temperature interval 350-450 °C and 3-6 kbar (Fig. 43). The field is limited by appearance of kynite towards the higher temperatures and by appearance of paragonite towards the lower temperatures and higher pressures. The modeled compositional isopleths for chlorite were used to further constrain the equilibration P–T conditions. The X_{Fe} in the analysed chlorite grains is ~ 0.18 which corresponds well to the stability field (not shown in pseudosection, see Fig. 44).

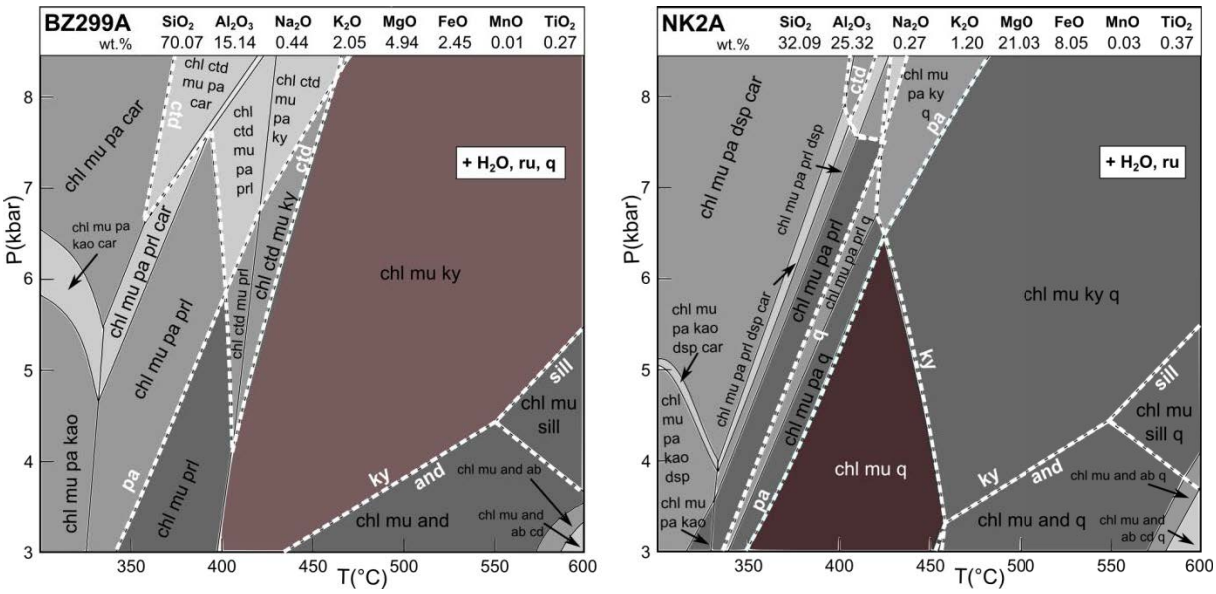

Fig. 43*: P-T pseudosections for the metagranite (BZ299A) and whiteschist (NK2A) sample. The section was calculated in MnNKFMASHT system using Perple_X 6.6.8. The bulk rock composition used for the calculation in weight proportion is indicated above the section.*

To check the influence of the bulk chemistry and in particular the possibility that the observe mineral assemblage do not represent different P-T conditions, but only reflect the progressive evolution of the effective bulk composition under constant pressure and temperature, we have calculated an isobaric T-X pseudosection (Fig. 44). This diagram displays the mineralogical variation as a function of temperature and chemical composition of the rock at 5 kbar. The bulk composition varies between that of the metagranite (BZ299A) to that of the whiteschist (NK2A). The geometric progression from the left to the right of the diagram models a progressive metasomatic evolution related to increasing fluid-rock interaction. Therefore the metagranite mineral assemblage and the whiteschist develop under distinct pressure and temperature conditions. This fact is furthermore supported by the modal proportion evolution of kyanite and chlorite and by the composional change of chlorite (Fig. 44). The amount of chlorite is rapidly increasing with the FeO and MgO income. Based on the observed mineral assemblage and its modal proportion we expect the reequilibration for the D_{A2} event to take place at 400-450 °C at 4-5 kbar.

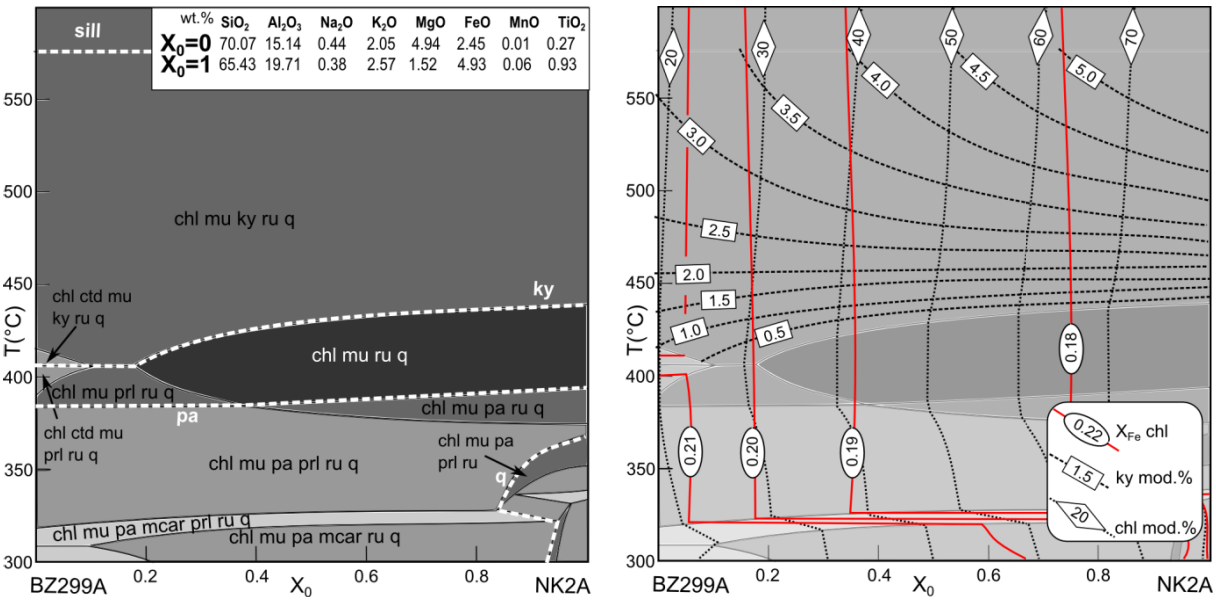

***Fig. 44**: T-X pseudosection calculated at 5 kbar for the samples. X=0 corresponds to the metagranite (BZ299A) composition and X=1 corresponds to whiteschist (NK2A) composition. This T-X section was constructed to show the mineral composition and proportion changes durig the isobaric metasomatic event. The modal proportion of kyanite, chlorite and the chlorite compositional isopleths (X_{Fe}) are shown.*

4.4.2 HANKOVÁ LOCALITY

To model the P-T pseudosection for chloritoid- kyniate schists (NK1I) proceeding to phyllonites (NK1F) the system $MnO\text{-}Na_2O\text{-}K_2O\text{-}FeO\text{-}MgO\text{-}Al_2O_3\text{-}SiO_2\text{-}H_2O\text{-}TiO_2$ (MnNKFMASHT) was used. The whole rock composition used to calculate the P-T section is presented in Fig. 45 and tab. 6. All CaO (0.20 wt.% in both samples) is combined with P_2O_5 to form apatite and therefore CaO component was excluded from the calculation. The mixing models for white mica (Auzanneau et al., 2010; Coggon et al., 2002), chlorite (Holland and Powell, 1998), chloritoid (Holland and Powell, 1998), garnet (White et al., 2000), ilmenite (White et al., 2000) and staurolite (Holland and Powell, 1998) were used. In the resulting P-T pseudosection for the sample NK1I (Fig. 45), the equilibrium assemblage chlorite, chloritoid, muscovite, kyanite, rutile and quartz corresponds to a narrow stability field. The stability filed is limited by disappearance of kyanite towards lower temperatures as well as towards higher temperatures. The modelled compositional isoplethes for chloritoid and chlorite were used to further constrain the equilibration P-T conditions (Fig. 45). The X_{Fe} in the analysed chlorite grains is ~ 0.33-0.35, yielding the narrow interval for temperature of 450-500°C in the stability field. In the chloritoid, the X_{Mg} is increasing towards the rim from 0.26 to 0.28 (see Fig. 46).

The modelled isopleths corresponds to 5-7 kbar and 450-500 °C. The observed fabric S_{A2} is represented by the chloritoid, muscovite(II), paragonite, chlorite (II, Fig. 38a) and this assemblage corresponds to 390-450 °C

For the NK1F sample in the resulting P-T pseudosection, the relic older equilibrium assemblage of chlorite(I), chloritoid, muscovite(I), paragonite, kyanite, rutile and quartz corresponds to a large stability field yielding a temperature interval 400-500 °C. The field is limited by disappearance of kyanite towards the lower temperatures and by appearance of garnet towards the higher temperatures. The modelled compositional isopleths for chlorite and chloritoid were used to further constrain the equilibration P–T conditions. The X_{Fe} in the analysed chlorite(I) grains is ~0.35-0.37 which corresponds to the higher temperatures within the stability field. In the chloritoid, the X_{Mg} ranges 0.26-0.30. These corresponds to ~5.5 kbar and ~ 520 °C in the calculated pseudosection (Fig. 45). In deformed domains the equilibrium assemblage is being obliterated by the chlorite(II) X_{Fe} ~ 0.37-0.39, muscovite(II) and paragonite assemblage, with relic chloritoid X_{Mg} ~0.23-0.26 (fig. 37d, fig. 38c). This assemblage correspons to lower PT estimates – 300-400 °C at 3-6 kbar.

To check the influence of the bulk chemistry and in particular the possibility that the observe mineral reequilibrated assemblage do not represent different P-T conditions, but only reflect the progressive evolution of the effective bulk composition under constant pressure and temperature, we have calculated an isobarical T-X pseudosection (Fig. 46). This diagram displays the mineralogical variation as a function of temperature and chemical composition of the rock at 5 kbar. The bulk composition varies between that of the ctd-ky schist (NK1I) to that of the phyllonite (NK1F). The geometrical progression from the left to the right of the diagram models a progressive metasomatic evolution related to increasing fluid-rock interaction. Therefore the ctd-ky schist mineral assemblage and the phyllonite develop under distinct pressure and temperature conditions. This fact is furthermore supported by the modal proportion evolution of chlorite where the modal amount is decreasing with progressive metasomatism and as the Na_2O increases, the amount of paragonite in deformed rocks rapidly increases (Fig. 46).

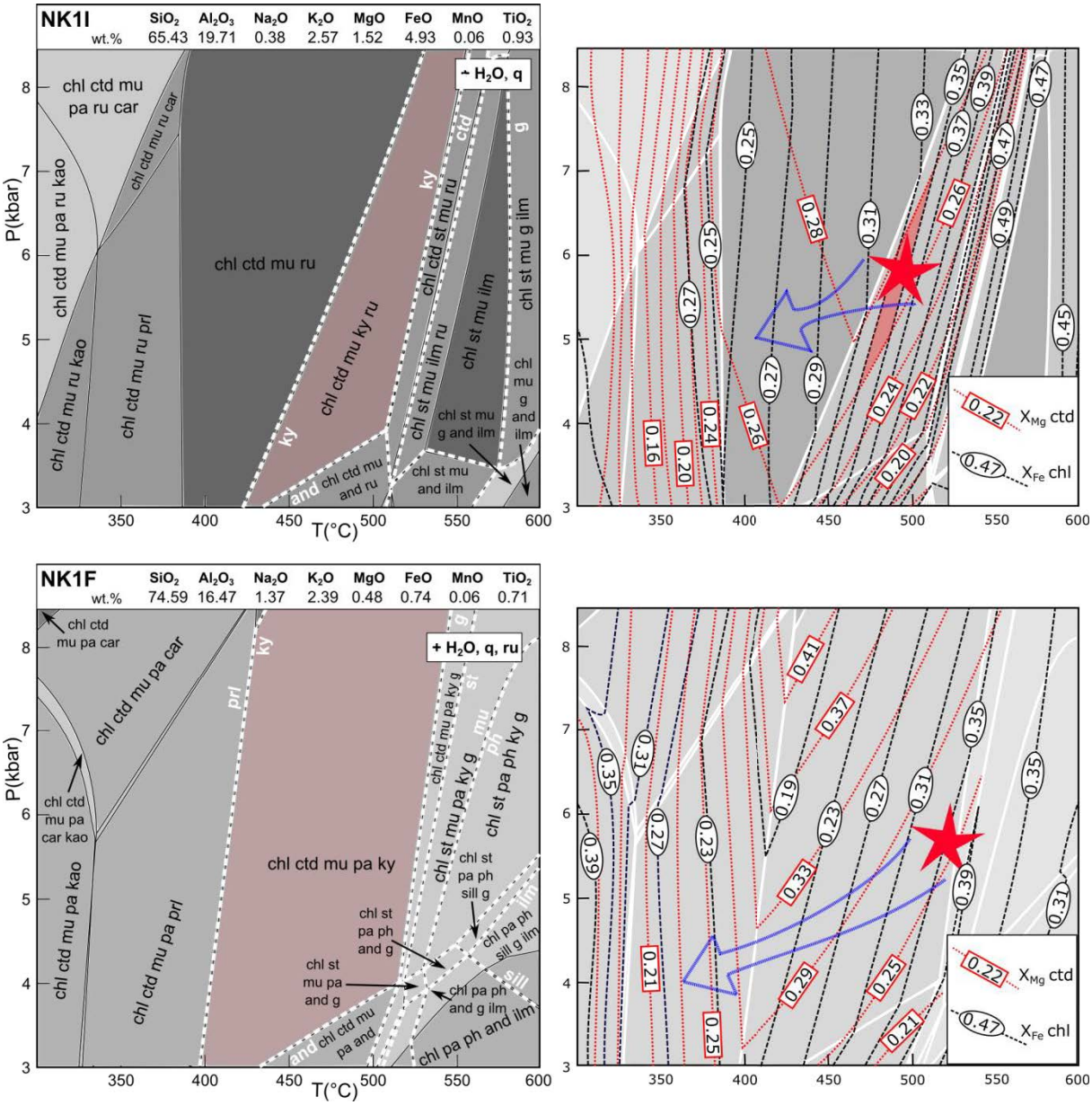

***Fig. 45**: P-T pseudosections for the ctd-ky schist (NK1I) and phyllonite (NK1F) sample with compositional isopleths of X_{Fe} in chlorite and X_{Mg} in chloritoid. Resulting P-T conditions are highlighted (by red in NK1I and by star in NK1F). The section was calculated in MnNKFMASHT system using Perple_X 6.6.8. The bulk rock composition used for the calculation in weight proportion is indicated above the section.*

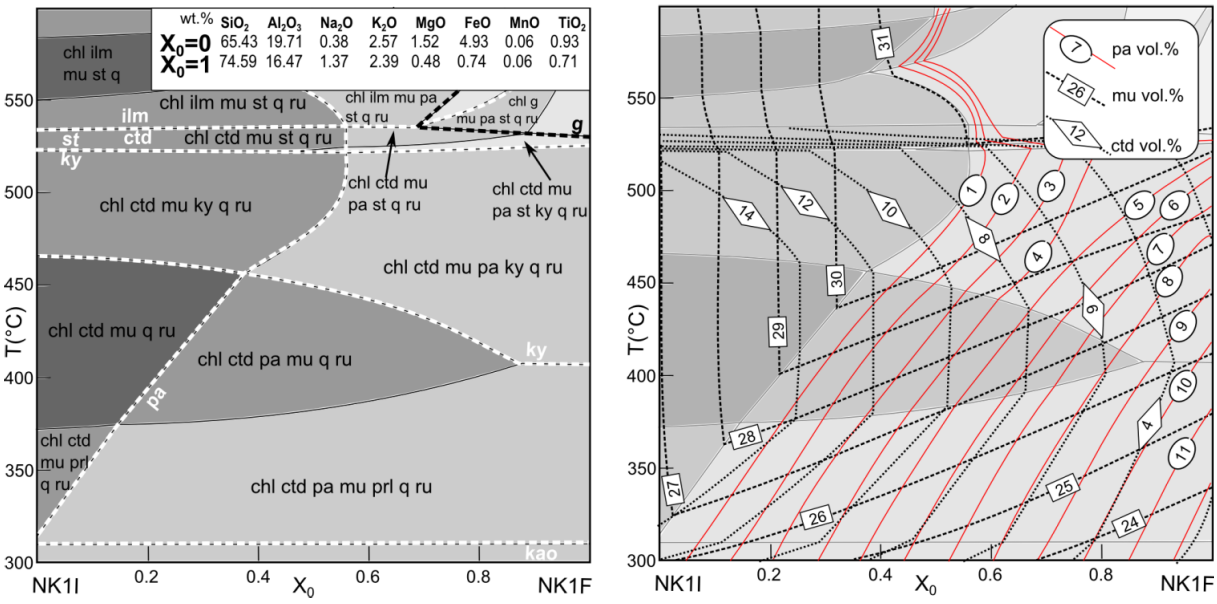

Fig. 46: *T-X pseudosection calculated at 5 kbar for the samples. X=0 corresponds to the ctd-ky schist (NK1I) composition and X=1 corresponds to phyllonite (NK1F) composition. This T-X section was constructed to show the mineral composition and proportion changes during the isobaric metasomatic event. The modal proportion of paragonite, muscovite and chloritoid are shown.*

4.5 DISCUSSION

4.5.1 THE P-T ESTIMATES AND ITS RELATION TO THE DEFORMATION HISTORY OF THE REGION

Besides the Variscan greenschist- to amphibolite-facies deformation and metamorphism, the studied area was affected by the post-Variscan extensional event associated with intrusion of the Permian Rochovce granite, and the polyphase tectono-metamorphic evolution during the Cretaceous (Jeřábek et al., 2012; Neméth et al., 2004; Novotná et al., 2015). During the Early Cretaceous evolution, the Vepor Unit was first buried (D_{A1}) due to the northward over-thrusting by the Gemer Unit (Lexa et al., 2003; Jeřábek et al., 2007, 2012). The ongoing northward movement and indentation of the Gemer Unit during the Cretaceous was followed by southward under-thrusting of the northerly Fatric domain below the Vepor Unit which led to doming and exhumation of deeper parts of the Vepor basement (D_{A2}) during the mid-Cretaceous (Plašienka 2003; Jeřábek et al., 2008, 2012). The doming was associated extensional unroofing of the Vepor Unit (Bukovská et al., 2013; Janák et al., 2001; Vojtko et al., 2016) and eastward lateral escape of the Gemer Unit (D_{A3}) along the transpressive Trans Gemer Shear Zone (Lexa et al., 2003; Jeřábek et al., 2012). Alpine metamorphic conditions reached generally amphibolite facies conditions in the Vepor Unit and greenschist facies conditions in the Gemer Unit (Janák et al., 2001; Jeřábek et al., 2008; Faryad et al., 1991a).

The obtained P-T estimates in this chapter correspond to the previously published data from the area (e.g. Jeřábek et al., 2008; Novotná et al., 2015) and to the Alpine metamorphic gradient (see Fig. 29). In the Vepor basement, the Alpine metamorphic conditions range in a variety of P–T conditions depending on the structural position of the studied samples (430-620 °C at 5-11 kbar; Janák et al., 2001; Jeřábek et al., 2012, 2008; Plašienka et al., 1999). In the metasedimentary cover overlying the central portion of the Vepor basement, the P–T conditions are 350-400 °C at 4-4.5 kbar (Lupták et al., 2003), whereas in the Gemer-Vepor Contact Zone the Permian cover recorded 530-560 °C at 4.5-8 kbar (Lupták et al., 2000), similar to the underlying Vepor basement schists.

For the Žabica locality, situated within the Carboniferous granitoid Complex in the close vicinity to the Gemer-Vepor Contact Zone, the sample BZ299A, which is the least affected by metasomatism, shows equilibrium assemblage of chlorite, muscovite, kyanite, rutile

and quartz. This assemblage spans over relatively large field of stability in the calculated PT section with estimated PT range of 450-700 °C at 4-12 kbar (Fig. 43) and it is interpreted to result from the prograde metamorphism during the burial of the Vepor Unit below the overthrusting Gemer Unit (Janák et al., 2001; Jeřábek et al., 2008, 2012). Similar conditions of the same burial event have been reported by Jeřábek et al. (2008) from nearby locality BL1 with estimated P-T conditions of 520-540 °C and 8-9 kbar. Although this event is typically associated with development of deformation fabric S_{A1}, the single deformation fabric observed in the studied Žabica locality is ascribed to the later exhumation fabric S_{A2} based on the dominating matrix minerals assemblage and progressive disappearance of kyanite in more deformed samples (see below). It is thus suggested that the S_{A1} fabric is either very weak or missing in the granitoids from the Žabica locality, which are likely only metamorphosed during the D_{A1} event. In samples showing higher degree of deformation kyanite as well as the muscovite(I) and chlorite(I) progressively disappear.

The secondary assemblage in the "white schist" Sample NK2A, shows equilibrium assemblage of chlorite, muscovite, rutile and quartz, where muscovite and chlorite show different composition with respect to muscovite(I) and chlorite(I) in the sample BZ299A. This assemblage corresponds to the estimated PT range of 350-450 °C and 3-6 kbar (Fig. 43), which is interpreted to reflect the exhumation conditions during the D_{A2} event. The kyanite-Mg-chlorite schists identified in the studied region were previously studied by Kováčik (1996). In his work, also only one deformation fabric has been identified however, the kyanite is interpreted to form together with Mg-chlorite during the development of deformational shear zones (Kováčik, 1996). In contrast in our study, the kyanite formation is associated with the prograde metamorphism during the D_{A1} metamorphic event while the formation of Mg-chlorite is associated with consumption of muscovite and forms later during the D_{A2}. This assumption is based on the results of our thermodynamic modelling and construction of T-X section (Fig. 44) showing that both metagranite (BZ299A) and whiteschist (NK2A) samples should contain kyanite at temperatures above ~425 °C (at 5 kbar). The lack of kyanite in the whiteschist sample NK2A, however, points to equilibrium at lower temperatures. This result is in accordance with two distinct PT estimates obtained for equillibrium assemblage in each of the samples which is in favor of the two events interpretation.

The increasing modal proportion of chlorite and its compositional change towards the composition of the whiteschist sample NK2A in the T-X section (Fig. 44) documents the

metasomatic process as the amount of chlorite is rapidly increasing with the FeO and MgO income. Based on the observed mineral assemblage and its modal proportion we expect the metasomatism and reequilibration to took place during the D_{A2} event at 400-450 °C and 4-5 kbar (Fig. 43).

In Hanková locality we were able to obtain the PT estimates for the older metamorphic fabric, associated with the D_{A1} metamorphic event. For the ctd-ky schist (NK1I) the PT estimates are 5-7 kbar and 450-500 °C and for the phyllonite (NK1F) ~5.5 kbar and ~ 520 °C in calculated pseudosection. Similar estimates (530-560 °C at 4.5-8 kbar) for this event has been presented by Lupták et al., 2000. For the S_{A2} fabric, interpreted to form due to exhumation and unroofing during the D_{A2} event, the assemblage corresponds to the temperature of 390-450 °C, 300-400 °C at 3-6 kbar respectively (Fig. 45).

The increasing modal proportion of paragonite towards the composition of the phyllonite sample NK1F in the T-X section (Fig. 46) documents the metasomatic process as the amount of paragonite is rapidly increasing with the K_2O and Na_2O income (see Fig. 38d for the Na distribution in deformed domain). The modal proportion of chloritiod is decreasing towards the phyllonite (NK1F) composition – this demonstrates the loss of Fe and Mg during the metasomatic process. Based on the observed mineral assemblage and its modal proportion we expect the metasomatism and reequilibration to take place during the D_{A2} event.

4.5.2 TIMING OF THE METASOMATISM AND APPLICATION ON THE TALC DEPOSITS EVOLUTION

Despite the extensive mining of magnesite on both sides of the Gemer-Vepor Contact zone in the so-called "Ochtiná zone" and "Sinec zone", the talc of economic accumulation could be found only within the Sinec shear zone. The magnesite ore deposits had been interpreted to form during the Upper Permian extensional tectonic regime (Neméth at al., 2004). The Permian extension regime allowed the Mg-bitter brines to penetrate along the extensional faults and interact with the Lower Paleozoic or Lower Carboniferous rocks (Radvanec et al., 2010 and reference therein). Identical model had been proposed to explain the magnesite formation in the Veitsch nappe of the Eastern Alps (Prochaska, 2000, Fig. 31).

The ore deposits in Sinec zone are surrounded by the rocks reaching up to amphibolite facies condition. The origin of these strongly mylonitized talc ore deposits remain unsolved. Some authors interpreted the magnesite ore deposits to be derived from Vepor basement (Molák at al., 1995). Another group of authors has proposed the model where calcite in Carboniferous limestone embedded in schists was replaced by talc and dolomite during the Permo-Triassic rifting stage at temperatures of 280-400 °C, determined using the combination of isochores with the data from geothermometers (Radvanec et al., 2010 and reference therein). The temperatures of ~ 370-420 °C were determined using the carbonate geothermometer for the magnesite in the Ochtiná Unit (Radvanec and Prochaska, 2001; Koděra and Radvanec, 2002).

Some more recent publications associate the formation of talc deposits with metasomatism related to Alpine tectono-thermal processes (Hurai et al., 2011; Kováčik, 1996). Based on the study of the kyanite-Mg-chlorite schist in the Sinec zone, it was proposed that the talc formation occurs due to the magnesite steatitization during the Cretaceous tectono-thermal reactivation of Vepor basement (Kováčik, 1996). Alternatively, the talc formation was interpreted to be the result of an increased thermal gradient during the unroofing of the Vepor Unit due to its crustal extension during the D_{A2} event, and its gradual continuation – change of kinematics from unroofing to regional transpressional shearing – D_{A3} (Neméth et al., 2004). However, the timing of these events remains discussed.

The Cretaceous polyphase evolution is documented by geochronological data. Lower Cretaceous deformation initiated 135-95 Ma by the so-called Gemer Cleavage Fan formation, which is the dominant structure observed in the Gemer Unit and it is represented by a lower-

grade E-W trending cleavage fan-like structure (Hurai et al., 2008, Lexa et al., 2003; Vojtko et al., 2016). Northward propagation of nappe stacking is responsible of crustal thickening due to overthrusting and continuous internal deformation of Gemer Unit together with prograde metamorphism in Vepor Unit due to its burial to the depth of ~ 15-40 km (Vojtko et al., 2016). $^{40}Ar/^{39}Ar$ data reveal hornblende ages of 115-105 Ma in Central Vepor Unit (Kováčik, 1996) and 105-100 Ma white mica ages in weakly metamorphosed southern Vepor cover (Dallmeyer et al., 1996; Putiš et al., 2009). This prograde event resulted into elevated temperatures and relatively cold orogenic geothermal gradient (Jeřábek et al., 2012).

Later, this convergent process in Central Western Carpathians switched from top driven to bottom driven, and the exhumation of the lower crust occurred due folding and doming of Vepor Unit along large-scale detachment and lead to the eastward unroofing of Vepor Unit (e.g. Jeřábek et al., 2012, Novotná et al., 2015). Two distinct phases of exhumation were recognized. The first phase took part at ~ 90 - 80 Ma and it could be connected to heterogeneous exhumation of the Vepor basement in the cores of large-scale antiforms and associated formation of detachment shear zones in the upper parts of the Vepor dome (Jeřábek et al., 2012; Vojtko et al., 2016). This process allowed exhumation of previous burial isotherms resulting into higher geothermal gradient during this D_{A2} event. The proposed timing of this event is also supported by the previous studies showing large quantity of $^{40}Ar/^{39}Ar$ white mica cooling ages ranging between 87 and 84 Ma associated with the detachment lower-grade cleavage (Dallmeyer et al., 2005; Putiš et al., 2009). The second phase of exhumation associated with continuous underthrusting of the Tatric-Fatric Unit is characterized by an en-block exhumation of the already finalized internal structure of the Vepor Unit. For this phase, Vojtko et al. (2016) suggested slow cooling from 300 ± 50 °C to 60 °C between ~80 – 55 Ma documented by the zircon and apatite fission track data from Gemer and Vepor Units spanning between 89-54 Ma (see also Kráľ, 1996; Plašienka et al., 2007).

It is anticipated that the exhumation process and associated deformation D_{A2} prior to en-bloc exhumation (i.e. between ~90-80 Ma) allowed the fluids to be released and transported through different lithological complexes of the Gemer-Vepor Contact Zone and cause the metasomatic changes.

4.5.3 COMPLEX CRUSTAL-SCALE MASS TRANSFER, THE SOURCE OF FLUID

Two types of shear zones with contrasting metasomatic record have been recognized in the Vepor Unit. Mg, Fe, Ni and Mn-enriched shear zones heterogeneously develop within the Carboniferous granitoids resulting in the formation of white schists. The formation of these schists is associated with the leaching of SiO_2 and K_2O and with 32 % volume loss (Fig. 41).

In contrast, the second type of shear zones developed within chloritoid-kyanite-bearing schists of the Veporic Permian cover is characterized by a loss of Fe, Mg and Ni, gain of Si and K leading to the formation of a chlorite-muscovite-quartz phyllonite by 22 % of volume increase (Fig. 42).

The strong enrichment in Mg, Fe, Ni and Mn in the first case, and the loss of Fe, Mg and Ni in the second case, suggest either two separate metasomatic events in the studied area or the complex crustal-scale mass transfer (fig. 47).

The D_{A2} deformation phase led to the development of large-scale detachment shear zones that allowed the fluids to circulate and exchange elements through different lithological complexes of the Gemer-Vepor Contact Zone. If it is so then the magnesite ore deposits situated within the Ochtiná Nappe were the source of the Mg-rich fluid that circulate through the Vepor basement granite by creation of the "white schists" in Žabica locality. We expect the volume loss in the Žabica to be the result of the Si-rich fluid release that is responsible for the generation of talc deposits. Based on our study the metasomatic event is a coupled process, where deeper parts are enriched in Mg, Fe, Ni and Mn, whereas the upper parts of the lithological complexes are depleted in these elements (Fig. 47).

The magnesite ore deposits in the Ochtiná zone are located in the tectonic superposition of talc deposits in the Sinec zone. The occurrence of talc in Ochtiná zone due to the steatitization is documented along brittle deformational structures – such as cracks and smaller faults within the magnesite ore bodies (Fig. 47, Radvanec et al., 2010 end reference therein). The talc ore deposits of economic importance are interpreted to evolve from the originally magnesites located in the Sinec zone during the Alpine reactivation of Vepor Unit along the major shear zones (Neméth et al., 2004) The precipitation of talc is related to increasing deformation and temperature along the shear zones. This situation resembles to the situation in the Greywacke Zone (Wölfler et al. 2015). The Si-rich fluid income to the upper

lithological complexes during the Alpine orogeny is supported by the study of shear zones (Fig. 47).

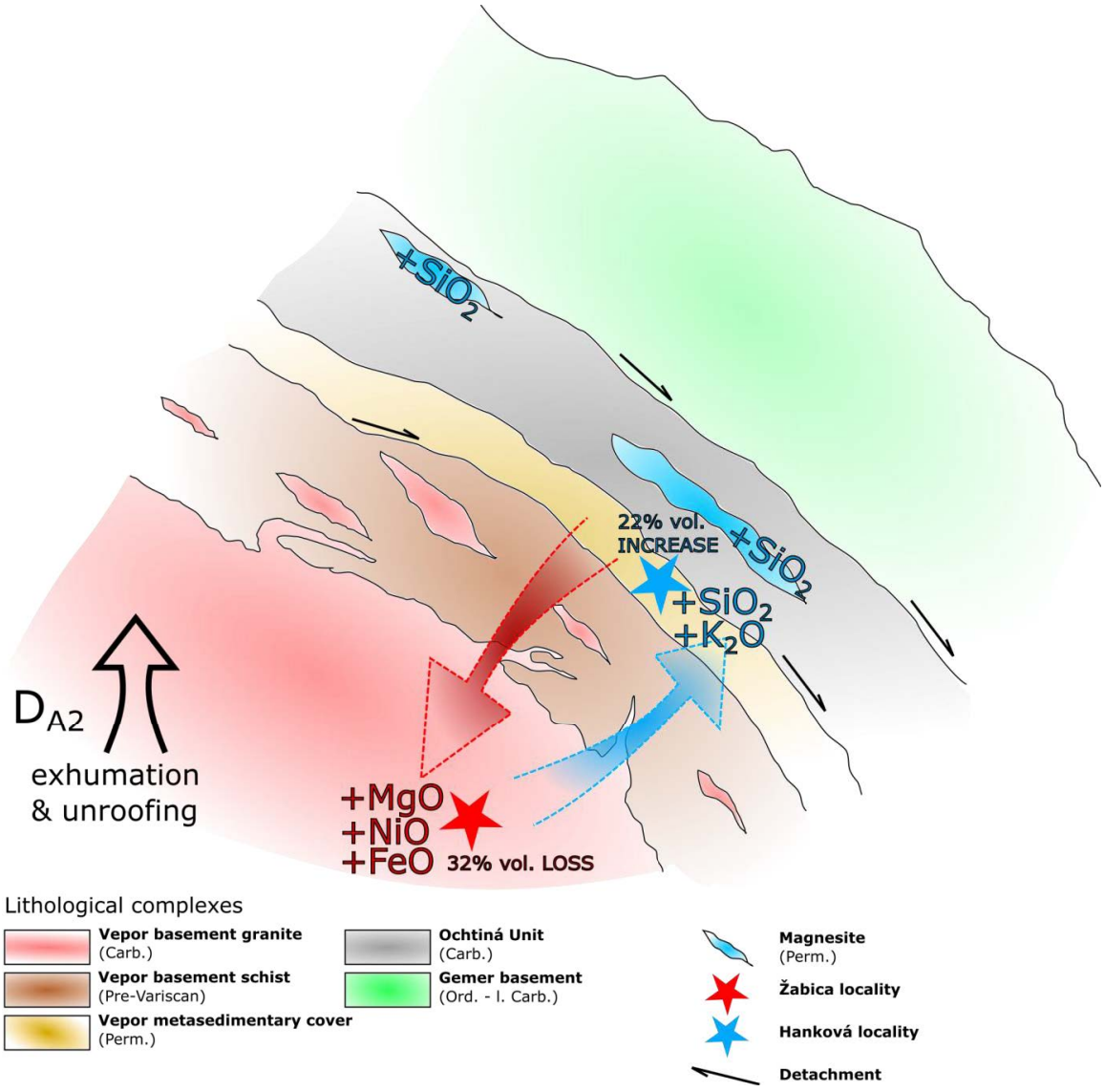

Fig. 47*: Schematic vertical section (not scaled) through the lithological complexes within the Gemer-Vepor Contact Zone of the proposed model of the crustal-scale mass transfer and fluid assisted element exchange. The income of Si due to the fluid circulation is documented in the studied Hanková locality as well as within the magnesite deposits located within the Ochtiná zone.*

4.6 PARTIAL CONCLUSIONS

Both sampled shear zones experienced prograde metamorphism during D_{A1} of higher grade. Later, as the process in Central Western Carpathians switched from top to bottom driven, the exhumation of the lower crust occurred due folding and doming of Vepor Unit D_{A2} and this process is recorded in the studied shear zones as well. The metasomatism is associated with formation of detachment shear zones and deformation fabric S_{A2} related to exhumation during D_{A2} deformation. The fluids were released from local sources during the early stage of exhumation and transported along large scale detachment shear zones in the Gemer-Vepor Contact Zone. At different crustal levels and within different lithological complexes, the fluids show heterogeneous behavior, related to gain or loss of different elements. It is a coupled process – the lower parts of the lithological complexes show gain in Mg, Fe, Ni and Mn, whereas the upper parts show depletion in the dam elements. The magnesite ore deposits present in the Gemer-Vepor Contact Zone probably served as the source for Mg-enrichement of fluids migrating through detachment shear zones during the doming and exhumation of the Vepor Unit. So far, such extent and type of the mass transfer has not been recognized in the studied area.

5. VEITSCH-NÖTSCH-SZABADBATTYÁN-OCHTINÁ ZONE –AGES OF DETRITAL ZIRCONS

In order to test the possible links between the Ochtiná Unit in the Gemer-Vepor Contact Zone of the Western Carpathians and the Veitsch Nappe in the Greywacke Zone of the Eastern Alps, the samples for provenance analysis of detrital-zircons from both zones were collected.

The Carboniferous syn- to late-orogenic sediments, which deposited in a narrow orogenic foredeep basin were described as the Veitsch-Nötsch-Szabadbattyán-Ochtiná Zone (VNSOZ, Neubauer and Vozárová, 1990). The VNSOZ in the ALCAPA-Megaterrane evolved after the formation of the Mediterranean Crystalline Zone in its foreland, or as remnant basin, related to Variscan orogenic belt in the Western Carpathians (Ebner et al., 1991; Ebner 1992; Ebner et al., 2008; Flügel 1977, 1990; Neubauer and Vozárová, 1990; Vozárová 1996).

The primary basement of the VNSOZ is uncertain, because the sedimentary sequence was later detached and overrode the continental margin (Ebner et al., 2008 and reference therein). There is no proof of Variscan deformation of the VNSOZ in the Veitsch Nappe (Ratschbacher 1987) but in the Ochtiná Unit the basin closure due to the continuation of convergence is documented by hiatus during the Lower Bashkirian (Fig. 49) in the Ochtiná Unit (Vozárová 1996, Ebner et al., 2008).

In this chapter samples of typical lithologies were systematically collected for detrital U-Pb zircon dating.

Three samples (GG69, GG89 and GG141) from the Veitsch Nappe (Fig. 48) and three samples from the Gemer-Vepor Contact Zone (NN142, R40 and TU5, Fig. 48) were analyzed in detail.

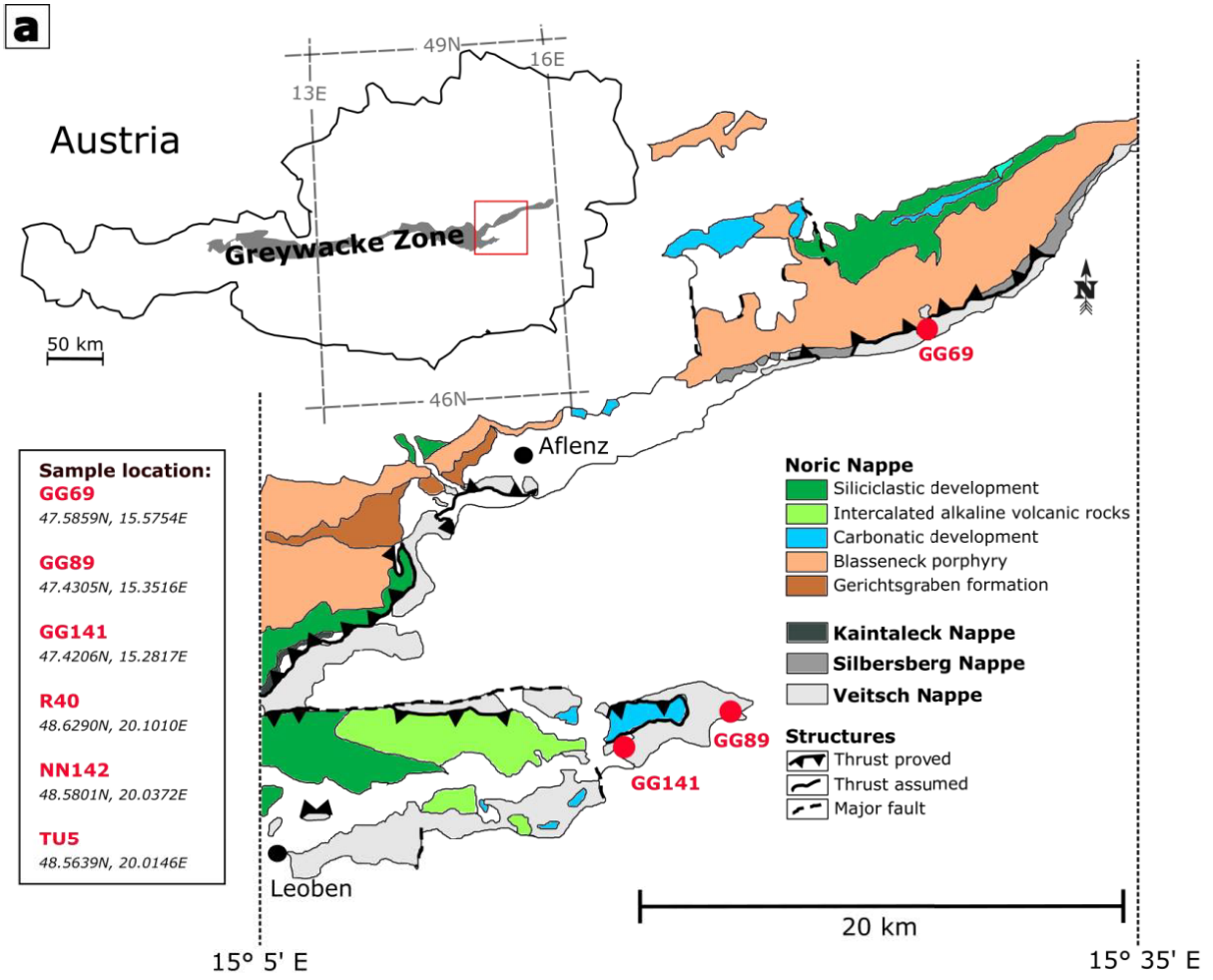
a
Austria
49N
16E
13E
46N
Greywacke Zone
50 km
GG69
Aflenz
Sample location:
GG69
47.5859N, 15.5754E
GG89
47.4305N, 15.3516E
GG141
47.4206N, 15.2817E
R40
48.6290N, 20.1010E
NN142
48.5801N, 20.0372E
TU5
48.5639N, 20.0146E
Noric Nappe
Siliciclastic development
Intercalated alkaline volcanic rocks
Carbonatic development
Blasseneck porphyry
Gerichtsgraben formation
Kaintaleck Nappe
Silbersberg Nappe
Veitsch Nappe
Structures
Thrust proved
Thrust assumed
Major fault
GG89
GG141
Leoben
20 km
15° 5' E
15° 35' E

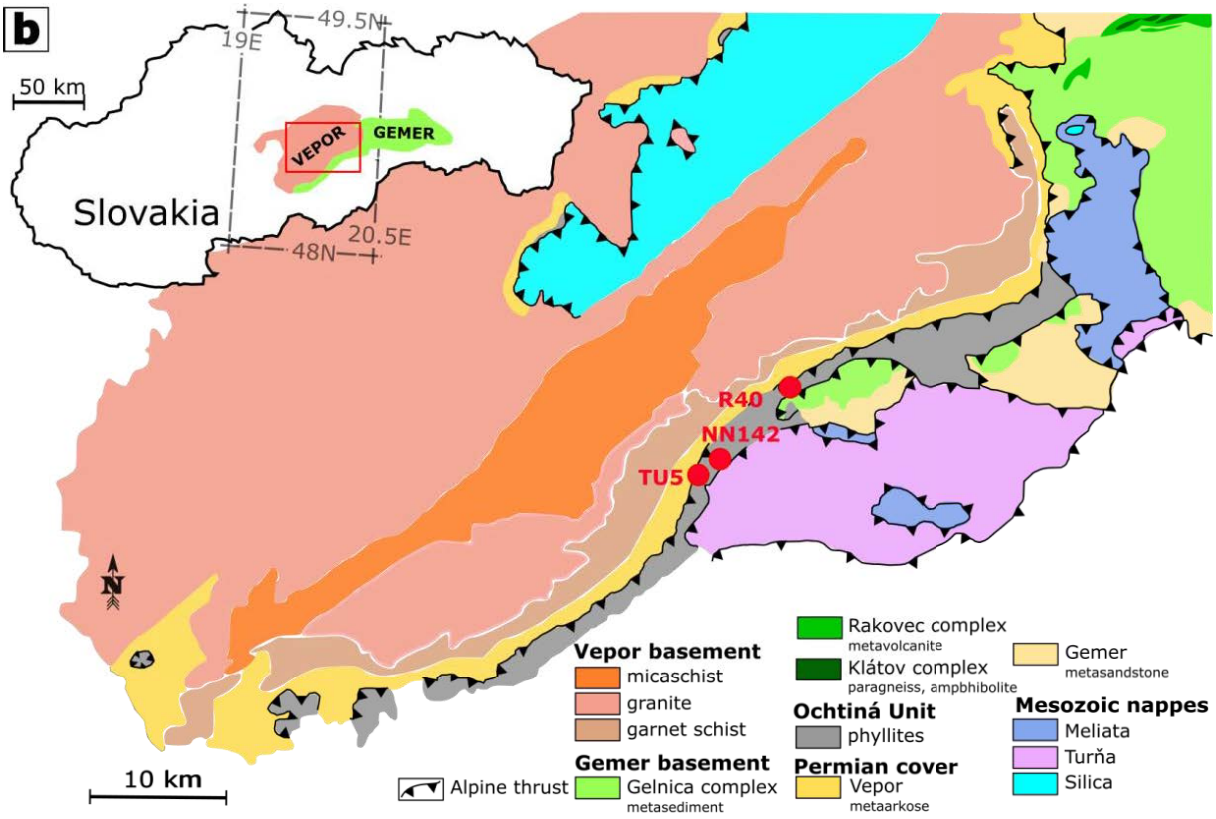
b
49.5N
19E
50 km
VEPOR
GEMER
Slovakia
20.5E
48N
R40
NN142
TU5
10 km
Alpine thrust
Vepor basement
micaschist
granite
garnet schist
Gemer basement
Gelnica complex
metasediment
Rakovec complex
metavolcanite
Klátov complex
paragneiss, amphibolite
Ochtiná Unit
phyllites
Permian cover
Vepor
metaarkose
Gemer
metasandstone
Mesozoic nappes
Meliata
Turňa
Silica

Fig. 48: *Simplified lithotectonic maps:* ***(a)*** *Greywacke Zone in the studied area with location of studied samples, modified after Gasser et al., 2009 and reference therein, the inset with the studied samples is shown.* ***(b)*** *Gemer–Vepor Contact Zone and surrounding units. Map based on the geological map of the Slovak Republic, 1:50 000 http://mapserver.geology.sk, the studied samples are marked with red dots.*

5.1 LITHOLOGICAL CHARACTERIZATION

5.1.1 VEITSCH NAPPE

The Veitsch Nappe comprises Carboniferous sequence that consists of syn- to late-orogenic sediments (Ebner et al., 2008). Locally, Permian clastic sediments are present (Neubauer and Vozarová 1990).

The Veitsch Nappe is furthermore subdivided into three formations (from bottom to top): the Steilbachgraben Formation, composed mainly of clastics and minor carbonates, the Triebenstein Formation with carbonates and some greenschists, and the Sunk Formation with quartz conglomerates and anthracite/graphite deposits (Gasser et al., 2009 and reference therein, Fig. 49). Locally, in the Mürz valley close to St. Marein, the hanging wall of the Sunk Formation is built up by the Graschnitz Formation (Neubauer and Vozarová 1990), which contains brownish to reddish sandstones and phyllites.

The samples from the Steilbachgraben Formation (GG141), the Triebenstein Formation (GG89) and the Sunk Formation (GG69) were analyzed in detail (Fig. 48 and 49).

The tectonic processes leave a distinctive geochemical signature to sediments. Different tectonic environments have distinctive provenance characteristics and they are characterized by distinctive sedimentary processes. Therefore the geochemical data are used to determine the rock sources and tectonic environments (for the whole rock analysis see Tab. 7).

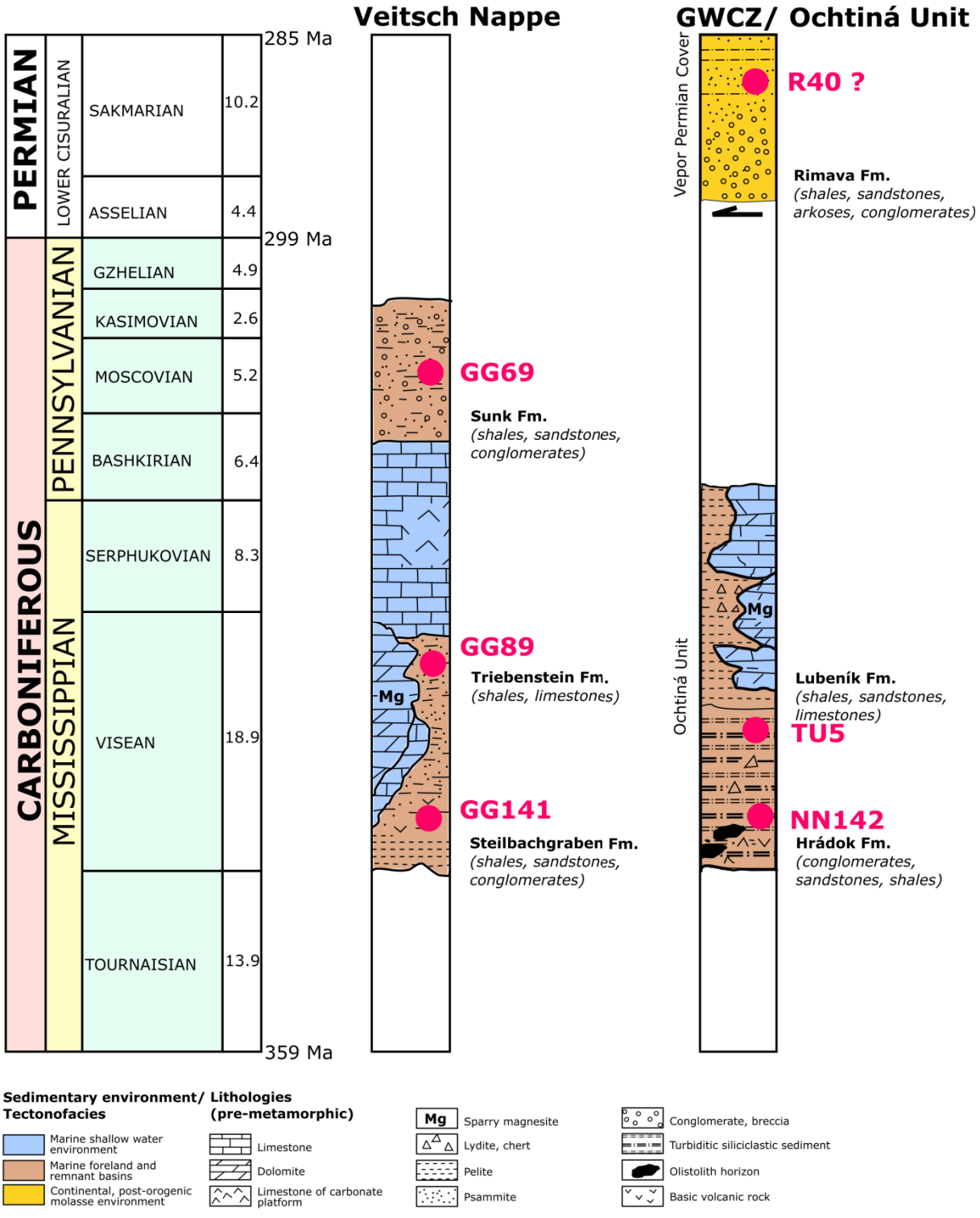

Fig. 49: *Carboniferous/Early Permian sequences in the studied area with the location of studied samples (modified after Ebner et al., 2008, Vozárová et. al., 2009 and Vozárová et al., 2013).*

Sample	GG 69	GG 89	GG 141	NN 142	R 40	TU 5		GG 69	GG 89	GG 141	NN 142	R 40	TU 5
SiO_2	74.03	90.81	47.48	65.19	71.30	58.58	Y	15.0	6.4	26.0	27.4	27.9	32.7
Al_2O_3	13.37	4.95	15.77	22.20	13.62	21.35	La	17.4	17.4	28.9	31.9	38.5	40.5
Fe_2O_3	3.45	1.02	11.02	2.27	2.21	6.52	Ce	35.6	34.2	57.3	79.7	78.8	78.8
MgO	2.20	0.27	6.44	0.35	0.68	1.49	Pr	4.34	3.86	7.10	8.44	8.78	10.92
CaO	0.05	0.04	8.91	0.07	2.07	0.19	Nd	14.4	12.5	27.7	27.9	31.0	40.5
Na_2O	0.48	0.14	3.03	2.06	2.04	0.91	Sm	2.28	1.88	5.74	5.48	5.75	8.03
K_2O	2.55	1.08	0.76	3.34	4.23	4.10	Eu	0.51	0.40	1.80	1.20	1.03	1.74
TiO_2	0.55	0.19	2.26	0.73	0.26	0.97	Gd	2.40	1.49	5.62	5.13	5.28	7.31
P_2O_5	0.04	0.02	0.47	0.02	0.06	0.07	Tb	0.40	0.21	0.87	0.80	0.83	1.08
MnO	0.03	0.02	0.18	0.03	0.05	0.04	Dy	2.31	1.11	4.70	4.83	4.80	6.06
Cr_2O_3	0.025	0.011	0.027	0.022	0.011	0.023	Ho	0.52	0.30	1.06	1.04	1.02	1.21
Ni	32	21	88	32	22	41	Er	1.64	0.65	2.82	2.86	2.99	3.74
Sc	9	2	22	15	7	21	Tm	0.24	0.10	0.38	0.46	0.42	0.52
LOI	3.1	1.4	3.4	3.5	3.4	5.6	Yb	1.33	0.74	2.67	3.17	2.82	3.65
Sum	99.89	99.98	99.74	99.83	99.90	99.81	Lu	0.21	0.08	0.34	0.50	0.44	0.52
Ba	432	246	189	810	519	720	TOT/C	0.14	0.08	0.18	0.07	0.42	0.10
Be	3	3	3	6	6	12	TOT/S	<0.02	<0.02	<0.02	<0.02	<0.02	<0.02
Co	4.0	4.8	36.6	9.1	4.8	10.2	Mo	0.1	0.2	0.7	0.2	0.2	0.4
Cs	2.5	1.7	0.7	6.5	3.0	5.7	Cu	2.5	2.4	40.0	11.4	4.1	32.9
Ga	14.9	5.6	15.7	23.6	14.8	23.0	Pb	2.8	1.9	8.8	3.6	2.2	3.2
Hf	3.4	1.4	4.8	5.4	2.9	5.6	Zn	27	11	76	19	4	70
Nb	8.8	3.6	27.6	14.7	9.5	13.8	Ni	20.2	7.3	67.2	12.7	7.1	39.5
Rb	78.8	40.2	20.7	143.4	120.8	162.1	As	10.3	3.8	<0.5	14.3	2.8	29.8
Sn	2	<1	1	4	2	3	Cd	<0.1	<0.1	0.1	<0.1	<0.1	<0.1
Sr	48.8	19.4	354.7	260.8	25.3	114.3	Sb	0.4	0.2	0.1	<0.1	0.3	0.4
Ta	0.7	0.3	1.7	1.2	0.9	1.1	Bi	0.2	<0.1	<0.1	0.5	<0.1	0.6
Th	5.1	4.2	3.0	14.8	14.8	15.0	Ag	<0.1	<0.1	<0.1	<0.1	<0.1	<0.1
U	1.4	0.8	1.4	2.9	2.6	5.8	Au	4.2	1.1	<0.5	35.6	<0.5	3.6
V	83	36	188	64	31	126	Hg	0.10	<0.01	<0.01	<0.01	0.01	0.02
W	1.5	0.6	1.1	1.9	2.2	2.3	Tl	<0.1	<0.1	<0.1	<0.1	<0.1	0.1
Zr	117.1	59.4	206.6	188.9	116.1	220.9	Se	<0.5	<0.5	<0.5	<0.5	<0.5	<0.5

Tab. 7: *Whole rock analyses of the studied samples. Values are of oxides are given in wt. %, of elements in ppm.*

The sample GG141 is dark fine-grained shale from the Steilbachgraben Formation. Based on the whole rock analyses the discrimination diagrams were used for further characterization . The SiO2/Al2O3 index, used to characterize the sedimentary maturation, ranges is ~3 – close to values characteristic for basic source rocks (Roser et al., 1996). To discuss the tectonic setting and the source rocks for the sedimentary protolith of the samples, the discrimination diagrams of Floyd and Leveridge (1987) and Bhatia and Crook (1986) were used. In the diagram La/Th vs. Hf, the GG141 sample show proximity to the andesitic arc source field and to the tholeiitic ocean island arc source (Fig. 50a). In the Ti/Zr vs. La/Sc and La-Th-Sc-Zr/10 diagrams (Fig. 50 b, c), the sample GG141 exhibit an affinity to ocean island arc source (fore-arc or back-arc basins, adjacent to a volcanic-arc developed on oceanic or thin continental crust).

The deformed shale, with large amount of quartz from the Triebenstein Formation (GG89) has an unusually high SiO_2/Al_2O_3 index (~ 18) -that is characteristic for acidic source rocks, with low Al_2O_3 content. In the discrimination diagram La/Th vs. Hf , the analyzed sample GG89 show proximity to the acidic arc source field (Fig. 50a). In the Ti/Zr vs. La/Sc and La-Th-Sc-Zr/10 diagrams (Fig. 50 b, c), the sample exhibit an affinity to the passive margin source (rifted continental margins developed on thick continental crust on the edges of continents).

The sandstone with graphite from the Sunk Formation (GG69) has the SiO_2/Al_2O_3 index of 5.5 indicating the acidic source rocks (Roser et al., 1996). In the discrimination diagram La/Th vs. Hf , the sandstone show proximity to the acidic arc source field (Fig. 50a). In the Ti/Zr vs. La/Sc and La-Th-Sc-Zr/10 diagrams (Fig. 50 b, c), the sample exhibit an affinity to the continental arc source (inter-arc, fore-arc or back-arc basins, adjacent to a volcanic-arc developed on thick continental crust or thin continental margin).

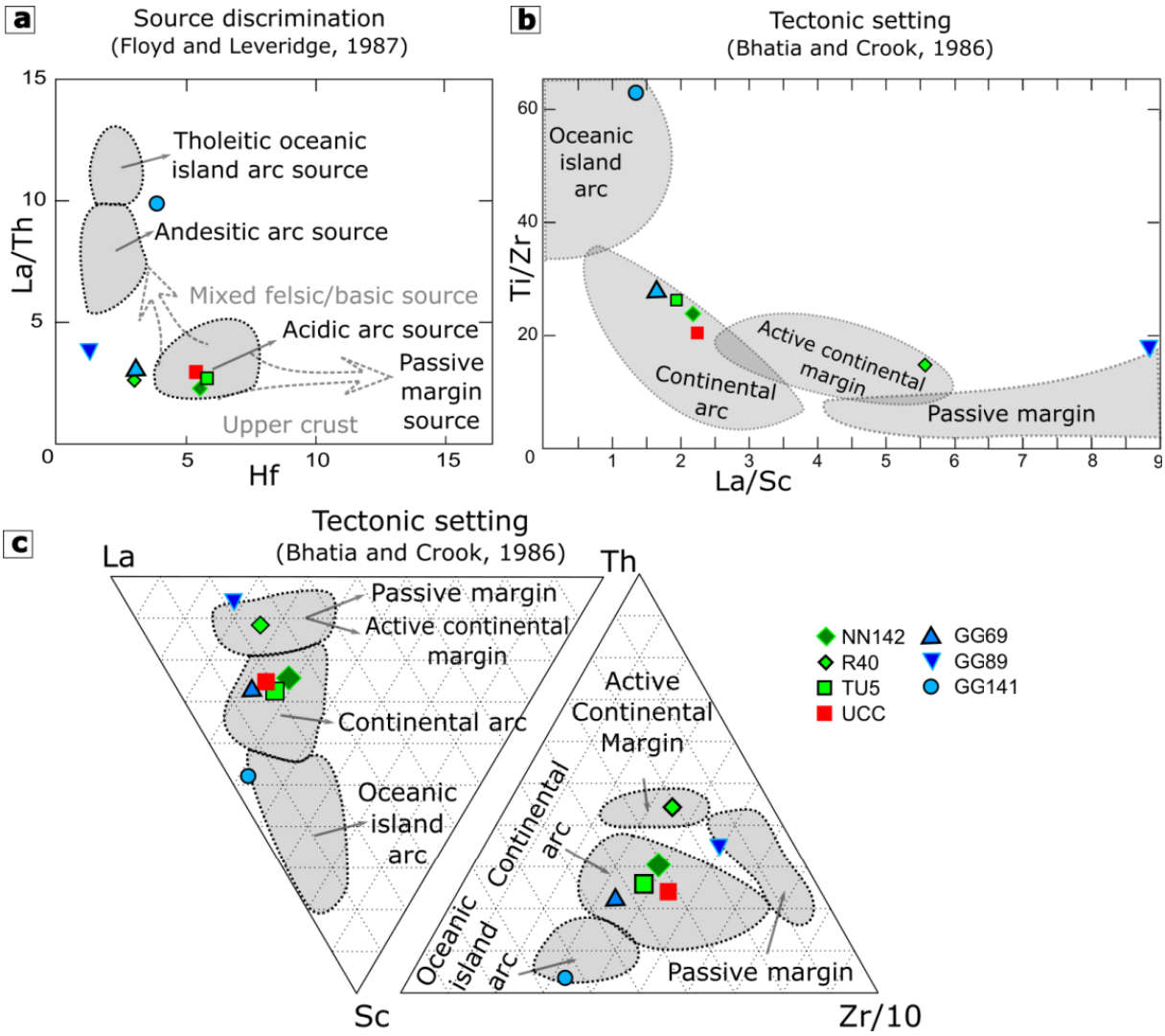

Fig. 50: *Source rock and tectonic setting discrimination diagrams for the Veitsch Nappe and Ochtiná Unit, the UCC (Upper Continental Crust after Rudnick and Gao, 2003) standard is plotted for comparism:* ***(a)*** *La/Th vs. Hf diagram (after Floyd and Leveridge, 1987), indicating mixing of felsic and intermediate sources with minor influence of an old sediment component.* ***(b)*** *Ti/Zr vs La/Sc diagram (after Bhatia and Crook, 1986.* ***(c)*** *Triangular trace element tectonic discrimination diagram (Bhatia and Crook, 1986).*

5.1.2 OCHTINÁ UNIT

The group of sediments of the Ochtiná Unit is furthermore subdivided into Hrádek, and Lubeník Formations in the studied area (Fig. 49). The group consists of Mississippian volcano-sedimentary sequence that includes deep-water turbidite sediments in the lower part (the Hrádok Formation) and shallow-water fine-rained siliciclastic and bioclastic carbonate sediments in the upper part (the Lubeník Formation; Vozárová 1996; Vozárová et al., 2013).

Two samples from the Hrádok Formation (NN142 and TU5) were analyzed in detail (Fig. 48 and 49).

The samples NN142 and TU5 are dark phyllites with a well developed slaty cleavage, due to the Alpine metamorphic overprint of the greenschist facies. Based on the whole rock analyses the discrimination diagrams were used for further characterization. The SiO2/Al2O3 index ranges from 2.7 to 2.9 – close to values characteristic for basic source rocks (Roser et al., 1996). To discuss the tectonic setting and the source rocks for the sedimentary protolith of the phyllites, again, the discrimination diagrams were used. In the diagram La/Th vs. Hf , the analyzed samples show proximity to the acidic arc source field (Fig. 50a). In the Ti/Zr vs. La/Sc and La-Th-Sc-Zr/10 diagrams (Fig. 50 b, c), the samples exhibit an affinity to continental arc source.

In the area of Gemer-Vepor Contact Zone, the strongly deformed and metamorphosed Southern Veporicum metasediments of Rimava Formation of Permian age are laying in the tectonic footwall of the Carboniferous Hrádok Formation of Ochtiná Unit (see Fig. 10 – Vepor metasedimentary cover). The Rimava Formation consists of coarse-grained arkosic metasandstones and rare metaconglomerates with abundant granitic detritus of Permian age.

One sample from Rimava Formation (R40) was analyzed (Fig. 48 and 49). The sample R40 is a coarse-grained metasandstone with large amount of detrital micas. Based on the whole rock analyses, the SiO_2/Al_2O_3 index ~5.2 is characteristic for acidic source rocks (Roser et al., 1996). In the diagram La/Th vs. Hf , sample R40 shows proximity to the acidic arc source field (Fig. 50 a). In the Ti/Zr vs. La/Sc and La-Th-Sc-Zr/10 diagrams (Fig. 50 b, c), the sample R40 exhibit an affinity to active continental margin (Andean-type basins developed on or adjacent to thick continental margins, strike-slip basins also developed in this environment).

5.2 U-PB DETRITAL ZIRCON DATING

5.2.1 STEILBACHGRABEN FORMATION

Zircon grains form the sample GG141 are 70-200 µm long. The zircons form often euhedral, subhedral or subrounded shapes with rounded crystal faces. In some zircons the truncated oscillatory zoning cores are preserved and are discordantly overgrown by thick outer parts and the subrounded cores with chaotic internal patterns were also extracted from the sample, as well as in some grains the corroded inherited cores are preserved. Also, anhedral grains could be occasionally found in this sample (see Fig. 51).

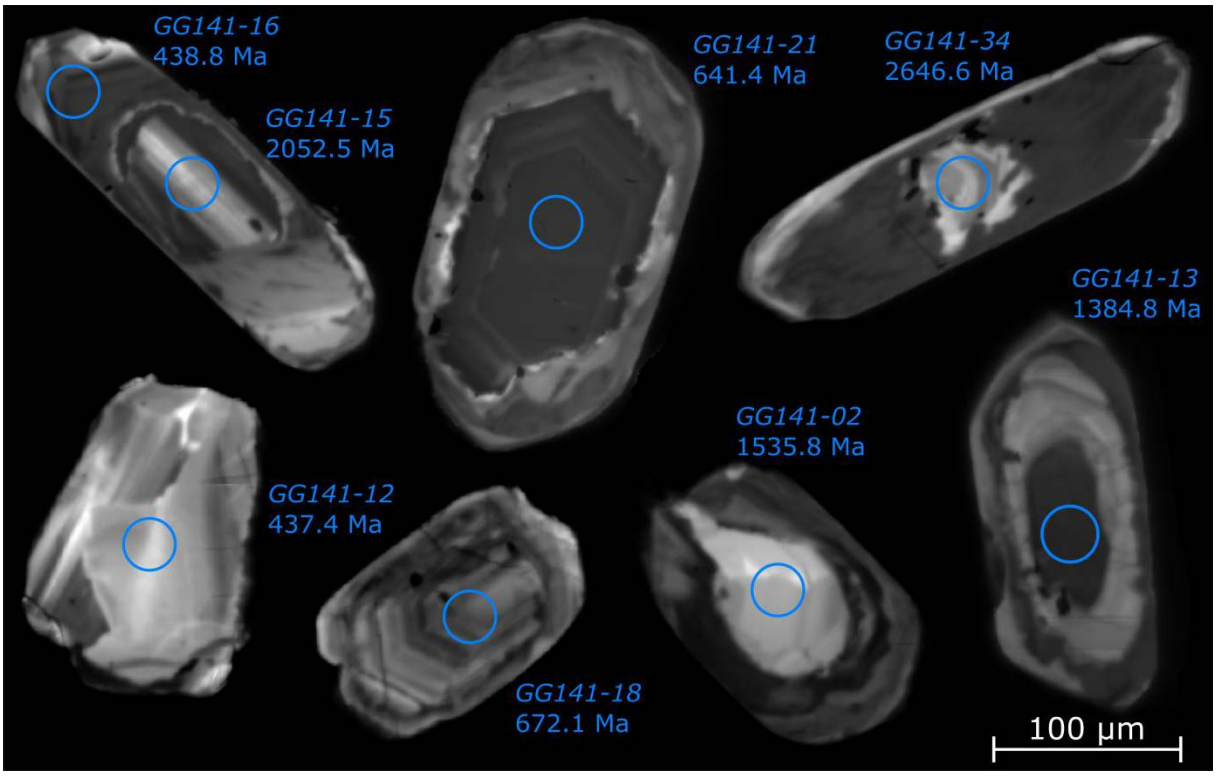

Fig. 51: *Cathodoluminescence image of the representative zircon grains from the sample GG141. Laser-ablation ICP-MS analysis spots are marked with concordant* $^{206}Pb/^{238}U$ *age.*

U-Pb dating of 50 grains yielded age population with the highest proportion of ages around 520-600 Ma with one subordinate peak at 420-480 Ma and significant peaks at 620-680 Ma, 1800-2200 Ma and 2600 Ma. Some individual age appear at 360 Ma (Fig. 52 and 53).

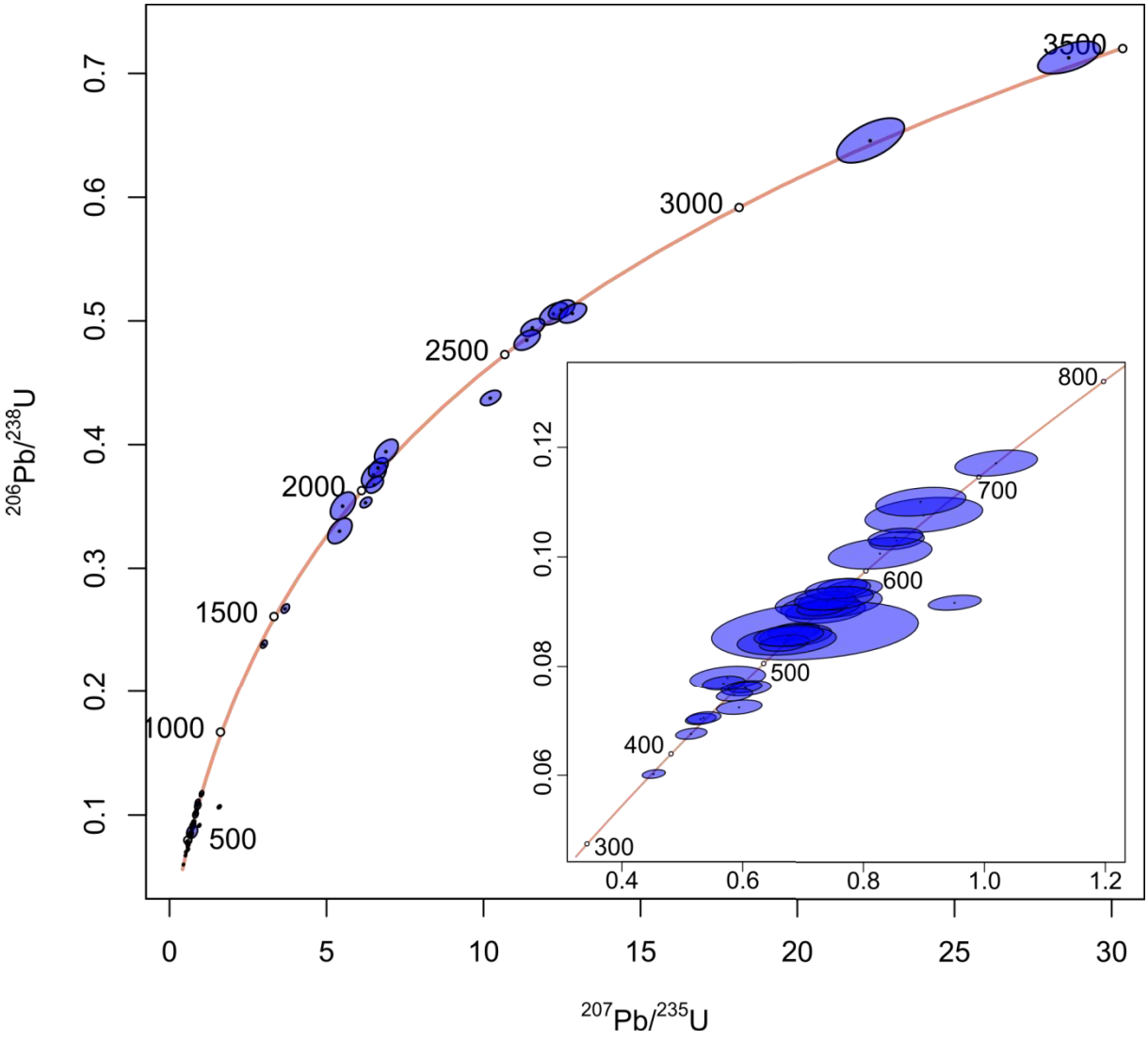

Fig. 52: *Concordia diagram for the GG141 sample.*

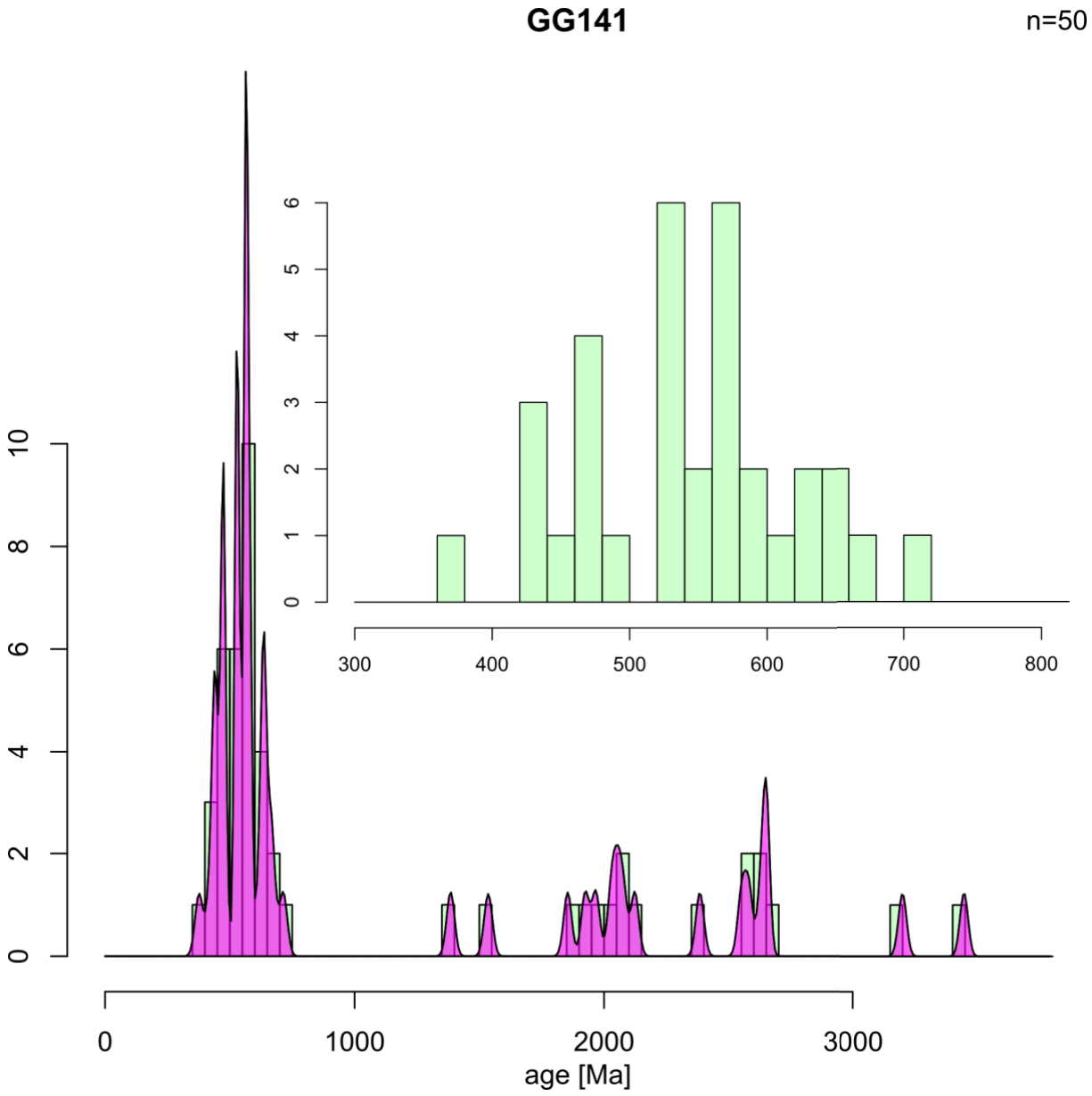

Fig. 53: *Frequency histogram with kernel density estimates showing detrital ($^{206}Pb/^{238}U$) zircon age distributions in the studied sample from the Steilbachgraben Formation.*

5.2.2 TRIEBENSTEIN FORMATION

The zircon grains extracted from the Triebenstein Formation sample GG89 are 50-250 µm long, the zircons often form subhedral shapes with rounded edges and these edges are overgrown by rims. The cores have often preserved oscillatory zoning. However, grains with patchy zoning could be found, as well as smaller (~ 60 µm) euhedral prisms with oscillatory zoning.

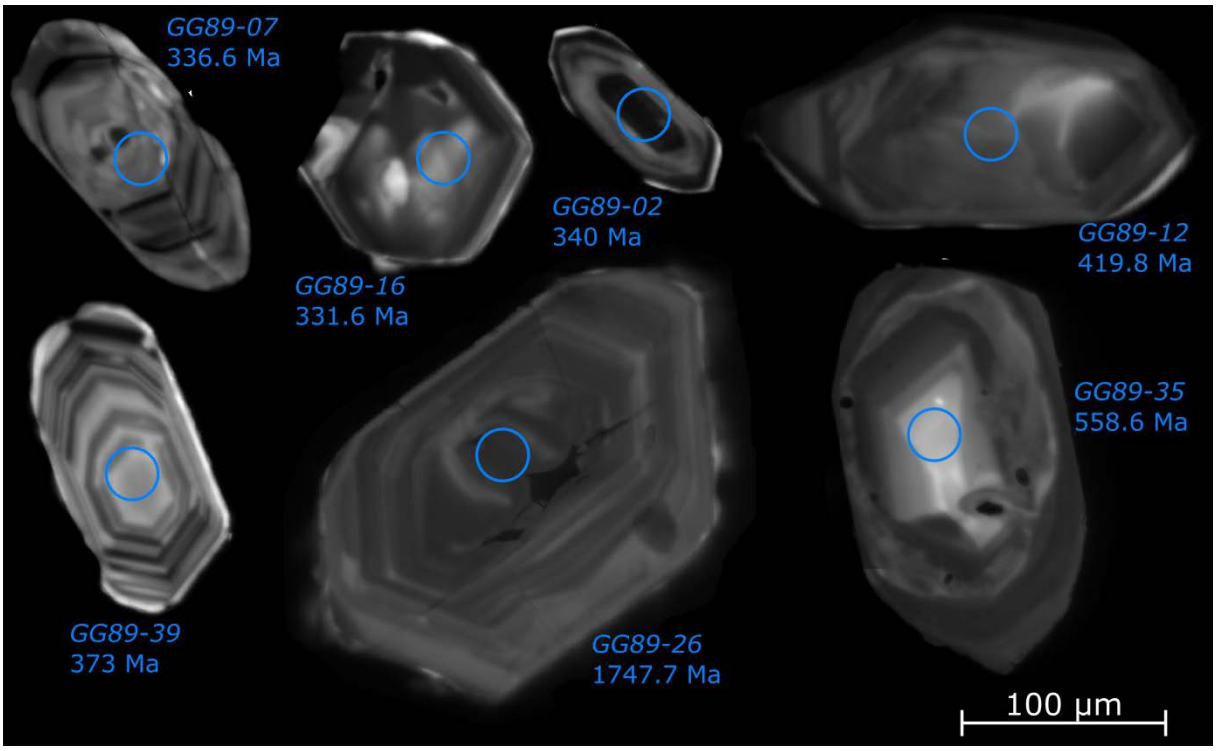

Fig. 54: *Cathodoluminescence image of the representative zircon grains from the sample GG89. Laser-ablation ICP-MS analysis spots are marked with concordant* $^{206}Pb/^{238}U$ *age.*

U-Pb dating of 49 grains yielded 2 age-populations with the highest proportion of ages around 330-380 Ma and 440-500 Ma, with significant peak at 510-530 Ma. Some individual ages appear at 780 Ma, 1070 Ma, 1750 Ma, 2065 Ma, 2516 Ma and 2694 Ma (Fig. 55 and 56).

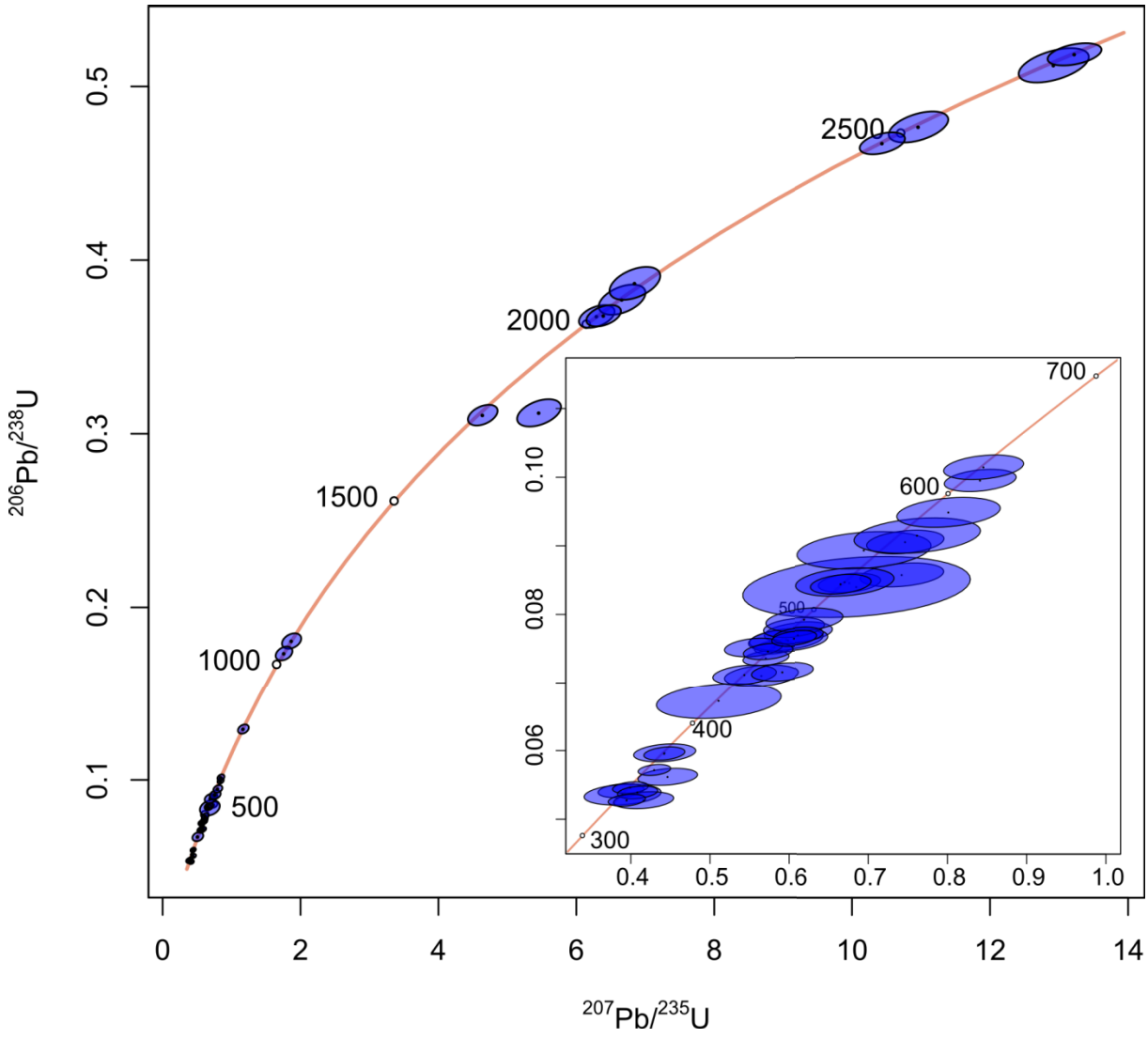

Fig. 55: *Concordia diagram for the GG89 sample.*

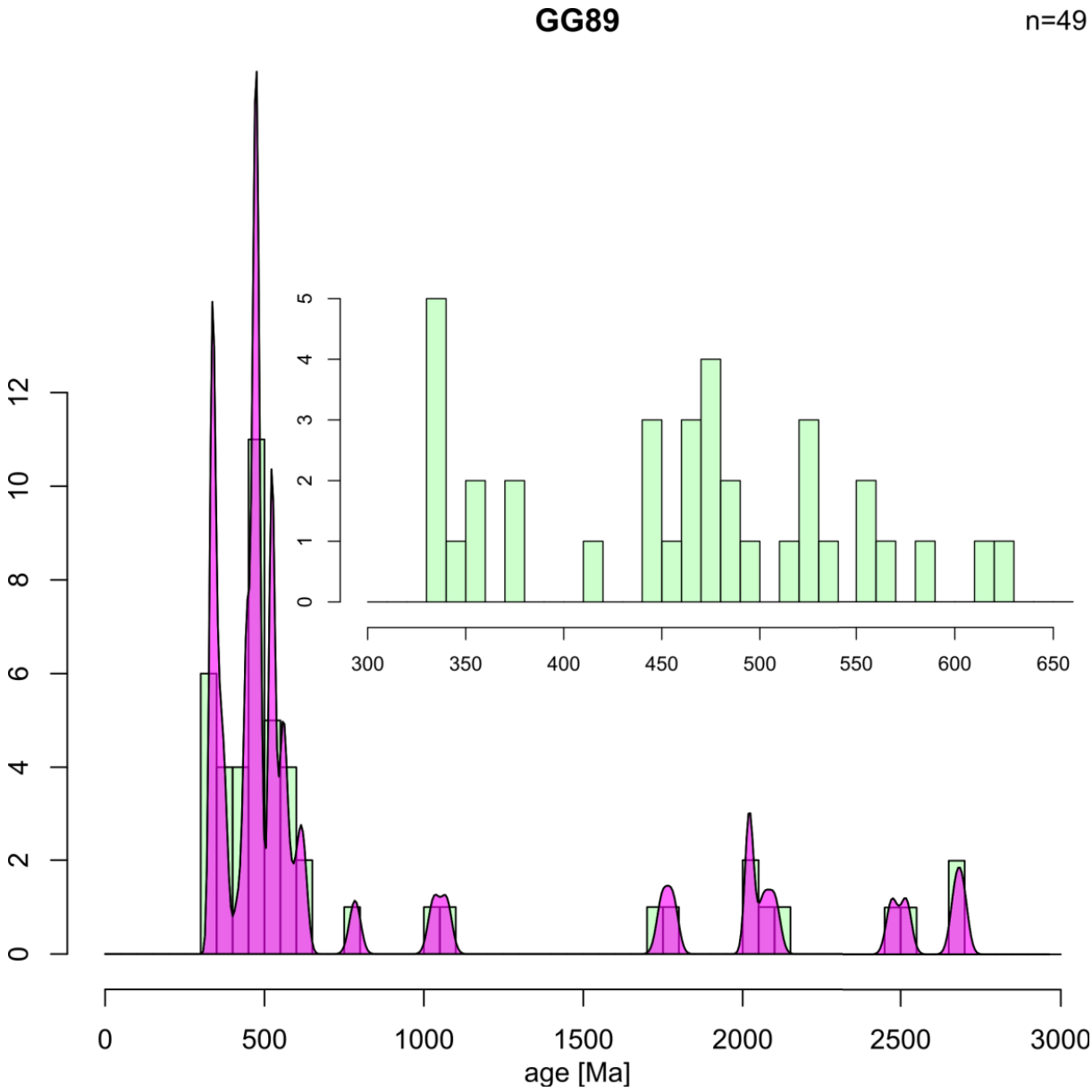

Fig. 56: *Frequency histogram with kernel density estimates showing detrital ($^{206}Pb/^{238}U$) zircon age distributions in the studied sample from the Triebenstein Formation.*

5.2.3 SUNK FORMATION

Zircons extracted from the GG69 sample are 50-200 µm long. Commonly they form the subhedral to euhedral shapes, sometimes they display truncated oscillatory zoning with thin rim overgrown. In this sample, some short prismatic grains with sector zoning were observed and also stubby grains with truncated internal pattern could be found, as well as the angular cores discordantly overgrown by thick outer parts (fig. 57).

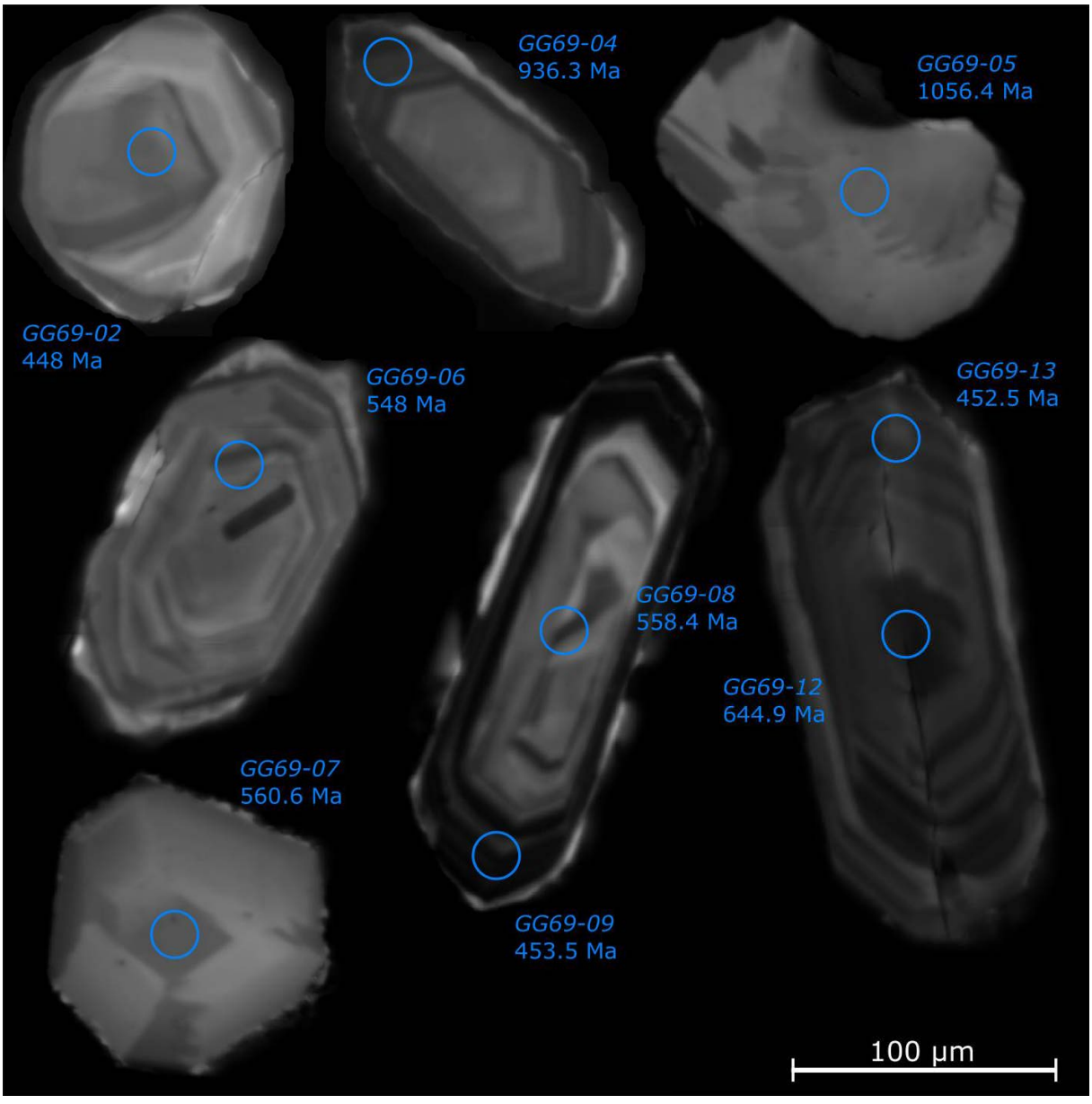

Fig. 57: *Cathodoluminescence image of the representative zircon grains from the sample GG69. Laser-ablation ICP-MS analysis spots are marked with concordant* $^{206}Pb/^{238}U$ *age.*

U-Pb dating of 86 grains yielded two main peaks for age population with the highest proportion of ages around 440-520 Ma and 540-580 Ma, with one subordinate peak at 330-370 Ma and significant peak at 2300-2450 Ma, 1800-2200 Ma. Some individual ages appear ~2700 Ma (Fig. 58 and 59).

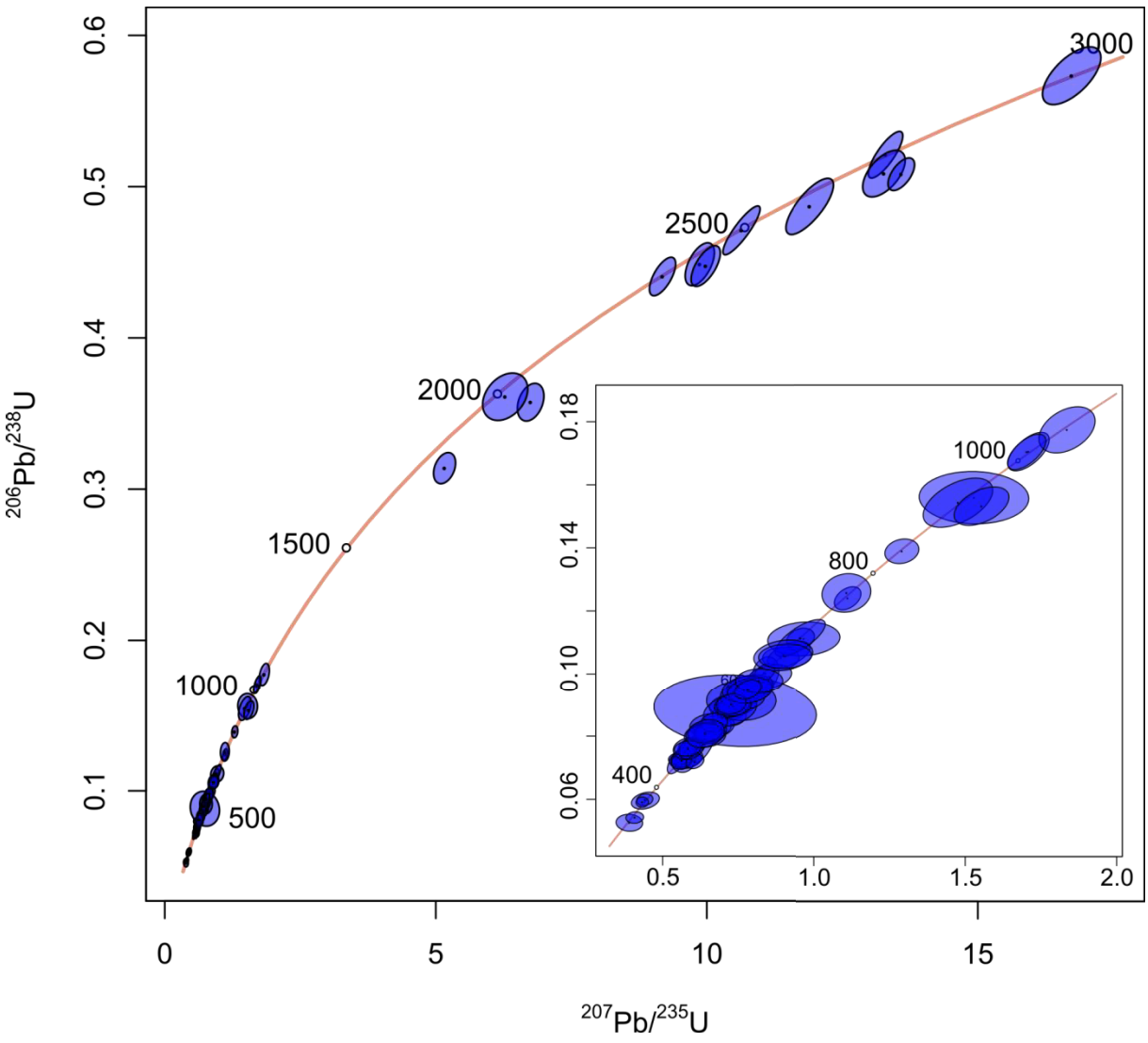

Fig. 58: *Concordia diagram for the GG69 sample.*

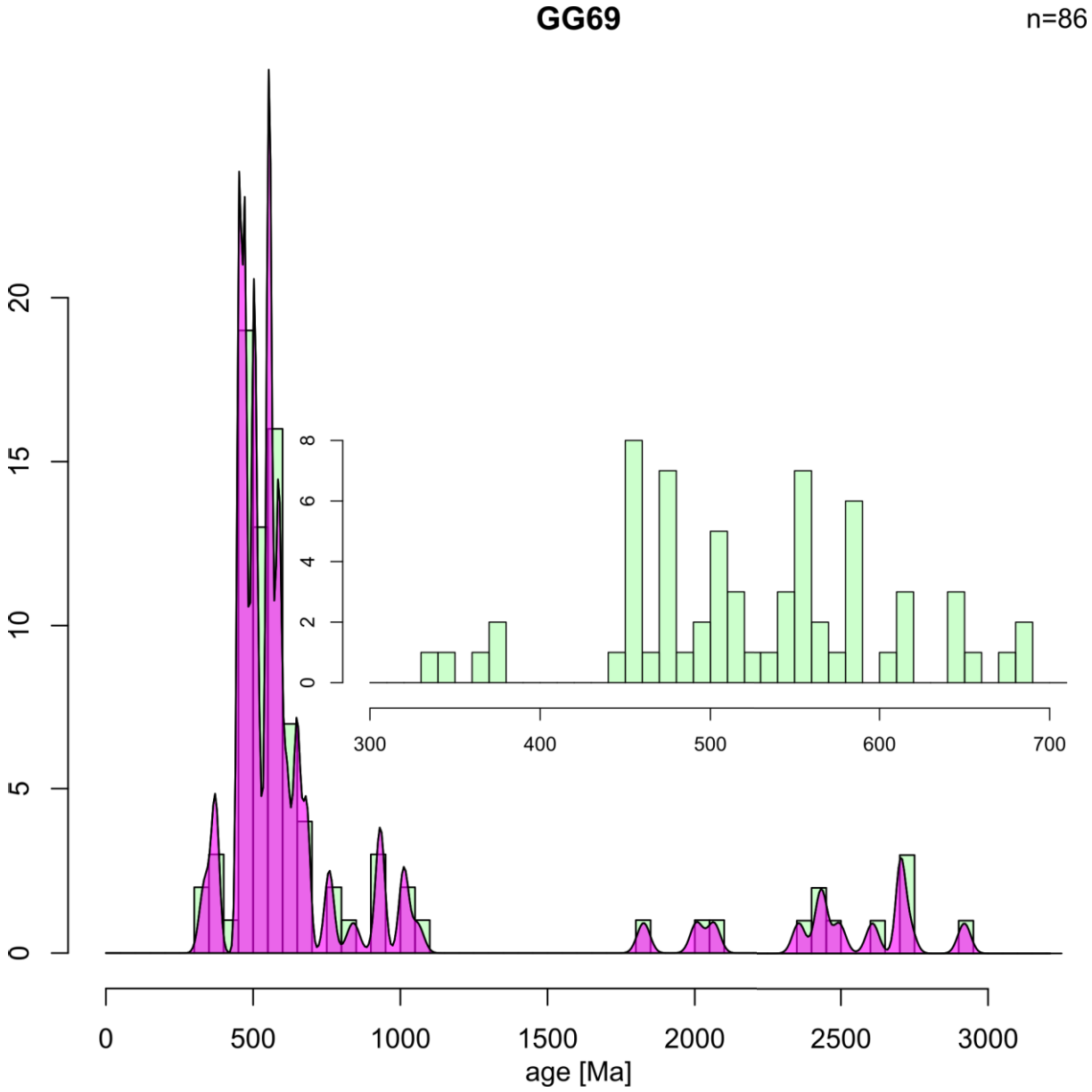

Fig. 59: *Frequency histogram with kernel density estimates showing detrital ($^{206}Pb/^{238}U$) zircon age distributions in the studied sample from the Sunk Formation.*

5.2.4 HRÁDOK FORMATION

The zircon grains extracted from the sample TU5 are 50-150 µm long. They usually form euhedral and subheral shapes with well preserved crystal faces with rounded edges and with oscillatory zoning, sometimes the grains display truncated oscillatory zoning. The crystals with overgrown rim were also observed (fig. 60)

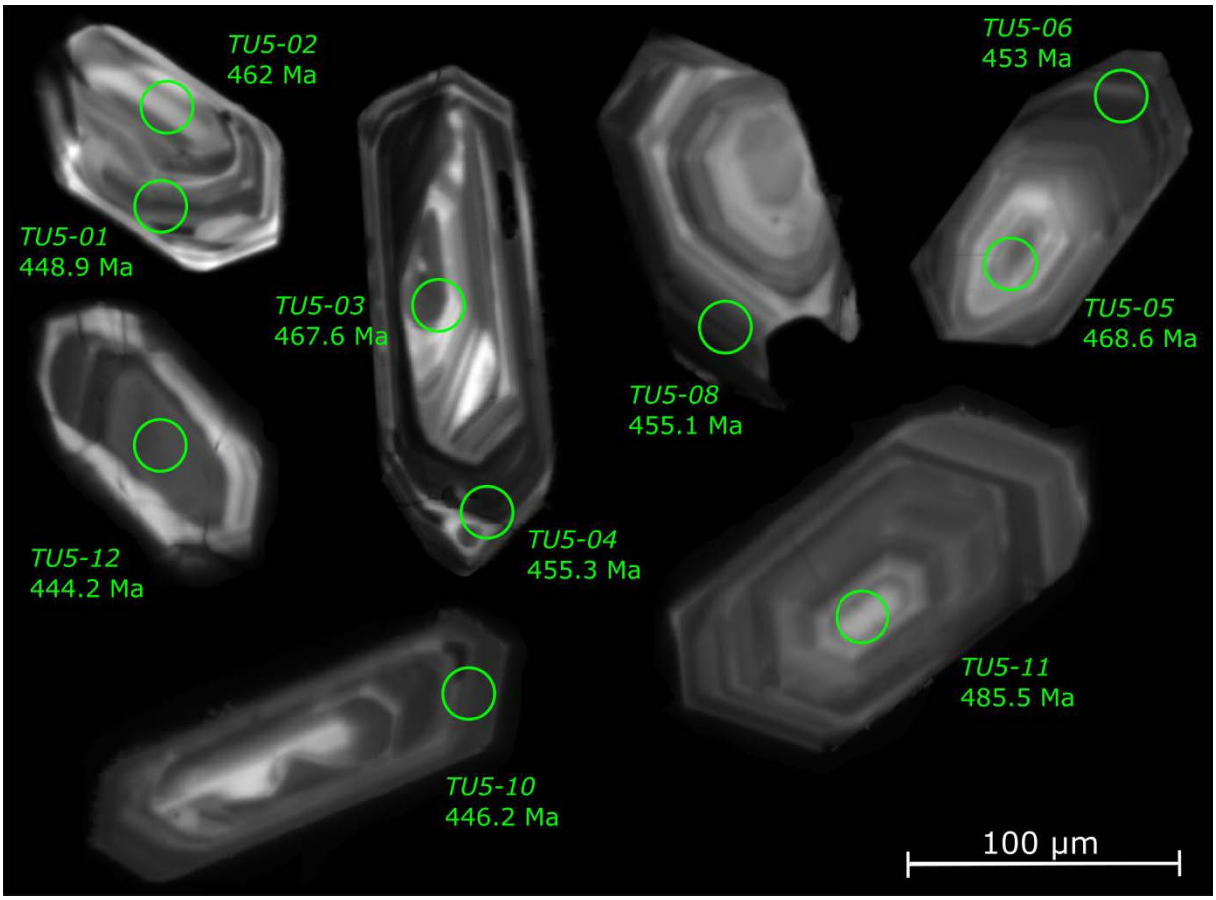

Fig. 60: *Cathodoluminescence image of the representative zircon grains from the sample TU5. Laser-ablation ICP-MS analysis spots are marked with concordant $^{206}Pb/^{238}U$ age.*

U-Pb dating of 112 grains yielded age population with the highest proportion of ages around 420-500 Ma, with two significant peaks at 530-560 Ma and 590-510 Ma. Some individual ages appear at 2422 Ma and 2664 Ma (Fig. 61 and 62).

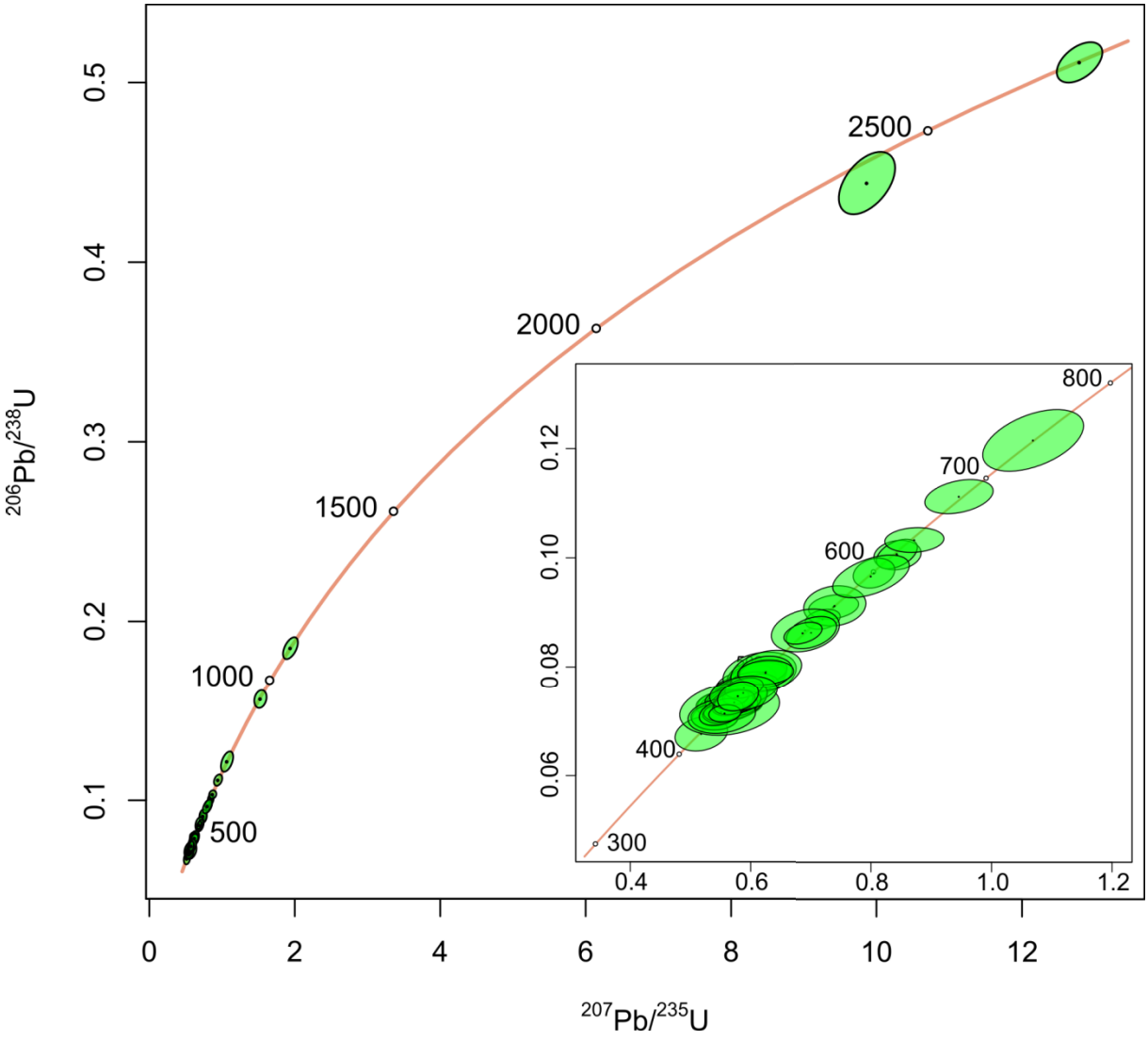

Fig. 61: *Concordia diagram for the TU5 sample.*

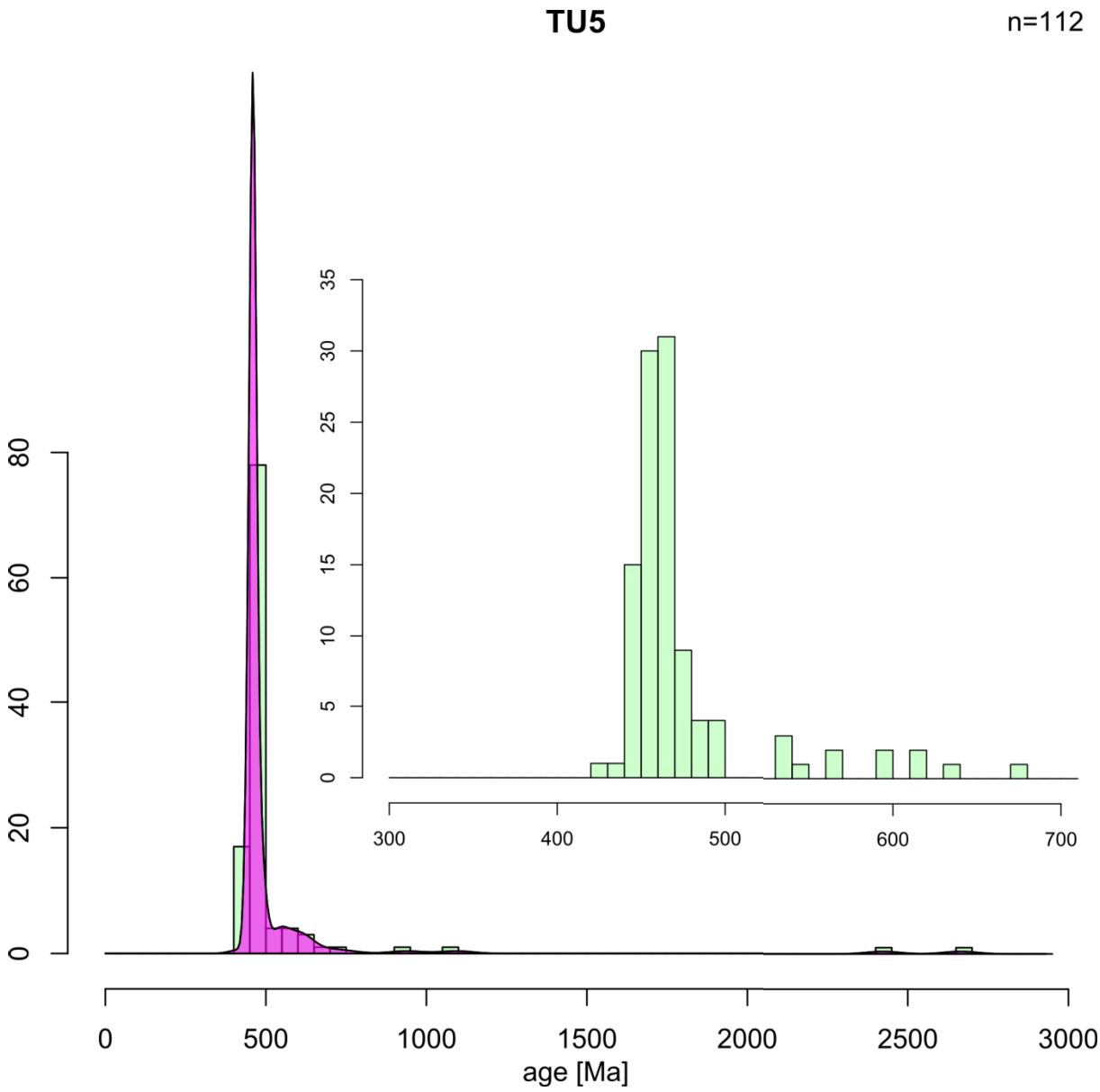

Fig. 62: *Frequency histogram with kernel density estimates showing detrital ($^{206}Pb/^{238}U$) zircon age distributions in the TU5 sample.*

The separated zircons from the NN142 sample are 20-200 μm long. The grains can form euhedral to subhedral shapes with preserved crystal faces. They usually form euhedral and subheral shapes with with rounded edges and oscillatory zoning, sometimes the inherited cores are overgrown by thin rims. The stubby zircons, with chaotic internal patterns could be found in this sample (fig. 63).

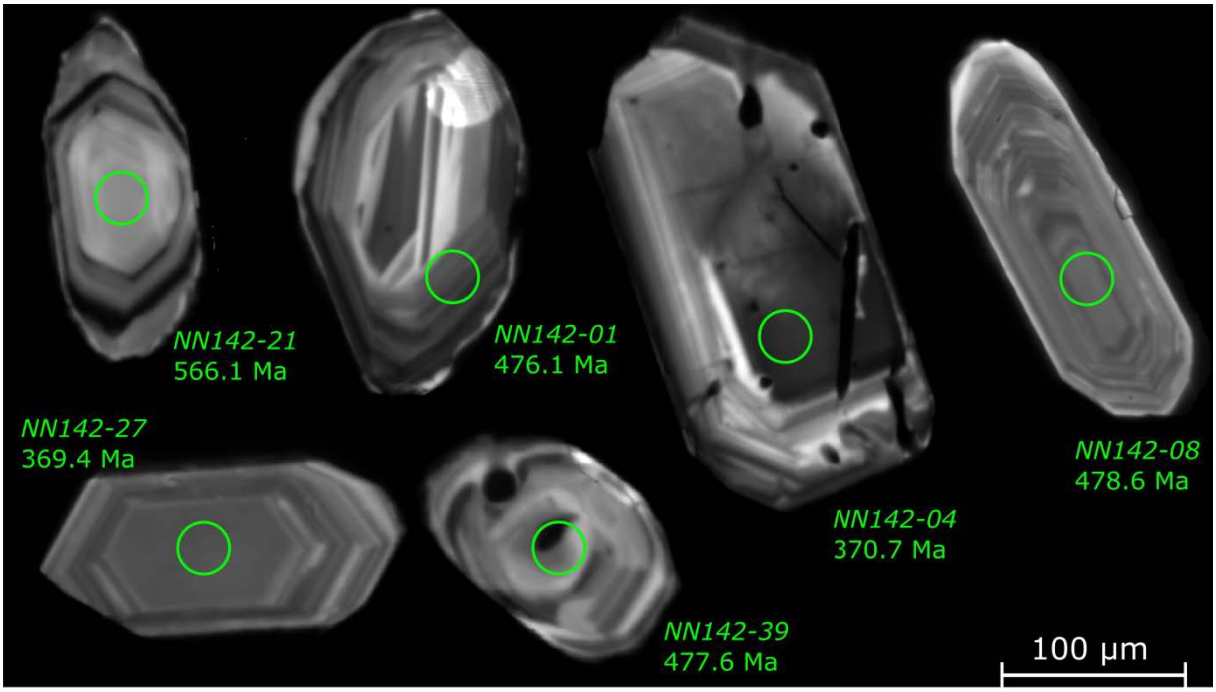

Fig. 63: *Cathodoluminescence image of the representative zircon grains from the sample NN142. Laser-ablation ICP-MS analysis spots are marked with concordant* $^{206}Pb/^{238}U$ *age.*

U-Pb dating of 48 grains from the NN142 sample, yielded 2 major age populations with the highest proportion of ages around 340-380 Ma and 440-500 Ma, with some individual ages appear at 1850 Ma, 1988 Ma and 2670 Ma (Fig. 64 and 65).

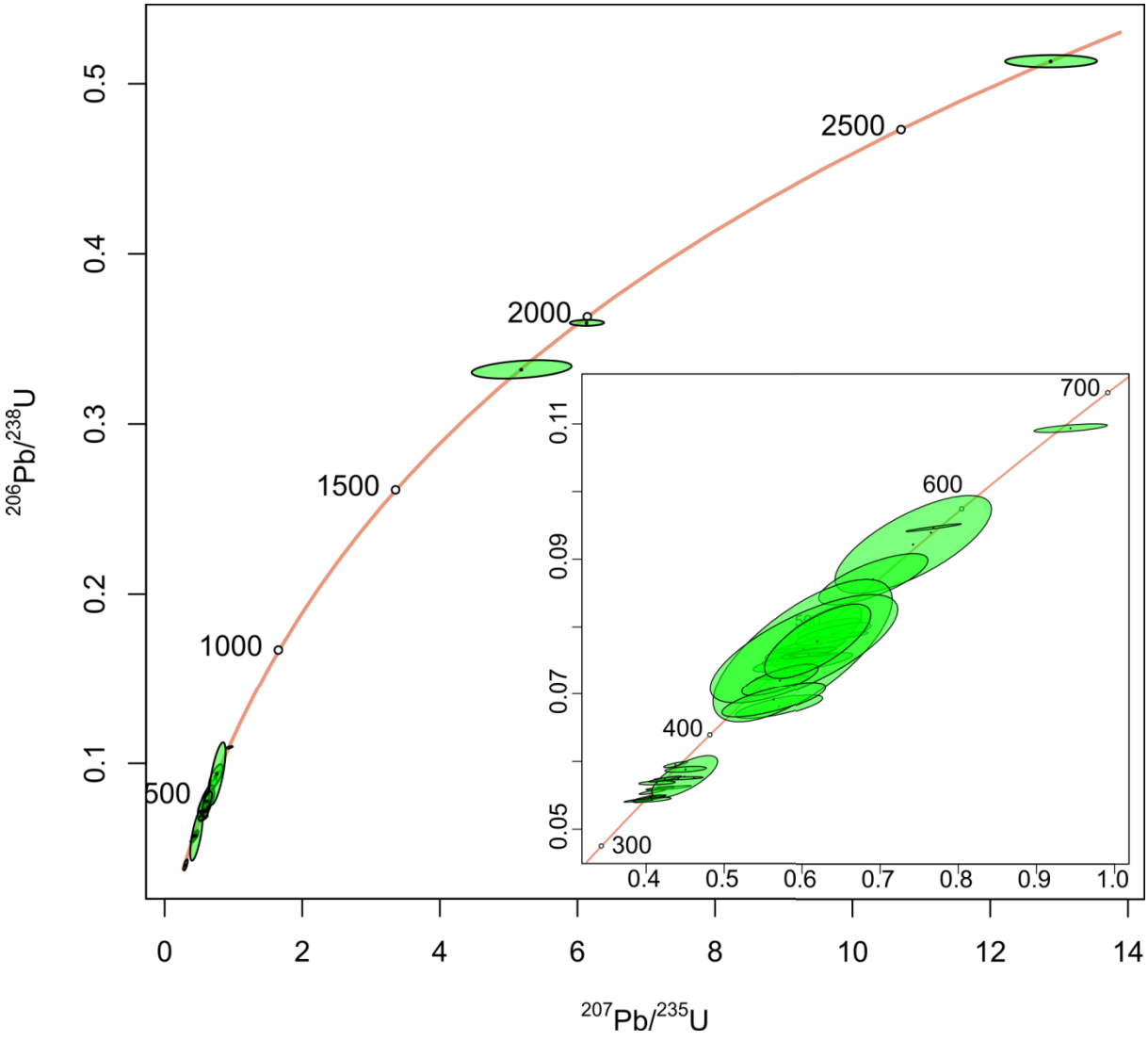

Fig. 64: *Concordia diagram for the NN142 sample.*

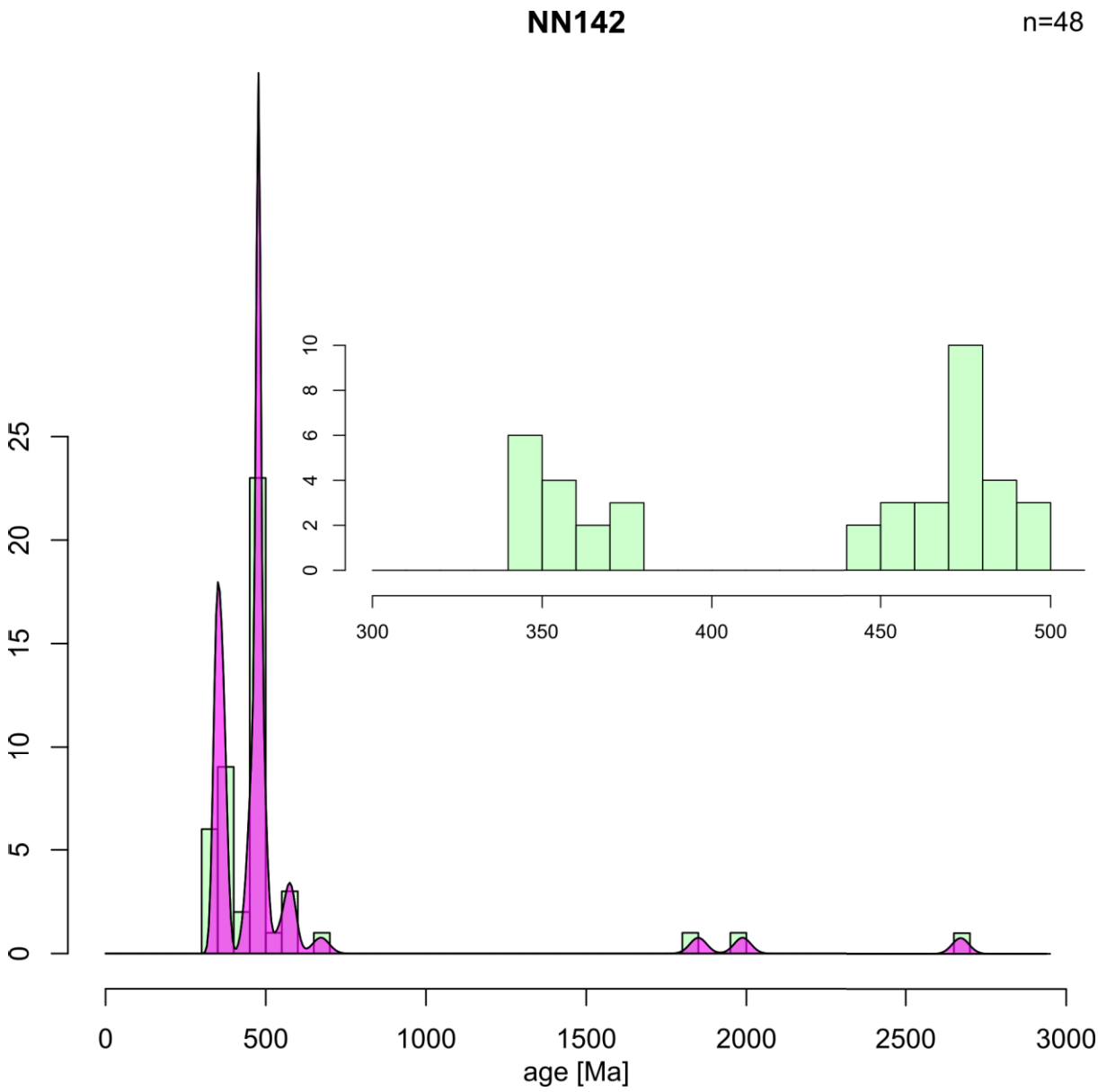

Fig. 65: *Frequency histogram with kernel density estimates showing detrital ($^{206}Pb/^{238}U$) zircon age distributions in the NN142 sample.*

5.2.5 RIMAVA FORMATION

Two main types of the zircon grains from the Rimava Formation R40 sample were identified. The grainsize is generally between 80-200 µm. The well preserved prismatic crystal shapes with oscillatory zoning are dominant in the sample, however stubby grains with rounded crystal faces without any internal zoning could be found as well.

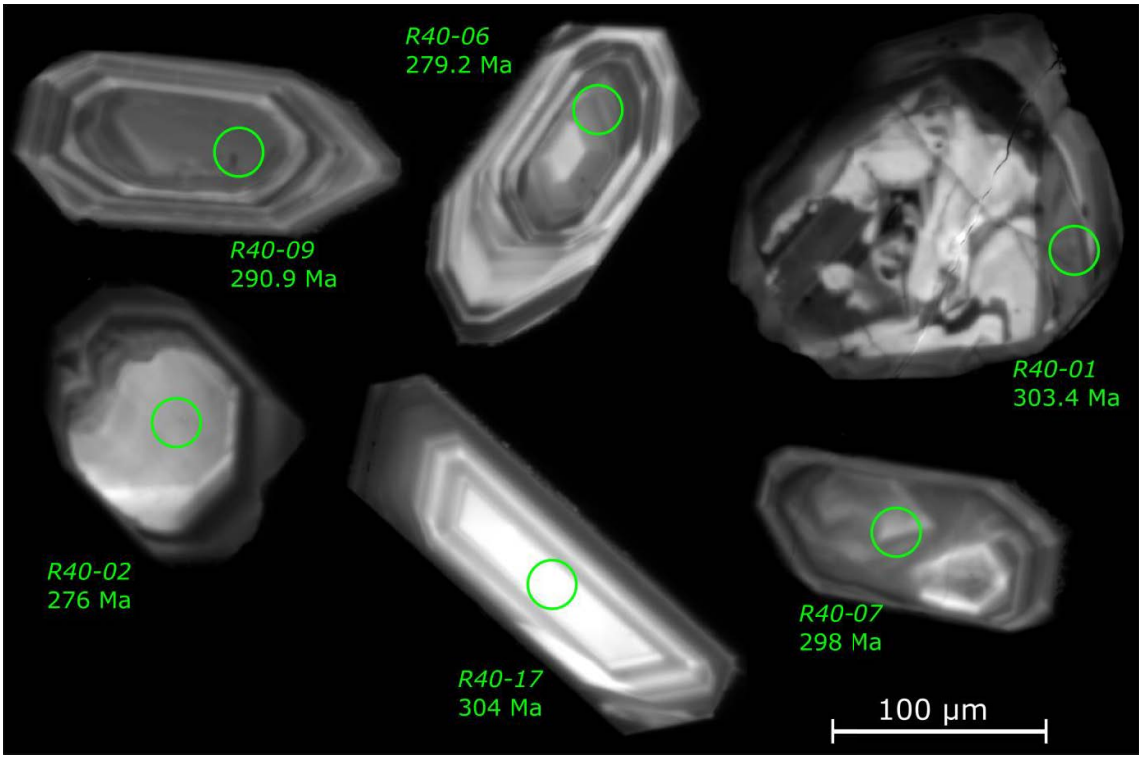

Fig. 66: *Cathodoluminescence image of the representative zircon grains from the sample NN142. Laser-ablation ICP-MS analysis spots are marked with concordant* $^{206}Pb/^{238}U$ *age.*

U-Pb dating of 48 grains from the R40 sample, yielded 2 major age populations of ages around 270-320 Ma and 330-370 Ma, with no other individual ages (Fig. 67 and 68).

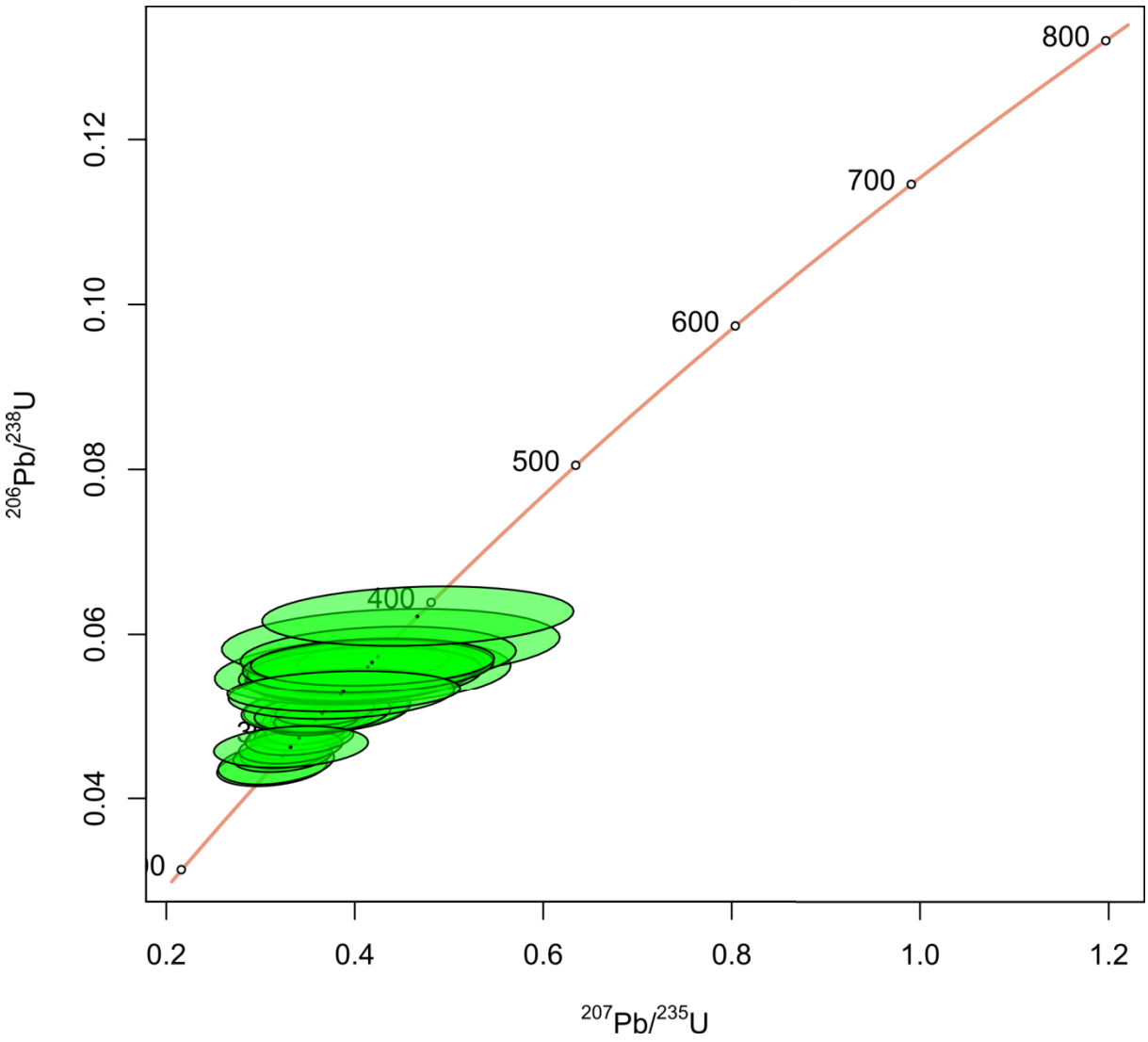

***Fig. 67**: Concordia diagram for the R40 sample.*

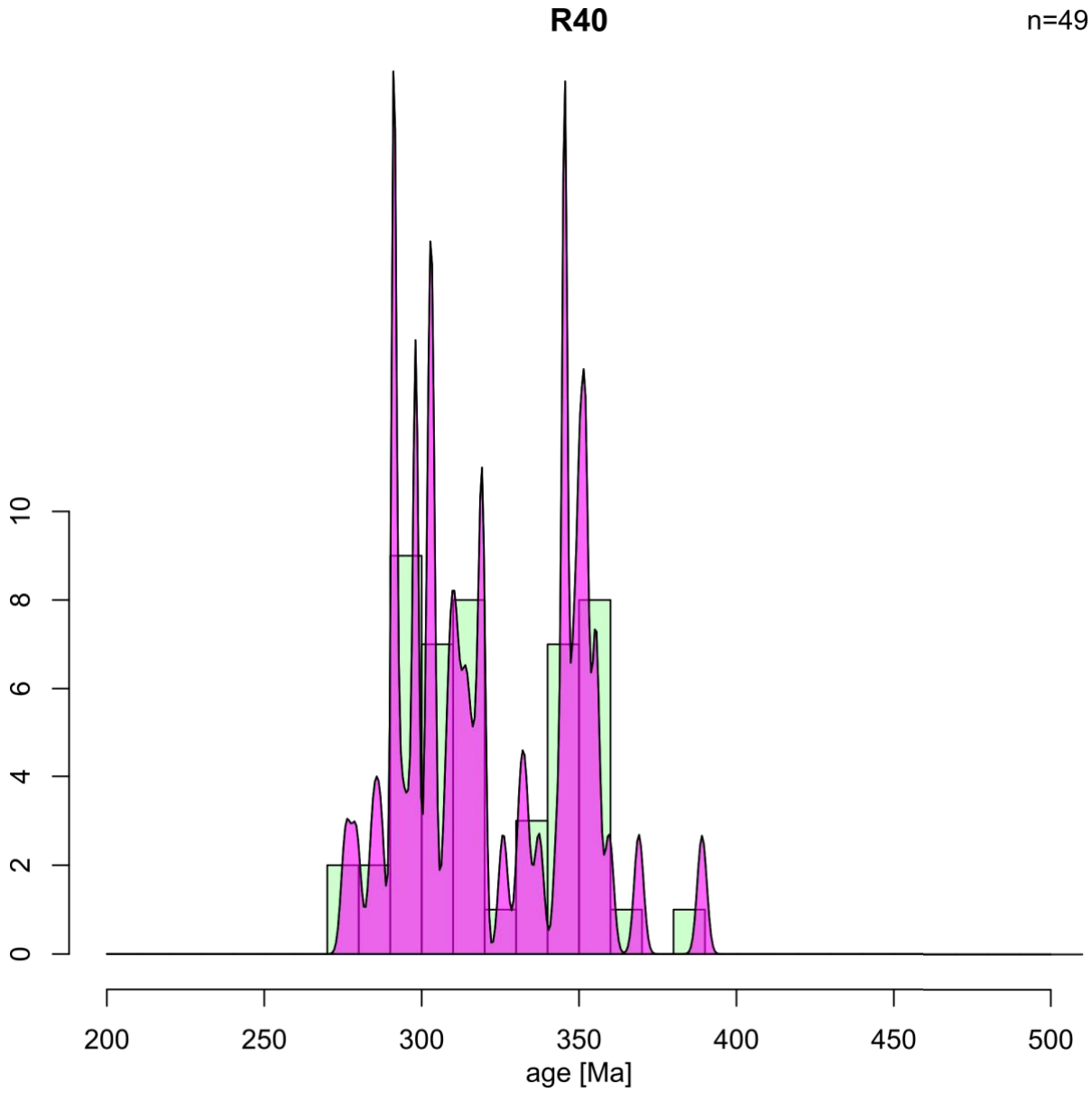

Fig. 68: *Frequency histogram with kernel density estimates showing detrital ($^{206}Pb/^{238}U$) zircon age distributions in the R40 sample.*

5.3 DISCUSSION

5.3.1 THE VEITSCH NAPPE

The Veitsch nappe is composed of Carboniferous marine to deltaic carbonates and clastic sediments (Ratschbacher, 1987) however, the source area of theses sediments still remains unknown (Ratschbacher, 1987; Handler et al., 1997; Neubauer et al., 2002). The possible sources of the detrital zircons are the Noric Nappe of the Greywacke Zone, the crystalline basement rocks in the vicinity of of the Greywacke Zone and/or the rocks from Graz Paleozoic.

The Greywacke Zone has a complex internal structure that consists of several tectonic nappes (Neubauer et al., 1994). The largest and uppermost Noric Nappe of the Greywacke Zone comprises a Lower Palaeozoic to Upper Carboniferous sedimentary successions. This is transgressively overlain by the Permian-age strata of the Tirolic Nappe System (Froitzheim et al., 2008 and references therein).The Noric Nappe consists of ignimbritic Late Ordovician Blasseneck porphyroid (Fig. 48), Silurian limestones, black shales and basic volcanic rocks. Platy, flaser/nodular and sometimes organodetritic limestones were deposited in the Devonian (Ebner et al., 2008).

The Crystalline basement units to the south underlie the Greywacke Zone can be separated again into several nappe systems (Schmid et al. 2004 and Froitzheim et al. 2008). The Drauzug-Gurktal nappe system (Fig. 6) represents the uppermost unit of the Austro-alpine nappe stack in the studied area that consists of low-grade metamorphic Paleozoic sedimentary rocks with a few relics of Permo-Mesozoic cover. Remnants of it are exposed as the Graz Paleozoic and the Gurktal nappes (Gasser et al., 2009 and reference therein). The Graz Paleozoic is located south from the studied area and it is divided into lower and upper nappe group. Both groups of nappes are built up of different sedimentary facies zones. The northern part of the lower nappe group is dominated by Devonian to probably Carboniferous calcareous schists and pelitic sediments (Gasser et al., 2009 and reference therein). The central and southern part of the lower nappe group is dominated by basal Silurian volcanic rocks, overlain by Silurian to Devonian siliciclastic and carbonaceous rocks and Middle Devonian limestones (Gasser et al., 2009). The upper nappe group is also characterized by basal Silurian volcanic

rocks. These are overlain by Carboniferous carbonaceous schists, sandstones and limestones (Gasser et al., 2009).

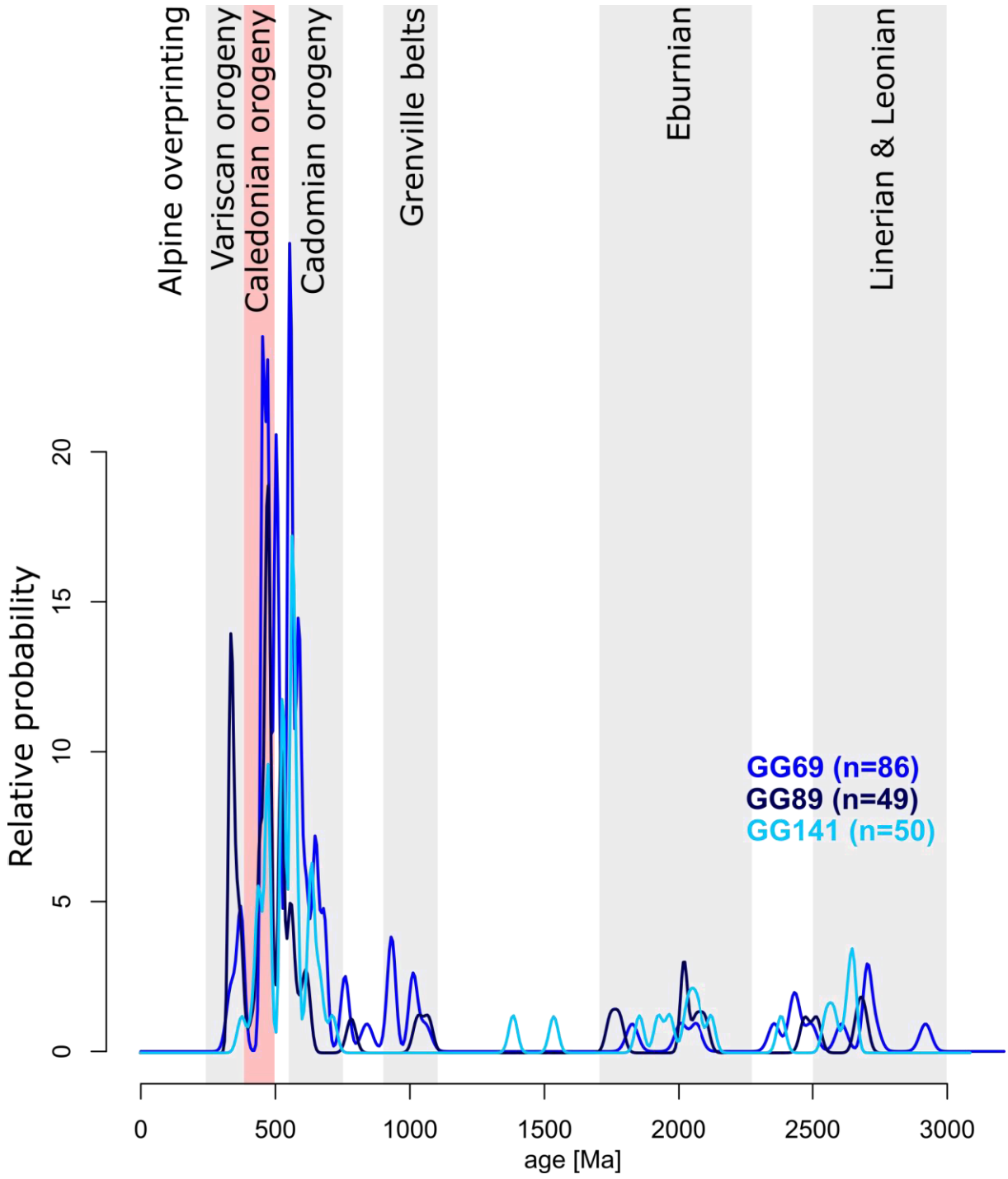

Fig. 69: *Compilation of age probability curves showing the detrital-zircon ages from the Veitsch Nappe. The main Paleozoic and Precambrian tectonothermal events and provenances are indicated.*

U-Pb dating of 180 grains from the Veitsch Nappe yielded age populations with the highest proportions of the ages 420-490 Ma, and 550-650 Ma, subordinate peak of 500-540 and significant peaks at 340-370 Ma and ~ 1900-2050 Ma and ~ 2500- 2700 Ma (Fig. 69,71, 73).

With the significant peak of 2.5 – 2.7 Ga, the peak at Eburnean (~ 2.1.; Fig. 69), the Grenvillian peak ~ 1 Ga and the significant amount of ~ 800 Ma (Fig. 69) ages, these older ages pattern resembles the characteristic age distribution of the East African-Arabian Zircon Province based on the main provenance features reported by Stephan et al. (2019).

The major peaks correspond to Cadomian evolution (550-650 Ma) and to the Ordovician rifting phase (420 – 490 Ma) associated with opening of the Rheic ocean (Fig. 69, 71). The scale and importance of the Ordovician event marked by LP-HT metamorphism and bimodal magmatism has been revealed in numerous recent studies of various massifs across the European Variscides (Edel et al., 2018; Peřestý et al., 2017; Pitra et al., 2012). The obtained Proterozoic ages could be interpreted as the recycled basin material from the older units. The possible source of the Ordovician ages could be interpreted the Blasseneck porphyry of the Noric Nappe.

Minor peak of the Variscan age was also recognized indicating time span of 340-370 Ma. These Variscan ages probably correspond to magmatic rock sources which are indicated by the fine-oscillation growth of zircons typical for magmatic rocks (e.g. Fig. 54 – GG89). The number of analyzed detrital zircons of Variscan age is increasing from the Steilbachgraben Formation (GG141) towards the Triebensten (GG89) and Sunk Formation (GG69, Fig. 69). This increase of the Variscan ages towards the hangingwall could be interpreted as the result of the continuous exhumation of Variscan crystalline basements.

5.3.2 THE OCHTINÁ UNIT

The Ochtiná Unit is located between two major units of the Central Western Carpathians. These Units are the possible sources of the detrital zircons in the studied samples. The basement of the structurally lower Vepor Unit is dominated by the Early Carboniferous granitoids (360- 340 Ma, Bibikova et al., 1988; Kohút et al., 1997; Kráľ et al., 1997; Michalko et al., 1998) with a Permian–Triassic cover (Foederata unit, Rozlosznik, 1935), while the structurally upper Gemer Unit consists mainly of Lower Palaeozoic volcano-sedimentary complexes (Faryad, 1991). The Gemer Unit includes the gneiss-amphibolite complex (The Klátov Group) interpreted in terms of an oceanic crust environment, the lower grade Rakovec Group is predominantly composed of tholeiitic metabasalts and metavolcanics and smaller amount of pelitic and Fe-rich metasediments. The Klátov and Rakovec Groups were incorporated into the Variscan collision suture proposed in the studied area (Vozárová and Vozár, 1996; 1997). The structurally uppermost Gelnica group in the south comprises volcano-sedimentary rocks intruded by Permian granitoids (Grecula, 1982; Poller et al., 2002).

The Gemer Unit is overlain by the Meliata accretionary wedge complex of Jurassic age (Kozur and Mock, 1973; Faryad and Henjes-Kunst, 1997) and uppermost Silica nappe system (Fig. 3).

Although the region was strongly deformed during the Alpine orogenic event of Cretaceous age, the Variscan metamorphic greenschist- to amphibolite-facies fabrics are dominant in Gemer Unit (Faryad, 1994; Faryad et al., 1999) and relics of a Variscan metamorphic amphibolite-facies fabric are locally preserved in the Vepor basement (Janák et al., 2007; Jeřábek et al., 2008).

In the Ochtiná Unit, the Mississippian volcano-sedimentary sequence includes deep-water turbidite sediments in the lower part and shallow-water fine grained siliciclastic and bioclastic carbonate sediments in the upper part (Vozárová, 1996). Although this complex was earlier interpreted as the cover of the Gemer Unit (Němejc, 1946; Planderová and Vozárová, 1978), more recently a separate evolution of the Ochtiná Unit was proposed based on the study of fluid inclusions and possible correlation of lithostragraphic horizons (Kozur and Mock, 1997; Németh et al., 2006).

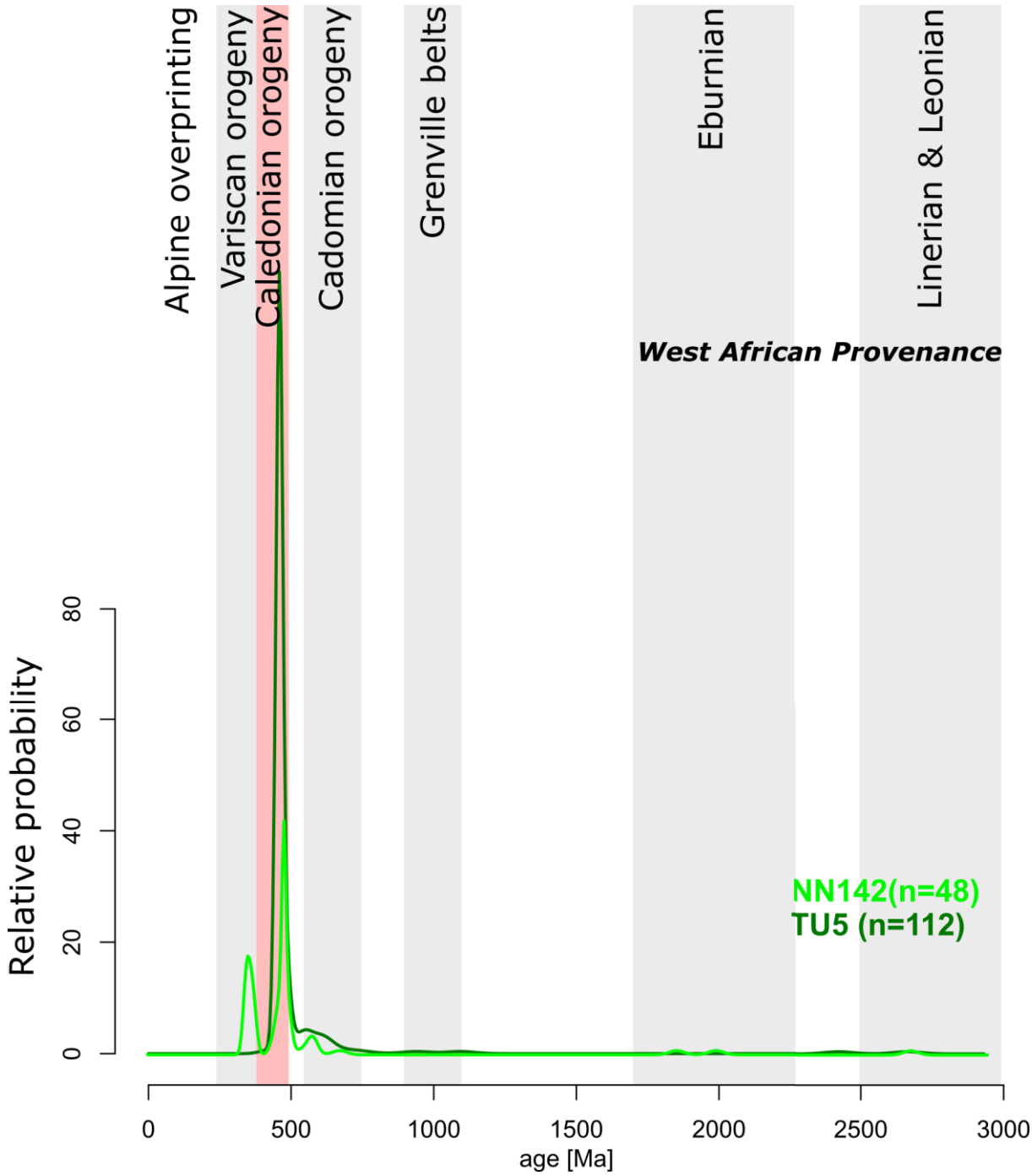

Fig. 70: *Compilation of age probability curves showing the detrital-zircon ages from the Ochtiná Unit. The main Paleozoic and Precambrian tectonothermal events and provenances are indicated.*

The detrital zircons have been recently analyzed from the basal part of Hrádok Formation (Vozárová et al. 2013). Based on the study the Hrádok Formation is dominated by Late Devonian-Mississippian ages within the range of 373-344 Ma (Vozárová et al. 2013).

In our study, U-Pb dating of 160 grains yielded age populations with the highest proportions of the ages 450-500 Ma. In the sample TU5 from basal part of Hrádek Formation this age was obtained from more than 84 % of the analyzed grains, in the stratigraphically higher sample NN142 this age was obtained from 52 % of the analyzed zircon grains.

From the rest of the analyzed grains, the dominant group of ages 340-380 Ma has been recognized only in sample NN142 (31 % of analyzed grains). The Variscan ages were derived from proximal magmatic rocks sources, which is indicated by the fine-oscillation growth zoning of zircons (e.g. Fig. 63 – NN142)

Furthermore, the significant peaks were recognized at 530-640 Ma, 1.7-2.0 Ga, 2.5-2.7 Ga. Single Grenvillian ages (~ 1 Ga) were observed and rare ages of ~ 800 Ma (Fig. 70, 71, 73). Based on the provenance features discussed by Stephan et al., (2019), these older ages pattern can be compared to the East African-Arabian Zircon Province. This relation seems to be more likely than the previously discussed relation to the West African Zircon Province suggested by Vozárová et al. (2013).

The dominant group of ages corresponds to the Ordovician rifting phase (420 – 490 Ma) associated with the Ordovician rifting and opening of the Rheic ocean in the studied area (Fig. 70, 71). The previously published ages from the basal part of the Hrádok Formation are dominated by Late Devonian-Mississippian ages within the range of 373-344 Ma pointing to the Vepor Unit source (Vozárová et al., 2013). In the uppermost sample from the Hrádok Formation no Variscan ages were found and the dominance of Ordovician ages points to the Gemer Unit source. This distinct evolution in ages along the stratigraphic column suggests an interesting change in the source area during Viseán from the Vepor dominating source to the Gemer dominating source. This is documented by the samples from basal part of the Hrádok Formation showing majority of the Variscan ages (Vozárová et al., 2013), sample NN142 from the upper part of the Hrádok Formation showing two dominant age populations of the Variscan and Late Cambrian-Ordovician ages (340-380 Ma and 440-500 Ma), and sample TU5 from the upermost part of the Hrádok Formation with Ordovician ages and no Variscan age. Thus the sample NN142 is expected to reflect the mixed source from both Gemer and Vepor Units.

5.3.3 RIMAVA FORMATION

The Permian sedimentary processes in the Gemer-Vepor Contact Zone are recorded by the Permian sample R40 from the Rimava Formation, which is interpreted to belong to the cover sequence of the Vepor Unit (Vozárová and Vozár, 1982). U-Pb dating of 48 grains from the Rimava Formation, yielded 2 major age populations of ages around 270-320 Ma and 330-370 Ma (Fig. 68). The well preserved prismatic crystal shapes with oscillatory zoning (Fig. 66), typical for magmatic rocks and absence of the older ages suggest a proximate source of Variscan and Permian magmatic rocks. Indeed, the Vepor crystalline basement is composed of large bodies of Carboniferous granitoids as well as some Permian smaller plutons and could serve as a source for the Rimava formation. At the same time, the Permian granitoids are also present in the Gelnica group of the Gemer Unit. The sample from Rimava Formation thus could reflect mixed source from both Vepor and Gemer units.

5.3.4 COMPARISON OF THE DATA FROM THE VEITSCH NAPPE AND OCHTINÁ UNIT

Based on the source rock and tectonic setting discrimination diagrams (Fig. 50) for the Veitsch Nappe, the samples from Veitsch Nappe show evolution from oceanic island arc (GG141) through continental arc (GG89) to passive margin settings (GG69). The samples from the Hrádok Formation with its whole rock composition correspond to the continental arc setting (NN142, TU5).

The reason for such a dramatic difference in source rock setting in the Veitsch Nappe might be explained by ongoing collision where the rocks of various sources are tectonically juxtaposed and thus provide a completely mixed source for sedimentation. In contrast, the situation in Ochtiná Unit is much more simple with the probable source rocks identified in the the volcanics of the Gemer Unit.

The studied samples from the Veitsch Nappe (GG141, GG89 and GG69) show gradual propagation of detrital zircons ages of the cumulative distribution curves (Fig. 71, 72). From the stratigraphically lower to the upper formations (Fig. 49, 72) the distribution curves show the increase of the absolute number of younger ages towards the hangingwall. This may indicate higher exhumation and erosion rates or change in sediment source due to the change in river network related to progress in Variscan collision (Fig. 71).

In the Ochtiná Unit, the stratigraphically lower sample (NN142) shows both, the Variscan and Late Cambrian-Ordovician ages (340-380 Ma and 440-500 Ma), the upper sample TU5 displays only Ordovician ages. This trend (Fig. 71 - opposite in the cumulative curves diagram than in Veitsch Nappe) is furthermore supported by the published data from the basal part of Hrádok Formation where the Variscan ages dominated the studied sample (Vozárová et al., 2013).

The samples from Veitsch Nappe show more complex age spectra with significant number of the older, even Archaican ages, than the studied samples in Ochtiná Unit (Fig. 69, 70, 71).

The diagram after Cawood et al., 2012 (Fig. 72) was constructed to further constrain the tectonic setting in which the sediment was deposited. Convergent plate margins are characterized by a large proportion of zircon ages close to the depositional age of the sediment,

whereas sediments in collisional, extensional and intracratonic settings contain greater proportions with older ages that reflect the history of the underlying basement. These differences are resolved by plotting the distribution of the difference between the measured crystallization ages and the depositional age of the sediment (Fig. 72). Based on the cumulative distribution curves of differences between the crystallization ages and the depositional ages (the depositional ages are inferred from Ebner et al., 2008)- the samples from Ochtiná Unit represent the active continental margin setting, contrary to the studied samples from Veitsch Nappe- they represent most likely the collisional tectonic setting (after Cawood et al., 2012).

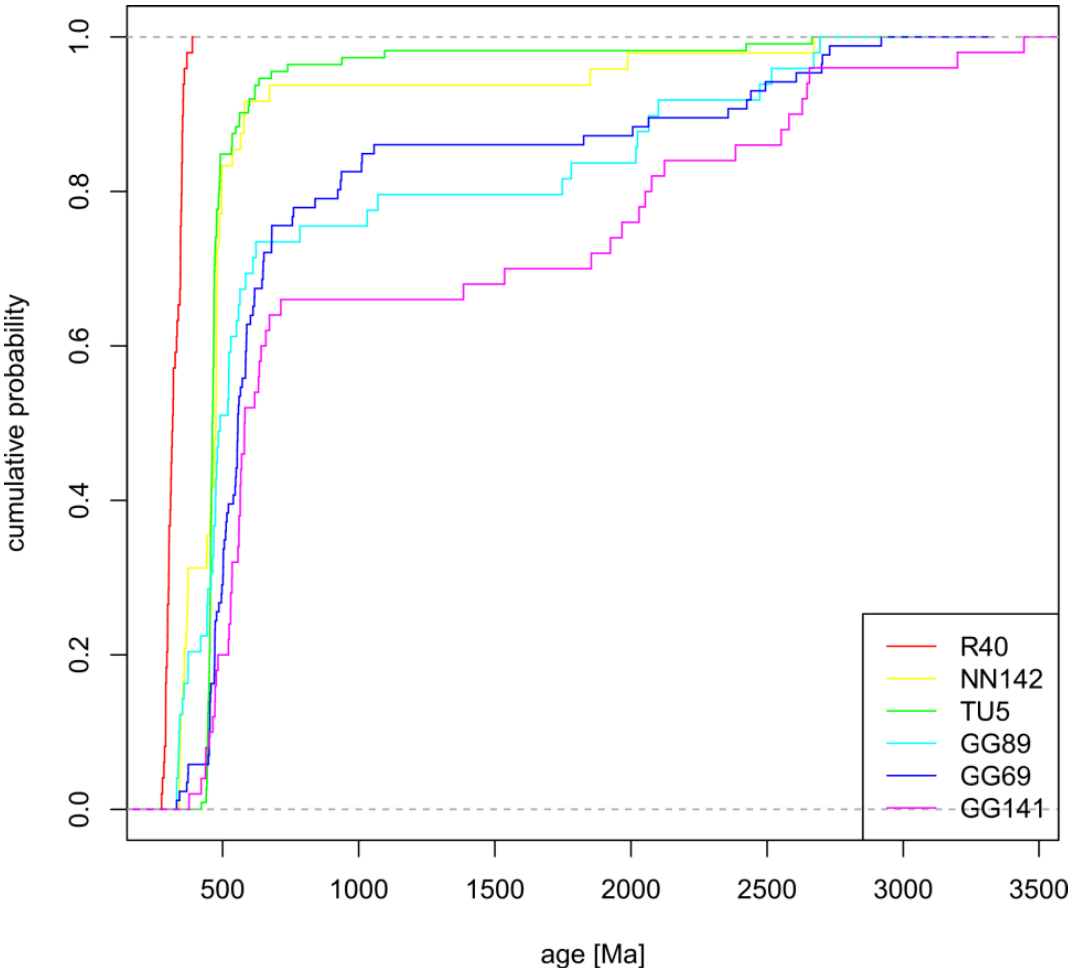

***Fig. 71**: Cumulative distribution curves of detrital zircons spectra from the Steilbachgraben Formation (GG141), Triebenstein Formation (GG89) and Sunk Formation (GG69) in the Veitsch Nappe; Hrádok Formation (TU5, NN142) in the Ochtiná Unit and Rimava Formation (R40).*

The active continental margin setting is supported by the geochemical data and by the age distribution in the Hrádok Formation of the Ochtiná Unit. In the Veitsch Nappe, the collision environment – the tectonic juxtaposition and proximity of different basement sources is responsible for the mixture of geochemical data and complex structure of the age spectra. This difference in tectonic setting between the two domains may reflect the large extent of the Veitsch-Nötsch-Szabadbattyán-Ochtiná Zone (VNSOZ, Neubauer and Vozárová, 1990). As previously discussed, the VNSOZ evolved after the formation of the Mediterranean Crystalline Zone in its foreland, or as remnant basin, related to Variscan orogenic belt in the Western Carpathians (Ebner et al., 1991; Ebner 1992; Ebner et al., 2008; Flügel 1977, 1990; Neubauer and Vozárová, 1990 Vozárová 1996), however along-strike variations in the tectonic setting are naturally expected.

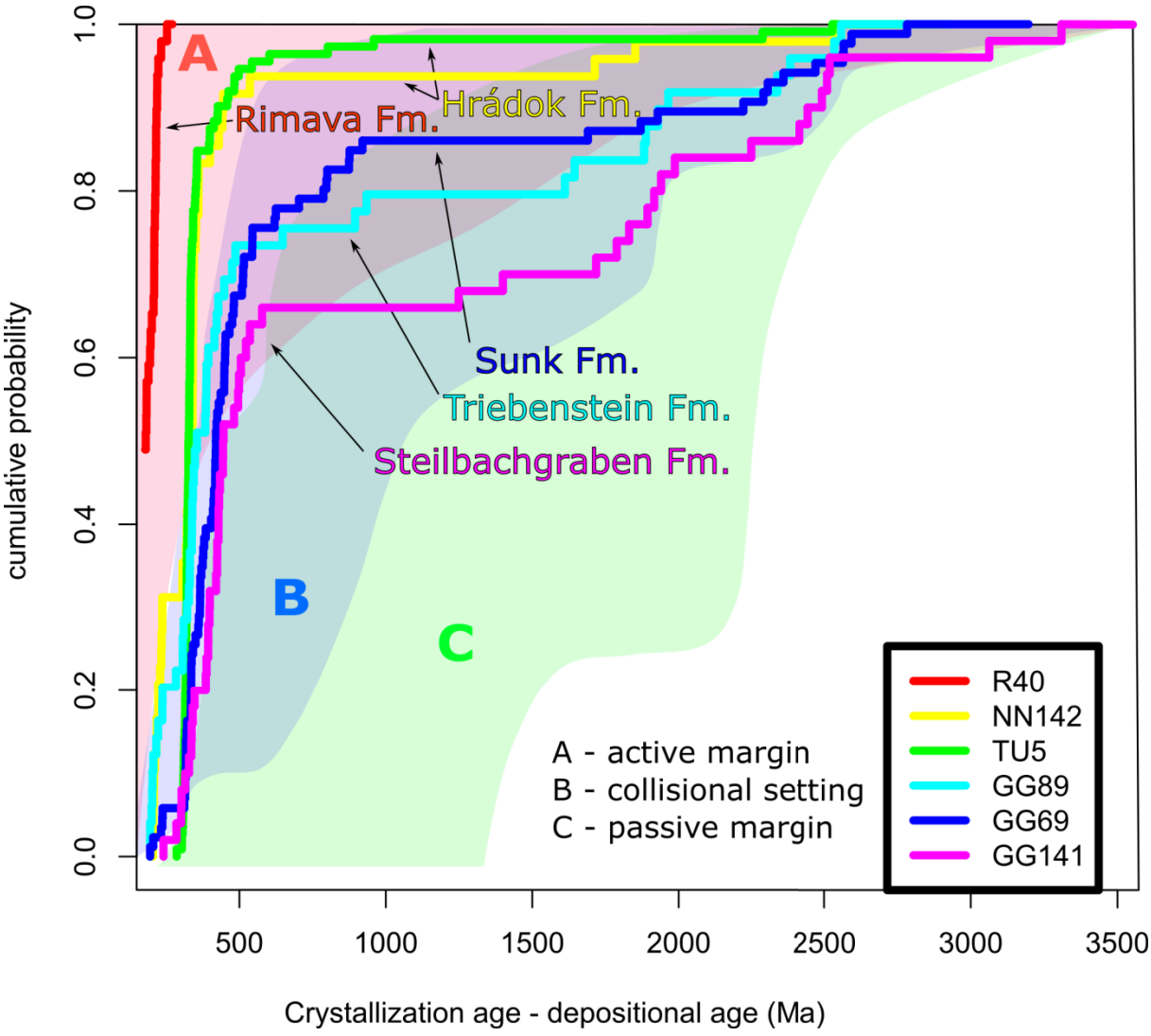

Fig. 72: *Cumulative distribution curves of differences between the crystallization ages and the depositional ages of detrital zircons form the Rimava, Hrádok, Sunk, Triebenstein and Steilbachgraben Formations. Depositional ages of individual formations are inferred from the stratigraphic record published in Ebner et al., 2008. Colour fields representing different tectonic settings of deposition are after Cawood et al., 2012.*

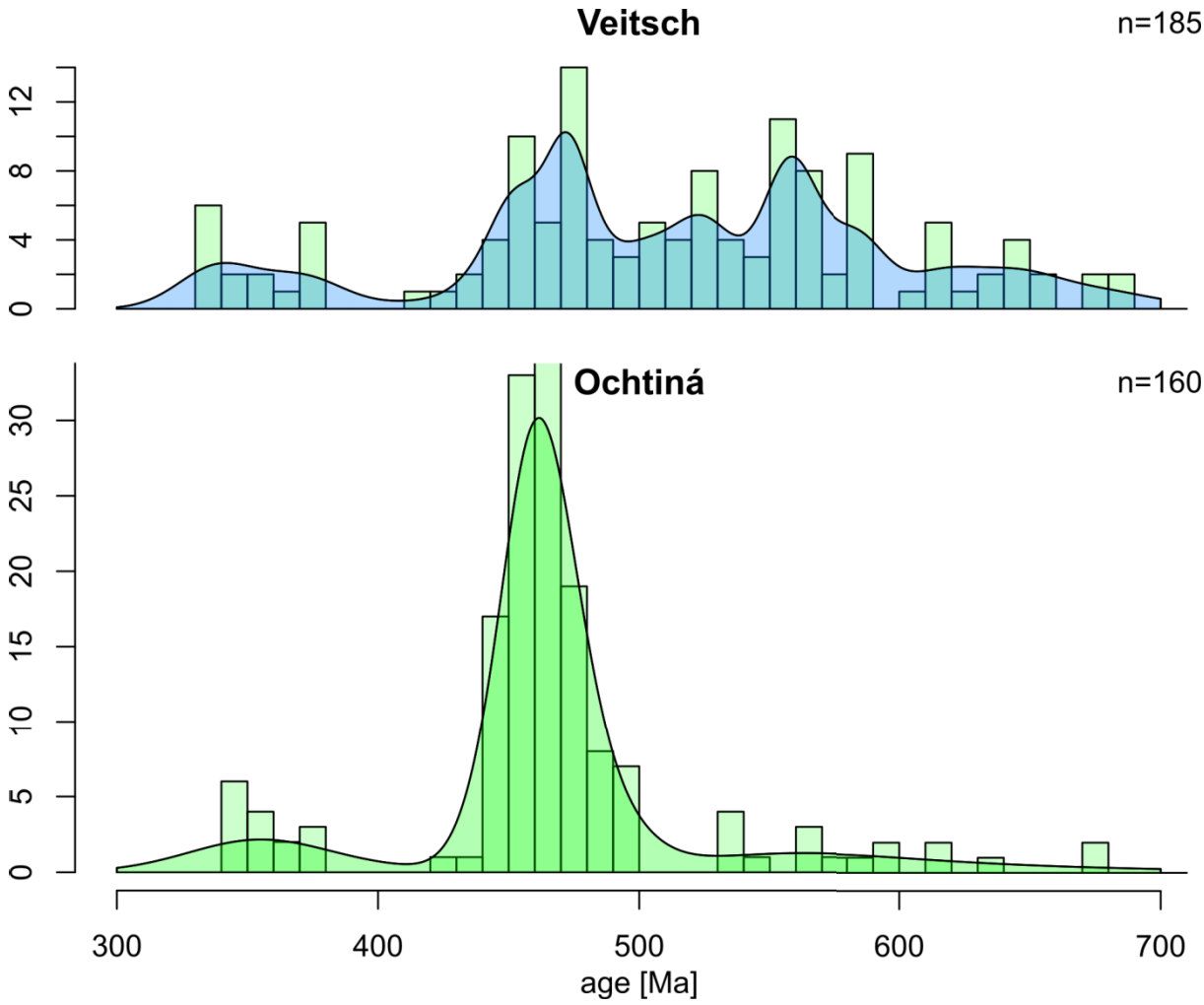

Fig. 73: *The detail on the zircon age distribution between 300-700 Ma in the studied areas; n – number of analyses.*

5.4 PARTIAL CONCLUSIONS

Both of the studied zones significantly show that the older ages patterns resembles to the East African-Arabian Zircon Province based on the main provenance features (Stephan et al., 2019).

Significant peak of ~ 440-490 Ma was observed in both domains. The Variscan ages (340-380 Ma) are also documented in both domains. However, the tectonic setting is different in each zone. The active continental margin environment in the Hrádok Formation of the Ochtiná Unit and on the other hand in the Veitsch Nappe, the collision environment – the tectonic juxtaposition and proximity of different basement sources is responsible for complex structure. Furthermore, this difference in tectonic setting between the two domains may reflect the large extent of the Veitsch-Nötsch-Szabadbattyán-Ochtiná Zone, however along-strike variations in the tectonic setting are naturally expected.

6. SUMMARY

This thesis represents the complex multidisciplinary work and it constitutes of answers to the three main objectives. The studied area extends from the Western Carpathians to the Eastern Alps. The Ochtiná Unit is situated in the ENE-WSW-trending contact zone between two crustal-scale nappes, the upper Gemer Unit and the lower Vepor Unit, in the Central Western Carpathians, Slovakia. The Ochtiná Unit consists mainly of Carboniferous phyllitic schists and sandstones enclosing lenses of diverse lithological nature and contrasting metamorphic history. The continuation of the Central Western Carpathians (CWC) in the Eastern Alps is regarded to be the nappe system of the Greywacke Zone. This Zone underlies the Tirolic Nappe System and includes from bottom to the top the Veitsch, Silbersberg, Vöstenhof-Kaintaleck and Noric nappes. The lowermost Veitsch Nappe mainly comprises Carboniferous clastic and carbonaceous metasediments and it is regarded to be the counter part of the Ochtiná Unit in the Eastern Alps. The Ochtiná Unit as well as the Veitsch Nappe is distinct in comparison with the surrounding Nappes and Units.

In Ochtiná Unit we have focused on the tectonic evolution and deformation record with respect to the Vepor Unit and we were furthermore been interested in the similarities of both domains in the Western Carpathians and Eastern Alps.

The Ochtiná Unit is characterized by a complex lithological assemblage of exotic hard blocks, lenticular in shape enclosed in a weak phyllite matrix. The heterogeneous lithological and metamorphic record is consistent with a block-in-matrix type of rock assemblage and consequently the Ochtiná Unit is interpreted as deep seated tectonic mélange which has formed during the Cretaceous Eo-Alpine collision at the boundary between two major crustal nappes of the Western Carpathians – the Gemer and Vepor Units.

The mélange evolved via repeated slip along the rheologically weak sediments of the Ochtiná Unit during the building and collapse of the Central Western Carpathians orogenic wedge. Deformation record indicates that the mélange separates two distinct structural domains marked by a decoupled behaviour, i.e. the orogenic suprastructure represented by the Gemer Unit and infrastructure represented by the Vepor Unit. With this respect, the Ochtiná Unit represents an unusual example of a suprastructure-infrastructure transition zone with its

position being controlled by the mechanical weakness of this sedimentary horizon and not by the usual thermal maturation.

To understand the distinct metasomatic processes recorded along the contact of Gemer and Vepor Units during the Alpine orogeny, the careful structural and petrological analysis was performed on local smaller shear zones in the Gemer-Vepor Contact Zone. Both sampled shear zones experienced prograde metamorphism during D_{A1} of higher grade. Later, as the process in Central Western Carpathians switched from top to bottom driven, the exhumation of the lower crust occurred due folding and doming of Vepor Unit D_{A2} and this process is recorded in the studied shear zones as well. The metasomatism is associated with formation of detachment shear zones and deformation fabric S_{A2} related to exhumation during D_{A2} deformation. The fluids were released from local sources during the early stage of exhumation and transported along large scale detachment shear zones in the Gemer-Vepor Contact Zone. At different crustal levels and within different lithological complexes, the fluids show heterogeneous behavior, related to gain or loss of different elements. It is a coupled process – the lower parts of the lithological complexes show gain in Mg, Fe, Ni and Mn, whereas the upper parts show depletion in the dam elements. The magnesite ore deposits present in the Gemer-Vepor Contact Zone probably served as the source for Mg-enrichement of fluids migrating through detachment shear zones during the doming and exhumation of the Vepor Unit.

To test the possible links between the Ochtiná Unit in the Gemer-Vepor Contact Zone of the Western Carpathians and the Veitsch Nappe in the Greywacke Zone of the Easten Alps the samples U-Pb detrital zircon dating was performed. Both of the studied zones significantly show that the older ages patterns resemble to the East African-Arabian Zircon Province based on the main provenance features.

Significant peak of ~ 440-490 Ma was observed in both domains. The Variscan ages (340-380 Ma) are also documented in both domains. The samples from the Veitsch Nappe show gradual propagation of detrital zircons ages of the cumulative distribution curves- from the stratigraphically lower to the upper formations. This increase of the number of Variscan ages towards the hangingwall could be interpreted as the result of the continuous exhumation of Variscan crystalline basements.

In Ochtiná Unit the dominant group of ages corresponds to the Ordovician rifting phase (420 – 490 Ma) associated with the Ordovician rifting and opening of the Rheic ocean in the studied area. In the uppermost sample from the Hrádok Formation no Variscan ages were

found and the dominance of Ordovician ages points to the Gemer Unit source. In the lower sample, the Variscan and the Ordovician ages were documented - this distinct evolution in ages along the stratigraphic column suggests an interesting change in the source area during Viseán from the Vepor dominating source to the Gemer dominating source.

The tectonic setting is different in each zone. The active continental margin environment in the Hrádok Formation of the Ochtiná Unit and on the other hand in the Veitsch Nappe, the collision environment – the tectonic juxtaposition and proximity of different basement sources is responsible for complex structure. Furthermore, this difference in tectonic setting between the two domains may reflect the large extent of the Veitsch-Nötsch-Szabadbattyán-Ochtiná Zone, however along-strike variations in the tectonic setting are naturally expected.

7. REFERENCE

Abonyi, A., 1971. Stratigraficko-tektonický vývoj karbónu Gemeríd západne od Štítnického zlomu (In Slovak). Geol. Práce, Správy 57, 339–348.

Abonyi, A., Abonyiová, M., 1981. Magnesite ore deposits of Slovakia (in Slovak). Miner. Slovaca, Monogr. pp. 1–125 (Alfa Bratislava).

Agard, P., Yamato, P., Jolivet, L., Burov, E., 2009. Exhumation of oceanic blueschists and eclogites in subduction zones: timing and mechanism. Earth Sci. Rev., 92, 53–79.

Ague, J. J., 1994. Mass transfer during Barrovian metamorphism of pelites, south-central Connecticut: II. Channelized fluid flow and the growth of staurolite and kyanite: American Journal of Science, v. 294, p. 1061-1134.

Andrusov, D., 1936. The subtatric nappes in the Western Carpathians (In Slovak). Carpatica 1, 3–50.

Auzanneau, E., Schmidt, M.W., Vielzeuf, D., Connolly, J. A. D., 2010. Titanium in phengite: a geobarometer for high temperature eclogites. Contrib. to Mineral. Petrol. 159, 1–24, doi: 10.1007/s00410-009-0412-7.

Bajaník, Š., 1976. To the petrogenesis of Devonian volcanic rocks of the Spišsko-gemerské rudohorie Mts. - Western Carpathians (In Slovak). Ser. Miner. Petrog. Geoch. Lož. 2, 75–94.

Bajaník, Š., Planderová, E., 1985. Stratigraphic position of the lower part of the Ochtiná Fm. (between Magnezitovce and Magura). Geologické Práce Správy, v. 82, p. 67-76 (in Slovak).

Beaumont, C., Nguyen, M.H., Jamieson, R.A., Ellis, S., 2006. Crustal flow modes in large hot orogens. Geol. Soc. London, Spec. Publ. 268, 91–145, doi: 10.1144/GSL.SP.2006.268.01.05.

Bernard, J. H., 1961. Mineralogie und Geochemie der Siderit Schwerspatgänge mit Sulphiden im Gebiet von Rudňany (Tschechoslowakei). Geologické Práce – Zošit, 58: 5–222.

Bhatia, M.R., Crook, K.A.W., 1986. Trace element characteristics of greywackes and tectonic setting discrimination of sedimentary basins. Contrib. to Mineral. Petrol. 92, 181–193, doi: 10.1093/petrology/25.4.956.

Bibikova, E. V., Cambel, B., Korikovsky, S.P., Broska, I., Gracheva, T. V., Makarov, V.A., Arakeliants, M., 1988. U-Pb and K-Ar isotopic of Sinec (Rimavica) granites (Kohút zone of Veporides). Geol. Carpathica 39, 147–157.

Bukovská, Z., Jeřábek, P., Lexa, O., Konopásek, J., Janák, M., Košler, J., 2013. Kinematically unrelated C—S fabrics: an Lexample of extensional shear band cleavage from the Veporic Unit (Western Carpathians). Geol. Carpathica 64, 103–116, doi: 10.2478/geoca-2013-0007.

Cawood, P.A., Hawkesworth, C.J., Dhuime, B., 2012. Detrital zircon record and tectonic setting. Geology 40, 875–878. https://doi.org/10.1130/G32945.1.

Chang, C.P., Angelier, J., Huang, C.Y., Liu, C.S., 2001. Structural evolution and significance of a mélange in a collision belt: the Lichi Mélange and the Taiwan arc–continent collision. Geol. Mag. 138, 633–651, doi: 10.1017/S0016756801005970.

Chopin, C., 1981. Talc-Phengite: a widespread assemblage in high-grade pelitic blueschists of the western Alps : Journal of Petrology,v. 22,p. 628–650.

Coggon, R., Holland, T.J.B., Street, D., 2002. Mixing properties of phengitic micas and revised garnet-phengite thermobarometers. J. Metamorph. Geol. 20, 683–696, doi: 10.1046/j.1525-1314.2002.00395.x.

Connolly, J.A.D., 2005. Computation of phase equilibria by linear programming: A tool for geodynamic modeling and its application to subduction zone decarbonation. Earth Planet. Sci. Lett. 236, 1-2, 524-541, doi: 10.1016/j.epsl.2005.04.033.

Culshaw, N.G., Beaumont, C., Jamieson, R.A., 2006. The orogenic superstructure-infrastructure concept: Revisited, quantified, and revived. Geology 34, 733–736, doi: 10.1130/G22793.1.

Dallmeyer, R.D., Németh, Z., Putiš, M. 2005. Regional tectonothermal events in Gemericum and adjacent units (Western Carpathians, Slovakia): Contribution by the $^{40}Ar/^{39}Ar$ dating. Slovak Geol. Mag. 11, 155—163.

Dallmeyer, R.D., Neubauer, F., Handler, R., Fritz, H., Müller, W., Pana, D., Putiš, M., 1996. Tectono-thermal evolution of the internal Alps and Carpathians: Evidence from $^{40}Ar/^{39}Ar$ mineral and whole-rock data. Eclogae Geologicae Helvetiae 89, 203–227.

Dela Pierre, F., Festa, A., Irace, A., 2007. Interaction of tectonic, sedimentary, and diapiric processes in the origin of chaotic sediments: An example from the Messinian of Torino Hill (Tertiary Piedmont Basin, northwestern Italy). Geol. Soc. Am. Bull. 119, 1107–1119, doi: 10.1130/B26072.1.

Demény, A., Sharp, Z.D., Pfeifer, H.-R., 1997. Mg-metasomatism and formation conditions of Mg–chlorite–muscovite–quartzphyllites (leucophyllites) of the Eastern Alps (W. Hungary) and their relations to Alpine whiteschists. Contrib. Mineral. Petrol. 128, 247–260.

Diener, J.F. a., Powell, R., 2012. Revised activity-composition models for clinopyroxene and amphibole. J. Metamorph. Geol. 30, 131–142, doi: 10.1111/j.1525-1314.2011.00959.x.

Ebner, F., Kovács, S., Schönlaub, H.P., 1991. Das klassische Karbon in Österreich und Ungarn – ein Vergleich der sedimentären fossilführenden Vorkommen. Jubiläumsschrift 20 Jahre Geol. ZuSouthern Alpsmmenarbeit Österreich-Ungarn 1, 263—294.

Ebner, F. 1992. Correlation of marine Carboniferous sedimentary units of Slovakia, Hungary and Austria. Spec. Vol. IGCP Project No. 276, (Dionýz Štúr Inst.), Bratislava 37—47.

Ebner, F., Vozárová, A., Kovács, S., Kräutner, H.G., Krstić, B., Szederkenyi, T., Jamićić, D., Balen, D., Belak, M., Trajanova, M., 2008. Devonian—Carboniferous pre-flysch and flysch environments in the Circum Pannonian Region. Geol. Carpathica 59, 159—195.

Edel, J. B., Schulmann, K., Lexa, O., Lardeaux, J. M., 2018. Late Palaeozoic palaeomagnetic and tectonic constraints for amalgamation of Pangea supercontinent in the European Variscan belt, Earth-Science Reviews, Volume 177, p. 589-612,ISSN 0012-8252, https://doi.org/10.1016/j.earscirev.2017.12.007.

Egger, H., Krenmayr, H. G., Mandl, G. W., Matura, A., Nowotny, A., Pascher, G., Pestal, G., Pistotnik, J., Rockenschaub, M.,Schnabel, W., 1999. Geologische Übersichtskarte der Republik Österreich 1:1.500.000. − Geologische Bundesanstalt, Wien.

Faryad, S.W., 1990. Gneiss-amphibolite Complex of the Gemericum. Miner. Slovaca 22, 303–318.

Faryad, S.W., 1991a. Pre-alpine metamorphic events in Gemericum. Miner. Slovaca 23, 395–402.

Faryad, S.W., 1991b. Metamorfóza sedimentov staršieho paleozoika gemerika (In Slovak). Miner. Slovaca 23, 315–324.

Faryad, S.W., 1994. Mineralogy of Mn-rich rocks from greenshist facies sequences of the Gemericum, West Carpathians. Neues Jahrb. fur Mineral. 10, 464–480.

Faryad, S.W., 1995. Phase petrology and P-T conditions of mafic blueschists from the Meliata unit, West Carpathians, Slovakia. Journal of Metamorphic Geology. J. Metamorph. Geol. 13, 701–714, doi: 10.1111/j.1525-1314.1995.tb00253.x .

Faryad, S.W., Bernhardt, H.J., 1996. Taramite-bearing metabasites from Rakovec (Gemeric Unit, The Western Carpathians). Geol. Carpathica 47, 349–357.

Faryad, S.W., Henjes-Kunst, F., 1997. Petrological and K-Ar and 40Ar-39Ar age constraints for the tectonothermal evolution of the high-pressure Meliata unit, Western Carpathians (Slovakia). Tectonophysics 280, 141–156, doi:10.1016/S0040-1951(97)00141-8

Faryad, S.W., 1999. Metamorphic evolution of the eastern part of the Western Carpathians , with emphasis on Meliata Unit. Acta Montan. Slovaca 4, 148–160.

Faryad, S.W., Dianiška, I., 1999. Alpine overprint in the early Paleozoic of the Gemericum. Miner. Slovaca 31, 485-490.

Ferrando, S., 2012. Mg-metasomatism of metagranitoids from the Alps: Genesis and possible tectonic scenarios, Terra Nova, 24(6), 423– 436.

Festa, A., Pini, G.A., Dilek, Y., Codegone, G., 2010. Mélanges and mélange-forming processes: a historical overview and new concepts. Int. Geol. Rev. 52, 1040–1105, doi: 10.1080/00206810903557704.

Festa, A., Dilek, Y., Pini, G.A., Codegone, G., Ogata, K., 2012. Mechanisms and processes of stratal disruption and mixing in the development of mélanges and broken formations: redefining and classifying mélanges. Tectonophysics 568–569, 7–24. http://dx.doi.org/10.1016/j.tecto.2012.05.021.

Floyd, P.A., Leveridge, B.E., 1987. Tectonic environment of the Devonian Gramscatho basin, south Cornwall: framework mode and geochemical evidence from turbiditic sandstones. J. Geol. Soc. London. 144, 531–542, doi:10.1144/gsjgs.144.4.0531.

Flügel, E. 1977: Environmental models for Upper Paleozoic benthic calcareous algal communities. In: Flügel E. (Ed.): Fossil algae. Springer, Berlin—Heidelberg—New York—Wien, 314—343.

Flügel, H.W., 1990. Das voralpine Basement im Alpin-Mediterranen Belt – Überblick und Problematik. Jb. Geol. B.—A. 133, 181—221.

Frisch, W., Gawlick, H.-J., 2003. The nappe structure of the central Northrn Calcareous Alps and its disintegration during Miocene tectonic extrusion – a contribution to understanding the orogenic evolution of the Eastern Alps. – Geologische Rundschau 92: 712–727.

Froitzheim, N., Plašienka, D., Schuster, R., 2008. Alpine tectonics of the Alps and Western Carpathians. – In: McCann T. (Ed.): The Geology of Central Europe. Volume 2: Mesozoic and Cenozoic. – Geological Society, London, 1141–1232.

Gánovský, J., 1995. Lubeník – reserve calculation of magnesite deposit, stand 1.1.1994. Bratislava: Geofond, 17 p (in Slovak).

Gasser, D., Gusterhuber, J., Krische, O., Puhr, B., Scheucher, L., Wagner, T., Stüwe, K., 2009. Geology of Styria: An Overview. – Mitt. Naturwiss. Ver. Steiermark 139: 5–36.

Goncalves, P., Oliot, E., Marquer, D., Connolly, J.A.D., 2012. Role of chemical processes on shear zone formation: an example from the Grimsel metagranodiorite (Aar massif, Central Alps). Journal of Metamorphic Geology 30, 703–722.

Grant, J.A., 1986. The isocon diagram – A simple solution to Gresens equation for metasomatic alteration. Econ. Geol., 81, 1976–1982.

Grecula, P., 1982. Gemericum - Segment of the Paleotethyan riftogenous basin. Miner. Slovaca- Monogr., Alfa Bratislava, pp.1-263.

Grecula, P. (Ed.), 1995. Mineral deposits of the Slovak ore mountains. Volume 1. Geocomplex, Bratislava, 1—834 Volume 1. Geocomplex, Bratislava, 1-834.

Grecula, P., Kobulský, J., Gazdačko, Ľ., Neméth, Z., Hraško, Ľ., Novotný, L., Maglay, J., 2009. Geological map of the Spiš-Gemer Ore Mts. at a scale 1:50000. Bratislava, State Geological Institute of Dionýz Štúr.

Handler, R., Dallmeyer, R. D., Neubauer, F., 1997. $^{40}Ar/^{39}Ar$ ages of detrital white mica from Upper Austroalpine units in the Eastern Alps, Austria evidence for Cadomian and contrasting Variscan sources. Geologische Rundschau, 86, 69-80.

Holland, T.J.B., Powell, R., 1998. An internally consistent thermodynamic data set for phases of petrological interest. J. Metamorph. Geol. 16, 309–343, doi:10.1111/j.1525-1314.1998.00140.x.

Holland, T., Powell, R., 2003. Activity composition relations for phases in petrological calculations: an asymmetric multicomponent formulation. Contrib. to Mineral. Petrol. 145, 4, 492-501, doi: 10.1007/s00410-003-0464-z.

Hoschek, G., 2004. Comparison of calculated P-T pseudosections for a kyanite eclogite from the Tauern Window, Eastern Alps, Austria. Eur. J. Mineral. 16, 59–72, doi: 10.1127/0935-1221/2004/0016-0059.

Hoschek, G., 2013. Garnet zonation in metapelitic schists from the Eclogite Zone, Tauern Window, Austria: comparison of observed and calculated profiles. Eur. J. Mineral. 25, 615–629, doi: 10.1127/0935-1221/2013/0025-2310.

Hovorka, D., Zlocha, J., 1974. Tectonics and origin of ultrabasic bodies of the Gemeride Mesozoic (West Carpathians). Sbor. geol. Věd 26, 185–193.

Hovorka, D., Ivan, P., 1985. Meta-ultrabasites in the Inner Western Carpathians: Implication for the reconstruction of the tectonic evolution of the region. Ofiolity 10, 317–328.

Hovorka, D., Ivan, P., Méres, Š., 1997. Leptyno-amphibolite complex of the Western Carpathians: Its definition, extent and genetical problems., in: Grecula, P., Putiš, D., Hovorka, M. (Eds.), Geological Evolution of the Western Carpathians. Miner. Slovaca-Monograf., Bratislava, pp. 269–280.

Huang, C.Y., Chien, C.W., Yao, B., Chang, C.P., 2008. The Lichi Mélange: A collision mélange formation along early arcward backthrusts during forearc basin closure, Taiwan arc-continent collision. Geol. Soc. Am. Spec. Pap. 436, 127–154, doi: 10.1130/2008.2436(06).

Hurai, V., Prochaska, W., Lexa, O., Schulmann, K., Thomas, R., Ivan, P., 2008a. High-density nitrogen inclusions in barite from a giant siderite vein: implications for Alpine evolution of the Variscan basement of Western Carpathians, Slovakia. J. Metamorph. Geol. 26 (4), 487–498. http://dx.doi.org/10.1111/j.1525-1314.2008.00775.x.

Hurai, V., Lexa, O., Schulmann, K., Montigny, R., Prochaska, W., Frank, W., Konečný , P., Kráľ, J., Thomas, R., chovan, M., 2008b. Mobilization of ore fluids during Alpine metamorphism: evidence from hydrothermal veins in the Variscan basement of Western Carpathians, Slovakia. Geofluids, 8: 181–207.

Hurai, V., Huraiová, M., Koděra, P., Prochaska, W., Vozárová, A., Dianiška, I., 2011. Fluid inclusion and stable CO isotope constraints on the origin of metasomatic magnesite deposits of the Western Carpathians, Slovakia. Russ. Geol. Geophys. 52, 1474–1490, doi: 10.1016/j.rgg.2011.10.015.

Ivan, P., 2008. Staropaleozoický bázický vulkanizmus Západných Karpát: Geochémie a geodynamická pozícia. Acta Geologica Universitatis Comenianae, Bratislava, pp. 1-94.

Jablonský, J., Sýkora, M., Aubrecht, R., 2001. Detritic Cr-spinels in Mesozoic sedimentary rocks of the Western Carpathians (overview of the latest knowledge).Miner. Slovaca 33, 487–498.

Jackson, S.E., Pearson, N.J., Griffin, W.L., Belousova, E.A., 2004. The application of laser ablation-inductively coupled plasma-mass spectrometry to in situ U–Pb zircon geochronology. Chemical Geology 211, 47–69.

Janák, M., Plašienka, D., Frey, M., Cosca, M., Schmidt, S.T., Lupták, B., Méres, Š., 2001. Cretaceous evolution of a metamorphic core complex, the Veporic unit, Western Carpathians (Slovakia): P–T conditions and in situ $^{40}Ar/^{39}Ar$ UV laser probe dating of metapelites. J. Metamorph. Geol. 19, 197–216, doi: 10.1046/j.0263-4929.2000.00304.x

Janák, M., Méres, Š., Ivan, P., 2007. – Petrology and metamorphic P-T conditions of eclogites from the northern Veporic unit, western Carpathians, Slovakia. – Geol. Carpath., 58, 121-131.

Janoušek, V., Farrow, C.M., Erban, V., 2006. Interpretation of whole-rock geochemical data in igneous geochemistry: introducing Geochemical Data Toolkit (GCDkit). J. Petrol. 47, 1255–1259, doi: 10.1093/petrology/egl013

Jeřábek, P., Stünitz, H., Heilbronner, R., Lexa, O., Schulmann, K., 2007. Microstructural-deformation record of an orogen-parallel extension in the Vepor Unit, West Carpathians. J. Struct. Geol. 29, 1722–1743, doi: 10.1016/j.jsg.2007.09.002.

Jeřábek, P., Faryad, S.W., Schulmann, K., Lexa, O., Tajčmanová, L., 2008. Alpine burial and heterogeneous exhumation of Variscan crust in the West Carpathians; insight from thermodynamic and argon diffusion modelling. J. Geological Soc. 165, 479–498, doi: 10.1144/0016-76492006-165

Jeřábek, P., Lexa, O., Schulmann, K., Plašienka, D., 2012. Inverse ductile thinning via lower crustal flow and fold-induced doming in the West Carpathian Eo-Alpine collisional wedge. Tectonics 31, 5, 1-26, doi: 10.1029/2012TC003097.

Kilík, J., 1997. Geological characteristic of the talc deposit in Gemerská Poloma—Dlhá dolina. Acta Montanistica Slovaca 2, 71—80 (in Slovak).

Klinec, A., 1966. On the structure and evolution of the Veporic crystalline unit. Geol. Zborník 6, 7–28.

Koděra, P., Radvanec, M., 2002. Comparative mineralogical and fluid inclusion study of the Hnúšťa-Mútnik talc-magnesite and Miková-Jedľová magnesite deposit (Western Carpathians, Slovakia). Boletím Paranaense de Geociências, 50: 131–150.

Kohút, M., Todt, W., Janák, M., Poller, U., 1997. Thermochronometry of the Variscan basement exhumation in the Veká Fatra Mts. (Western Carpathians, Slovakia). Terra Abstracts, EGU 9, Strassbourg 9, 1, 494.

Kováčik, M. 1996. Kyanite–magnesian chlorite schist and its petrogenetic significance (the Sinec massif, southern Veporic unit, Western Carpathians). Geologica Carpathica, 47, 245–255.

Kozur, H., Mock, R., Mostler, H., 1976. Stratigraphische Neue-instufung der Karbonategesteine der unteren Schichtenfolge von Ochtiná (Slovakei) in das oberste Vise Serpukchovian (Namur A). Geol. Paläont. Mitt. 6, 1–29.

Kozur, H., Mock, R., 1997. New paleogeographic and tectonic interpretations in the Slovakian Carpathians and their implications for correlations with the Eastern Alps and other parts in the Western Tethys. Part II. Inner Western Carpathians. Miner. Slovaca 29, 164–209.

Kráľ, J., Frank, W., Bezák, V., 1996. ^{40}Ar—^{39}Ar spectra from amphibole of Veporic amphibolic rocks. Miner. Slovaca 28, 501—513 (in Slovak, English summary).

Leake, B.E., Woolley, A.R., Birch, W.D., Burke, E.A., Ferraris, G., Grice, J.D., Whittaker, E.J., 1997. Nomenclature of amphiboles: additions and revisions to the International Mineralogical Association's 1997 recommendations. Can. Mineral. 41, 1355–1362, doi: 10.2113/gscanmin.41.6.1355.

Lexa, O., Schulmann, K., Ježek, J., 2003. Cretaceous collision and indentation in the West Carpathians: View based on structural analysis and numerical modeling. Tectonics 22, 6, 1–16, doi: 10.1029/2002TC001472.

Lillie, R. J., Bielik, M., Babuška, V., Plomerová, J., 1994. Gravity modelling of the lithosphere in the Eastern Alpine-Western Carpathian-Pannonian Basin region. Tectonophysics, Volume 231, Issue 4, 215-235, ISSN 0040-1951, https://doi.org/10.1016/0040-1951(94)90036-1.

Lisý, E., 1971. Talc deposits of Slovakia. Mineralia Slovaca, 3: 343–348 (in Slovak).

Liu, Y., Hu, Z., Gao, S., Günther, D., Xu, J., Gao, C., Chen, H., 2008. In situ analysis of major and trace elements of anhydrous minerals by LA-ICP-MS without applying an internal standard, Chemical Geology, Volume 257, Issues 1–2, Pages 34-43, ISSN 0009-2541, https://doi.org/10.1016/j.chemgeo.2008.08.004.

López-Carmona , A., A., Pitra, P., Abati, J., 2013. Blueschist-facies metapelites from the Malpica–Tui Unit (NW Iberian Massif): phase equilibria modelling and H2O and Fe2O3 influence in high-pressure assemblages. Journal of Metamorphic Geology, 31, 3, 263-280, doi: 10.1111/jmg.12018.

Ludwig, K.R., 2008. User's Manual for Isoplot v. 3.6, a Geochronological Toolkit for Microsoft Excel. vol. 4. Berkeley Geochronological Center Special Publications, pp. 1–77.

Lupták, B., Janák, M., Plašienka, D., Schmidt, S.T., Frey, M., 2000. Chloritoid-kyanite schists from the Veporic unit, Western Carpathians, Slovakia: implications for Alpine (Cretaceous) metamorphism. Schweizerische Mineral. und Petrol. Mitteilungen 80, 213–223.

Lupták, B., Janák, M., Plašienka, D., Schmidt, S.T., 2003. Alpine low grade metamorphism of the Permian-Triassic sedimentary rocks from the Veporic superunit, Western Carpathians: phyllosilicate composition and „crystallinity“ data. Geol. Carpathica 54, 367–375.

Manatschal, G., Marquer, D., FrühGreen, G.L., 2000. Channelized fluid flow and mass transfer along a riftrelated detachment fault (Eastern Alps, SE Switzerland). Geol. Soc. Am. Bull., 112, 21–33

Marquer, D., 1987. Transfert de matière et déformation progressive des granitoïdes. Exemples des massifs de l'Aar et du Gotthard (Alpes central suisses), Thesis Université de Rennes, 250 pp.

Matějka, A. and Andrusov, D., 1931. Aperçu de la géologie des Carpathes occidentales de la Slovaquie centrale et des régions avoisinantes. Knihovna Státního geologického ústavu 13A, 19–163.

Michalík, J., lintnerová, o., Gażdzicki, a. and Soták, J. 2007. record of environmental changes in the triassic/Jurassic boundary interval in the zliechov basin, Western Carpathians. Palaeogeography, Palaeoclimatology, Palaeoecology, 244, 71–88

Michalko, J., Bezák, V., Hraško, Ľ., 1998. U/Pb zircon data from the Veporic granitoids (Western Carpathians). Krystalinikum 24, 91–104.

Mihalík, F., Tréger, M., 1995. The Ochtiná deposit – magnesite – prospecting, reclassification of reserves, stand 1995. Spišská Nová Ves: Geological Survey of Slovakia, 16 p (in Slovak).

Mock, R., Sýkora, M., Aubrecht, R., Ožvoldová, L., Kronome, B., Reichwalder, P., Jablonský, J., 1998. Petrology and stratigraphy of the Meliaticum near the Meliata and Jaklovce Villages. Slovakia. Slovak Geol. Mag. 4, 223–260.

Molák, B., Hraško, L., Pristas, J., 1995. Metallogenic investigation in the area of Rimavská Baňa village. Manuscript, Geological Survey of Slovak Republic. 1-50 (in Slovak).

Němejc, F., 1946. Further critical remarks on Sternberg's Lepidodendron dichotomum and its relations to the cones of Sporangiostrobus Bode. Rozpr. II. třídy České Akad. Věd 47, 7, 1-11.

Németh, Z., Prochaska, W., Radvanec, M., Kováčik, M., Madaras, I., Koděra, P., Hraško, L., 2004. Magnesite and talc origin in the sequence of geodynamic events in Veporicum, Inner Western Carpathians, Slovakia. Acta Petrologica Sinica, 20: 837–854.

Németh, Z., Radvanec, M., Hraško, Ľ., Madarás, J., 2006. Ochtinská zóna z pohľadu nových výsledkov mapovacieho a petrologického výskumu v stykovej zóne veporika a gemerika. Geol. práce, Správy 15 (in Slovak).

Neubauer, F., Vozárová, A., 1990. The Noetsch-Veitsch-North gemeric zone of the Alps and Carpathians: Correlation, paleogeography and significance for Variscan orogeny., in: Thirty Years of Geological Coooperation Between Austria and Czechoslovakia, *Ústr. Ústav geologický, Praha,* pp. 167–171.

Neubauer, F., Handler, G., Hermann, S., Paulus, G., 1994. Revised Lithostratigraphy and Structure of the Eastern Graywacke Zone (Eastern Alps). - Mitt. Österr. Geol. Ges., 86 (1993), 61-74, Wien.

Neubauer, F., Frisch, W., Hensen, B.T., 2002. Early Palaeozoic tectonothermal events in basement complexes of the Eastern Greywacke zone (eastern Alps): Evidence from U-Pb zircon data: International Journal of Earth Sciences, v. 91, p. 775–786, doi:10.1007 /s00531-001-0254-7.

Novotná, N., Jeřábek, P., Pitra, P., Lexa, O., Racek, M., 2015. Repeated slip along a major decoupling horizon between crustal-scale nappes of the Central Western Carpathians documented in the Ochtiná tectonic mélange. Tectonophysics 646, 50–64.

Paton, C., Woodhead, J.D., Hellstrom, J.C., Hergt, J.M., Greig, A., Maas, R., 2010. Improved laser ablation U–Pb zircon geochronology through robust downhole fractionation correction. Geochemistry, Geophysics, Geosystems 11, 1–36. https://doi.org/ 10.1029/2009GC002618 (Q0AA06).

Pawling, S. and Baumgartner, L.P., 2001. Geochemistry of a talc-kyanite-chloritoid shear zone within the Monte Rosa granite, Val dAyas, Italy. Schweiz. Mineral. Petrogr. Mitt., 81, 329–346.

Pearce, J.A., Norry, M.J., 1979. Petrogenetic implications of Ti, Zr, Y and Nb variations in volcanic rocks. Contrib. to Mineral. Petrol. 69, 1, 33–47, doi: 10.1007/BF00375192.

Peřestý, V. , Lexa, O. , Holder, R. , Jeřábek, P. , Racek, M. , Štípská, P. , Schulmann, K., Hacker, B., 2017. Metamorphic inheritance of Rheic passive margin evolution and its early-Variscan overprint in the Teplá-Barrandian Unit, Bohemian Massif. J. Metamorph. Geol., 35: 327-355. doi:10.1111/jmg.12234

Pitra, P., Poujol, M., Driessche, J. V. D., Poilvet, J.-Ch., Paquette, J.-L., 2012. Early Permian extensional shearing of an Ordovician granite: The Saint-Eutrope "C/S-like" orthogneiss (Montagne Noire, French Massif Central), Comptes Rendus Geoscience,Volume 344, Issue 8, p. 377-384, ISSN 1631-0713, https://doi.org/10.1016/j.crte.2012.06.002.

Planderová, E., Vozárová A., 1982. Biostratigraphical correlation of Late Paleozoic formations in the West Carpathians. In: Sassi F. P. (Ed.): Newsletter 4, IGCP Pr. No. 5, Padova, 67-71.

Planderová, E., Vozárová, A., 1978. Upper Carboniferous in the Souther part of Veporic Unit. Geol. práce, Správy 70, 129–141.

Plašienka, D., Grecula, P., Putiš, M., Kováč, M., Hovorka, D., 1997. Evolution and structure of the Western Carpathians: an overview, in: Grecula, P., Hovorka, D., Putiš, M. (Eds.), Geological Evolution of the Western Carpathians. Miner. Slovaca, Bratislava, p. 1-24.

Plašienka, D., Janák, M., Lupták, B., Milovský, R., Frey, M., 1999. Kinematics and metamorphism of a cretaceous core complex: The veporic unit of the Western Carpathians. Phys. Chem. Earth, Part A: Solid Earth Geod. 24, 8, 651-658, doi: 10.1016/S1464-1895(99)00095-2.

Plašienka, D., Soták, J., 2001. Stratigraphic and tectonic position of Carboniferous sediments in the Furmanec valley (Muránska planina). Miner. Slovaca 33, 29–44.

Plašienka, D., 2003. Development of basement-involved fold and thrust structures exemplified by the Tatric–Fatric–Veporic nappe system of the Western Carpathians (Slovakia). Geodinamica Acta, 16,1, 21-38, doi: 10.1016/S0985-3111(02)00003-7.

Poller, U., Uher, P., Broska, I., Plašienka, D., Janák, M., 2002. First Permian–Early Triassic zircon ages for tin-bearing granites from the Gemeric unit (Western Carpathians, Slovakia): connection to the post-collisional extension of the Variscan orogen and S-type granite magmatism. Terra Nov. 14, 1, 41–48, doi: 10.1046/j.1365-3121.2002.00385.x.

Powell, R., Holland, T.J.B., 1988. An internally consistent dataset with uncertainties and correlations: 3. Applications to geobarometry, worked examples and a computer program. J. Metamorph. Geol. 6, 2, 173–204, doi: 10.1111/j.1525-1314.1988.tb00415.x.

Prochaska, W., 1985. Talk- und Leukophyllitbildung als Folge hydrothermaler Metasomatose. Mitt. O ¨sterr. Geol. Ges., 78, 167–179.

Prochaska, W., 1991. Leukophyllitbildung und Alteration in Scherzonen am Beispiel der Lagerstätte Kleinfeistritz (Steiermark). Arch. f. Lagerst.forsch. Geol. B.-A., 13, 111–122.

Prochaska, W., 1999. Die Bedeutung der chemischen Zusammensetzung von Einschlussfluiden und laugbaren Salzen für die Genese von hydrothermalen und sedimentären Karbonatgesteinen in den Ostalpen. Mitteilungen der Österreichischen Geologischen Gesselschaft, 90: 175–183.

Prochaska, W., 2000. Magnesite and talc deposits in Austria. Miner. Slovaca 32, 6, 543–548.

Prokešová, R., Plašienka, D., Milovský, R., 2012. Structural pattern and emplacement mechanisms of the Krížna cover nappe (Western Carpathians, Slovakia). Geol. Carpath. 63 (1), 13–32. http://dx.doi.org/10.2478/v10096-012-0001-y.

Putiš, M., Frank, W., Plašienka, D., Siman, P., Sulák, M., Biroň, A., 2009. Progradation of the Alpidic Central Western Carpathians orogenic wedge related to two subductions: constrained by $^{40}Ar/^{39}Ar$ ages of white micas. Geodin. Acta 22, 1, 31–56.

Radvanec, M., Prochaska, W., 2001. Successive replacement of Upper Carboniferous calcite to dolomite and magnesite in Dúbrava magnesite deposit (Western Carpathians, Slovakia). Mineralia Slovaca, 33: 517–525.

Radvanec, M., Bajtoš, P., Németh, Z., Koděra, P., Prochaska, W., Roda, Š., Tréger, M., Baláž, P., Grecula, P., Cicmanová, S., Kráľ, J., Žák, K., 2010. Magnesite and talc in Slovakia – genetic and geoenvironmental model. Štátny geologický ústav Dionýza Štúra, Bratislava, 189 pp.

Rakusz, G., 1932. Die Oberkarbonischen Fossilien von Dobsina (Dobišina) und Nagyisnyó. Inst. Regni Hungariae Geologicum, Geologica Hungarica, 8.

Ratschbacher, L., 1986. Kinematics of Austro-Alpine cover nappes: changing translation path due to transpression. Tectonophysics 124, 4, 335–356, doi: 10.1016/0040-1951(86)90170-8.**Ratschbacher, L. 1987.** Stratigraphy, tectonics, and paleogeography of the Veitsch nappe (Greywacke Zone, Eastern Alps, Austria): A rearrangement. Miner. Slovaca Monogr. 1987, 407—417.

Raymond, L.A., 1984. Classification of melanges. In: Raymond, L.A. (Ed.), Melanges: Their Nature, Origin and Significance. Geological Society of America Special Papers 198, pp. 7–20 (Boulder, Colorado).

Roser, B.P., Cooper, R.A., Nathan, S., Tulloch, A.J., 1996. Reconnaissance sandstone geochemistry, provenance, and tectonic setting of the lower Paleozoic terranes of the West Coast and Nelson, New Zealand. New Zeal. J. Geol. Geophys. 39, 1, 1-16, doi: 10.1080/00288306.1996.9514690.

Rozlozsnik, P., 1935. Die Geologische Verhältnisse der gegend von Dobšiná. Geologica Hungarica, Ser. Geol 5, 1-118.

Rudnick, R.L., Gao, S., 2003. The composition of the continental crust, in: The Crust. Elsevier-Pergamon, Oxford, 1–64, doi:10.1016/B0-08-043751-6/03016-4.

Schmid, S. M., Fügenschuh, B., Kissling, E., Schuster, R., 2004. Tectonic map and overall architecture of the Alpine orogen. – Eclogae Geologicae Helvetiae 97: 93–117.

Silver, E.A., Beutner, E.C., 1980. Melanges. Geology 8, 32–34.

Schertl, H.-P., Schreyer, W., Chopin, C.,1991. Thepyrope-coesiterocksandtheircountry rocks at Parigi, Dora Maira Massif, Western Alps: detailed petrography, mineral chemistry and PT-path. Contributions to Mineralogy and Petrology 108, 1–21.

Sláma, J., Košler, J., Condon, D.J., Crowley, J.L., Gerdes, A., Hanchar, J.M., Horstwood, M.S.A., Morris, G.A., Nasdala, L., Norberg, N., Schaltegger, U., Schoene, B., Tubrett, M.N., Whitehouse, M.J., 2008. Plešovice zircon – a new natural reference material for U– Pb and Hf isotopic microanalysis. Chemical Geology 249, 1–35.

Stephan, T., Kroner, U., Romer, R., 2019. The pre-orogenic detrital zircon record of the Peri-Gondwanan crust. Geological Magazine, 156(2), 281-307. doi:10.1017/S0016756818000031

Šucha, V., Eberl, D.D., 1992. Burial metamorphism of the Permian sediments from the Western Carpathians. Miner. Slovaca 24, 399–405.

Tomek, Č., Hall, J., 1993. Subducted continental margin imaged in the Carpathians of Czechoslovakia. Geology, 21, 6, 535-538, doi: 10.1130/0091-7613(1993) 021<0535:SCMIIN>2.3.CO;2.

Tréger, M., Malachovský, P., Mesarčík, I., Kilík, J., Mihál', F., 2004. Position of Betliar Formation in Gemericum geological structure. Mineralia Slovaca, 36: 51–60 (in Slovak).

Varga, I., 1992. Possible resources of the mineral raw materials of Slovakia – magnesite, prospecting, stand 31.12.1991. Geological Survey, Spišská Nová Ves, 177 p (in Slovak).

Vermeesch, P., 2018. IsoplotR: a free and open toolbox for geochronology. Geoscience Frontiers, v.9, p.1479-1493, doi:10.1016/j.gsf.2018.04.001.

Vojtko, R., Králiková, S., Jeřábek, P., Schuster, R., Danišík, M., Fügenschuh, B., Minár, J., Madarás, J., 2016. Geochronological evidence for the Alpine tectono-thermal evolution of the Veporic Unit (Western Carpathians, Slovakia). Tectonophysics 666, 48—65.

Vozárová, A., 1990. Development of metamorphism in the Gemeric/Veporic contact zone (Western Carpathians). Geol. Carpathica 41, 5, 475–502.

Vozárová, A., 1996. Tectono-sedimentary evolution of Late Paleozoic basins based on interpretation of lithostratigraphic data (Western Carpathians, Slovakia). Slovak Geol. Mag, 3-4.

Vozárová, A., 1998. Hercynian development of the external-Gemeric zone., in: Rakús, M. (Ed.), Geodynamic Development of the Western Carpathians. Dionýz Štúr Publication, Bratislava, 47–61.

Vozárová, A., Vozár, J., 1982. New lithostratigraphic units in the southern part of the Veporicum. Geol. Práce, Spr. 79, 27—54 (in Slovak).

Vozárová, A., Vozár, J., 1996. Terranes of West Carpathian-North Panonian Domain. Slovak Geol. Mag. 1, 61—83.

Vozárová, A., Vozár, J., 1997. Terranes of the Western Carpathian North Panonian Domain. In: Papanikolau D. (Ed.): Terrane map and terrane descriptions. IGCP No. 276. Ann. Géol. Pays Helén. 37, 245—270.

Vozárová, A., Šarinová, K., Larionov, A., Presnyakov, S., Sergeev, S., 2010. Late Cambrian/Ordovician magmatic arc type volcanism in the Southern Gemericum basement, Western Carpathians, Slovakia: U–Pb (SHRIMP) data from zircons. Int. J. Earth Sci. 99, 1, 17–37, doi: 10.1007/s00531-009-0454-0.

Vozárová, A., Ebner, F., Kovács, S., Kräutner, H-G., Szederkényi, T., Kristić, B, Sremac, J., Aljinovič, D., Novak, M., Skaberne, D., 2009. Late Variscan (Carboniferous to Permian) environments in the Circum Pannonian Region. Geologica Carpathica 60, 71–104.

Vozárová, A., Laurinc, D., Šarinová, K., Larionov, A., Presnyakov, S., Rodionov, N., Paderin, I., 2013. Pb ages of detrital zircons in relation to geodynamic evolution: Paleozoic of the Northern Gemericum (Western Carpathians, Slovakia). J. Sediment. Res. 83, 11, 915–927.

Vozárová, A., Konečný, P., Šarinová, K., Vozár, J., 2014. Ordovician and Cretaceous tectonothermal history of the Southern Gemericum Unit from microprobe monazite geochronology(Western Carpathians, Slovakia).Int. J.Earth Sci.103(4), 1005–1022. http://dx.doi.org/10.1007/s00531-014-1009-6.

Vrána, S., 1964. Chloritoid and kyanite zone of alpine metamorphism on the boundary of the Gemerides and the Veporides (Slovakia). Krystalinikum 2, 125–143.

White, R.W., Powell, R., Holland, T.J.B., 2007. Progress relating to calculation of partial melting equilibria for metapelites. J. Metamorph. Geol. 25, 5, 511–527, doi: 10.1111/j.1525-1314.2007.00711.x.

White, R.W., Powell, R., Holland, T.J.B., Worley, B.A., 2000. The effect of TiO_2 and Fe_2O_3 on metapelitic assemblages at greenschist and amphibolite facies conditions: mineral equilibria calculations in the system K_2O-FeO-MgO-Al_2O_3-SiO_2- H_2O-TiO_2-Fe_2O_3. J. Metamorph. Geol. 18, 5, 497–511, doi: 10.1046/j.1525-1314.2000.00269.x.

Wiedenbeck, M., Alle, P., Corfu, F., Griffin, W.L., Meier, M., Oberli, F., von Quadt, A., Roddick, J.C., Spiegel, W., 1995. Three natural zircon standards for U–Th–Pb, Lu–Hf, trace element and REE analyses. Geostandards Newsletter 19, 1–23.

Winchester, J.A., Floyd, P.A., 1977. Geochemical discrimination of different magma series and their differentiation products using immobile elements. Chem. Geol. 20, 325-343, doi: 10.1016/0009-2541(77)90057-2.

Wölfler, A., Prochaska, W., Fritz, H., 2015. Shear zone related talc mineralization in the Veitsch nappe of the Eastern Greywacke Zone (Eastern Alps). Austrian Journal of Earth Science, 108: 50–72.

Wood, D.A., 1980. The application of a ThHfTa diagram to problems of tectonomagmatic classification and to establishing the nature of crustal contamination of basaltic lavas of the British Tertiary Volcanic Province. Earth Planet. Sci. Lett. 50, 1, 11-30, doi: 10.1016/0012-821X(80)90116-8.

Xia, X., Sun, M., Geng, H., Sun, Y., Wang, Y., Zhao, G., 2011. Quasi-simultaneous determination of U-Pb and Hf isotope compositions of zircon by excimer laserablation multiple-collector ICPMS. J. Anal. Atomic Spectrom. 26, 1868e1871.

8. SUPPLEMENTARY